

Propulse NTNU - Project Stetind

Team 16 Technical Report to the 2021 EuRoC

Hannah Chaplin Laugaland - Project manager, Ask Haugerud Hovik - Chief Mechanical Engineer, Anders Indrebø Hestad - Chief Avionics Engineer, Vebjørn Gulbrand Bratlie - Chief recovery engineer, Johannes Eiriksønn Mørkrid - Simulation engineer, Hege Grytten - Recovery engineer, Ola Vanni Flataa - Ground station and telemetry Engineer, Sheikha Al-Nasser - Avionics Engineer, Andreas Fanebust - Avionics Engineer, Ane Kirstine Havstad Mørkemo - Avionics Engineer, Svein Jostein Husa - Avionics Engineer, Kristian Hope - Avionics Engineer, Tina Torsdatter Davidsen - Deputy project manager, Erik Fjeldstrøm Trydal - Chief Inner Structure, Cecilie Aurelia Olsnes - Inner Structure Engineer, Simen Flåtter Flo - Inner Structure Engineer, Steven Xu - Inner Structure Engineer, Tea Christiansen Rasmussen - Chief Outer Structure Engineer, Fabian Camillo Eitzen - Computational Fluid Dynamics Specialist, Erlend Lokna - Simulation Engineer, Amrinder Dhillon - Outer Structure Engineer, Fredrik Fossan-Waage - Chief Payload Engineer, Sven Amberg - Payload Engineer, Young-In Falck - Payload Engineer, Hans Kristian Lorentzen - Payload Engineer, Astrid Christine Zieritz -Payload Engineer, Adelina Ghindaoanu -Payload Engineer

Norwegian University of Science and Technology (NTNU), 7031 Trondheim, Norway

Propulse NTNU presents the rocket Stetind, slated to participate in the European Rocketry Challenge of 2021, and aims to reach a target apogee of 9000 m with a commercial off-the-shelf Cesaroni Pro 98 solid rocket motor. Stetind builds on the experience from the organization's two forerunning projects, and is a step towards our long term goal of reaching the Karman line. Our project goals are to develop a high-performing sounding rocket, and for our members to evolve into competent engineers. Stetind has the following design characteristics: The airframe is made out of two segments of filament wound fiber composite, and is aerodynamically optimized with a Haack series shape both on the nose and the tail of the rocket. The recovery system incorporates a student researched and developed main parachute deployment mechanism with no energetic elements. The avionics system controls and monitors the recovery system using barometers, thermometers and cameras, transmitting all this data to the ground station during the flight. Both software and printed circuit boards are student researched and developed. Stetind's payload is developed by our sister organization Orbit NTNU, with purpose to examine the behaviour of ferrofluid during flight, with high acceleration, strong vibrations and free fall. This report will present the technical details and validation of the different systems comprising the rocket.

Nomenclature

A	- Area
A_P	- Projected Area
a	- Average Attraction Between Particles
b	- Volume Excluded by a Mole of Particles
C_D	- Drag Coefficient
CG	- Center of Gravity
CP	- Center of Pressure
D	- Maximum Diameter
d_i	- Distance Between the Component's Centre of Gravity and the Nose Tip
F	- Force
F_D	- Drag
$F_{D,aft}$	- Drag Aft
$F_{D,forward}$	- Drag Forward
g	- Gravitational Acceleration
m	- Mass
P	- Pressure
q_∞	- Dynamic Pressure
R	- Universal Gas Constant
ρ	- Density
ρ_∞	- Freestream Density
α	- Angle of Attack
β	- Oblique Shock-wave Angle
σ	- Stress
T	- Temperature
V	- Volume
V_∞	- Freestream Velocity
v	- Velocity
W_t	- Total Rocket Weight
W_i	- Component Weight

Contents

I	Introduction	4
II	System Architecture	5
II.A	System overview	5
II.B	Propulsion System	6
II.C	Trajectory calculations	7
II.D	Outer structure	9
II.E	Inner structure	20
II.F	Recovery	28
II.G	Avionics	34
II.H	Payload	43
III	Mission concept overview of operations	47
IV	Conclusion and Outlook	49
V	Appendix	50
V.A	System data	50
V.B	Test reports	58
V.C	Hazard analysis	111
V.D	Risk assessment	118
V.E	Assembly, Preflight and Launch checklists	131
V.F	Engineering drawings	138
V.G	Aerodynamics	174
V.H	Constraints and requirements appendix	203
V.I	Calculations and Analysis	206
V.J	Production methods	258
V.K	Component overview	263
V.L	Detailed Telemetry Architecture	278
V.M	Detailed Software Architecture	283
V.N	Detailed Electrical Architecture	289
V.O	Mechanical Interface Control Document for Payload	295
V.P	Detailed Software Architecture Payload	302
V.Q	Electrical Interface Control Document	311
V.R	Requirements Payload	318
V.S	Payload Sub-assembly checklist	324

I. Introduction

1. Organization

Propulse NTNU is a volunteer-based student organization whose goal is to provide students knowledge and enhanced engineering abilities through design, development, and construction of sounding rockets. The organization is currently working on three technical projects that consist of developing a sounding rocket, a hybrid engine, and a flight trajectory simulator. These projects are steps on the way towards our long term goal of reaching the Karman line. Other functional areas in the organization are business, marketing and administration. There are 37 members in total from 12 different fields of studies, supported by 13 mentors. Members working on the main project are split between system related groups.

2. Project Stetind

Project Stetind is the current main project of Propulse NTNU, and the subject for this report. The objective is to develop a sounding rocket capable of carrying a 4 kg payload to 9000 m , with a Commercial off-the-shelf (COTS) solid propulsion system. These are the underlying project goals:

- 1) The project must be economically viable.
- 2) Create a good environment for learning and social interaction.
- 3) Perform a successful flight.
- 4) Build competence on Finite Element Analysis(FEA), Computational Fluid Dynamics (CFD)-analysis, composite, data cleaning and testing.

As a result of these goals, requirements set by the team for the rocket are related to price, achievable production, reliability, and validation through analysis and tests. These are stated in Appendix V.H. The rocket is a cooperation of subsystems. Therefore subsystems must be developed in a way that they complement each other, with a goal of maximizing the rocket's performance as a whole. Requirements systems pose on each other are also stated in Appendix V.H. To find solutions fulfilling all requirements, members are encouraged to compare known methods and technologies to new ideas. The solutions are evaluated through design reviews, where professors, sponsors, alumni and the team are present. New designs and solutions are made iteratively based on feedback from said reviews, as well as test results, analysis, risk assessment and production constraints.

The main technical challenges of the project have been designing and validating high performing aerodynamic aspects of the rocket, using a mechanical parachute deployment system without energetic devices, and developing software on embedded systems.

3. Orbit NTNU

As part of the Project Stetind Propulse NTNU cooperates closely with the student organization Orbit NTNU, which is working with design, development and testing of satellites. This year, a subgroup within Orbit NTNU constructed the payload for the rocket, described in Section II.H Payload. The purpose of this subgroup is to provide new members in Orbit NTNU an introduction to the process of making a satellite.

4. Stakeholders

The primary stakeholders in the project are the team members. EuRoC and the Spaceport America Cup (SA Cup) have certain demands for the project, while our sponsors and the Norwegian University of Science and Technology (NTNU) have contributed to the project in the form of expertise, production and funding. Kongsberg Defence & Aerospace is the main sponsor. The organization is also sponsored by Radionor Communications, the Faculty of Information Technology and Electrical Engineering at NTNU, the Faculty of Engineering at NTNU, NCAB Group, NORBIT, Simpro, 4Test Instrument, Norwegian Defence Research Establishment (FFI), WindTec, Nammo and Eidsvoll Electronics.

II. System Architecture

A. System overview

The Stetind rocket consists of four main systems; structure, recovery, avionics and payload. Structure is divided into two subsystems, outer and inner structure. An overview of the systems is illustrated in Figure 1 and 2. Outer structure features a forward airframe (OU.FA)¹ composed of fiberglass, and an aft airframe (OU.AA) composed of carbon fibre. The aft airframe tapers in towards the boat tail (IAE.B) following a Haack series shape. There are four symmetric trapezoidal fins (OL.F) located at the bottom of the aft airframe. The fins are mounted with fin brackets (OL.FP). The inner structure of the rocket can be divided into three parts: the upper half, lower half, and the coupler section. The upper half of the inner structure houses the avionics system, the payload and most recovery subsystems. The structural integrity of this section is ensured by bulkheads and threaded rods. The threaded rods are also the main mounting points for the inner subsystems, such as the avionics mount and the hawk system. The lower half houses the COTS Cesaroni pro 98 6GXL solid rocket motor (IAE.M), the boat tail assembly, four trapezoidal fins (OL.F) and a motor centering ring (IAE.MCR). The coupler section is where the rocket decouples after apogee, and houses the drogue parachute (RC.DC) and the main parachute (RC.MC). There are three reasons for why the rocket splits at the middle. Firstly, having all the avionics on one side of the split simplifies cabling, yielding one “smart” half with avionics, recovery and payload, and one “dumb” half with the motor and related components. Secondly, it allows the placement of the payload to be as far up into the nose cone as possible, raising the center of mass. Thirdly, it prevents the need for several composite and metal sections, reducing the complexity of the fuselage. Fig 16 in section II.E Inner structure, shows an interface diagram between the systems, while figure 3 and 4 contain force diagrams showing how the forces from the motor and from the parachutes are translated through the structure.

The rocket contains a two-stage recovery system. The first stage is the rocket separation module. The separation is enabled by a surge of gaseous carbon dioxide from the hawk system pressurizing the airtight compartment within the coupler system, thereby breaking the shear screws (F.14) holding the upper coupler (IC.UC) and lower coupler (IC.LC) together, which allows the drogue parachute to deploy from the rocket. The second stage of recovery is programmed to initiate at the preset altitude of 475 m above ground level (AGL), where the main parachute is deployed by a student researched and developed (SRAD) mechanical release system (RM.MCRS). The main function of the avionics systems is to activate the two stages of the recovery system. This function can be fulfilled by either the SRAD Flight Computer, or the redundant COTS system. The SRAD system also has a function of collecting, storing and transmitting sensor data. Figure 33 and Figure 32 in section II.G Avionics, shows the information flow and power flow in the system. There are two cameras (A.C1, A.C2) which record the exterior surroundings of the rocket, whilst a third camera (A.C3) records the inside of the coupler section containing the parachutes. The requirements for all the systems are listed in Appendix V.H, which provides further details on the aforementioned design choices.



Fig. 1 The Rocket Stetind.

¹ This is a component ID referring to the component. An overview of all components comprising the rocket, and corresponding component IDs can be found in Appendix V.K.



Fig. 2 Cross sectional view of the rocket.



Fig. 3 Force diagram motor force.



Fig. 4 Force diagram parachute forces.

B. Propulsion System

The Cesaroni Pro98 6GXL motor (IAE.M) with the 21062O3400-P fuel grain was chosen early in the concept phase. This resulted in the rocket being designed based on the performance and size properties of the motor. This particular motor was chosen because it is a high power motor at an acceptable price for our organization. Additionally, it has a high impulse to diameter ratio, which makes reaching the 9 000 m altitude target feasible, albeit a challenge, with the 21062 N·s of impulse the motor provides. The interface between the motor and the mechanical structure of the rocket is described in Section II.E.

C. Trajectory calculations

1. Flight profile

The trajectory analysis consists of simulations from the software OpenRocket as well as a numerical simulation of the recovery phase. Further information on the recovery simulation can be found in the Appendix V.I *Parachute trajectory simulations*. The results from the analysis are shown below in Figure 5 and Figure 6, where Figure 5 shows the rocket in a quick ascent plus coasting to 8771.3 m followed by release and deployment of the parachutes for a slow descent. The flight plus descent is estimated to last 400 s. Note the slower descent after 323 s, where the main chute is deployed.

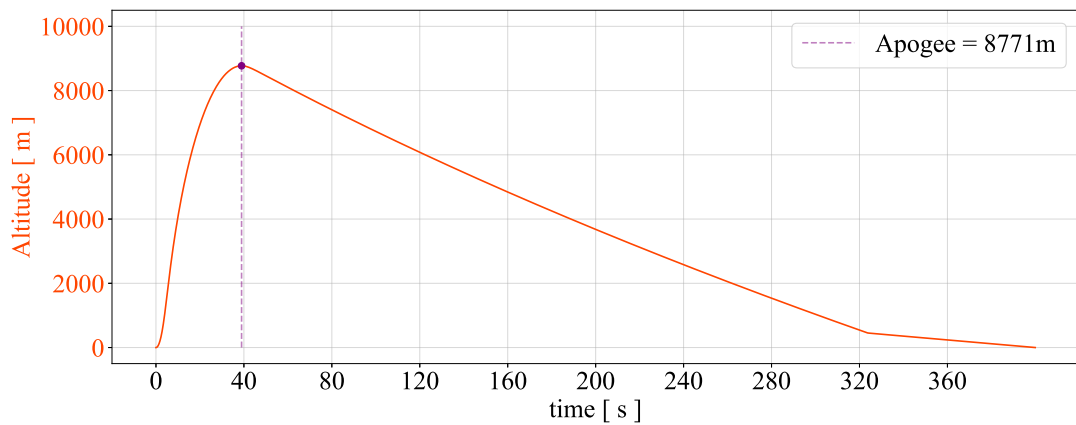


Fig. 5 Simulated flight profile displaying all flight phases, and highlighting apogee expected at 39 s.

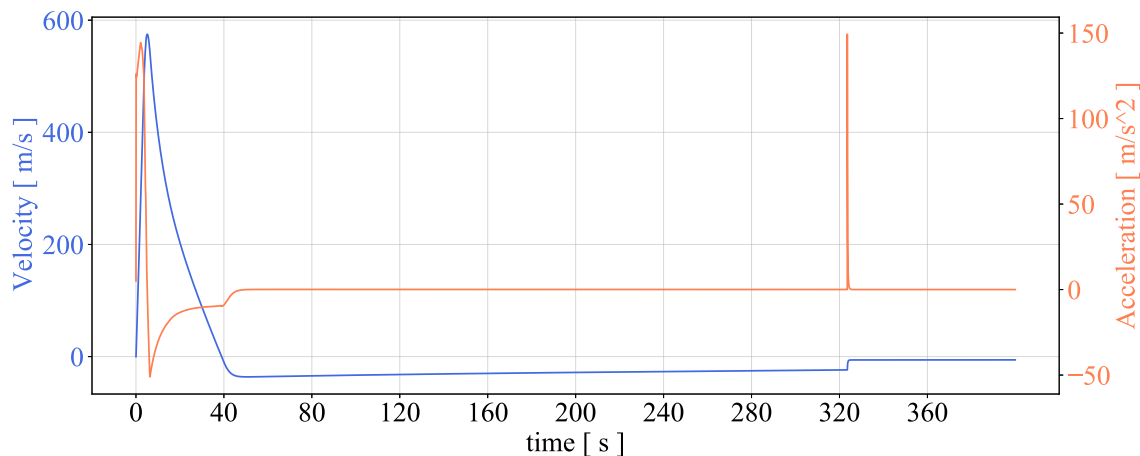


Fig. 6 Predicted velocity and acceleration during flight. The rapid change in acceleration at around 323 s is due to the main parachute being deployed.

2. MaxQ / Mach number

The maximum dynamic pressure can be found using the velocity and altitude values from OpenRocket, where Eq. (1) is the equation for dynamic pressure:

$$q_\infty = \frac{1}{2} \rho_\infty V_\infty^2 \quad (1) \quad \rho(z) = \rho_0 \cdot e^{-(\frac{gMz}{RT_0} - \frac{Lz}{T_0})} \quad (2)$$

International Standard Atmosphere (ISA) provides models for calculating the density at different altitudes, shown in Eq. (2). The results are shown in Figure 7, where the dynamic pressure is calculated using Eq. (1).

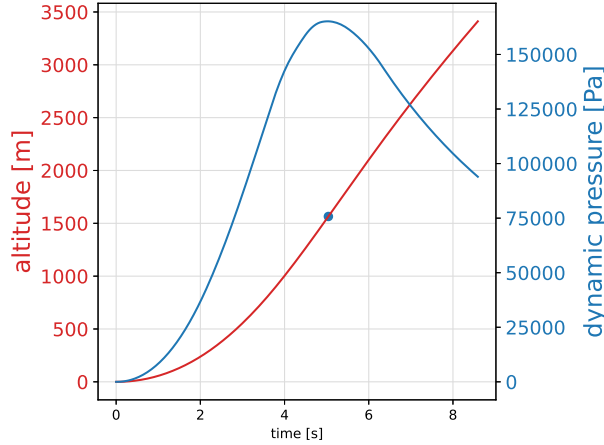


Fig. 7 OpenRocket maxQ prediction. The blue point represents Max Q.

The maximum dynamic pressure prediction allows locating the point in space and time where the rocket should experience the maximum aerodynamic loads. The data collected in this analysis are presented in Table 1.

Table 1: Maximum dynamic pressure

MaxQ	Value
Altitude (m)	1692
Velocity (m/s) [mach]	577 [1.73]
Density (kg/m ³)	1.0413
Pressure (Pa)	82992
Time (s)	5.2

3. Parameters

The simulation conditions for OpenRocket are:

Table 2: Simulation conditions and results

Simulation conditions	Value
Launch alt (m.)	119 [1]
Rail angle (deg.)	5
Rail Length (m.)	12
Avg. windspeed (m/s.)	0
Atmospheric conditions	ISA
Results	
Apogee (m.)	8771
Launch rod clearance velocity (m/s.)	55.8
Max velocity (m/s.)[Mach]	577 [1.73]
Max acceleration (m/s^2)	145
Time to apogee (m.)	39

An average wind speed is chosen to be 0 m/s in order to avoid unnecessary cumulation of errors. This is also based on the uncertainty of how OpenRocket handles winds and when the simulation potentially can become unstable.

D. Outer structure

1. System function and system overview

Outer structure defines the aerodynamic element of the rocket and the structural integrity of the airframe, fins and fin brackets. A figure of the outer structure can be found in Section II.A *Systems Overview*. The following section addresses the aerodynamic aspect of the planned flight trajectory, such as stability margin, drag and air turbulence encompassing the rocket. Design justification is based on results obtained from CFD, FEA and hand calculations. In addition, manufacturing decisions are presented and discussed.

OpenRocket and RASAero II have been used to estimate the rocket's stability and derive data on aerodynamic coefficients and forces. Furthermore, CFD has been used for two reasons: one, to capture the entire flow field around the rocket's full geometry (as OpenRocket and RASAero II do not add full geometric details). Secondly, as CFD is a powerful tool, Propulse NTNU wants to increase knowledge and skills to improve key design elements, accuracy and precision, and to minimize error propagation within the calculations. Detailed outline on error estimation for OpenRocket, RASAero II and CFD, can be found in Appendix V.G.

Table 3: Function diagram

Part	Reference	Manufacturing method	Validation method	Functions				
				Tool for production	Load bearing	Mounting point	Reduce drag	Gain stability
Mandrel	OP.M	Turning	FEM					
Forward Air-frame	OU.FA	Winding	CFD					
Aft air-frame	OL.AA	Winding	CFD					
Fins	OL.F	CNC machining	CFD, FEM					
Fin brackets	OL.F	CNC machinig	CFD, FEM					

2. Aerodynamics

Stability Margin

One must examine the rocket's stability in order to predict its flight trajectory, and thereby obtain a stable and safe flight profile to the desired apogee.

The stability margin presented in Eq 3 is a way to measure the rocket's stability based on the CP-CG distance, measured in calibers (body tube diameter), being expressed as.

$$SM = \frac{CP - CG}{D} \quad (3)$$

where CP is the center of pressure, and CG is the center of gravity. Note that the CP is closest to the boattail meaning the CP-CG distance is positive.

At liftoff, the rocket motor mass is at its maximum where the distance between the nose tip and CG is greatest. In order for the SM to be optimal, the fins must move the CP towards the boattail such that the CP-CG distance is sufficient, ensuring stability. This is why EuRoC states that the rocket must have an offrail velocity of minimum 30.0 m/s [Design test and evaluation guide (DTEG) 8.2]. As the moving airstream surrounding the rocket accelerates, the CP shifts downwards, while the CG naturally shifts upwards until burnoff due to loss of fuel mass.

The CG was estimated by using Eq 4 for every rocket component, and its corresponding weight and distance from nose tip [Appendix V.A]. The distances were retrieved from Catia 3D.

$$CG \cdot W_t = \sum_{n=i}^n w_i \cdot m_i \quad (4)$$

The CP placement was predicted using three software programs.

- 1) RASAero II
- 2) OpenRocket
- 3) AnsysFluentCFD

The method for analysing the stability margin at different Mach numbers was combining the CG values from OpenRocket with CP values from RASAero and CFD into Eq 3. The CFD simulations are described in the next section. RASAero provides two methods for predicting the CP placement:

- Roger Modified Barrowman (RMB) approximation.
- Regular Barrowman approximation.

RASAero's user manual states that the regular barrowman approximation is a decent choice for the subsonic regime, although for the transonic and supersonic velocities the modified barrowman handles the effects of the rocket's geometry better. This includes the effects of the fin sweep angle, nose cone shape and fin airfoil. Also it is a better choice for approximating parasitic drag and the corresponding CP placement [2].

Table 4 presents the criteria for instability and overstability set by EuRoC [DTEG 8.3 - 8.4]. The lower limit for desired stability is also set by EuRoC, while the upper limit for desired stability is recommended by a member of the Tripoli Rocket Association with a certified level 3, Arve Tokheim, based on his own experiences [3].

Table 4: Requirements for a stable flight.

Criterias	SM [cal]
Unstable	$SM < 1.5$
Desired stability	$2.0 < SM < 4.75$
Overstable	$6.0 < SM$

Figure 8 and Table 5 summarize the results from the stability analysis. Uncertainties related to these results are discussed in Appendix V.G. SM provided by OpenRocket and RASAero is within a desirable range during most of the flight. CFD predicts a desired SM up to the velocity Mach 1.2. Greater velocity results in a marginally overstable flight, but this is still acceptable. Based on comparison between all three simulation methods and the discussion around uncertainties, the risk of an unstable flight is considered to be low [Appendix V.D].

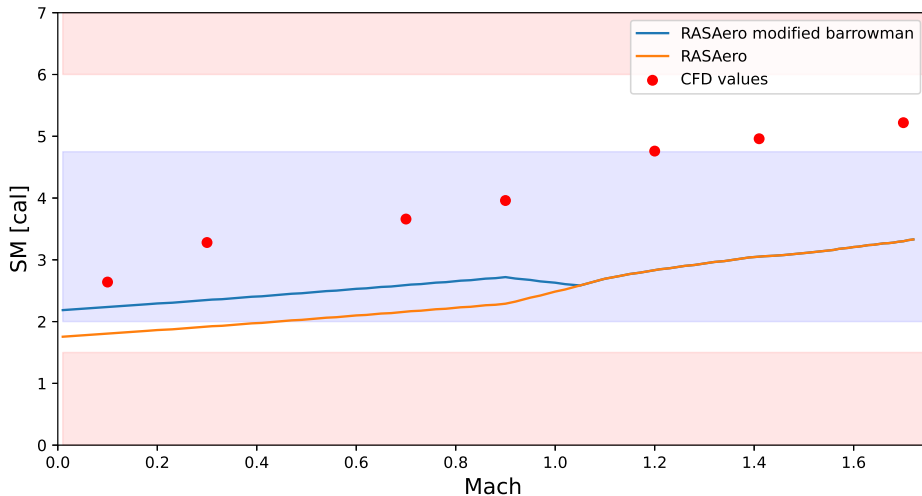


Fig. 8 Comparing stability results from RASAero and CFD analysis. Blue area is the desired range and the red areas is the unstable range

Table 5: Green indicates a SM desirable interval shown in Table 4. The yellow values are not nominal but acceptable.

	Minimum SM [cal]	Maximum SM [cal]
OpenRocket	2.02	5.13
RASAero	1.90	3.94
RASAero RMB	2.29	3.94
ANSYS Fluent CFD	2.59	5.65

Computational Fluid Dynamics

A total number of 16 simulations have been made on the final rocket, ranging from incompressible flow to supersonic speeds. For each region of interest, which is $M \in \{0.1, 0.3, 0.7, 0.9, 1.2, 1.41, 1.73\}$, simulations for $\alpha = 0^\circ$ and $\alpha = 2^\circ$ have been derived. Additional simulations for $\alpha = 5^\circ$ and $\alpha = 7^\circ$ have been made at MaxQ to capture the maximum dynamic load the rocket will experience.

AoA at 0° was selected as this will simulate nominal flight, where 2° AoA was selected due to comparison with data from RASAero II. Furthermore, in cooperation with a simulation specialist within outer ballistic at Nammo, AoA at 5° was selected as an intermediate critical case, whereas 7° was selected as the highest critical case expected during flight [4][5].

From an aerodynamic aspect, features that have been analysed are:

- Shock wave propagation and Mach angles
- Pressure distribution
- Thermal effects
- Turbulence intensity and boundary layer

Assumptions, observations and critical results are highlighted in this section. Here, starting with the findings on velocity field and shock wave propagation, followed up by a presentation of the static pressure distribution and thermal evaluation. See Appendix V.G for a detailed outline, as well as an in depth discussion of all results regarding the elements presented above.

Shock wave propagation and Mach angles

As the rocket reaches the transonic region (Mach 0.8 to 1.2), the fins upper and -leading edge (LE), as well as the area around the nose cone's transition, will experience a local critical Mach number ($M_{cr} \geq 1$). This is shown in Figure 9 by the dark green color region. Above the fin it was measured to be Mach 1.13, and at the nose cone transition it was measured to be just above Mach 1.02. This results in small shock wave fluctuations which will increase drag. However, unfortunately these shock waves were not observed, due to difficulty in numerical simulations, which is common for these types of phenomena [6]. No simulations have been done at Mach 1 because these simulations would be numerically unstable.

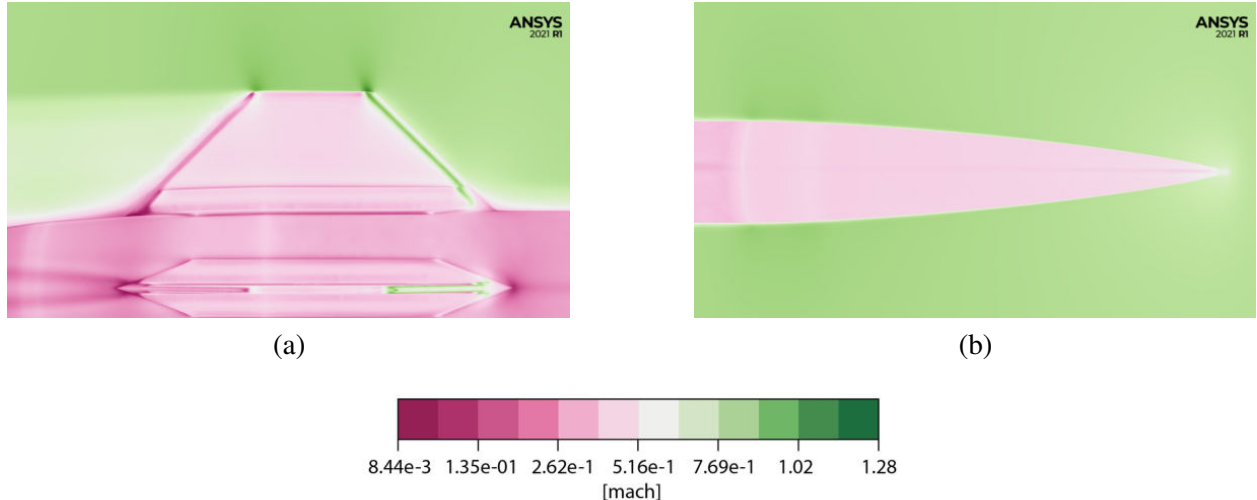


Fig. 9 Green scale contour of super critical flow. a) Shows the critical Mach number at the fins. b) Shows critical Mach number at nose cone transition. Results derived from Mach 0.9, zero AoA.

Between Mach 1 and MaxQ, the Mach angle is expected to decrease with increasing Mach number [7]. This can be observed by comparing the contours from simulations made in the supersonic region, which can be seen in Appendix V.G.

In Figure 10, oblique shock waves can be observed propagating from the nose tip. Additional Prantl-Meyer expansion fans can be observed both at the nose cone transition, the LE tip of the fins, and at the von Kármán transition at the back. This validates the simulation results, as these results reflect physical behavior.

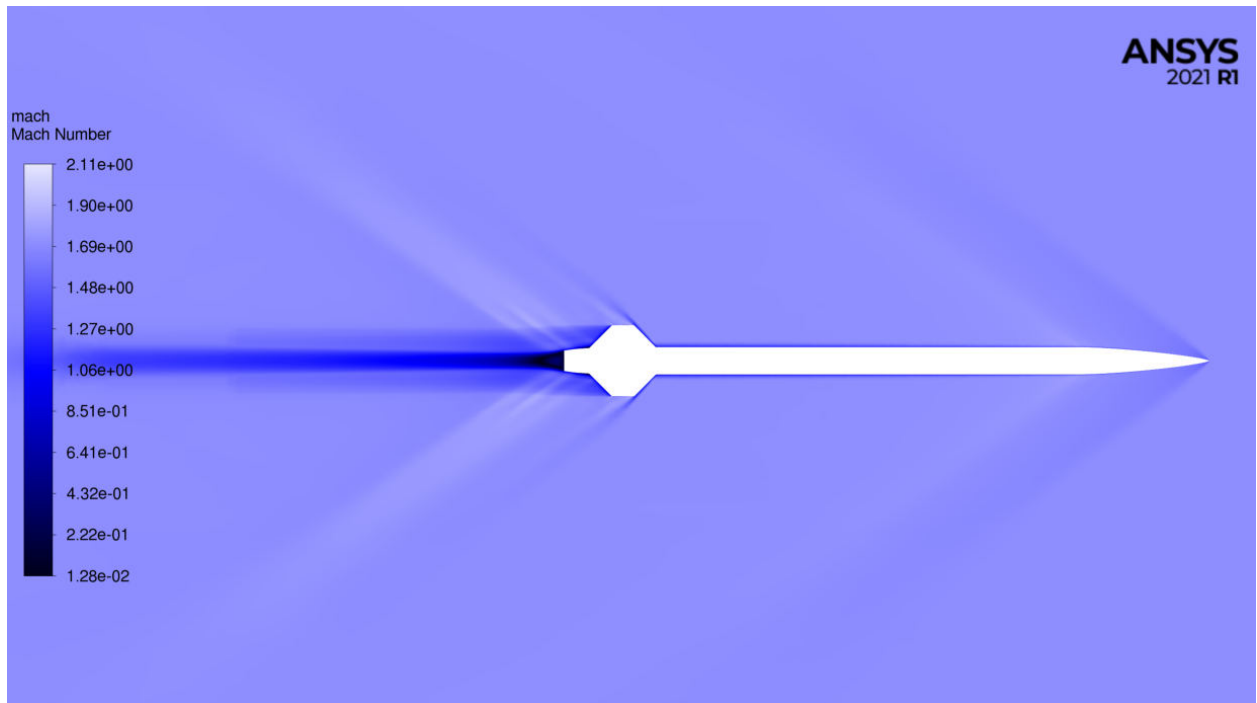


Fig. 10 Mach contour simulated at Mach 1.73 with = 0°

Pressure distribution and thermal effects

A stagnation pressure point at the nose cone can be observed in Figure 11 a), and a high pressure distribution along the LE of the fins can be seen in Figure 11 b). These results reflect physical behavior as the pressure is expected to increase as the velocity field decreases [7]. The highest temperature readings are expected to be at the stagnation point on the nose cone. This observation can be seen by the yellow contour at the side and at the nose tip in Figure 11 c). The high temperature at the side of the fins is due to the particular AoA chosen (7 degrees AoA). Even higher temperatures have been measured along the LE of the fins, reading 174 Celsius shown by the red contour from Figure 11 d).

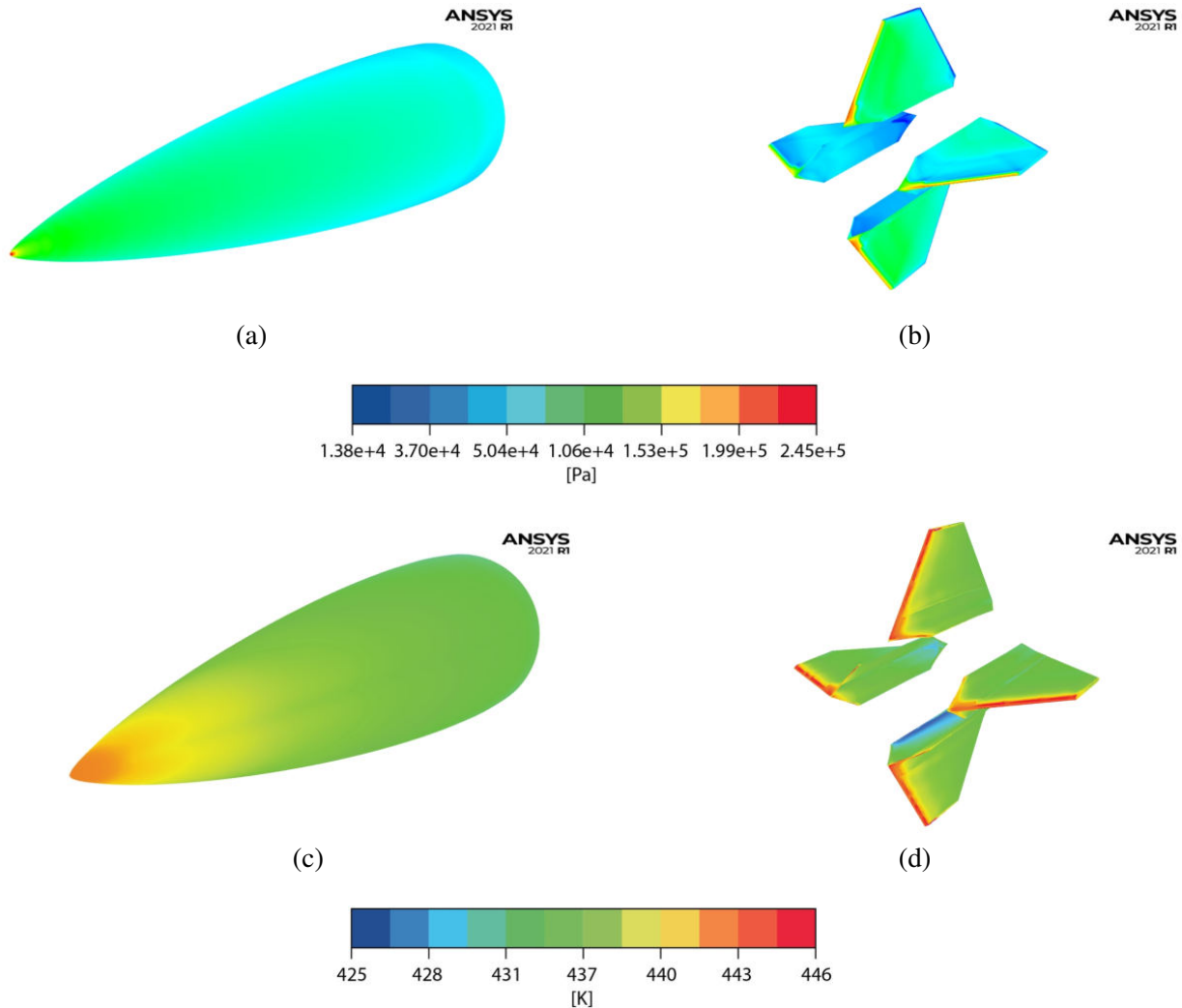


Fig. 11 a) Static pressure contour of nose cone. b) Static pressure distribution on the fins. In the colorbar, dark blue represents 0.0138 MPa, and increases towards 0.245 MPa represented by the dark red color. c) Wall temperature distribution on nose cone. d) Wall temperature distribution on the fins. Results from Mach 1.73 with AoA = 7°. In the colorbar, dark blue represents 152 degrees Celsius, and increases towards 173 degrees Celsius represented by the dark red color.

3. Design

Airframe overview

The function of the airframe is to provide an aerodynamic shell, and accommodate fastening points for the inner structure in the rocket. Fastening mechanisms between the airframe and inner structure are described in Section II. E Inner structure. In order to reduce complexity, the airframe consists of two parts, the forward airframe (OU.FA) and the aft airframe (OU.AA). Additional aerodynamic components are the nose tip, couplers and boattail, discussed in Section II. E. 2.Threaded rods, 3. Coupler system and 4. Aft end, respectively.

Airframe design

A minimum body diameter is desirable due to the dependency between drag and the cross sectional area of the rocket; an increase in diameter results in increased drag [8]. The lower limit for the diameter is bounded by the size of the Pressure Based Separation System [Appendix V.H S4.3.3]. The OD is therefore set to 128 mm. The nose cone shape is von Karman in the Haack series because the Haack series is shown to reduce drag the most. Open rocket simulations give us close to Mach 2 as shown in Section II.C.2 Max Q/Mach number, which is where the von Karman shape is optimal [9]. The nose cone should be as long as possible, in order to minimize shear stress and the generation of expansion waves, but also be reasonable to manufacture. A axial length of 600mm is therefore selected as a compromise between the two. See Appendix V.G for more details on aerodynamics for the nose cone. The forward airframe will be coated in silver lacquer in order to avoid overheating the inner components. See Appendix V.I, *Choosing color of forward airframe*, for calculations on the heat transfer.

Validation airframe

Load evaluation

Table 6 summarizes data retrieved from CFD. The forces and moment presented should be used to study the possibility of excessive high tear-out stresses, however, due to limited timeframe, no further evaluation was made.

Table 6: Data retrieved from CFD at Max Q (Mach 1.73) with 7 degrees AoA

Parameters	Direction	Value [min, max]	Units	Comments
Total Force	X	213	N	Pressure force 23% Viscous force 77%
	Y	816	N	Pressure force 98% Viscous force 2%
	Z	1285	N	Pressure force 99% Viscous force 1%
	Total	1336	N	Pressure force 92% Viscous force 8%
Moment	Z Pitch	923	Nm	Moment about CG
Temperature	-	[151, 169]	°C	

Frequency analysis

The possibility of the rocket vibrating at its eigenfrequency is a potential hazard during launch which may lead to fractures in the airframe and inner components [Appendix V.D]. A frequency analysis was therefore

conducted to validate the structure holistically. This analysis is seen in Appendix V.I, *Eigenfrequency*. The result was an eigenfrequency of 56.9Hz for the first mode in frequency analysis [10]. An estimate for the highest value for what the rocket might experience during flight is considered to be 30Hz according to the Kongsberg group [11][12]. Therefore, it is sought to have the rocket's eigenfrequency well above 30Hz. However, bonded connection has been used in some areas in the analysis. This is probably not realistic, and leads to a large uncertainty around the frequency analysis result.

Two actions have been made based on the findings from the frequency analysis:

- 1) Not reducing the wall thickness of the airframe further than 2 mm , as this results in a high eigenfrequency.
- 2) To increase the stiffness, and thereby the eigenfrequency, loctite have been used on all bolted connections. All bolted connections will also be pre-strained.

Airframe manufacturing

The airframe is manufactured using filament winding. The process is as follows:

Table 7: Manufacturing strategy

Before winding	Winding	After winding
<ul style="list-style-type: none"> • Polish Mandrel • Insert o-rings • Apply release agent 	<ul style="list-style-type: none"> • Wind pre impregnated fiber in desired layup • Wind shrinking peel ply around forward airframe • Wind shrink tape around aft airframe 	<ul style="list-style-type: none"> • Cure between 99 and 121°C • Apply heat resistant lacquer to the forward airframe • Sand aft airframe • Apply clear lacquer to both airframe parts to ensure a smooth surface

Due to the requirement from avionics [Appendix V.H S4.3.1], the forward airframe is chosen to be made out of 758 ZenTron glass fiber. The aft airframe on the other hand, is made out of Toray T700S carbon fiber due to its high strength to weight ratio, and also its high stiffness. The epoxy system for both frames are UF3369 TCR resin. These were chosen due to their availability at the winding company. The fiber layup of choice is based on rules of thumb from “Structural Materials Handbook” and resulted in -5/+5/+45/-45/-85/+85/+45/-45 [13]. See Appendix V.J for more details on this.

Fin overview

The overall function of the fins is to provide aerodynamic stability to maintain a safe straight trajectory from leaving the launch rail, and till reaching apogee. The shape of the fin is selected to move CP towards the motor end of the rocket to maintain sufficient stability through flight.

Fin design

When choosing fin design, a balance has to remain between the following factors:

- Large area at the aft end of the rocket in order to move the CP further down
- Protection against breakage when the rocket hits the ground
- Strong attachment to the rocket body
- Drag reduction
- Fin stiffness
- Weight

The chosen fin shape is a symmetric trapezoid with a sweep angle of $\Lambda = 45^\circ$, and there are in total 4 fins. The selected wedge angle is 40° , as it results in a lower drag coefficient within the expected Mach region [14]. The selected fin contour reduces the chance of breakage when the rocket hits the ground. Additionally, the root of the fin is considerably longer than the tip, as it absorbs most of the aerodynamic loads and results in stronger attachment to the rocket at the fins base. In Figure 10, one can observe that the oblique shock-wave angle, β , is smaller than the complementary angle to the fins sweep angle², which leads to higher wave drag [15]. However, since a larger sweep angle will lead to less drag on the fins, the CP will not be sufficiently moved towards the motor end, and possibly lead to understability. Having 4 fins also moves CP sufficiently towards the motor end. The fins are illustrated in Figure 1 in Section II.A.Systems overview.

Validation fins

Data retrieved from CFD, shown in Table 8, are used to validate the fins through FEA analysis in ANSYS Mechanical. “Epoxy Carbon Woven (230 GPa) Prepreg” from ANSYS Engineering Database was used in the simulation. The results of the FEA analysis of the fins are shown in Table 9.

It is expected that some amount of the kinetic energy due to perturbation in the flow field, is transferred into momentum as the rocket angles itself into the freestream. However, as the transfer rate is unknown, the total force in the Y direction has been used to deform the fin to derive conservative estimations. In Figure 12, the highest calculated stress value are observed near the centered hole, with a value of 146 MPa. This value is expected due to stress concentrations around the holes. Comparing max stress value obtained with tensile stress limit (805 MPa) yields a safety factor of 5.5. This is well above the required safety factor of 2 and thus the fins are able to handle the stresses of the flight. The deformation of 11.3 mm is non-critical as a less load on the fins is expected. The validation of fin brackets are discussed in Section II.D.3.Validation fin brackets.

Table 8: Data retrieved from CFD at Max Q (Mach 1.73) with 7° AoA

Parameters	Value [min, max]	Units
Total force	1150	N
Moment	35.7	Nm
Temperature	[151, 174]	°C

Table 9: Data from FEA in ANSYS Mechanical with input force from CFD at Max Q with AoA = 7°

Critical factors	Value	Units
Input force, normal to surface	1150	N
Deformation at upper edge	11.3	mm
von Mises Stress	146	MPa
Stiffness factor	101.8	N/mm
Safety factor	5.5	nd

² Oblique shock-wave angle is the angle between the shock wave and the upstream flow direction, while the sweep angle is the angle between the fin's leading edge and the vertical plane [7]

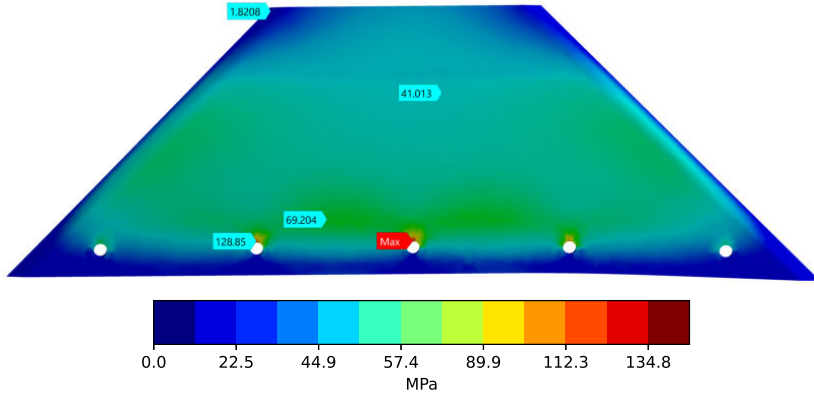


Fig. 12 von Mises Equivalent stress [MPa] analysis on the fins at Mach 1.73 with 7° AoA and force at 1150 N

Fin fluttering

The flutter velocity can be modeled using approximations for pressure, temperature and the boundary flutter condition. The complete calculation can be found in Appendix V.I, *Fin fluttering*. The fin material shear modulus (G) is within the range (3.5 - 5) GPa. From here a simulation can be made using the altitude values from an OpenRocket simulation. By comparing the velocity profile and the flutter velocity as a function of the rocket's altitude, we can predict whether the fins will flutter or not.

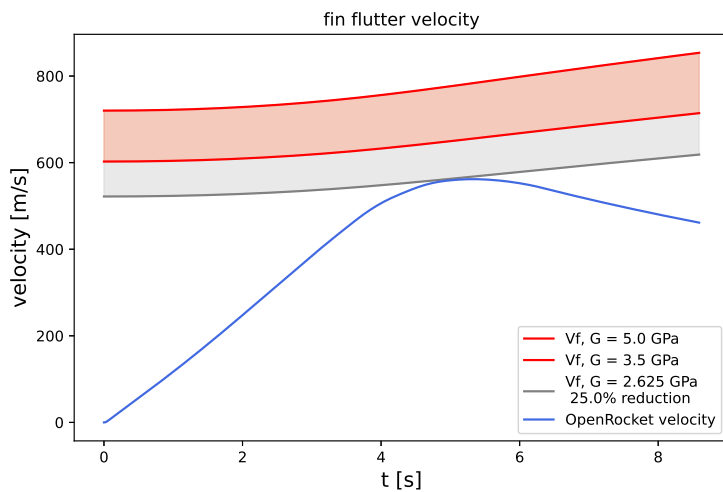


Fig. 13 Plot comparing the flutter velocity (vf) at altitude and the OpenRocket velocity profile

As seen in Figure 13, the OpenRocket velocity is far from the flutter velocity at the maximum velocity (red area). CFD analysis shows that an expected high frictional heating can result in a reduction of the shear modulus. Thereby, analysis shows that a 25% reduction can lead to fin fluttering, as seen at the bottom grey line in Fig 13. However, the time interval during the heating is short, so the inner temperature of the material is not expected to rise substantially before the airstream decelerates. A heat resisting spray can help to ensure that the shear modulus reduction does not exceed the 25% threshold.

Fin manufacturing

The fins are CNC-machined out of 4.76mm thick quasi-isotropic solid carbon fibre sheets. These sheets are carbon reinforced epoxy matrices composed of multiple layers of woven carbon fibre fabric without core material. The fins will have a high stiffness due to properties of carbon fiber as mentioned in Section II.D.3.Airframe manufacturing, and a high number of layers with symmetrical lay-ups of 0/90 and +45° fabric. The manufacturer's profile- and chamfer tolerance equals 0.254 mm and 0.381 mm respectively, which are considered to be non-critical. To increase safety against overheating and reduction in yield strength for the carbon fiber, a thermal coating will be applied to all four fin areas.

Fin brackets overview

The fin brackets is the fastening mechanism between the fins and the aft airframe. In Figure 1 in Section II.A.Systems overview, one can see the fin bracket alongside the root chord.

Validation fin brackets

It is expected that a significant portion of the normal force resulting from the transverse flow will be transformed into momentum, and not deformation of the fins, fin brackets and the rocket body. A static analysis, such as the one presented above, assumes that the entire force value will be transferred from the fins to the fin bracket, leading to substantial stress levels. Furthermore, AoA of 7° is far larger than what is expected at Mach 1.7. Due to these factors, the calculated stress value is expected to be much larger than the actual stress value in the bracket. Thus, the intention of showing this analysis is that the stress on the fin bracket is definitely smaller than the stress derived from the analysis.

Using 1150 N load from CFD simulations, the highest calculated stress level is 272.7 MPa, located in one of the hole cavities of the bracket, as shown in Figure 14. The result is expected due to stress concentration, however, the area marked by the label "Max" is considered small, where a plastic deformation at this point would not affect the brackets operating condition. Furthermore, the highest calculated stress value in the green-yellow region is 189.5 MPa. According to the producer of aluminum 6082-T6 [16], the expected tensile yield strength is 260 MPa. The conclusion from this analysis is therefore set to be non-critical as fundamental parts of the bracket calculate a tensile stress value within the given tensile stress limit.

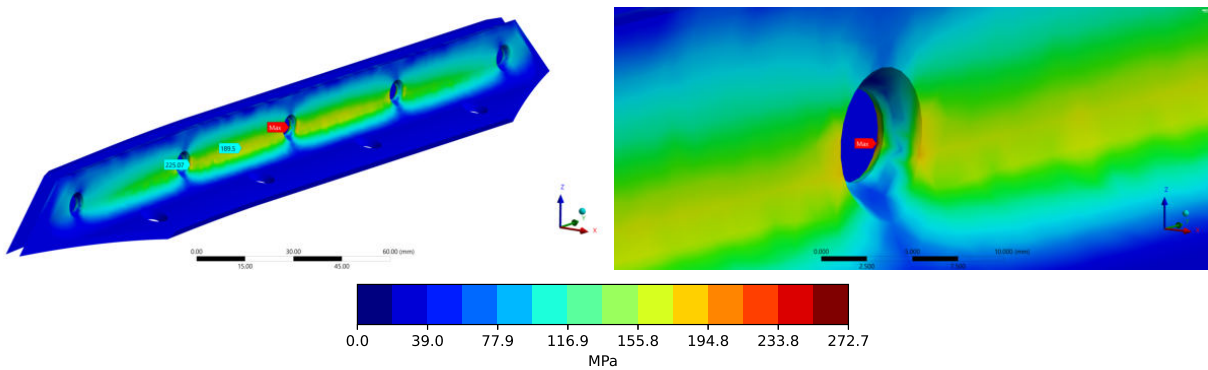


Fig. 14 von Mises equivalent stress [MPa] analysis on the brackets at Mach 1.73 with 7 degrees AoA and force load of 1150 N.

Fin bracket manufacturing

Since the fin brackets have a double curved surface in order to fit the von Karman shape of the aft airframe, CNC machining is needed for manufacturing. The brackets are glued and bolted with a brass washer on the

inside of the airframe in order to distribute the forces as evenly as possible. The fins themselves are detached from the brackets by unscrewing the five barrel nuts that clamp the brackets against the fins.

E. Inner structure

1. System function and system overview

The function of the inner structure is to establish a structurally reliable and reusable way of organizing and fitting the inner systems of the rocket.

Overview of subsystems

Inner structure consists mainly of three subsystems:

- The threaded steel rods supporting the nose tip, avionics, recovery and payload infrastructure
- The coupler section which includes the motor mount (IC.MM) and the recovery plate (RR.RP)
- The aft end, which includes motor centering ring (IAE.MCR) and a boat tail assembly

Out of these components, the couplers (IC.UC + IC.LC) are the ones experiencing the highest loads and are the most critical parts of the system. Figure 15 shows the inner structure without the airframe.

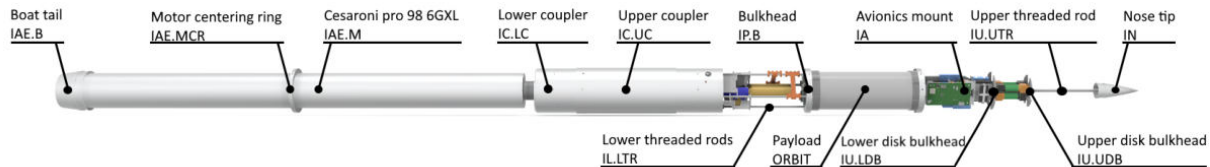


Fig. 15 The rocket components

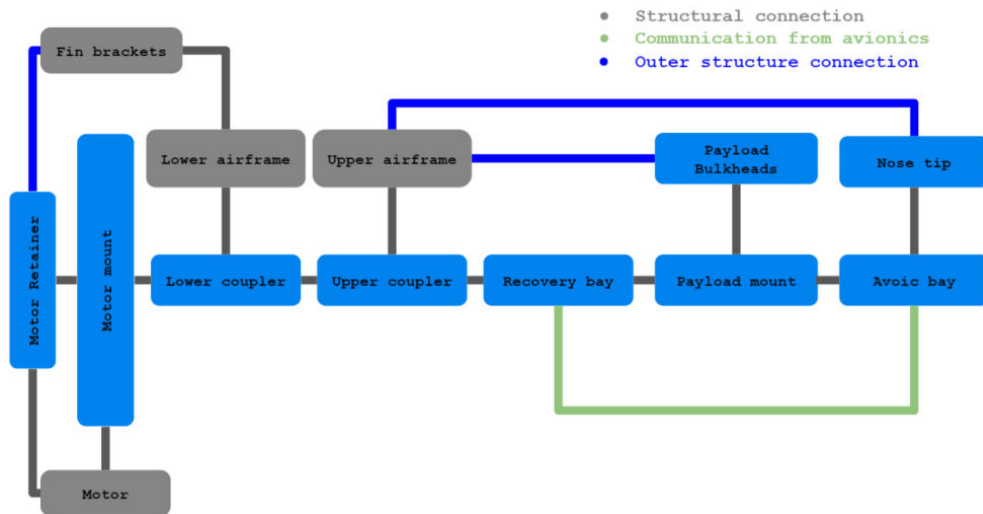


Fig. 16 Connections between the different component groups

Validation

Several FEA and two integration tests have been conducted. The FEA results are seen in Table 11. The integration tests have utilized 3D-printed parts and laser cut medium density fiberboard on the two first tests.

Table 10: Function diagram

Part	Reference	Manufacturing method	Validation method	Functions				
				Load bearing	Mounting point	Resist vibrations	Reduce drag	Ease of assembly
Nose tip	IN.	Turning	Integration test		Upper threaded rod			
Upper threaded rod	IU.UTR	COTS	Integration test, calculation		Avionics mount, battery holder			
Disk bulkheads	IU.UDB, IU.LDB	Milling	Integration test					
Battery holder	IU.BH	COTS	Integration test		Batteries			
Avionics mount	IA.	Water cut	Integration test, FEA		Avionics			
Bulkhead and bulkhead ring	IP.B, IP.BR	Turning	Integration test		Payload, lower threaded rods			
Lower threaded rods	IL.LTR	COTS	Integration test, calculations		Cameras, hawk system			
Couplers and motor mount	IC.	Turning and welding	Integration test, FEA		Motor, airframe, recovery plate			
Motor centering ring	IAE.MCR	Turning	Integration test					
Boat tail	IAE.B+	Turning	Integration test		Motor, airframe			
Recovery plate	RM.RP.	Turning	Integration test, FEA		Lower threaded rods			
Camera mount	IL.CM, IL.CP	Water cutting, bending	Integration test		Cameras			

A third integration test is planned after all parts have been produced. These tests ensure that the parts fit as intended and that the assembly process is not only possible, but also practical. The full test reports are included in Appendix V.B *Integration test 1 & 2*.

Table 11: FEA results

Part	Reference	Experienced stress [MPa]	Material yield strength [MPa]	FoS
Upper coupler and lower coupler	IC.UC, IC.LC	556	250	4.48
Motor mount (5 mm)	IC.LC IC.MMS IC:MMP	113	130/230 (not heat-treated/heated)	1.15/2.05
Motor mount (8 mm)	IC.LC IC.MMS IC:MMP	49	130/230 (not heat-treated/heated)	2.68/5.68

2. Threaded rods

Function

The inner structure works by utilizing two skeleton-like structures to mount the inner components of the rocket and distribute the forces throughout the rocket, see Figure 17 below. The premise of the threaded rod system is to mount all the components to the threaded rods using mounting structures. Nuts are fastened on each side of the mounts, to hinder them from moving up and down the rods. After all systems have been mounted, the threaded rods are fastened to their corresponding bulkheads (IP.B), which functions as adapters and structure between the threaded rods, payload and the airframe. In addition the bulkheads are designed asymmetrical to guarantee hole alignment. This modular mounting scheme aims to achieve an efficient and simple assembly process.



Fig. 17 Threaded rod subsystem fully assembled

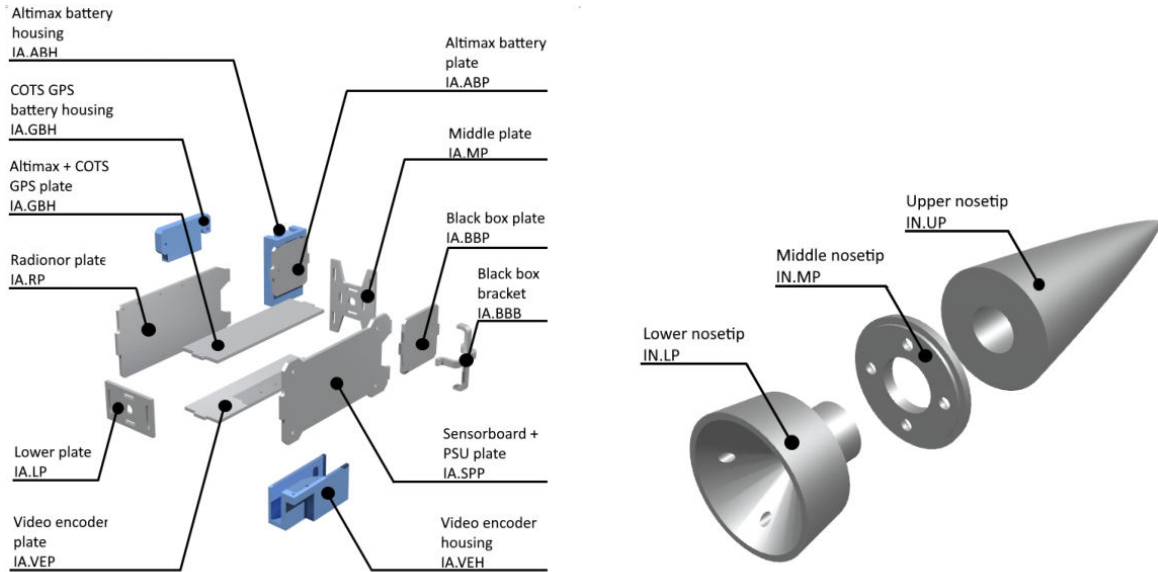


Fig. 18 Exploded view of Upper threaded rod sub-assembly and nosetip

Upper threaded rods design

The upper threaded rod (IU.UTR) is a M8 steel rod aligned with the tip of the rocket (Figure 18). The avionics mount and disk bulkheads are mounted to the rod, and are made out of fibreglass to reduce interference with the avionic components. The avionics mount is held in place by one M8 nut on each side of the mount. This design results in modular and easy assembly/disassembly of the rocket's avionics. The upper and lower disk bulkheads (IU.UDB + IU.LDB) are mounted on the rod to reduce vibrations. By adding contact points between the forward airframe (OU.FA) and the threaded rod, the unsupported length of the rod is reduced, resulting in an increased eigenfrequency [Appendix V.I, *Eigenfrequency*]. These designs were chosen as they are easy to assemble and manufacture, but also provide vibration damping for the components while maintaining the system requirements[Appendix V.H].

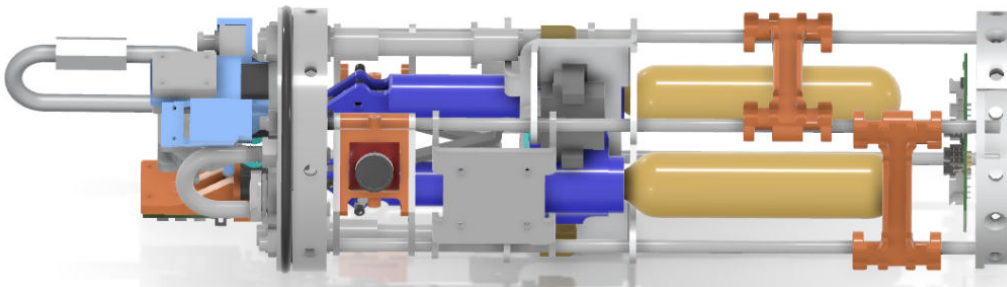


Fig. 19 Lower threaded rods

Design lower threaded rods

The lower threaded rods are four M6 steel rods (IL.LTR) placed with equal distance to the center axis of the rocket (19). The system is connected to the lower bulkhead (IP.B) on one end and the recovery plate (RP.RP) at the opposite end. This subsystem is designed to fit cameras (A.C1, A.C2, A.C3), the main sensor board (A.MB) for the avionics, hawks for the recovery system, and their respective mounts. It is also designed to have enough space to swap the CO_2 canisters (RH.CO2) when this subsystem is fully assembled. The camera mount (IL.CM) on the threaded rod is designed to have the cameras be flushed with the airframe to minimize the drag induced by the camera protrusion. Additionally, the recovery plate (RR.RP) is designed to be a mounting point for the Mainchute release system (MCRS) system, while also being airtight to maintain pressure inside the couplers.

Manufacture decisions

Sheet metals are suitable for the mounts, as the mounting points are not load bearing structures. They are simple and lightweight while also being relatively inexpensive to manufacture. The recovery plate and bulkheads will be machined as they are subjected to more forces, so they need increased thickness in addition to having more complex shapes.

Validation strategy

The validation strategy consists of integration tests, and calculations on buckling and strength of the rods. The three integration tests assure that the components mounted to the rods fit as intended. The tests have resulted in changes to the bulkheads, lower threaded rods and camera mount mainly in terms of proper fitting or not having enough space to assemble the system. The findings and solutions can be found in Appendix V.B, *Integration test 1 & 2*.

The calculations are done on the lower threaded rods and are seen in Appendix V.I, *Lower threaded rods*. These calculations are very conservative, but only show a stress of $108.8MPa$. This means that the rods have no problem withstanding the loads from impact, which is higher than both main and drogue chute deployment forces.

3. Coupler section

Function

The functions of the coupler sub-system are listed below. The subsystem consists of the upper coupler (IC.UC), the lower coupler (IC.LC) and the motor mount (IC.MM), as shown in Figure 20.

- Main function: Split the rocket in two halves, enabling drogue and parachute deployment (Section II.F.2).
- Structural: Enable rigid connection between the two halves of the rocket in accordance with requirement from EuRoc [DTEG 6.2.3. Implementing Coupling Tubes].
- Airtight: Keep coupler section housing parachutes airtight by using an O-ring.

Upper coupler design

The upper coupler (IC.UC) is designed such that it allows the forward airframe (OU.FA) to slide over the outside of the upper end, and the lower coupler (IC.LC) can slide into it on the lower end (Figure 20). It also has 20 holes for hawk arming, camera and mounting, see Figure 20.

Lower coupler and motor mount design

The lower coupler and motor mount (IC.MM) consist of three parts in total being welded together. The lower end of the lower coupler is glued and screwed together with the aft airframe (OU.AA). There is also

a groove allowing for mounting an O-ring, and 8 holes for the shear screws on the upper half of the lower coupler, where it overlaps with the upper coupler. The O-ring keeps the coupler section airtight to guarantee the separation of the rocket when pressurized by the hawk system.

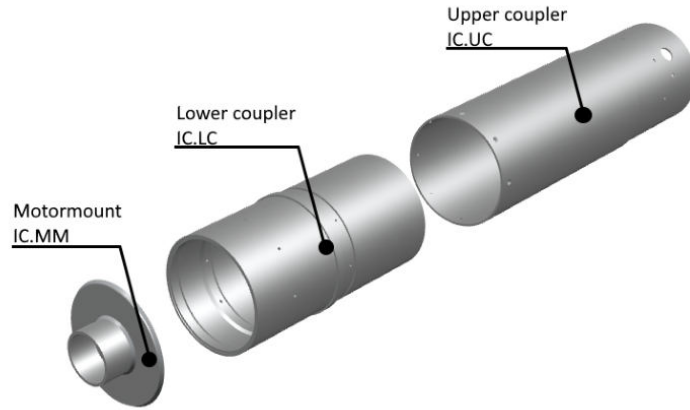


Fig. 20 Exploded view of Coupler section.

Validation strategy

The validation strategy consists of a decoupling test that has been conducted using the hawk system and shear screws on the ground. FEA have also been done on the couplers and on the motor mount. The ground test showed that the couplers had no problems with breaking the shear screws and separating when pressurized. Further details can be seen in the full report [Appendix V.B *Ground test - Rocket separation*].

Validation Coupler section

Both couplers are analyzed in SolidWorks using the motor force and the maximum aerodynamic forces with an AoA of 7° . The analysis resulted in high safety factors, with the upper coupler having the lowest safety factor of 4.48 (Figure 21). This is well above the required safety factor of 2 and thus be able to handle the stresses of the flight.

The decoupling test showed that the couplers had no problems separating when pressurized. The full test is seen in Appendix V.B. In addition to a friction test, the coupler system has also been fitted into the rocket by performing multiple integration tests. This was to ensure the placement and fitting of the couplers and the coupler holes.

Validation Motor mount

FEA was done using the motor force of 4750 N on a 8 mm and a 5 mm thick version of the motor mount to verify our requirements in terms of minimum weight and safety factor. The resulting safety factors were 2.05 for the 5 mm version and 4.54 for the 8 mm version. As a factor of safety of 2 is deemed necessary for this component the 5 mm version is adequate after heat treatment and is therefore selected to minimize weight. The full analysis is given in Appendix V.I, *Motor mount*.

Manufacturing decisions

As the couplers and motor mount are circularly symmetric they are suited for turning. To minimize the amount of material and time needed to produce the couplers, a $130\times10\text{ mm}$ pipe was used. Both couplers, as well as the motor mount, will be machined out of 6082-T6 aluminium. The motor mount is produced in two

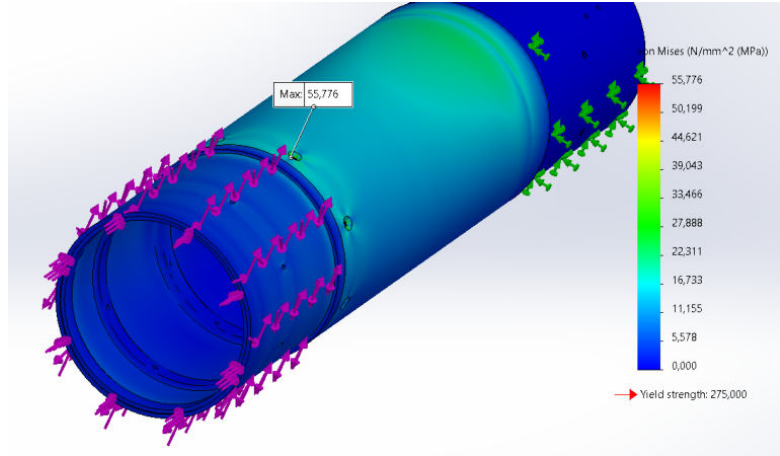


Fig. 21 FEA on the coupler section. The results show a max stress of 55.8 MPa at the holes.

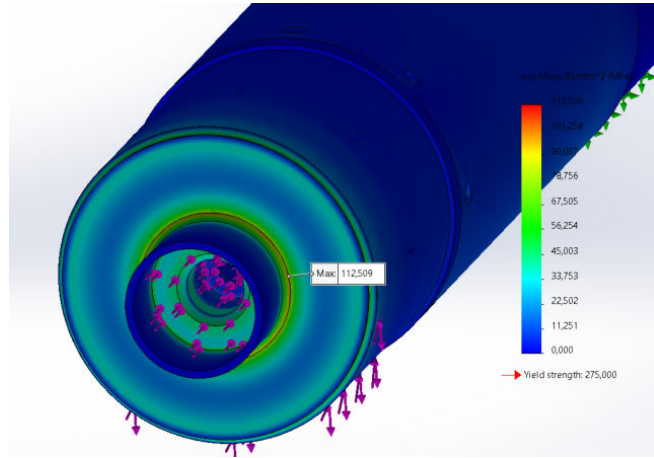


Fig. 22 Stresses from motor force on 5 mm motor mount. The max stress is 113 MPa and is seen in red.

parts that are welded together, and then welded to the lower coupler. The reason for this was to save material, as machining it in one piece would waste most of the billet and would take a long time. By welding the two parts together the strength of the material is somewhat reduced, but by heat treating the aluminium the T6 properties can be almost completely restored.

4. Aft end

Function

The functions of the aft end subsystem are listed below. The subsystem consists of the motor centering ring (IAE.MCR) and the boat tail assembly comprised of the boat tail (IAE.B), the boat tail centering ring (IAE.BCR), and the wedge ring (IAE.BW), as shown in Figure 23 .

- Main function: Retain and center the motor within the rocket while also reducing the drag forces on the rocket during ascent. The latter is discussed in Section II.D.2 Aerodynamics.
- Motor centering ring: Keep the motor centered in the rocket by hindering significant radial movement.
- Boat tail: Reduce aerodynamic drag during flight by narrowing the rear end area in a smooth transition, and to withstand impact with the ground.

- Boat tail centering ring: Mounting point between the boat tail to the aft airframe (OL.AA).
- Wedge ring: Ensures a tight fit between the boat tail centering ring and aft airframe.

Together with the motor mount (IC.MM), the boat tail assembly ensures that the motor is safely mounted, by providing a fastening point for the bottom of the motor.

Design

The motor centering ring sits between the motor (IAE.M) and aft airframe, and is fastened permanently to the fuselage with adhesive and four screws (F.40). When the wedge ring is wedged between the aft airframe and the boat tail centering ring, all mentioned parts are secured together with four screws (F.42). The boat tail has a conical shape, with a tapering angle of 8° . It has threads that coincide with those in the boat tail centering ring. According to expertise from Nammo, a longer transition with low gradient for the boat tail will result in a decrease in wake generation. Nevertheless, the length of the boat tail is limited to 46 mm due to the short distance between the boat tail and the exhaust plume.

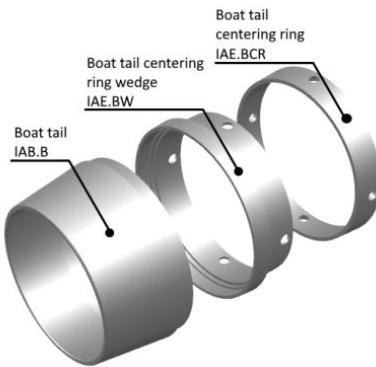


Fig. 23 Exploded view of boat tail assembly

Manufacturing decisions

The boat tail, boat tail centering ring and wedge ring are all designed to be circularly symmetric. This makes them suited for turning. The boat tail, wedge ring, boat tail centering ring and motor centering ring are made out of aluminium 6082-T6.

Validation strategy

For validation, the subsystem had to pass the third integration test. The test has not yet been conducted. The boattail has also been simulated when it impacts the ground. The results are seen in Appendix VI, *Boattail Impact Simulation*

F. Recovery

1. Overview recovery

The recovery system is a dual-event parachute recovery. The system features a drogue chute and a main chute. The drogue chute (RC.DC) will be deployed shortly after apogee using a pressure-based separation system (PBSS). While the main chute (RC.MC) is deployed at 450m above ground level (AGL) using a SRAD main chute release system (MCRS). Figure 24 shows the recovery setup inside the rocket.

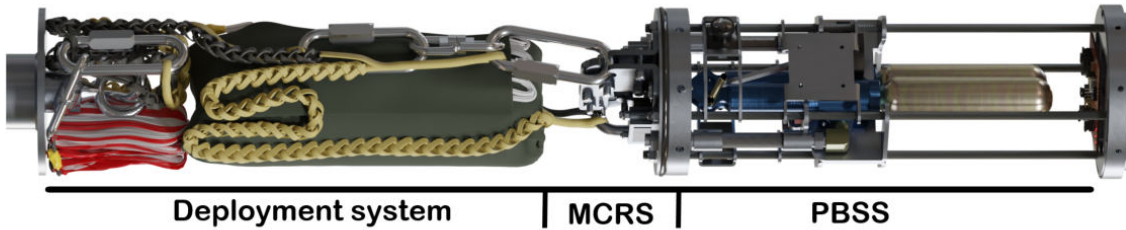


Fig. 24 Overview Recovery

Table 12: Function diagram

System	Manufacturing method	Validation method	Functions			
			Energetic device	Load bearing	Initial deployment	Final deployment
Pressure based separation system	COTS	Separation test, Ground test				
Main chute release system	Laser cut parts, sheet metal bending	FEA, MCRS-function test				
Deployment system	COTS	Hand calculations				

2. Pressure based separation system

The main function of the PBSS is to separate the rocket in order to deploy the drogue chute. The servo motor in the PBSS is activated when apogee is detected. The motor rotates the release arm that unleashes the piston. As a result, the CO₂-canister is punctured, and gas flows into the recovery bay. The force from the pressure breaks the shear screws that holds the couplers together, causing the rocket to separate, and the drogue chute is able to deploy.

The PBSS consists of a CO₂-canister (RH.CO2), a servo motor (RH.HSM) and a Hawk (RH.HB) which are mounted to an aluminium plate (RH.HP). The Hawk is a COTS-system and features a spring-loaded piston (RH.P) that is held in place by a release arm (RH.RA). This is shown in Figure 25. Note that a duplicate of the PBSS is also installed in the rocket to increase the reliability. Where one PBSS is connected to the COTS

flight computer and the other to the SRAD flight computer.

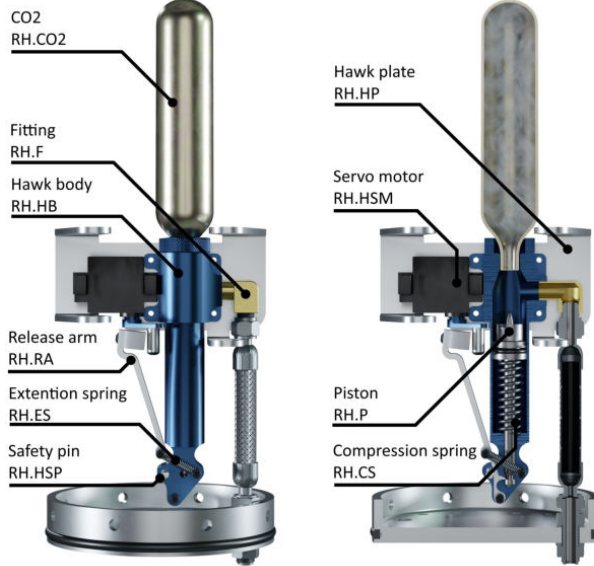


Fig. 25 Pressure based separation system

The Hawk is considered an energetic device once the spring is loaded. As stated in the rules from EuRoC, all energetics needs to comply with the energetics requirements [DTEG 4.1. *Stored-energy Devices - Energetic Device Safing and Arming*]. To accommodate this the Hawk features a safety pin (RH.HSP) that is installed once the system is loaded. The pin has a wire at its end, that is led through an opening in the airframe, Which allows the system to be armed externally at the launch pad.

Shear screws

The shear screws (F.14) function as a controlled structural weak point. The shear screws need to be dimensioned to break as intended when the PBSS is activated, but be strong enough to withstand the forces experienced during ascent and handling of the rocket. During ascent, the difference in drag on the aft and forward results in a shear force on the shear screws. This force is given by,

$$\Delta F_D = F_{D,aft} - F_{D,forward}. \quad (5)$$

At 7° AoA the maximum difference in the drag experienced by the rocket is found to be 26 N through CFD analysis [Appendix V.I *Drag difference aft and forward*].

Another force experienced is the pressure gradient at apogee. Assuming an airtight recovery chamber, there will be a pressure gradient of 0.75 kPa giving a total shear force of 845 N. The pressure gradient has been calculated using Van der Waals Equation,

$$P = \frac{RT}{V - b} - \frac{a}{V^2}. \quad (6)$$

See Appendix V.I *Pressure calculations* for detailed calculations. As a result the minimum force the shear screws must withstand is the force from the natural pressure gradient.

On the other hand, the shear screws can not be too strong, as this would prevent separation. The maximum strength as well as the amount of shear screws is therefore dependent on the type of CO_2 canister (RH.CO2) chosen. The selected combination is a 33 gram CO_2 canister and 8 M3x0.5 shear screws [Appendix V.I *shear screw calculations*]. The Van der Waals equation gives a pressure of 5.0 bar for this canister. Using the equation for stress,

$$\sigma = \frac{F}{A}, \quad (7)$$

and adding the natural pressure gradient to the pressure from the canister, a stress force of 6391 N is found [Appendix V.I *Pressure calculations*]. The resulting safety factors are presented in Table 13.

Table 13: Separation safety factors

CO_2 -canister size (gram)	ISO metric thread designation	Number of screws	FoS early separation	FoS intended separation
33	M3x0.5	8	3.27	2.11

O-rings

Two O-rings are used in order to seal the recovery bay and make it airtight. One O-ring is placed in the groove of the recovery plate (RR.RP), whereas the other O-ring is placed in the groove of the lower coupler (IC.LC). The selected O-rings are shown in Table 14 and detailed calculations can be found in Appendix V.I *O-ring calculations*.

Table 14: O-ring properties

O-ring load case	Dimension [mm]	Material	Temperature range [°C]
Static	110x4	EPDM	-50 to 150
Dynamic	107.62x2.62	EPDM	-50 to 150

Validation

Several tests have been conducted in order to validate the system. These tests include pressure tests and separation tests. The results from the tests are shown in the table below, while detailed test reports are presented in Appendix V.B.

Table 15: Test results

Pass criteria	Status	Reference
The shear pins can withstand a pressure force of 845 N equal to the expected pressure force at apogee (estimated to be 8771.3 m)	Pass	Appendix V.B <i>Pressure test 4</i>
The couplers are separated	Pass	Appendix V.B <i>Ground test - Rocket separation</i>
The drogue chute is deployed	Pass	Appendix V.B <i>Ground test - Rocket separation</i>

3. Deployment system

Parachutes

According to [DTEG 3.1.1. *Initial Deployment Event* and 3.1.2. *Main Deployment Event*], the descent rate for the drogue chute should be 23 - 46 m/s, while the main chute descent rate shall be below 9 m/s. The chosen parachutes are a 30" elliptical parachute and a Iris 96" compact parachute delivered by the company Fruity Chutes. The selection of parachutes is based on the drag force equation solved for velocity,

$$v = \sqrt{\frac{2mg}{\rho A C_D}}. \quad (8)$$

The resulting velocity for the drogue chute is estimated to be 24.16 m/s at 450 m, while the resulting velocity for the main chute is 5.87 m/s before ground impact. The velocity and altitude profile is shown in Figure 26. In addition, a self-imposed requirement was taken into account, which states that the highest release force shall be below 4 kN [Appendix V.H S2.1.2]. Using the drag force equation,

$$F_D = \frac{1}{2} \rho v^2 C_D A, \quad (9)$$

the maximum release force is found to be 3298 N from the main chute [Appendix V.I *Chute Calculations and Parachute Trajectory Simulations*].

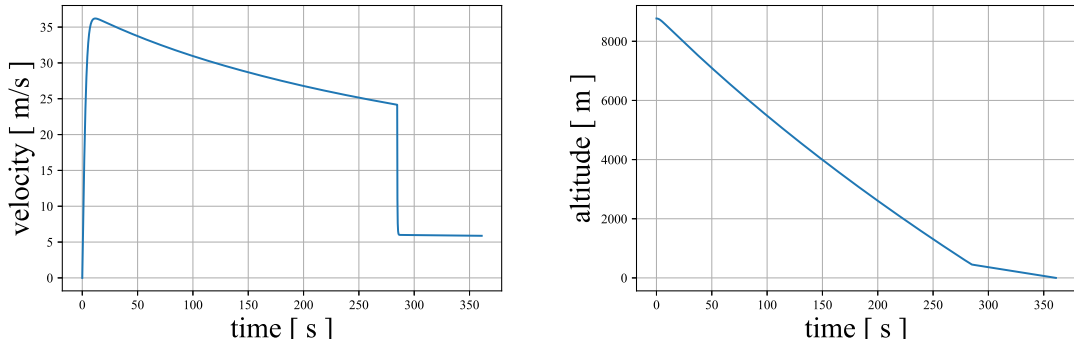


Fig. 26 Velocity and altitude profile when drogue is deployed at apogee and main chute is deployed at 450 m

Shock cords

The shock cord setup consists of a straight cord (RC.SCS) connected to the aft and drogue chute, and a Y-cord (RC.SCY) connected to the parachutes and the forward. This is illustrated in Figure 24.

The shock cord has several features in the deployment system. Its main purpose is to connect the fuselage to the parachutes and absorb the shock from the parachute's release force. Another function is to prevent zippering³. The amount of shock absorbed and the chance of zippering is dependent on the length of the shock cord. A longer shock cord corresponds to a lower chance of zippering. The straight shock cord has a total length of 12 m and each leg of the Y-shock cord has a length of 6 m. This conforms with apogee rocket's statement [17], that the shock cord connecting the aft and drogue chute should be three times the length of the rocket.

³ Zippering is known as the phenomenon when the shock cord rips the fuselage. This usually happens during initial deployment, when the rocket has a horizontal velocity, in which the shock cord is pulled along the airframe, ultimately leading to tearing due to friction forces.

Another risk is that the shock cord can snap when it is being pulled along the airframe. To mitigate this a surface extender (RC.SE) is installed at the cord where it is in contact with the airframe. This increases the contact area between the shock cord and the airframe, and therefore relieves the pressure on the cord.

The shock cord setup is designed in such a way that the aft and forward does not collide in mid-air. An additional effect of having the shock cord connecting the main chute and the aft as the longer one, is that the aft will hit the ground first. This will cause the forward, with the internal systems, to hit the ground with a velocity of 4.38 m/s [Appendix V.I *Parachute trajectory simulations*], and therefore increases the chance of securing sensor data from the flight.

4. Main chute release system

The MCRS is a mechanism with the primary function of deploying the main parachute. At 450 m altitude, the flight computer will activate the servo motor belonging to the MCRS. The motor rotates the release arms which results in deployment of the main chute. The MCRS features two servo motors (RM.SMO), an upper release arm (RM.URA) and a lower release arm (RM.LRA) that are mounted onto two steel plates (RM.MCRD). In addition a quick link (RC.QL), that is connected to a shock cord (RC.SCY) holding the main chute and the drogue chute, is locked between the upper release arm and the steel plates. This is shown in Figure 27. Note that there are two servo motors, where one is connected to the SRAD flight computer and the other to the COTS flight computer, making the system more reliable.



Fig. 27 MC RS overview (left), MC RS locked position (middle) and MC RS open position (right)

Another function of the MC RS is to be a fastening point between the forward and the drogue chute. When a load is applied to the system, rotation of the upper release arm is prevented by the lower release arm. A higher load implies that a higher force is needed to rotate the lower release arm in order to deploy the parachute. This reduces the risk of early deployment and allows it to function as a fastening point.

Another risk is that the system is not mechanically locked when no load is applied. Because of heavy vibrations during ascent, the release arm can vibrate out of its position. As a mitigation, two extension springs (RM.ES) are installed that connect the release arm to the main chute release docking.

The system is designed for easy manufacturing. The parts have been produced, with laser cutting

technology, from 6 mm and 4 mm steel plates of type S650MC. Then bending has been used to bend the main chute docking 90° to its wanted shape. Laser cutting is a highly automated process while bending is a simple manual operation, making the system easy to produce and cost effective.

The system has been verified using FEA. In order for the system to function properly it cannot experience any significant deformation. This could result in jamming of components and prevent the release of the main parachute. Therefore, the chosen material is a high strength steel, S650MC. The high strength results in the high safety factors that can be found in Table 16.

Recovery plate

The recovery plate (RR.RP) is the mounting plate for most of the recovery system. The plate consists of two holes to connect the hoses from the Hawk system (RH.GH), two holes for the U-bolt (RC.UB), one hole for the cable gland, one hole for each threaded rod and two holes for the MCRS. The recovery plate will be fastened to the fuselage from the outside with 8 M4 screws. Steel inserts are installed in these holes since steel threads are more durable than aluminium threads. Furthermore, the plate is designed to withstand a force of 2032 N from the main chute. This has been verified using FEA analysis [Appendix V.I *FEA on MCRS components and recovery plate*]. The results are shown in Table 16.

Table 16: FEA results

Part	Reference	Experienced stress [MPa]	Yield strength [MPa]	FoS	Deformation [mm]
Main chute docking	RM.MRD	62.8	650	10.3	0.804
Upper release arm	RM.URA	123	650	5.28	0.018
Lower release arm	RM.LRA	124	650	5.25	0.009
Recovery plate	RR.RP	92.4	270	2.92	0.009

To validate the system several tests have been conducted. These are described in more detail in Appendix V.B, while the results are presented in the following table.

Table 17: Test results (MCRS)

Pass criteria	Status	Reference
The system is able to release the main chute when under a load equal to the weight of the forward (123 N).	Pass	Appendix V.B <i>MCRS Pull Test</i>
The system is mechanically locked when a load is applied	Pass	Appendix V.B <i>MCRS Pull Test</i>

Note that a drop test from a helicopter has been conducted. The results from this test are still under evaluation and will be submitted before 4th of October.

5. Deployment forces

The forces experienced by the system during deployment have been calculated using Eq. (8). It is also assumed that the experienced force on the parachute is distributed differently to the aft and forward based on their weight [Appendix V.I *parachute trajectory calculations*]. The calculated results are presented in Table 18.

Table 18: Structural overview

Part	Reference	Deployment Stage	Experienced Load [N]	Rated maximum load [N]	FoS
Main chute	RC.MC	Main	3298	21356	6.48
U-bolt	RC.UB	Main	1834	4227	2.30
Drogue chute	RC.DC	Initial	1466	7828	5.34
Quick link	RC.QL	Initial	3298	9344	2.83
Swivel link	RC.SWL	Initial	3298	13349	4.05
Shock cord	RC.SC	Initial	3298	9789	2.97
Eye-bolt	RC.EB	Initial	1464	6376	4.36

G. Avionics

1. System overview

Function

The avionics system in the rocket is designed to perform two functions: the main function being to activate the recovery system; the secondary function being to safely store and transmit sensor data and display this live on the ground station.

The system is designed to make the main function reliable, keeping the design efficient and compact, without sacrificing functionality. The avionics system can be separated into two parts, COTS and SRAD. The main function is fulfilled by both a COTS and a SRAD system, which are completely independent. The SRAD system also fulfills the secondary function of storing sensor data on the rocket and transmitting it to the ground station. To fulfill the main function the SRAD system utilises a Finite State Machine (FSM), to keep track of its flight trajectory, and a Kalman filter for suppressing noise in the barometer data, and to accurately detect apogee in order to trigger the recovery system at the optimal time. The SRAD system collects sensor data from barometers, IMUs and a GPS for use in the FSM. Additionally the SRAD system collects sensor data to monitor the state of the recovery system. These sensor data are both saved on a blackbox and transmitted to the ground station via a 5GHz transceiver where it is displayed live and stored.

In figure 28,29,30 and 31 you can see renders of the avionics components placement in the rocket. In Figure 32 and 33 you can see system interface diagrams showing how all the different components in the avionics are connected, visualizing how the system distributes power, where signals are being sent and in which protocol.



Fig. 28 Render of rocket without forward airframe, highlighting the two general locations of avionics.

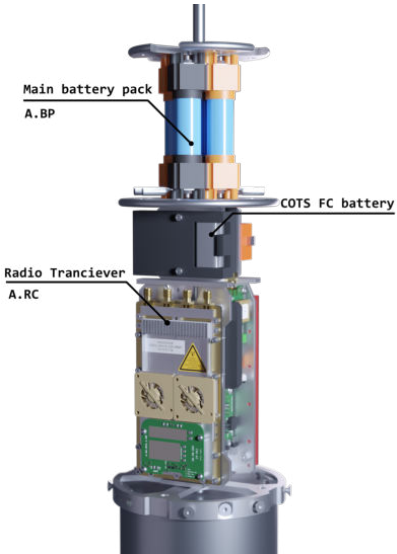


Fig. 29 Upper avionics.

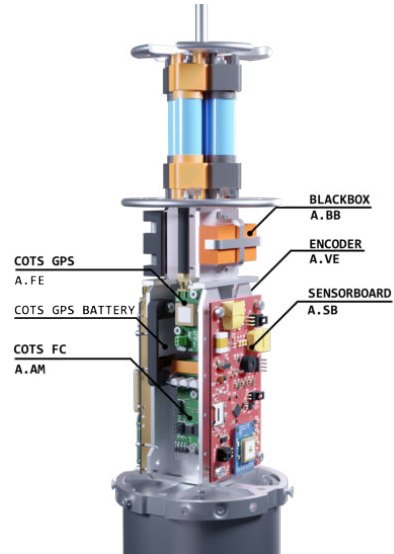


Fig. 30 Upper avionics.

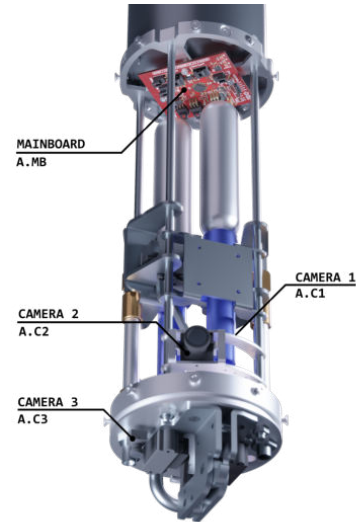


Fig. 31 Lower avionics.

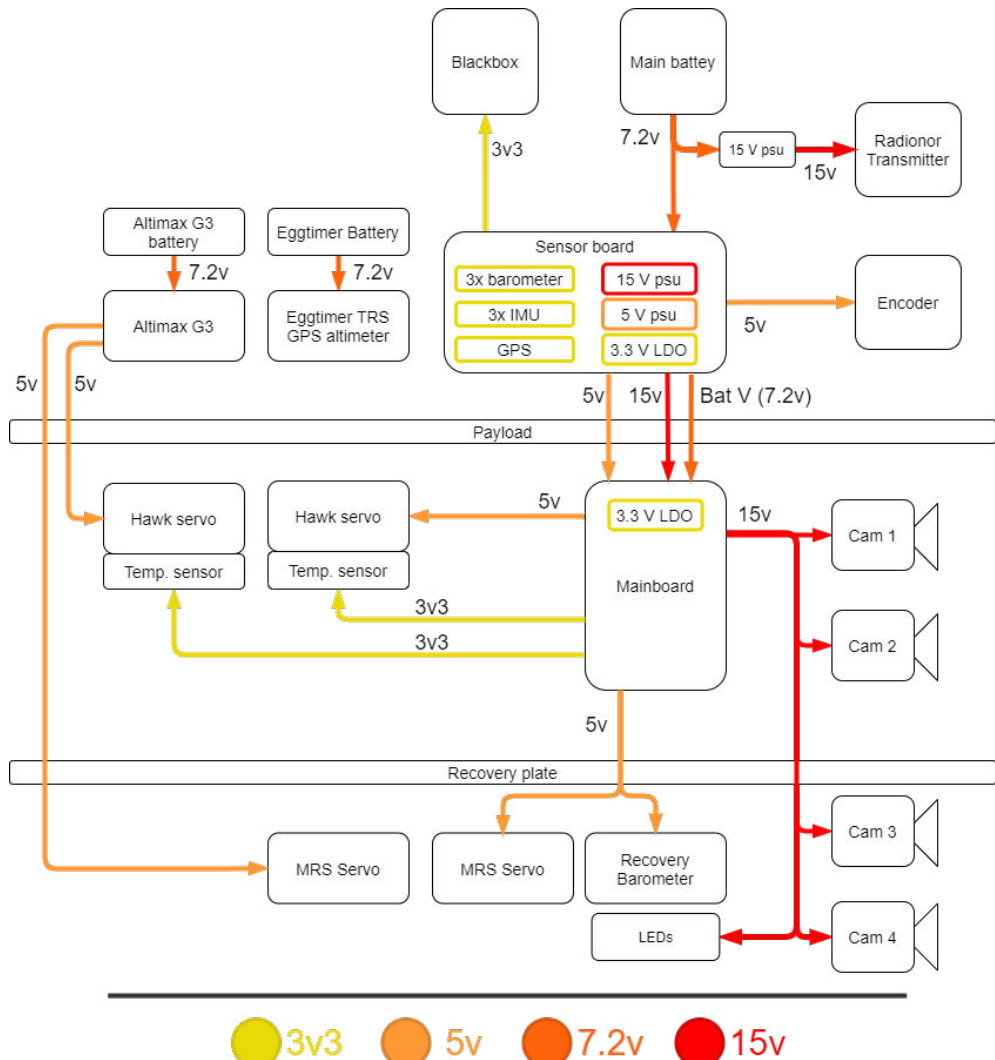


Fig. 32 Power delivery overview.

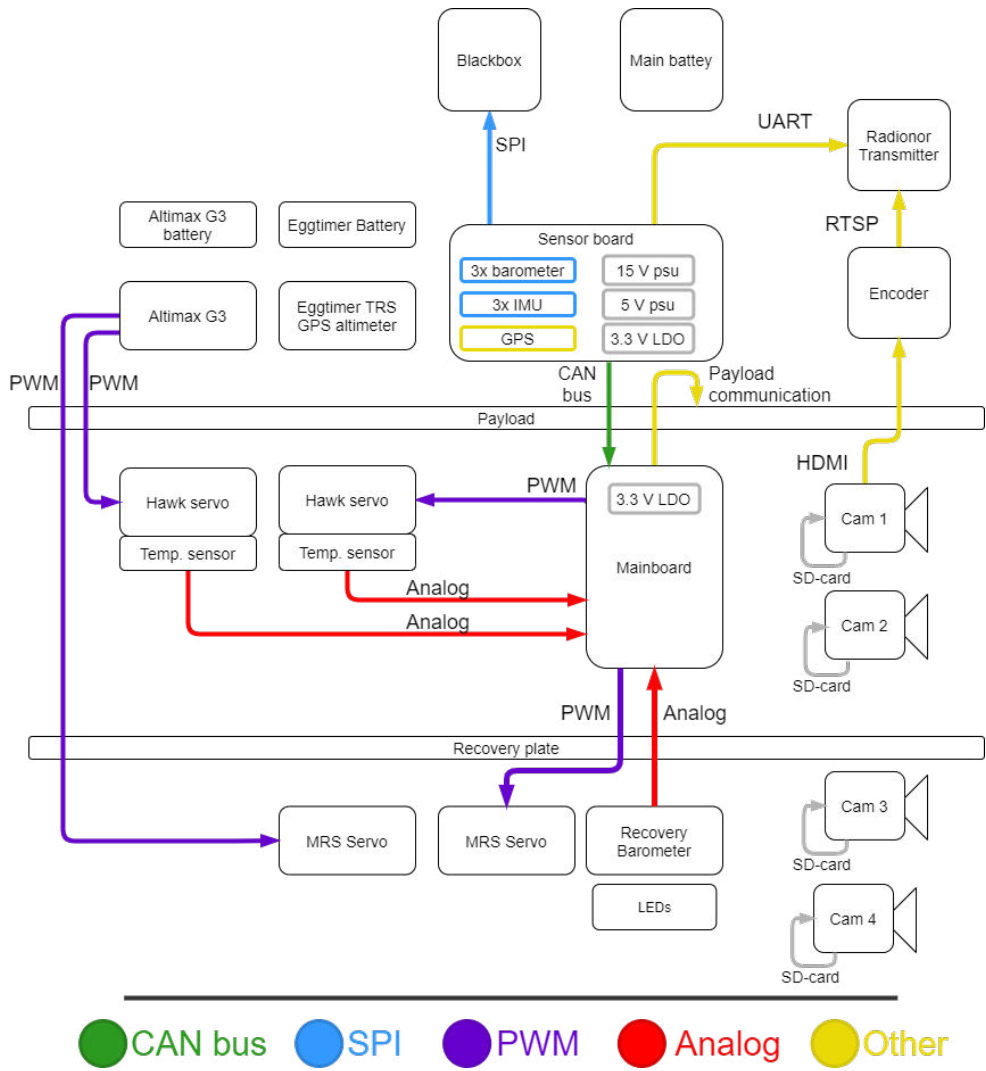


Fig. 33 Information delivery overview.

Table 19: Overview of the major components in the avionics system along with their function.

Part	Reference	Validation method	Short function description	COTS
Sensor board + Power Supply Unit (PSU)	A.SB	Small scale rocket launch, stress test	Voltage conversion, collect, store and transmit sensor data.	
Main board	A.MB	Small scale rocket launch, stress test	Triggers recovery and collects sensor data for recovery status monitoring.	
Blackbox	A.BB	Durability test	Backup storage of sensordata.	
Main battery	A.BP	Ground testing	Provide sufficient power for the entire flight.	
Rocket Radio transceiver	A.RC	Ground and range tests	Transmit sensor data and video feed to ground and receive commands from ground.	
Ground Radio transceiver	A.RCG	Ground and range tests	Receive data from Rocket Radio transceiver.	
Ground station computer	A.PC	Ground testing	Computer for data handling and displaying live information during flight.	
Cameras	A.C1, A.C2, A.C3, A.C4	Ground and test	3x cameras for recording flight from the rocket at different angles.	
Encoder	A.VE	Ground and plane test	Encodes HDMI to Real Time Streaming Protocol (RTSP).	
Eggtimer GPS TRS altimeter	A.FE	Ground testing	For tracking rocket after flight and logging official altitude of the rocket.	
COTS Flight Computer (FC)	A.AM	Small scale rocket launch	Official flight logger and redundant flight computer for recovery activation.	
Arming switch	A.SW	Ground testing	Magnetic arming switch for connecting power to the electronics.	

2. COTS components

Table 20: Overview of requirements from EuRoC regarding COTS hardware.

Req nr.	Req description	Solution
8.1 RR	Launch vehicles shall carry a COTS barometric pressure altimeter with on-board data.	The Eggtimer TRS GPS altimeter is a COTS FC which locally logs barometric height data.
3.3 DTEG	Launch vehicles shall implement completely independent and redundant recovery systems to include: arming switch, sensors/flight computers, power supply, energetics, and "electric initiators".	The Altimax G3 FC is completely independent. It runs on its own battery with its own arming switch, separate from any other electronics.
3.3.1 DTEG	At least one redundant recovery system electronics subsystem shall implement a COTS flight computer.	The Altimax G3 FC has Servo motor control output, meaning it can activate the recovery systems regardless of what the SRAD does.
3.3.2 DTEG	EuRoC will require teams to implement a common mandatory altitude logging and GPS tracking device in all rocket systems	The Eggtimer TRS GPS altimeter tracker makes it possible to comply with all sub requirement 3.2.1.

Requirements fulfilled by COTS system

To satisfy requirement 3.2.1 in DTEG, the avionics will use the Eggtimer TRS GPS altimeter. It operates in the 70cm band which is a relatively low frequency, thereby allowing for long range communication. The altimeter can interface with a common tracking unit which is sold alongside the altimeter. This allows us to track and find the rocket after landing.

3. SRAD Components

Flight computer hardware

The SRAD flight computer consists mainly of two custom Printed Circuit Boards (PCB): the main board, and the sensor board and power supply unit [Appendix V.F *Engineering Drawings*]. The sensor board has the main task of collecting and storing sensor data, while the main board is responsible for releasing the drogue and main chute by controlling the two servo motors with a power modulated (PWM) signal.

Both the main and sensor board feature a STM32F103C8T6 microcontroller(A.MCU), which has a 32-bit ARM Cortex-M3 CPU architecture and runs at 72MHz. On the sensor board there are three barometers(A.S1), three inertial measurement units(A.S2), and a GPS(A.S5). These were mainly chosen for their accurate measurements and well documented use. The triple redundancy on both the barometer and IMUs is to reduce noise and measurement error.

To increase the redundancy and reliability of the system, the sensor data is stored in multiple places. All data is sent to the ground station via a radio transmitter(A.RC), and saved in an SD-card that's placed in a blackbox to ensure that no data is lost in case the rocket crashes. See Appendix V.N for more information on the blackbox. The sensor board communicates with the main board using a Controller Area Network (CAN) bus to transmit the sensor data.

Flight computer software

The finite state machine (FSM) is used to keep track of the flight phase of the rocket and execute the code corresponding to the state it is in. It is crucial to make sure that certain systems run at the correct phase, e.g. the drogue should not deploy when the rocket is armed. The states and transitions were designed so that they all have a unique purpose and are necessary for the flight. To avoid any loops in the transitions, each one is dependent on sensor data and the previous state. The FSM will run through all the states in a specific order. It cannot deviate from this order and the system will therefore avoid skipping any state. A diagram of all the states and transitions can be seen in Figure 34.

The FSM uses a moving average as input. This suppresses sensor noise and ensures that we do not transition to the next state prematurely. The moving average is calculated during the entire flight for both altitude and acceleration as these are the crucial measurements the FSM uses to change states. Apogee detection, the most critical transition, is based on comparing the previous maximum average altitude and the current average altitude. If the difference between them is larger than a set margin, a timer is set. If the maximum altitude does not increase in the duration of the timer, apogee is detected and the drogue can be deployed. See Appendix V.M for further information on all the states and transition triggers used in the FSM.

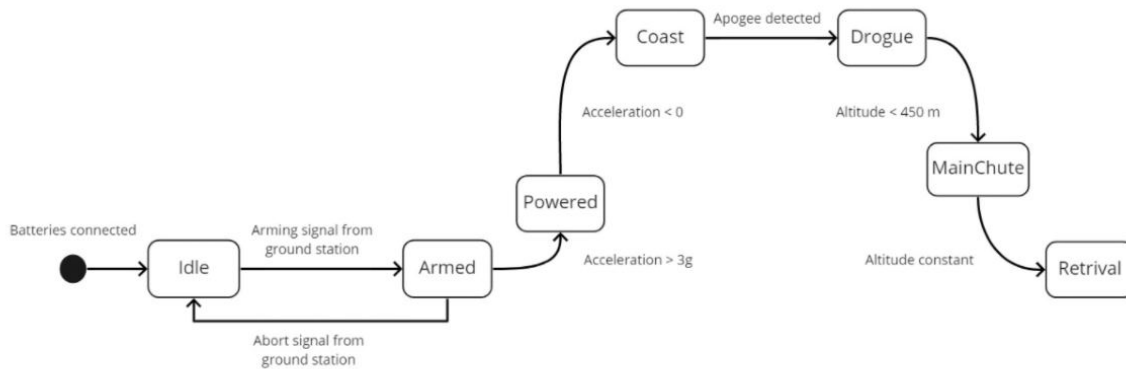


Fig. 34 FSM states and transitions.

4. Kalman Filter

As the collected sensor data contains uncertainties, it is desirable to filter the data to get smoother and more accurate measurements, and to estimate trajectory in case of loss in sensor measurements. With less sensor noise we can have tighter margins on the threshold for transitioning between states in the FSM, meaning that recovery activation can happen closer to apogee. The discrete linear Kalman Filter provides exactly this functionality in real-time. Using both a model of the rocket's trajectory and positional data, it estimates the translational motion of the rocket. It is implemented in C++ and runs on the main board (A.MB). See Appendix V.M for more on the implementation of the algorithms and details about how the sensors are being used in the two separate filters.

5. Recovery monitoring

Implemented in the avionics system is functionality for monitoring the state of the recovery system during rocket separation. The goal is to know what state the recovery system is in, and discern whether the COTS or SRAD FC was the system to successfully activate the recovery system and separate the rocket. To do this there is an analog temperature sensor (A.S3) located on the Hawk system's CO₂ canisters. When the Hawk

system releases the gas from these canisters, the temperature will drop. By recording this we will know when each of the Hawks activates and releases the CO₂ from the canisters.

Furthermore we will have an analog barometer(A.S4) inside the recovery bay of the rocket. This will record when the Hawk system pressurises the chamber, and then measure the drop in pressure once the rocket separates. By looking at these data points, and transmitting them to the ground station during flight, we will be able to know which Hawk actually pressurised the recovery bay and separated it. This is displayed live during the flight. Additionally these data should make it possible to detect a leak in both Hawk systems or a leak in the recovery bay(during flight), which could save the rocket in case it's detected before launch, or it could help decide the reason for a failure in the rocket if it should happen.

6. Cameras

There are four onboard cameras recording the flight from different angles, one of which will be live streamed down to the ground station. In Figure 35 there is an illustration of the different camera locations and views, and Table 21 contains their specifications.

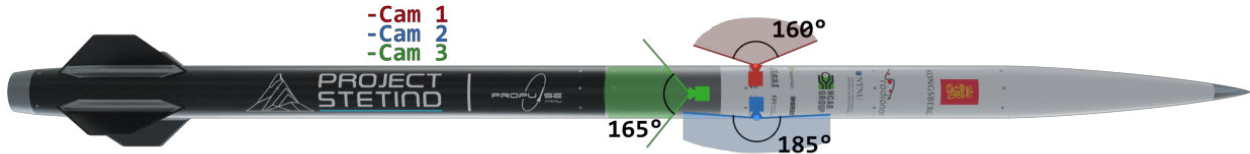


Fig. 35 Illustration of camera positions and view angles.

Table 21: Camera specifications.

Cam nr.	Camera model	Component name	Resolution	Framerate	Field of view	Streamed
1.	Firefly split 4k	A.C1	4096x2160	30 fps	160	No
2.	Firefly split 4k	A.C2	1920x1080	60 fps	185	Yes
3.	RunCam Split 3 Nano whoop	A.C3	1920x1080	60 fps	165	No
4.	RunCam Split 4	A.C4	4096x2160	30 fps	140	No

Camera 2 (A.C2) uses a special 185° field of view lens, which allows us to capture the fins of the rocket in the recording while still keeping the camera inside the rocket, having only the lens stick out a couple millimeters in order to have a minimal effect on drag and stability. The camera will send an HDMI signal to the video encoder(A.VE), which then converts it to RTSP 1080p 30fps and sends it to the radio transceiver onboard the rocket which transmits it down to the ground station. More detailed information on the camera system can be found in Appendix V.N.

7. Telemetry

The purpose of the radio is to transmit data for displaying and storing on the ground station, in case of a failure. The radio used is a CRE2-144-LW (A.RC) on the rocket, and a CRE2-189 (A.RCG) on the ground station. The rocket's radio is connected to the sensor board through Universal Asynchronous Receiver-Transmitter (UART) and to camera 2 (A.C2) through an encoder (A.VE). A detailed view of the telemetry information flow can be seen in figure 36 below. The radios have an operational range of 20 km, and can transmit at rates up to 15 Mbps. The CRE2-189 is directional with a coverage of 90°. The frequency used will be between 4900 and 5900MHz. The protocols used for transmission are User Datagram Protocol (UDP) for telemetry data and RTSP for video streaming. On the ground, the data will be streamed to a computer, where it will be displayed live and stored locally. The graphical user interface which displays the sensor data will also contain an arming switch for toggling the rocket between the armed and idle state. See Appendix V.L for more information regarding the ground station hardware and software, and details on the telemetry.

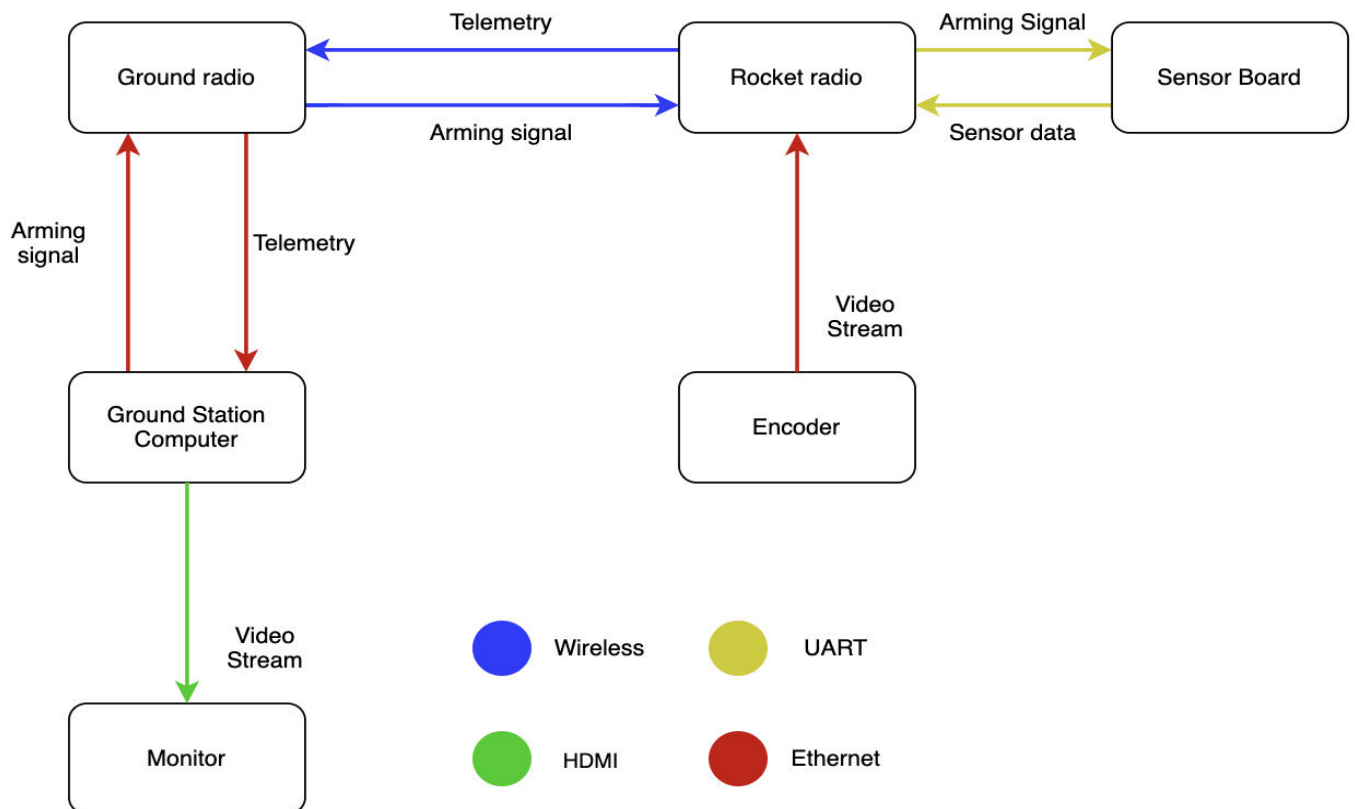


Fig. 36 Telemetry information flow overview.

8. Validation

All components have been tested for proper functionality on the ground to initially verify them. Most systems have gone through more extensive testing as well which you can see noted in the table below. See Appendix V.B for details on the procedure and results of all the tests performed on the avionics system.

Table 22: Overview of tests performed/to be performed.

Test reference	Parts Tested	Short test description	Result
Small scale rocket launch	SRAD flight computer system and COTS GPS tracker	Launching a model rocket to 400m to validate software functionality such as FSM, Kalman Filter and Sensor reading on a prototype PCB. Also to practice handling COTS hardware.	Success, Software performed as expected. COTS GPS was operated successfully. Noticeable room for improvement in sensor polling rate.
Test flight medium rocket	SRAD flight computer system and COTS GPS	Launch of rocket to 1400m to test final* SRAD FC software and production PCB, along with COTS GPS. *software could be changed after test, but in theory final	Success, software performed as expected. Most of FSM was validated
Durability test	Blackbox	Test to see what forces the blackbox is able to handle. This is to validate if it can survive a crash of the rocket.	Not yet conducted
Drop test from helicopter	SRAD flight computer system + recovery	Drop test from a helicopter to test whether the SRAD FC system can properly activate the recovery system in a realistic environment.	Pending
Range test using helicopter	Radio transceiver system + camera 1	To test power draw and see how much bandwidth we have at 10km distance between ground station and rocket transceiver. Potential to test the maximum range of the system as well.	Not yet conducted

H. Payload

1. System function and system overview

The payload consists of three main interfaces: software, electrical and mechanical. In addition there is an experiment, where the team aims to investigate the behaviour of ferrofluids during high acceleration, strong vibrations and free fall. To gain more context around the design choices that have been made, see the Appendix V.R.



Fig. 37 The structure of the payload.

2. Mechanical

The mechanical structure consists of a cylinder (P.CF), two screwable lids (P.PLL, P.UL), threaded rods (P.ROD), and plates as shown in Figure 37. The components of the payload are mounted on threaded rods, which attach to one of the payload lids. The lid with all components attached can be inserted into the casing and screwed on. Screwable lids are implemented for their decent water resistance, in case there is any leakage from the ferrofluid container. The mechanical interface between the payload and the structure is described in Section II.E Inner structure.

3. Electrical

The electrical interface consists of an on-board computer (P.OBC) as the main computer, and a Raspberry Pi (P.PI) as the secondary computer. The communication protocol used between them is UART. The SenseHat (P.SH) is a sensor board designed for the Raspberry Pi, from which this mission mainly uses the accelerometer. Microphones (P.MIC) are connected to the Raspberry Pi through an analog to digital converter (P.ADC), to measure the noise levels from the rocket. A Raspberry Pi camera (P.CMR) will be used to observe the behaviour of the ferrofluid. Led diodes (P.LED) are used to light up the fluid container, for the camera to be able to record. In addition, the OBC will have an IMU (P.IMU). Since data from two different sensors are collected, this improves the redundancy. An SD-card is used as a storage unit, and is located in a black box. The black box is meant to give extra safety for the data in case of a crash. An electrical power supply (P.EPS) is used to deliver power from two batteries (P.BLI) to the electrical system. After the avionics system is armed, it will send an arming signal to the payload. The signal will be sent via a cable through the upper lid. An overview is shown in Figure 38, while further details of the Electrical interface can be found in Appendix V.Q.

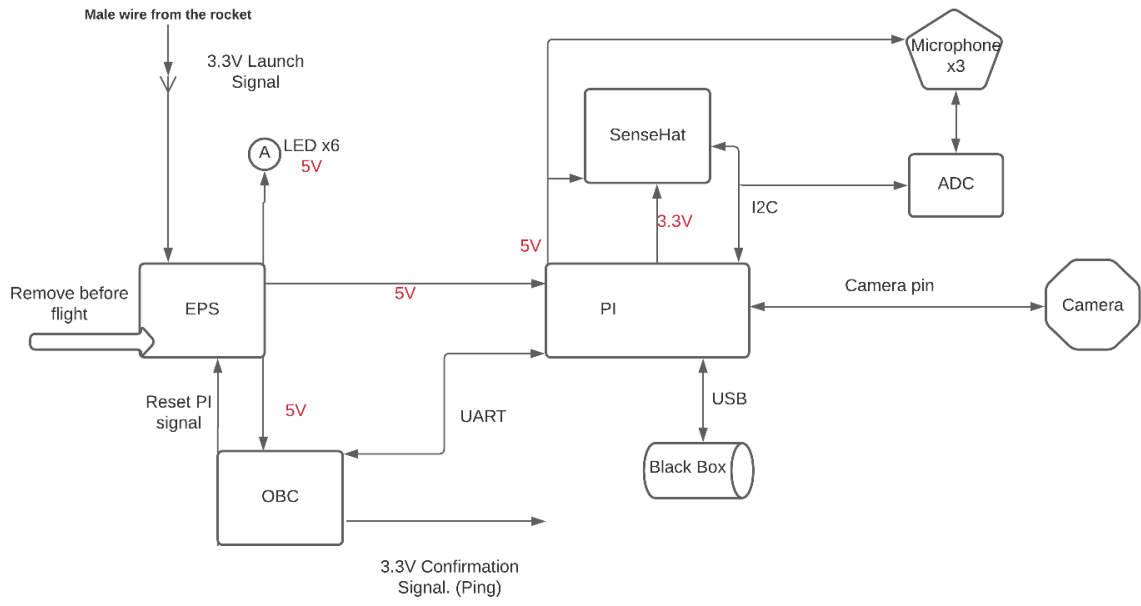


Fig. 38 Power and information delivery overview

4. Software

The operating system on the On-Board Computer (OBC) is developed by Orbit NTNU. When all systems are running, the OBC will send a signal to the flight computer, indicating that all systems are ready for launch. Figure 39 shows an overview of the software. In case some sensors are not functioning as expected, or there is some other type of malfunction, the system is programmed to restart. This will be done both before launch and during flight, although with some differences to which systems will be rebooted. Further details can be found in Appendix V.P.

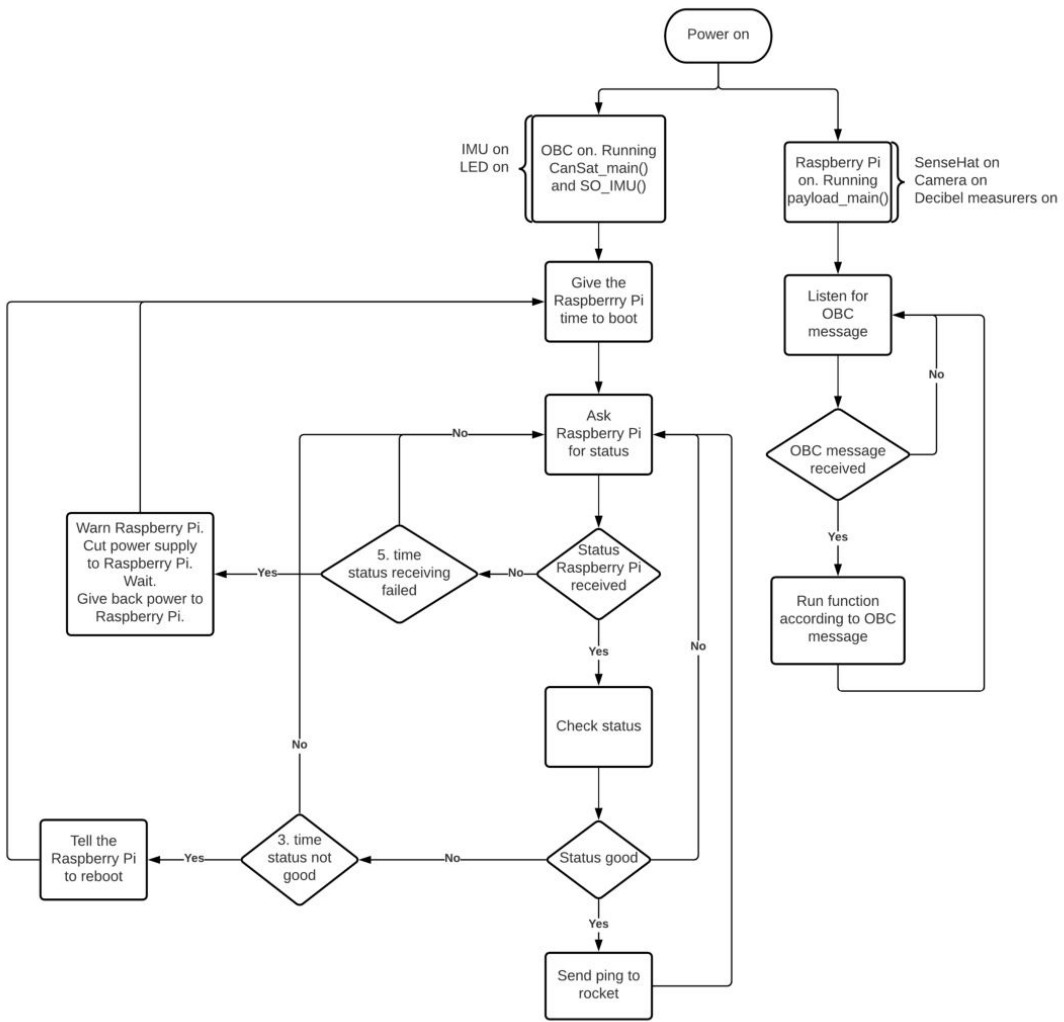


Fig. 39 Software overview

5. Experiment

The fluid container has magnets placed underneath, to induce the characteristic behaviour of the ferrofluid. We expect the ferrofluid to be flattened out as a result of the acceleration, and to shake as a result of the vibration. The goal of the experiment is to observe if the characteristic spikes are affected during high acceleration events, and how vibration resistant the fluid is.



Fig. 40 The ferrofluid in its container

6. Validation

A summary of the tests performed to validate the reliability of the payload functionality, is presented in table 23. Detailed descriptions of the tests can be found in Appendix V.B.

Table 23: Overview of performed tests

Test	Objective and test description	Result
Leakage test	Verify that the mechanical structure is water resistant by filling the cylinder frame with water.	Leaked when the cylinder was completely filled with water. The amount of fluid that leaked was very small, and the fluid smeared itself out on the surface inside of the cylinder. Deemed not to be a problem.
G-force test	Verify that the mechanical structure can handle the acceleration up to 15g. Components were weighted with 20 times their own weight, to simulate the acceleration from the rocket and stress from the vibration.	All the components handled the weight.
Black box test	Verify that the blackbox can keep the SD card intact by dropping it from the fifth floor and smashing it with a sledge.	The SD-card was protected by the black box to a degree.
Magnet interference test	Verify that the magnetic field does not cause disturbance to the signals between avionics and recovery. Magnets were placed next to wires and metal casing, while sending different signals through the wires.	No disturbance observed.

III. Mission concept overview of operations

The rocket's flight is arranged in eight phases, shown in Figure 41. In each phase it is indicated what criteria must be fulfilled for operations to be nominal. Risks to mission success, during each phase, are stated in Appendix V.D *Risk assessment*.

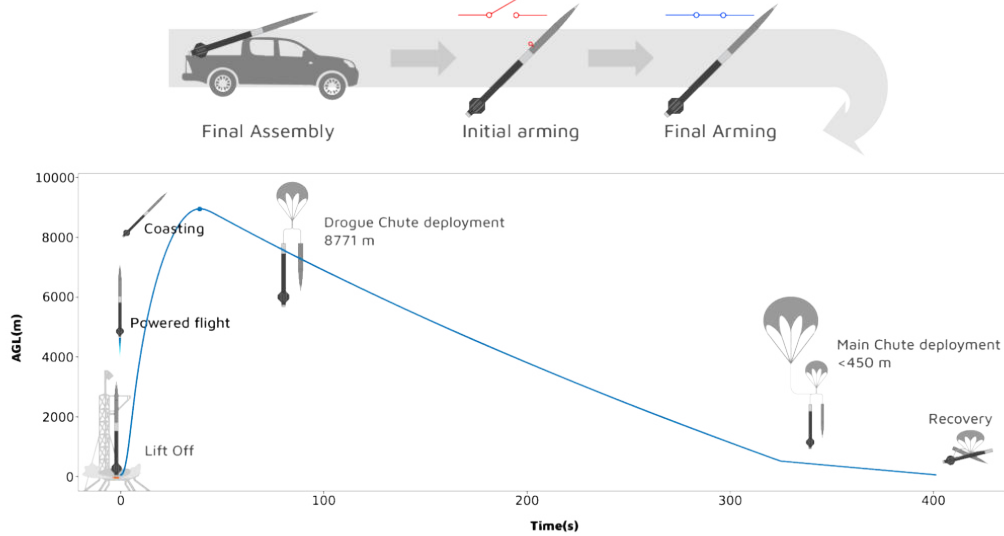


Fig. 41 Illustration of the mission phases, as well as final assembly.

Phase 1: Initial arming

The initial arming phase starts when the rocket is attached to the launch rail. The rocket will stay on the launch pad for an undefined amount of time, waiting for launch approval.

Pass criteria:

- Pre launch procedures (described in Appendix V.E) have been completed correctly.
- Ground control has established a connection with the avionics system.
- Received a “Go for launch” signal.

Phase 2: Final Arming

The final arming phase starts when an arming signal is sent from the ground station to the avionics system.

Pass criteria:

- The avionics system is armed.
- The payload is activated and logging data.
- Ground control receives and displays sensordata from avionics.
- All sensors are deemed nominal.

Phase 3: Lift off

Lift off is initiated when a “FIRE” signal is sent to the igniter.

Pass criteria:

- The avionics system detects acceleration above 3 g, and thus enters the “Powered” state of the FSM.
- The rocket obtains a minimum velocity of 30 m/s before clearing the launch rail, in accordance to DTEG 8.2 *Launch stability*. See Table 7 *simulation conditions and results* for the calculated velocity.

Phase 4: Powered flight

Powered flight starts when the rocket leaves the launch rail. Max Q occurs during this phase. See Section II.C.2 *Max Q/Mach number*.

Pass criteria:

- The structure withstands forces at Max Q.
- The rocket remains stable. See Section II.D.20 *Aerodynamics* for a detailed analysis.
- Successful propulsion completed.

Phase 5: Coasting

Coasting starts when the motor has burned out, expected at $T = 6.16\text{s}$ [18]. The rocket will coast upwards until it reaches apogee. Apogee is estimated by OpenRocket to be 8771.3 m AGL and occur at $T = 38.9\text{s}$. See Section II.C *Trajectory calculations*.

Pass criteria:

- The rocket remains stable. See Section II.D.2 *Aerodynamics* for a detailed analysis.
- The avionics system detects apogee. See Section II.G *Avionics* for detection methods.

Phase 6: Drogue chute deployment

The drogue chute deployment is initiated when apogee is detected. The drogue chute is first deployed near apogee, and is estimated to descend with a velocity of 36.20 m/s . As the atmosphere gets thicker it is estimated to slow down to 24.16 m/s at 450 m AGL [Appendix VI *Parachute trajectory simulations*].

Pass criteria:

- Drogue chute deployed. See Section II.F.3 *Deployment system*.
- The MCRS system does not deform [Appendix VI *Forces on MC RS and recovery plate*].
- The structure withstands the release force.
- The rocket slows down to a velocity between 23 m/s and 46 m/s in accordance with *DTEG 3.1.1 Initial deployment event*.
- The avionics system detects a pressure altitude below 450 m AGL . See Section II.G *Avionics* for detection details.

Phase 7: Main Chute deployment

The Main chute deployment phase is initiated when the avionics system detects an altitude below 450 m AGL based on barometric readings. The main chute is then deployed, leading to a deceleration of 149.3 m/s^2 [Appendix VI *Parachute trajectory simulations*].

Pass criteria:

- Main chute is deployed. See Section II.F.3 *Deployment system*.
- The structure absorbs the release force.
- The rocket slows down to a velocity lower than 9.0 m/s in accordance with *DTEG 3.1.2 Main deployment event*.

Phase 8: Recovery

The recovery phase starts when the lower part of the rocket hits the ground with a velocity of 5.87 m/s [Appendix VI *Parachute trajectory simulations*]. The rocket will be collected and inspected for damage, following the post flight checklist in Appendix V.E.

Pass criteria:

- The structure withstand the landing impact force calculated in Appendix VI *Impact force calculation*.
- Sensor data is intact.
- Successfully tracked down the rocket using GPS.
- Rocket collected.

IV. Conclusion and Outlook

Propulse NTNU Team 2021 has achieved building a rocket which they judge to fulfil the requirements set by the stakeholders, and are therefore confident that it will be a successful flight. Compromises have been made in order to increase reliability. For instance a javelin design, that would have permitted a cubesat payload while reaching 9000 m, was considered too high a risk, and therefore not pursued.

Having evolved into a well-functioning team is also an achievement. Despite extraordinary circumstances due to the pandemic, the team has been able to maintain efficiency and good communication, and the rocket has been finalized as planned. One of the main goals for the project has been to mature members as engineers. It is difficult to measure to which degree this goal has been fulfilled, however, this report is a manifestation of how much knowledge and understanding has been acquired by the members. The project has been economically viable, as a result of sound financial management and several new sponsor deals. Nonetheless there are several areas of improvement and lessons learned, which are listed below.

Design

- Multiple groups experienced that advanced solutions are not necessarily good. The avionics group chose a microcontroller and software for the ground station that led to a more complicated solution than necessary. While developing the main chute release system, the recovery team learned that a large number of moving parts decrease reliability. This led to a complete redesign of the subsystem, which is simpler and more reliable.
- The team learned through discussion with experienced engineers, late in the design period, that it is possible to have bolts through composite material, while preserving the structural strength that is required. Subsequent changes were made to the design.
- Risks related to vibration were also highlighted through this discussion with experienced engineers from our sponsors. Consequently disk bulkheads and more fasteners were added to the inner structure, and a vibration test of the inner structure, the recovery system, avionics and payload will be performed.
- The team has gained a better understanding of the importance and procedures of systems engineering.
- Specific requirements related to interfacing should have been made by both Propulse NTNU and Orbit NTNU at the beginning of the project and followed up closely. This way the payload and the rocket would complement each other better, the same way as the subsystems of the rocket complement each other.

Validation

- Some systems have been harder to validate than others, e.g. strength of composite structures. The validation process must be considered from the beginning of the development process.
- Not all planned test were executed within the deadline for the report. These test will be done before the rocket is launched.

Production

- More care could have been taken in defining realistic tolerances when requesting production. A tolerance which is tighter than necessary is likely to increase cost and production time.
- Supply issues with electronic components have placed severe challenges on the team's progression. Components with standard interfaces could have been selected to reduce the impact of supply issues.

In order to raise the technical level in the organization, experience from every project, such as the lessons mentioned above, must be passed on. The main part of corporate knowledge transfer will go through earlier members playing a role as mentors for next year's team. Knowledge transfer will be critical when embarking on Propulse NTNU's future project, of integrating and launching the hybrid propulsion system that the team has been working on since 2019. This is a step on the way to reaching the ultimate goal of launching a fully student researched and developed rocket to space.

V. Appendix

A. System data

System data appendix

Table of contents:

Propulsion system	1
Trajectory calculations	1
Structure	2
Recovery	2
SRAD Avionics system	3
COTS Avionics system	3
SRAD Telemetry	3
Detailed weight and positioning of components	4

1. Propulsion system

Propulsion system	Cesaroni Pro98-6GXL 21062O3400-P
Motor letter classification	O
Total impulse	21062 Ns
Average thrust	3421 N
Burn time	6.16 s
Loaded motor weight	16.842 kg
Empty motor case weight	5.57 kg
Propellant weight	10.93 kg

2. Trajectory calculations

The following values are further discussed in section II.C. Trajectory Calculations.

Liftoff thrust- weight ratio	14
Launch rod clearance velocity	55.8 m/s
Launch rod length	12 m
Altitude at maxQ	1692 m
Velocity at maxQ	577 m/s (1.73 Mach)
Atmospheric pressure at maxQ	82992 Pa
Time to apogee	39 s
Simulated apogee	8771 m

3. Structure

The following values are further discussed in section II.D. Outer structure.

Total length	3021 mm
Maximum diameter of airframe	128 mm
Number of fins	4 pts
Fin Semi Span	104 mm
Fin flutter velocity	793 m/s (2.42 Mach)
Lift off mass	33.30 kg
Dry mass	22.00 kg
Average Center of Pressure off rail ¹	2108 mm [dist. from nose tip]
Center of Gravity off rail	1826 mm [dist. from nose tip]
Average Center of Pressure at maxQ	2279 mm [dist. from nose tip]
Center of Gravity after motor burnout	1682 mm [dist. from nose tip]

¹ This is an average between values presented in table 5 II.D.2. Stability margin.

4. Recovery

The following values are further discussed in section II.E.Recovery.

Approximate Drogue chute release altitude	8771 m (apogee)
Descent rate drogue chute	24.16 m/s
Drogue parachute diameter	30" elliptical parachute (Fruity Chutes)
Drogue parachute coloration	Alternating red and white
CO2-canister (drogue chute release mechanism)	33 g
Number of CO2-canisters	2
Approximate Main chute release altitude	450 m
Descent rate main chute	5.87 m/s
Main parachute diameter	Iris 96" compact parachute (Fruity Chutes)
Main parachute coloration	Alternating orange and black
Length straight shock cord	12 m
Length Y-shock cord	6 m (each leg)

5. SRAD Avionics system

The following values are further discussed in section II.G Avionics.

Battery size	42 Wh
Battery type	2S2P li-ion
Battery idle time	3 hours
Battery armed/flight time	30 min
Max power draw ide	8 W
Max poraw armed	36.5 W

6. COTS Avionics system

The following values are further discussed in section II.G Avionics.

COTS GPS	Featherweight GPS tracker
COTS GPS battery life	11 hours
COTS GPS frequency	915 MHz band
COTS GPS range	>90 000 meter (line of sight)
COTS FC	Altimax G3
COTS FC battery life	4 hours

7. SRAD Telemetry

The following values are further discussed in section II.G Avionics.

Ground station transceiver	Radionor CRE2-189
Ground station antenna type	Phased array antenna (directional)
Ground station transceiver field of view	90 degrees (conical shape)
Rocket transceiver	Radionor CRE2-144-LW
Rocket transceiver antenna type	4x omnidirectional monopole antennas
Frequency	4900 - 5100 MHz
Range	>20 km (line of sight)
Data rate at 20km	7 Mbps (line of sight)
Data rate max	15 Mbps (line of sight)

8. Detailed weight and positioning of components

Division:	Part name	Mass [g]	Qty.	Position relative to nosecone [m]	Part ID
Avionics	CRE2-144-LW (radio transmitter)	153	1	0.56	A.RC
	Black box	85	1	0.4559	A.RC
	Battery assembly	238	1	0.4586	N/A
	Runcam split 3 nano whoop	10.5	2	1.2556	A.C3
	Camera, Hawkeye 4K Firefly Split mini	23	2	1.2116	A.C2
	Video Encoder, AVC-2K, H.264 V	20	1	0.5511	A.VE
	wires grams/meter	23	11	1.0246	N/A
	Sensor board pcb	35	1	0.5542	A.SB
	Main board pcb	25	1	0.9436	A.MB
	COTS FC altimax	14	1	0.5614	A.AM
	COTS GPS	18	1	0.4806	A.FW
	COTS FC altimax battery	6	1	0.455	N/A
	COTS GPS battery	8	1	0.5446	N/A
Recovery	Hawkbody+servo+fitting	225	2	1.235	N/A
	Hoseassembly	79	2	1.282	N/A
	Main chute	465	1	1.42	RC.MC
	Drogue chute	88	1	1.6	RC.DC
	U-bolt	71	1	1.349	RC.UB
	Eyebolt	75	1	1.732	RC.EB
	MRS-system	389	1	1.36	N/A
	Shock cords [g/m]	10	25	1.42	RC.SCY/S
	CO2 45g	201	2	1.122	RH.CO2
	Servo motor	13	2	1.349	RH.HSM
	Swivel links	62	2	1.468	RC.SWL
	Quick links (location 1)	112	1	1.269	RC.QL
	Quick link (location 2)	112	1	1.468	RC.QL
	Hawk plate	64	2	1.202	RH.HP
	Cable gland	10	1	1.336	RR.CG
	Recovery plate	272	1	1.332	RR.RP
Payload	Payload	4000	1	0.7675	N/A
Engine bay	Motor	16842	1	2.339	N/A

Structure	Nose tip assembly	190	1	0.08	IN.UP/MP /LP
	Upper threaded rod	231	1	0.34	IU.UTR
	Upper disk bulkhead	21	1	0.326	IU.UDB
	Lower disk bulkhead	32	1	0.4274	IU.LDB
	Altimax battery mount	6	1	0.4277	IA.ABP
	Altimax battery bracket	23	1	0.455	IA.ABP
	Black box mount	7	1	0.4547	IA.BBP
	Middle plate	18	1	0.4814	IA.MP
	Encoder bracket	45	1	0.5589	IA.VEP
	Encoder mount	14	1	0.5498	IA.VEP
	Altimax + GPS mount	14	1	0.55	IA.AGP
	GPS Battery housing	9	1	0.546	IA.GBH
	Radionor mount	23	1	0.5521	IA.RP
	PSU + Sensorboard mount	22	1	0.5514	IA.SPP
	Lower plate	11	1	0.4814	IA.LP
	Upper bulkhead	108	1	0.6253	IP.B
	Upper bulkhead ring	27	1	0.6277	IP.BR
	Lower bulkhead	108	1	0.9346	IP.B
	Lower bulkhead ring	27	1	0.9307	IP.BR
	Lower threaded rods	69	4	1.0955	IL.LTR
	Camera plate	28	2	1.1406	IL.CP
	Camera mount (3d print)	36	2	1.2116	IL.CM
	Upper coupler	1022	1	1.3783	IC.UC
	Lower coupler	777	1	1.5766	IC.LC
	Motor mount	221	1	1.6956	IC.MM
	Motor centering ring	91	1	2.3646	IAE.MCR
	Boat tail wedge	49	1	2.9536	IAE.BW
	Boat tail centering ring	57	1	2.9626	IAE.BCR
	Boat tail	130	1	2.9956	IAE.B
	Rec bay M6 nut	2.5	76	1.101	N/A
	Fin brackets	60	8	2.748	OL.FB
	Fins	152	4	2.748	OL.F
	Fore Airframe	1678	1	0.755	OU.FA
	Aft Airframe	1733	1	2.2680	OU.AA
	Nuts and bolts on fin brackets	91	1	2.7480	N/A
M =	33272	<i>Total mass of the rocket [g]</i>			
W =	326.3	<i>Total weight of the rocket [N]</i>			
CG =	1.826	<i>CG position relative to nose [m]</i>			

B. Test reports

PROJECT TEST REPORTS



Ground test - Rocket separation

Date: dd/mm/yyyy

2	9	0	4	2	0	2	1
---	---	---	---	---	---	---	---

Purpose:

The purpose of this test was to determine if our rocket design is able to separate and deploy the drogue chute. In addition to successfully activate the system remotely and be able to transmit data between the radio transmitter and the ground station.

Signatures:

Vebjørn G. Bratlie, Johannes E. Mørkrid, Hege Grytten, Anders Hestad, Kristian Hope, Ane Morkemo, Ola Flaata

Test Equipment & Set-Up Description:

From top left to bottom right in figure 1:

- Recovery plate and cable gland
- 2x25 gram CO_2
- 1x33 gram CO_2
- Hawk plate
- Weight 10 kg
- Upper coupler
- Lower coupler
- Threaded rods
- Hawk fitting
- Hawk with safety pin
- Servo motor
- Camera
- PTFE-tape
- Drogue chute
- Deployment bag with main chute
- Shock cords
- Battery packs
- PCB
- Power converter

In addition to wires, fasteners and a radiometry system.

Figure 2 shows the test rig that the



Figure 1: Test equipment



Figure 2: Test rig

components were mounted to.

Figure 3 shows the test setup.

Figure 4 shows the avionics inside the recovery bay. Consists of a camera with a circuit board, and a barometer with a sample rate of 1.68Hz. Note the use of a cable gland to ensure minimal leakage.



Figure 3: Test setup

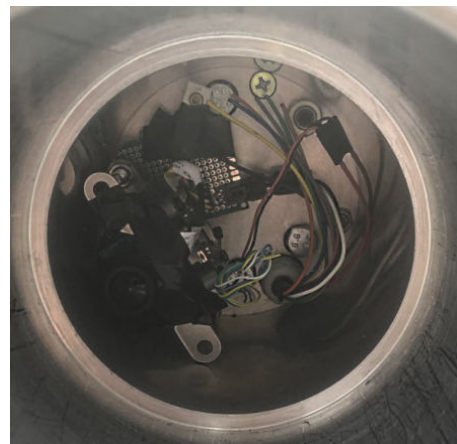


Figure 4: Avionics inside the recovery bay (not like this in actual rocket!)

As-Ran Test Procedure:

Test run 1#

Function test of avionics. Tested the activation of the hawk system. Testet that system was able to transmit data between radio antenna and ground station. Note that the system was not armed during this test.

Test run 2#

Separation with remote activation using 25 gram CO_2 with weight

Test run 3#

Separation with remote activation using 25 gram CO_2 with weight and parachutes

Test run 4#

Separation with remote activation using 33 gram CO_2 with weight and parachutes

Safety concerns:

Due to the high forces the test couplers will function as a “canon”, therefore everyone should keep a safe distance to the couplers, and not stand in front of the setup. The Hawk has a loaded spring, so a safety pin was used when loading the system with CO₂. The system was not armed until right before activation. Safety goggles were used by test participants to prevent eye injury from potential flying shear pins.

Test Criteria:

Pass criteria	Fail/Success
Successful separation with 25g CO_2	Success
Successful separation with 33g CO_2	Success
Drogue chute is deployed	Success
Able to sample the pressure accurately	Fail
Able to activate the servo motor remotely	Success
Able to transmit data from radio to ground station	Success
Successfully save data on a micro SD-card	Success
Able to detect a spike in pressure readings	Fail

Test Results:

Test run 1#

Able to transmit pressure data from radio antenna to ground station and to send a signal from the ground station to the antenna to activate the servo motor.

Test run 2#

Able to activate the servo motor using the ground station.

Distance separated: 171cm.

All shear screws sheared.

Able to detect a spike in pressure reading, although not correctly sampled. Max reading: 43.38 psi (2.99 bar).

Test run 3#

Able to activate the servo motor using the ground station.

Distance separated: 181cm

All shear screws sheared.

Able to detect a spike in pressure reading, although not correctly sampled. Max reading: 24.53 psi (1.69 bar)

Drogue chute successfully deployed.

Test run 4#

Able to activate the servo motor using the ground station.

Distance separated: 308cm

All shear screws sheared.

Not able to detect a spike in pressure reading.

Drogue chute failed to deploy.

Discussion of Results:

Both the 25 gram and 33 gram CO_2 canister provided enough force to successfully separate the couplers.

The parachutes were only packed for **test run 3#** and **test run 4#**. Only **test run 3#** were successful at deploying the drogue chute. The only difference between **test run 3#** and **test run 4#** was that in **test run 3#** the shock cords were braided, See figure 9, while in **test run 4#** they were just put in the couplers without being braided. Also a different CO_2 canisters were used in these attempts.

Since the shock cord is shorter when braided it is able to pull out the drogue chute before the braided shock cord disentangles. This is shown in figure 5 and figure 6. The shock cord is much longer when not braided and is therefore not able to pull out the drogue chute in **test run 4#**. This can be seen in figure 7 and figure 8 respectively.

Notice the difference in mess with the cords. For **test run 4#** the ropes were entangled in contrast with **test run 3#** where the shock cord was pulled out nicely together with the chutes. Fully pulled out chute is shown in figure 10.



Figure 5: Test run 3#



Figure 6: Test run 3#



Figure 7: Test run 4#



Figure 8: Test run 4#



Figure 9: Braided shock cords and shroud lines neatly packed



Figure 10: Shock cords and chutes successfully pulled out with no entanglement

Conclusion:

The separation was successfully triggered by the avionics for all attempts. To increase the chance of drogue chute deployment we learned that the shock cord needs to be braided. The avionic system transmitted sensor data successfully between the ground station and the radio transmitter. The sample rate was too low, 1.68Hz, to give accurate pressure data from the separation process. Since we were not able to verify the pressure calculations done in Appendix VI *Pressure calculations*, we have chosen to go with the 33 gram canister over the 25 gram. The 33 gram canister gave a satisfactory separation in addition to being shorter than the 45 gram canister which we considered to have before this test. The 33 gram option is also more available and cheaper than the 45 gram canister.

Dual redundancy:

The recovery system features dual redundancy in order to increase its reliability. The system has two separate power supplies, one for the COTS altimax flight computer and the other for the SRAD flight computer. The SRAD flight computer consists of a sensor board and a main board. The flight computers are connected to two separate pressure based separation systems (PBSS). With this redundancy the rocket will still be able to separate, should one of the flight computers fail to detect apogee or one of the PBSS be malfunctioning. In the event that both systems are activated the rocket will still separate and the excessive gas will flow out to the surrounding air. Each of the flight computers are also connected to two independent servo motors that activate the main chute release system (MCRS). The system with it's redundant components are shown in figure (11)



MCRS Pull

Test

Figure 11: Highlighted redundant components

Date: dd/mm/yyyy

0	3	0	5	2	0	2	1
---	---	---	---	---	---	---	---

Purpose: Write down the purpose of the test

The purpose is to validate the functionality of the main chute release system.

Signatures:

Vebjørn G. Bratlie, Johannes E. Mørkrid, Hege Grytten and Kristian Hope

Test Equipment & Set-Up Description:

Components from top left to lower right.

- 2x Main chute release docking
- Upper release arm
- Lower release arm
- Fasteners
- Force gauge
- Power converter
- PCB
- Batteries
- Servo motor
- Shock cord
- Test rig (Plank)
- Quick link

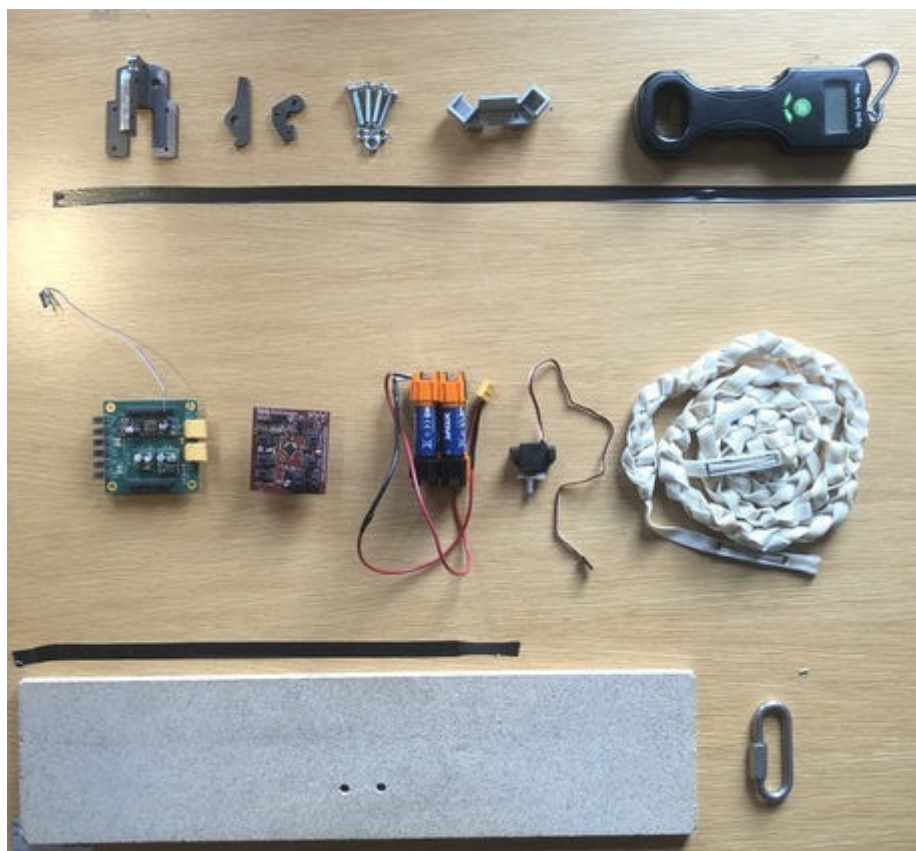


Figure 1: Test equipment

As-Ran Test Procedure:

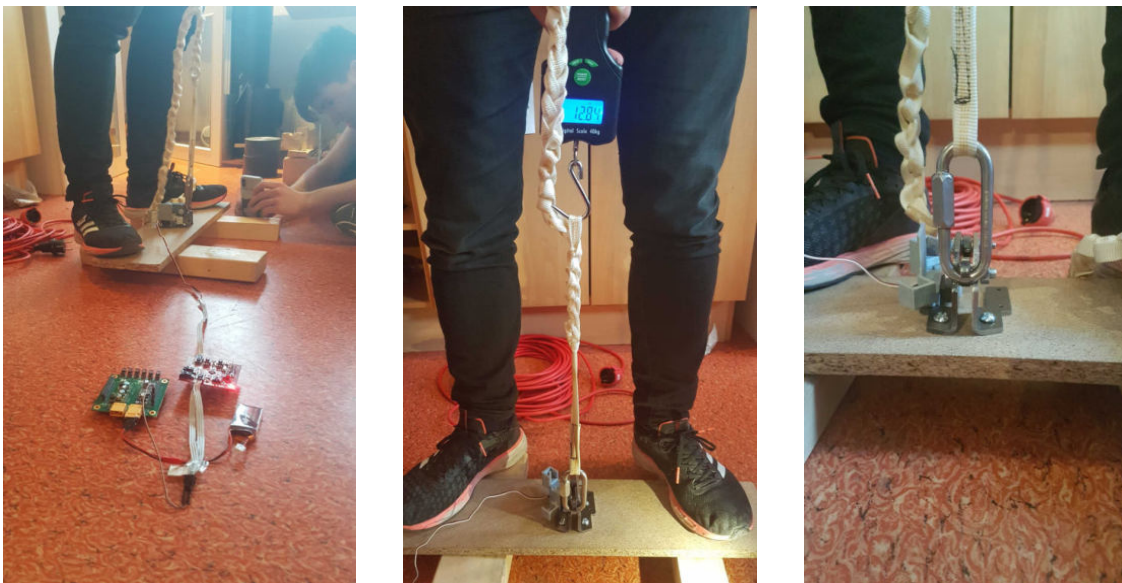


Figure 2: Test setup

The MCRS was mounted to the test rig. A quick link connected to a shock cord was used to pull the upper release arm to simulate the drogue chute release force. A force gauge was used to read the force applied. A signal from the PCB was used to activate the servo motor.

Safety concerns:

N/A

Test Criteria:

Pass criteria	Fail/Success
Servo can deploy the system under a load of 133.4 N(13.6kg), equal to the weight of the aft.	Success
The release arm is mechanically locked when the load is applied	Success

Test Results:

Test run 1#

Avionics test, servo rotates, and opens up with no load.

Test run 2#

Servo not able to rotate release arm.

Mitigation(turn the servo around)

Test run 3#

Servo not able to rotate release arm

Test run 4#

Servo able to rotate release arm

Reduced load (5kg)

Test run 5#

Servo motor able to rotate release arm

Reduced load (7kg (max))

Test run 6#

Servo motor was no able to rotate

Reduced load (9 kg), this time when we slowly reduced the load, we needed to have a load of 5kg before the system released the quicklink.

Test run 7#

Tried with different angles

No angle worked with a load of around 13 kg. Not even when the servo pointed 90 degrees up

Test run 8#

Tried to move the lower release arm by hand. Noticed that it became quite difficult to release the lower release arm. In other words, it required quite a large force to release the lower release. With a low load, it was quite easy to release.

Test run 9#

This attempt used the mitigation approach of filing down the edge on the lower release and adding a spacer. This resulted in releasing the quick link under a maximum load of 245.25 N.

Discussion of Results:

We were initially not able to successfully release the quick link when we had a load of 133.4N (13.6kg).

Factors of failure:

- Servo motor too weak
- Geometry of the lower release arm locks the system too tight.
- Angle of attack is not entirely 90 degrees.

Mitigation:

- Get a stronger servo motor
- Change the geometry of the release arm



Figure 3: Filed release arm (left) and original

Based on **attempt 7#** we found that the angle had minimal effect

Last attempt showed that the edge on the lower release arm was too sharp and therefore caused a lot of resistance. By filing this down it reduced the friction and the servo was able to rotate the release under a load of 245.25N with no problems. We conducted no further tests, but it's possible that the system can be activated with an even higher load. In addition we added a spacer that made sure that the servo arm did not crash into any other parts. Note that the system was still able to be mechanically locked when the load was applied.

Conclusion:

The system was successfully able to function under a load greater than 133.4N (weight of the rocket) and to be locked when the load was applied. **Note that the weight of the aft is inconsistent with the weight given in [Appendix I *system data appendix*]. The aft is actually lighter than approximated. This will only provide us with a higher safety margin.**

Pressure test 3

Date: dd/mm/yyyy

2	4	0	4	2	0	2	1
---	---	---	---	---	---	---	---

Purpose:

This was a pre-test with the purpose of testing the test set-up to validate the shear strength of the shear screws. Note that nylon shear screws of unknown origin were used in this test.

Signatures:

Vebjørn G. Bratlie, Johannes E. Mørkrid, Hege Grytten

Test Equipment & Set-Up Description:

- Test couplers
- Compressor
- 7x Shear screws
- PTFE-tape
- O-rings
- Test rig

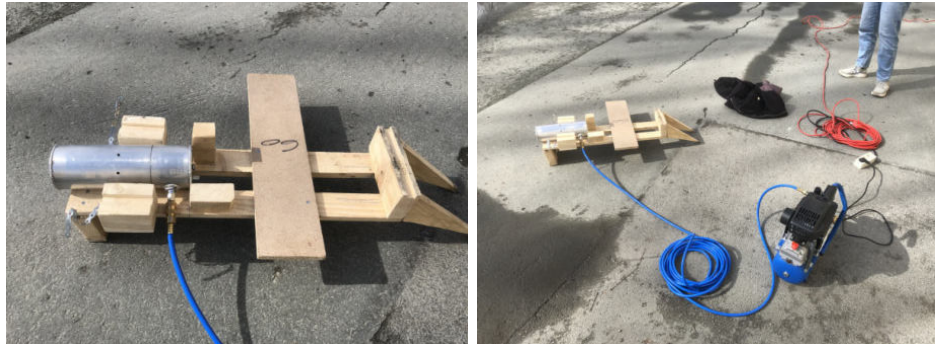


Figure 1: Test setup

Safety concerns:

Due to the high forces on the empty test couplers it will function as a “canon”, therefore everyone should keep a safe distance to the couplers, and not stand in front of the set up.

Test Criteria:

Pass criteria	Fail/Success
Withstand pressure of 1.76 bar	Success
Measure pressure the shear screws withstands (Reason: High variety of shear strength for nylon)	Success

screws)

Test Results:

Attempt #1

Built up pressure to about 1.5/1.6 bar. This pressure was too low, so it was ultimately a failed attempt, as we could not test the pass criterias.

Attempt #2

Build up pressure to 2.5 bar and result in breaking the shear screws. This was a successful test, gives an estimate of the pressure needed to break 7 shear screws. From calculations this gives the screws a combined shear strength of 1590 N and each screw a shear strength of 227 N.



Figure 2: Test measurement at burst pressure 2.5 bar

Discussion of Results:

Note that this test used nylon screws available to us at this time, and were not the ones we intend to use. Because the mechanical properties vary to a large degree this test must be repeated with the actual shear screws. And multiple tests should be conducted to get a good estimate of the shear screws ultimate tensile strength and its variance.

We expected the ultimate tensile strength of the M3x0.5 nylon screw to be between 66.2-72.4 MPa and the force needed to break them to be between 346-378 N. The test showed that the screws only had a strength of 1590 N.

One possible source of error is that there were only 7 screws used in the test and not 8 as intended. This could cause an uneven distribution of force and cause extra shear on the screws opposite to where the missing screw was supposed to be. We find this unlikely. Because the difference in actual force needed to break the shear screws and the expected force was very large.

Therefore we believe that the shear screws were of another type than we first expected. From matweb.com we found a type of shear screw that could fit our measurements[20]. This screw type has a tensile strength

range from 45-200MPa.

Another source of error could be aging. The screws have been laying in a closet for over a year. As a result, they have a reduction in strength.

Conclusion:

We cannot conclude which type of shear screw we have, we can only know that these screws have a tensile strength of 49 MPa. More tests are needed to compute an average tensile strength for these screws. Still these screws pass the test of withstanding a pressure of 1.76 bar. And because they break at 2.5 bar, CO₂ canisters of size 25g, 33g and 45g will suffice to break the shear pins(see appendix V.I *pressure calculations*), according to this test.

Note that this test must be repeated with the actual shear screws when they arrive.



Pressure test 4

Date: dd/mm/yyyy

2	5	0	8	2	0	2	1
---	---	---	---	---	---	---	---

Purpose:

This was a test with the purpose of testing the shear strength of the shear screws that will be used in the rocket. Another purpose was to test the consistency of the shear strength to validate them.

Signature(s):

Vebjørn G. Bratlie, Johannes E. Mørkrid, Kristian Hope, Ane Morkemo, Ola Flaata, Svein J. Husa

Test Equipment & Set-Up Description:

- Compressor
- Test rig
- Test couplers
- O-ring
- 8 x Shear screws wrapped in PTFE tape
- Safety goggles and headset



As-Ran Test Procedure:

Checked that the valve was closed and the hose was at atmospheric pressure before connecting the hose to the test coupler nipple. After this we video recorded the manometer while slowly opening the valve until the shear screws sheared.

Safety concerns:

An aluminum part will fly with a high velocity. Mitigated by making sure the area in front is cleared before the test is conducted. Also making sure that no one was standing behind the test set up.

The separation will cause a lot of noise, Mitigated by using headphones and earplugs.

Parts of nylon screws can spread and hit the eyes of the test participants. Mitigated by using safety goggles

Test Criteria:

Pass criteria	Fail/Success
Withstand pressure of 1.32 bar (double of pressure gradient expected at apogee in Portugal)	Success
Measure pressure the shear screws withstands (Reason: High variety of shear strength for nylon screws)	Success
Consistent shear strength	Success

Test Results:

Attempt #1



Measured 2.5 bar

Attempt #2



Measured 2.5 bar

Attempt #3



Measured 2.7 bar

Discussion of Results:

The test showed a consistent result of 2.5 bar. On the last attempt we built the pressure up more rapidly. This can explain the deviation of 0.2 bar.

The build up pressure of 2.5 bar resulted in breaking the shear screws. This was a successful test and gives an estimate of the pressure needed to break 8 shear screws. From calculations this gives the screws a combined shear strength of 1590 N and each screw a shear strength of approximately 198 N.

We expected the ultimate tensile strength of the M3x0.5 nylon screw to be between 66.2-72.4 MPa and the force needed to break them to be between 346-378 N. The test showed that the screws only had a combined strength of 1590 N. The lack of strength could be caused by uneven shearing. By this we mean that the shear screws are sheared one by one, or four by four, rather than all at once.

Conclusion:

We expected the shear strength to be larger than the first test we conducted on April 24th 2021, but the shear strength was the same this time around. The reason we expected a larger strength was because we used 7 shear screws back then, and this time we used 8 shear screws. So either the shear screws are weaker than the first pair we used, or there is no difference between using 7 than 8 shear screws due to uneven shearing.

Still these screws passed the test of withstanding a pressure of 1.76 bar. And because they break at 2.5 bar, CO₂ canisters of size 25g, 33g and 45g will suffice to break the shear pins(see appendix V.I *pressure calculations*), according to this test. And they can proceed to be used in the rocket and the drop test.

2	2	0	3	2	0	2	1
---	---	---	---	---	---	---	---

Purpose:

Want to measure the pressure to verify the pressure calculation, as well as to calculate the force. Also want to test out the Hawk system and see if the shear screws break uniformly.

Signatures:

Vebjørn G. Bratlie, Johannes E. Mørkrid and Hege Grytten

Test Equipment & Set-Up Description:

- Manometer: Keller LEO2
- 8 M3 shear screws
- NBR o-ring, 90mmx2mm
- Test aluminum couplers: ID 90mm, OD 100mm, height: 200mm
- Hawk system with 25g CO2 canisters and safety pin
- Launch rack and safety blockage
- Cameras



Figure 1: Test setup

Safety concerns:

Due to the high forces on the empty test couplers it will function as a “canon”, therefore everyone should keep a safe distance to the couplers, and not stand in front of the set up. The Hawk has a loaded spring, so use the safety pin when loading the system with CO₂. Do not arm the system until just before firing.

Test Criteria:

Pass criteria	Fail/Success
Successful separation	Success
Shear all shear screws	Success
Measure pressure	Fail

Test Results:

Attempt	Successful separation	Sheared all shear screws	Measured pressure
1	Success	Success	No reading
2	Success	Success	No reading
3	Success	Success	2.6 bar

Discussion of Results:

All three attempts had successful separation where all the shear screws sheared uniformly see Figure 2. Unfortunately the manometer did not give a reading of the pressure in the first two attempts. From the manual we read that the manometer measures pressure only twice per second, which we did not know when conducting the test.

Using Van der Waals equation we found that the expected pressure was going to be 9.8 bar, in this scenario , while the LEO2 [19] measured a pressure of 2.6 bar. We believe this difference is due to inaccurate readings from the manometer. When reviewing the videos we find that there was a delay in the manometers readings. Since the pressure varies so rapidly we believe that the manometer didn't catch the highest pressure experienced.

The calculated force needed to break the shear screws is 2680 N [Appendix 8 *Shear screw calculations*]. While with 2.6 bars we only get 1650 N. Using Tracker [21] and the impulse force equation $F = m \frac{\Delta v}{\Delta t}$, a force of 2332.8N was calculated. With m = 405g, Δt = 1/240s and Δt = 24m/s. This a more reasonable force, and errors in the tracking could be the reason for the force being lower than expected.

Other observations:

The material experienced a slight deformation. See Figure 3.

Conclusion:

Since the measurements were unreliable, there is no way to verify the pressure calculations. Thus, the pressure test was ultimately a failed test. However, on the good side it seems the canisters packs a punch, and we got 3 successful separations. As mentioned, the manometer had a 2Hz sample rate, which was too slow to get a good reading.. This can be solved with a manual manometer.

The separation was much more powerful than anticipated, so next time use goggles and earplugs to avoid shrapnels and hearing loss.

Figures:



Figure 2: Shear screws sheared



Figure 3: Deformation of the test coupler after impact

THIS PAGE INTENTIONALLY LEFT BLANK

THIS PAGE INTENTIONALLY LEFT BLANK



Avionics test flight - Andøya Space Center

Date: dd/mm/yyyy

1	1	0	8	2	0	2	1
---	---	---	---	---	---	---	---

Purpose:

The purpose of this test was to determine if the avionics would reliably retrieve and store sensor data to be used in finalizing the kalman filter, and then use this to send the correct signals for the drogue and main chute deployment. In addition, we wanted to test if we could track the rocket during the flight using the COTS GPS.

Signature:

Anders I. Hestad, Ane K. H. Morkemo, Kristian Hope and Andreas Fanebust

Test Equipment & Set-Up Description:

- Sensor board PCB
- Main board PCB
- Featherweight GPS and tracker
- Battery for GPS module
- Main battery
- Wires
- Duct tape
- 2U CanSat rocket with parachutes & motor ([Cesaroni Pro38-6G](#))
- Parachute for our payload
- Other launch equipment and services provided by Andøya Space



Figure 1: Assembly of the rocket



Figure 2: The payload

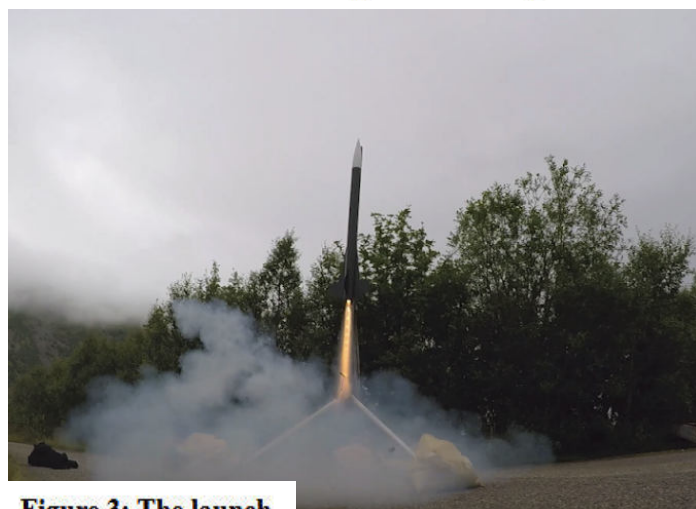


Figure 3: The launch

As-Ran Test Procedure:

We assembled the avionics payload and covered it in duct tape to make it as water-proof as possible, attached the parachute and turned on the power. We waited for the buzzer to signal that the SD-card had been successfully initialized, and that the program had started, and for the embedded GPS to get a fix, before inserting our system into the rocket. We also waited for the COTS GPS to connect. From then on, the professionals at Andøya Space Center (ASC) were in charge of the actual launch, flight and retrieval of the payload.

Safety concerns:

Due to the risk of an anomaly with the rocket motors, a large safety perimeter should be set around the launch pad and the possible trajectory for the rocket. The safety of both the Propulse team and the general public was handled by the professionals at ASC, which minimized the potential risk. Every safety regulation from ASC should naturally be followed.

Test Criteria:

Pass criteria	Fail/Success
FSM state switched to “Powered” at liftoff	Success
FSM state switched to “Coast” after engine burnout	Success
FSM state switched to “Drogue” at apogee	OK
FSM state switched to “Main Chute” at 500m	Success
FSM state switched to “Retrieval” shortly after landing	Fail
Able to receive FeatherWeight GPS coordinates during descent	Success
Successfully store and retrieve sensor data and flight computer state on a micro SD-card	Success

Test Results:

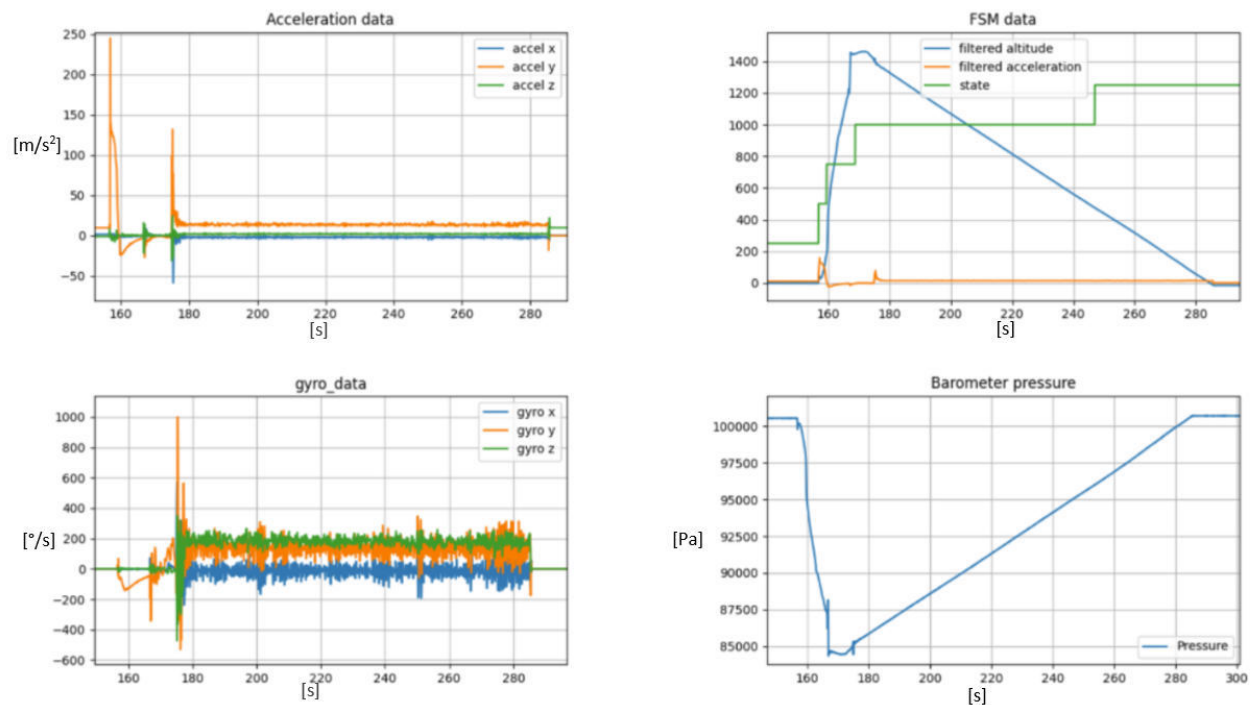


Figure 4: Graphs of data from the accelerometer and gyroscope, and barometric height and y-axis acceleration against a visual representation of the change in FSM state.

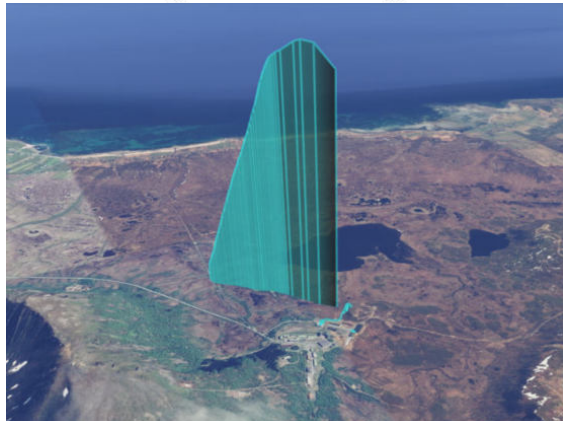


Figure 5: Data from the COTS GPS plotted in Google Earth. Apogee was at 1460 meters.

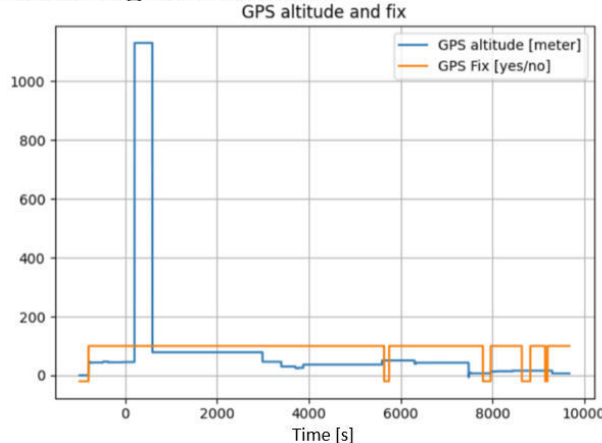


Figure 6: Altitude data from the embedded GPS, and whether it had a fix or not.

The ASC spotter team successfully recovered the payload in excellent condition. The spotter team was assisted by the featherweight GPS data and the continuous sound from the buzzer. The 25MB large data file was recovered from the SD card as expected without any issue with corruption of the data.

Discussion of Results:

The finite state machine performed nearly as intended, by changing to most states at the right time. There were two exceptions to this; the apogee detection and the (non-critical) last state transition. The software assumed that the spike/anomaly in pressure at 167 seconds in *Figure 4* was apogee, causing the somewhat (100-200 m early) early change in state, and the landing algorithm didn't work as expected. This is useful knowledge for choosing the right thresholds for transitioning between states for Stetind.

In addition, the sensor data that was successfully stored on the SD-card will help with tuning the kalman filter. The polling of data was slower than we had initially hoped, with the program on the sensor board mainly running at about 20Hz. For this reason, we chose to only use one IMU and barometer to have a faster polling rate rather than more redundancy with three of each. We will work on improving this.

The GPS on the sensor board did not function as expected, as can be seen in *Figure 4*. It had an extremely low update frequency, even though it had a fix during the entire flight. This is not something we have noticed before, so further investigation is required to determine whether it was caused by hardware limitations or a software issue. However, the COTS GPS worked exactly as expected; losing connection during the high acceleration after launch, and reconnecting closer to apogee. This is good to know, as it never managed to reconnect during the first Kvik Launch test.

Conclusion:

In conclusion, the test went exactly as well as one could have hoped for. Bugs with the GPS and a FSM transition were discovered, but they did not affect the rest of the system in any major negative way. This resulted in a test where both issues were discovered in addition to validating most of our FSM.



KL1 - small scale rocket launch

Date: dd/mm/yyyy

1	4	0	2	2	0	2	1
---	---	---	---	---	---	---	---

Purpose:

Test software of the avionics system by launching it as a payload on a small rocket; See if the FSM performs as expected, test software for reading sensor data and checking their performance, test SD-card storing software and see if vibrations cause problems, software performance, and lastly use the COTS GPS tracker to give us experience operating it.

Signatures:

Anders Hestad, William R. Schmidt, Kristian Hope, Ane Morkemo, Andreas Fanebust, Svein J. Husa and Sheikha Al-Nasser, Ola Flaata

Test Equipment & Set-Up Description:

Location was at a quite open area, a golf course, with some benches nearby which we used to assemble the rocket. The rocket was a small cardboard rocket with plastic nose tip and fins, it used 6 small rocket engines. Expected apogee was at ~400 meters.

The software was running on a stm32 blue pill prototyping board, this uses the same microcontroller as the final design will. The different sensors (ms5611 barometer, BMI088 IMU), sd card adapters, psu and UART to usb adapter were all mounted together on two prototyping boards connected by some wires.



Figure 1: Preparing for test launch



Figure 2: At launch site doing final preparations

Safety concerns:

There will be other people at the golf course which could get hit by the rocket, the rocket could also hit property nearby. This is mitigated by launching the rocket as far from houses and other people as possible, also keeping in mind the power and direction of the wind. Additionally we will have people responsible for warning nearby people to make sure everyone is aware of the launch.

Test Criteria: *Describe shortly what the test is supposed to determine, i.e. what would constitute success and failure.*

Pass criteria	Fail/Success
FSM passes through all states	Success
Sensordata is collected and saved on the SD card	Success
COTS gps successfully operated	Partial Success

Test Results:

The rocket launched nominally and reached an apogee of 360 meters, but the charge in the motor which deploys the parachute fired early making the parachute not deploy properly. The rocket then got dragged by the wind and landed in a tree. This is shown in figure 5.

Once the rocket was recovered it was still running, and sensor data was collected from the sd card successfully. The data is shown in figure 3.

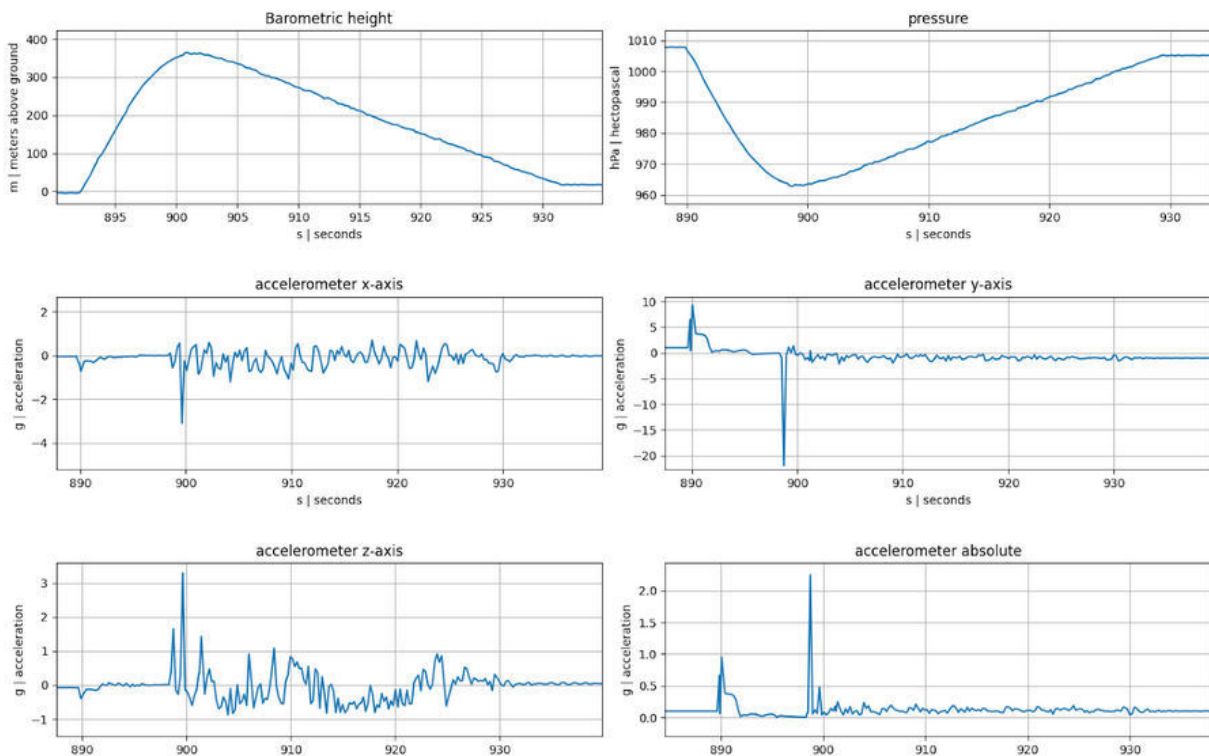


Figure 3: Successfully stored sensor data

The COTS GPS was tracking properly before launch, during launch it lost connection, and it was regained once the rocket “landed” in the tree.

Discussion of Results:

Although the flight/landing of the rocket wasn't ideal it was sufficient for testing the software. The recovered data showed that the FSM passed through all states, although there was an issue discovered. The final state, “landed”, was programmed to get triggered once the rocket reached a calculated height of ~0 meters, but since the rocket landed in a tree it did not reach a height of 0 meters until it was recovered, meaning it switched to the last state ~30 minutes after it initially landed.

This issue needs to be fixed by changing the transition function.

Sd-card saved nearly all data flawlessly, only 4 of about 16000 lines of data was damaged to some degree. Other than this another issue was the speed at which data was saved, sensordata data was collected at about 4Hz. This was found to be because data was written to UART at a far lower speed than what was possible, fixing just this increased sampling rate to about 16Hz.

The reason for the COTS GPS tracker losing connection during launch is unknown, and although we didn't receive any flight data from the GPS because of this, it's not a big issue as we were able to track the rocket as it landed, which is the main goal of the tracker.

Conclusion:

The test was a success, general functionality of the software was successfully validated, and weaknesses in the software were detected. SD-card storage worked and was satisfactory. COTS GPS tracker operation was rehearsed and performed its main function successfully.

Figures:



Figure 4: Loading the rocket

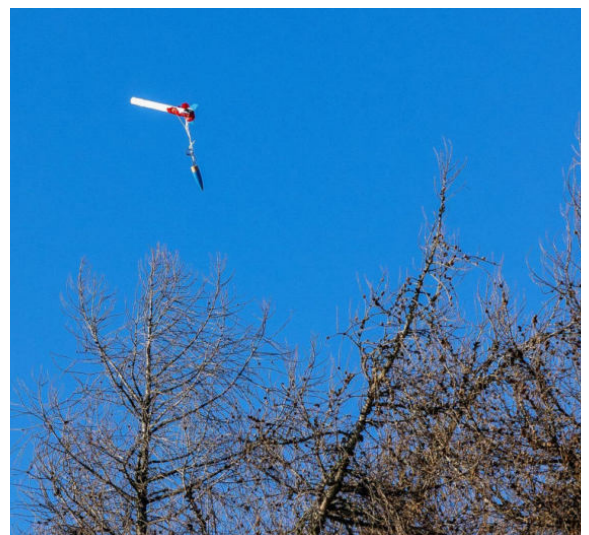


Figure 5: Faulty deployment and tree crash



Figure 5: Rocket launch



Figure 6: Kvikk lunsj(launch) is the testname and a norwegian chocolate

ADDITIONAL TESTS THAT ARE NOT SPECIFIED BY THE IREC DESIGN, TEST &
EVALUATION GUIDE

Integration test 1



Date: dd/mm/yyyy

2	4	0	1	2	0	2	1
---	---	---	---	---	---	---	---

Purpose:

The purpose of this test is to detect flaws and areas of improvement for our current rocket design.

Signatures:

Vebjørn G. Bratlie, Anders Hestad, Ask H. Hovik, Erik F. Trydal, Simen F. Flo, Peder Nervik

Test Equipment & Set-Up Description:

Actual components along with 3D-printed replicas of components were used to perform this test. The test followed the procedure described in a preliminary assembly checklist. The setup is shown in figure 1.

Safety concerns:

N/A

Test Criteria:

Pass criteria	Fail/Success
Detect flaws in our current design	Success
Detect sources of possible error and areas of possible errors and areas of improvement	Success
All components successfully integrated	Fail

Test Results:

Alteration in assembly method:

1. Avionics mount needs to be assembled with its components before assembled to the threaded rod above payload.

2. Assemble hawk bay, components on lower threaded rods, before connecting the rods to the recovery plate. (**Image 3**)

Design Flaws:

1. The server arm has no room to move because it crashed with the hawk mount. (**Image 4**)
2. Hawk pipe crashes with hawk mount (**Image 5**)
3. Hawk plate hole is too close to edge (**Image 6**)

4. Screws are not flush with the middle nose tip. (**Image 7**)
5. The servo arm crashes in the threaded rod (**Image 8**).
6. Gap between Hawk plate and terminal block plate. (**Image 9**)
7. Hawk plates are not flush. (**Image 10**)
8. Altimax too tight (**Image 11**)
9. Wires around hawk bay were too tight. (**Image 3**)
10. Main chute release looks like it won't function as wanted.
11. Hard to get the upper threaded rod threaded through the nose tip.
12. Payload do not rest on the threaded rods (**Image 12**)
13. The recovery plate did not fit inside the assembly.
14. Avionics mounting seems weak, does not have the right holes and is hard to assemble.
15. Need sufficient space between mounting plates and electronics. (**Image 13**)

Other discoveries:

1. "(Countersink bore) Can be useful"
2. Buy new boxes to organize screws, bolts and nuts for assembly.
3. Considering moving down the altimax under payload in order to redesign the avionics bay.
4. The payload casing needs rounded edges. Inform Orbit.

Discussion of Results:

Alteration in assembly method:

1. The test showed that it was more convenient to assemble the avionics mount with the electronics before assembling it to the threaded rod.
2. The same goes for the hawk bay.

Design flaws:

1. The hawk mount must be redesigned to be able to function properly.
2. Hawk mount must be redesigned so the pipe can be mounted to the hawk.
3. Hawk mount must be redesigned because the marked hole is too close to the edge.
4. Middle nose tip needs more screw depth to screw in order to make the upper nose tip flush with the middle nose tip.
5. Buy a shorter servo arm or make one ourselves in order to make it move past the threaded rod.
6. Redesign to eliminate gap between hawk plate and terminal block plate.
7. Design holes in the hawk plate on each side to stabilize and make them flush.
8. Locate the altimax at a different location.
9. Route the wires on the inside of the hawk bay instead of outside.
10. Main chute release system needs to be redesigned with a leading rod, otherwise the release arm is in danger of being activated. See other alternatives for placement of turning point for release arm, how to activate the release arm and casing.
11. Funnel shape lower nose tip to guide the upper threaded rod in the nose cone hole.
12. Use long nuts on the 4 threaded rods to let the payload rest at det for threaded rods.
13. Could be caused by inaccurate 3D-printing. Go over the recovery plate and make sure to have the right tolerances and dimensions.
14. Upper avionics mount need to be redesigned. The test showed it hard to assemble with the other components. The construction seems also to be too weak.
15. Use plastic stand-offs, 9-8mm, to get the right spacing between electronics and their mounting plates. Especially the PCBs.

Other:

The test showed there was enough room for a 120" parachute tightly packed. Therefore a 96" chute should fit just fine.

We had some lack of material and components. For example we did not have all the screws. Therefore some components couldn't be mounted properly. In addition, several parts missed the right holes to fasten them. The rocket was not fully up to date as the design is now due to alterations that have been made the past week. For example placement and integration of o-rings couldn't be tested because it was not taken into account in the 3D-printed part. And the desired o-rings were not yet acquired.

Conclusion:

We became aware of many issues with our current design. We can therefore now fix them. Some parts were not ready for the integration test. These parts must be worked on and made ready for the next integration test. The 120" parachute has enough room meaning a 96" will also fit.

Figures:



Figure 1: Component overview



Figure 2: Avionics mount on threaded rod



Figure 3: Hawk bay assembly



Figure 4: Servo arm crashing in hawk mount



Figure 5: Pipe crashing in hawk plate



Figure 6: Hawk mount



Figure 7: Counter sunk screws is not flush with middle nose tip

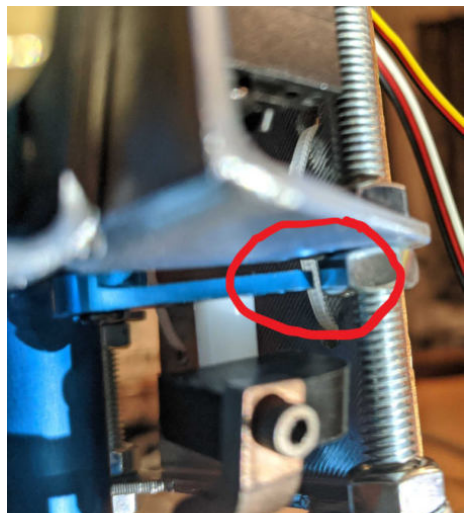


Figure 8: Servo arm crashes in nut on threaded rod



Figure 9: Gap betweent hawk plate and terminal block plate



Figure 10: Hawk plates not flush



Figure 11: Altimax to close to rocket body

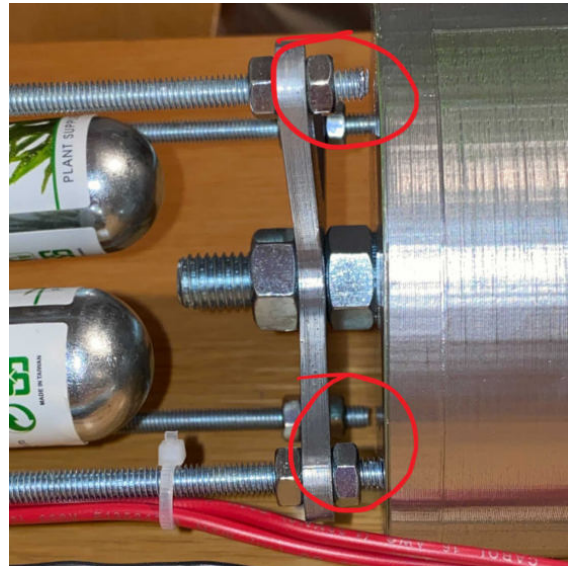


Figure 12: Threaded rods not in flush with payload casing



Figure 13: Plastic standoffs



Figure 14: Assembled rocket body

Integration test 2

Date: dd/mm/yyyy

0	7	0	3	2	0	2	1
---	---	---	---	---	---	---	---

Purpose:

The purpose of this test is to detect flaws and areas of improvement for our current rocket design with emphasis on flaws from the previous integration test.

Signatures:

Vebjørn G. Bratlie, Ask H. Hovik, Anders Hestad, Simen F. Flo, Peder Nervik, Hege Grytten, Steven Xu, Cecilie A. Olsnes, Johannes Mørkrid

Test Equipment & Set-Up Description:

Actual components along with 3D-printed replicas of components were used to perform this test. The test followed the procedure described in the assembly checklist with the setup as shown in figure 18.

Safety concerns:

N/A

Test Criteria:

Pass criteria	Fail/Success
Detect flaws in our current design	Success
Detect sources of possible error and areas of possible errors and areas of improvement	Success
All components successfully integrated	Fail

Test Results:

Alteration in assembly method:

1. Added a M3 hole to the hawk plates

Design Flaws:

1. Video encoder housing did not fit (**Figure 3**)
2. COTS GPS battery did not fit its casing(**Figure 4**)
3. COTS GPS battery sticks out of casing (**Figure 5**)
4. Black box casing missing(**Figure 6**)
5. Nuts in avionics mount is touching components (**Figure 7**)

- 6. Cables between main board and sensor board need to pass around payload bulkhead (**Figure 8 & Figure 9**)
- 7. Holes to mount the hawk plate are not align with actual hawk or the servo motor (**Figure 10**)
- 8. Mainboard might not fit under the payload (**Figure 11**)
- 9. Radionor antennas crashes in avionics mount (**Figure 12**)
- 10. Nuts crashes with camera mount

Other:

- 1. Radionor card uses 2.5mm screws 1922
- 2. Camera mount are thin around the threaded rods
- 3. Some of the 3D printed parts became hard to assemble due to expanding under production

Discussion of Results: *the real environnement.*

Alteration in assembly method:

- 1. Additional holes were added to the hawk plates to keep it flush

Design flaws:

- 1. Change design on 3D-print.
- 2. Change design on 3D-print.
- 3. Change design on 3D-print.
- 4. Make black box casing using epoxy
- 5. Move the battery mount 2 mm away from the threaded rod. Just make sure this component does not crash with the Radionor antenna.
- 6. Redesign bulkheads with bigger openings for the cables .
- 7. Relocate the mounting points for the hawk to align properly.
- 8. Move the location of the hawks down and payload along with the upper threaded closer in relation to the nose tip
- 9. Add bolts to move antennas further from the avionics mount.
- 10. Remove the two nuts, they are redundant.

Other:

The integration test showed design flaws at the recovery bay and bulkheads. In addition the 3D-prints can be further sliced with thermal expansion during printing in mind as it reduced the effectiveness of assembly.

Conclusion:

The team became more informed of the elements that work, as well of the issues of the current structure. Most of the changes will be restructuring of the placement of the inner structure, but also design changes with bulkheads and mounting points . We will also resize future 3D-prints to compensate for thermal expansion of the material.

Figures:



Figure 1: Test setup



Figure 2: Finished rocket



Figure 3: Video encoder atop of its casing

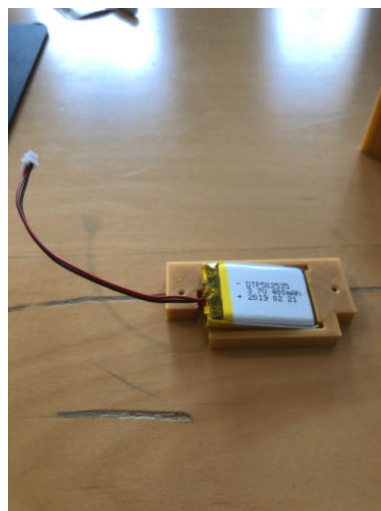


Figure 4: Battery is too big for its casing

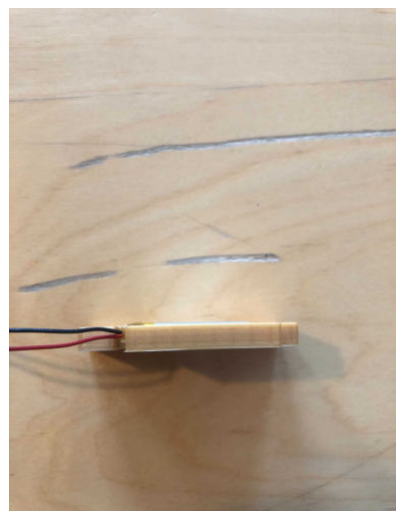


Figure 5: Battery is sticking out of the casing



Figure 6 : No existing blackbox

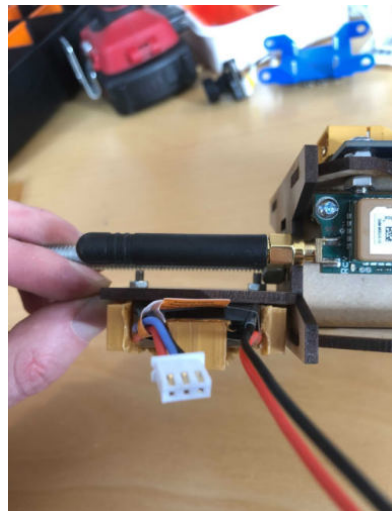


Figure 7: Components crashing with nuts

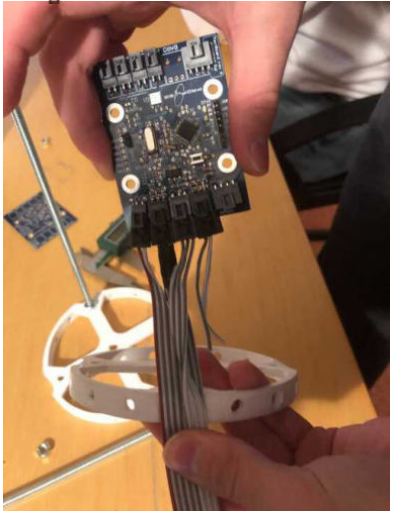


Figure 8: Cables to wide for bulkhead

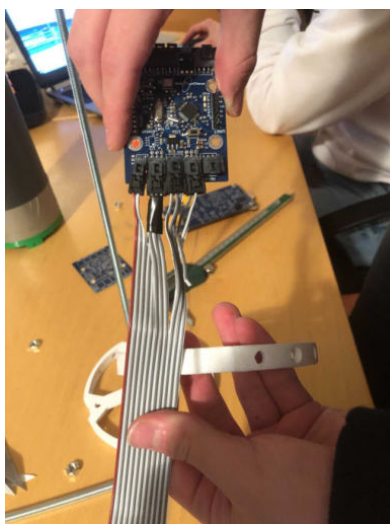


Figure 9: The bulkhead needs to pass 18 cables

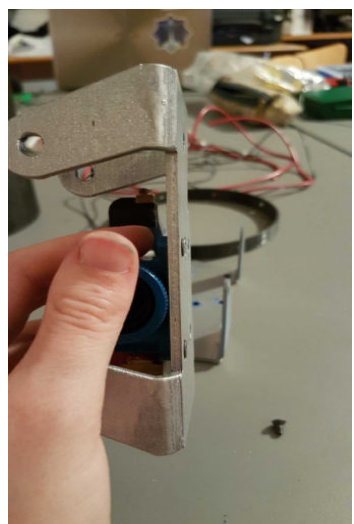


Figure 10: 3D-printed hawk plate not fitting



Figure 11 : Mainboard not fitting because of CO2 canisters



Figure 12: Antennas too close avionics mount on right hand side

Additional tests yet to be performed

The following tests will be performed before the 4. october.

Test name	Description	Goal with test
Drop test	Drop a qualification model from a target height to simulate flight after apogee.	Test the avionic system together with the mechanical system in a realistic environment in order to validate the rocket's functions.
Avionics vacuum chamber test	Place the avionics system inside a vacuum chamber and decrease the pressure to about 0.8 bar (expected pressure at 10 000 meter)	Make sure sensors are capable of accurately measuring pressure at high altitude.
Final assembly test	Do a full scale assembly test using flight hardware.	Check that all components fit together as intended, and that assembly is feasible.

Test for Payload



Satellite definition

In this document, the rocket's payload is referred to as the satellite and the payload's experiment referred to as the satellite's payload. The reason for this is that the Sub-Orbital team views the experiment as a sub-payload, and this is to avoid confusion between the rocket's payload and the satellite's payload.

Overview:

Magnet interference test

Leakage test

Black Box test

G-force test

Magnet interference test

Test ID: SOT-TR-003-MIT Magnet interference test	
Responsible: Fredrik Fossan-Waage	Test date: 2021-03-13
Report Authors: Fredrik Fossan-Waage	
Attending: Sven Amberg, Fredrik Fossan-Waage	
Purpose of test: Verify that the magnet field does not cause disturbance to the signal in the cables that go between the rocket's systems.	
Test summary: Good. No disturbance was observed.	
Result summary: No disturbance observed.	
Test conclusion: Safe to keep the magnets in the payload section.	
Issues and weaknesses with the test:	

1. Introduction

The purpose of this test is to verify that the magnetic field from the magnets does not cause any disturbance to the cables that will be outside the satellite. These cables run from the rocket's avionics, and if there is any disturbance in these cables, it may cause fatal error.

2. Method

2.1.1 Equipment

- Analog Discovery 2
- Waveforms on PC
- Cables
- Magnets
 - 2 x 2.3 kg strength
 - 2 x 1.5 kg strength
 - 2 x 3.9 kg strength

These magnets were used, because we will not use any more magnets than these in the satellite. Therefore, the magnet field that was tested with will be the upper limit for the strength of the field that will be used in the satellite.

2.1.2 Setup

- Using the Analog Discovery 2 and the Waveforms program to produce different signals and sending them through wires with the wavegen option.
- Measuring the signal from the wire with the scope option in Waveforms and Analog Discovery 2.
- Placing the wire next to the magnets, next to the metal casing with magnets.

2.2 Which tests are conducted?

2.2.1 Test #1

Test description:	Test: Run cables across the outside of the cylindrical frame while the magnets are placed in the payload section. Verify that the magnet field does not cause disturbance to the signal in the cables.
Test rationale:	Verify that the magnet field does not cause disturbance to the signal in the cables.
What are we looking for:	No disturbance.
How is data measured:	With Analog Discovery 2 and Waveshare. Using the scope program.

3. Procedure

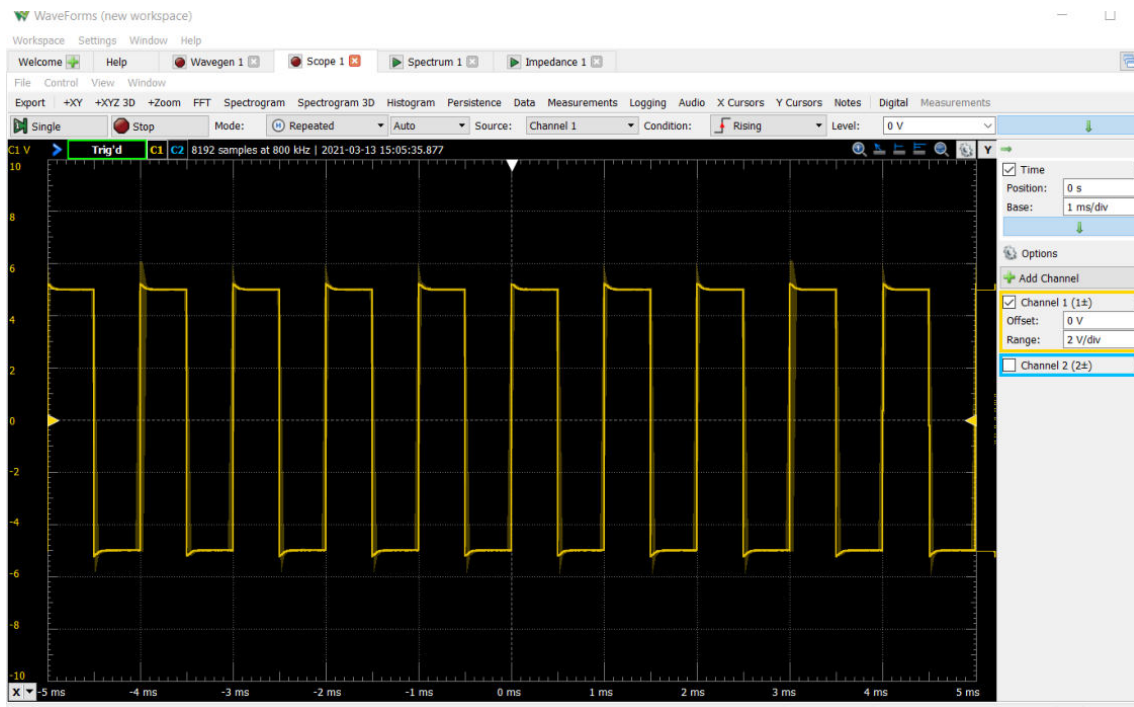
Step	Description	Comments
1	Set up Analog Discovery 2 Digilent and	

	Waveshare	
2	Place magnets in the payload section of the satellite.	
3	Run cables on the outside of the cylinder and look for disturbance on the signal.	

4. Results



This picture shows the signal in. A normal square pulse. 1kHz and Amp 5V.



This picture shows the signal reading in after it has gone next to the satellite outer cylinder. The pulse is unchanged. Continuous observation with movement of the cable and magnets did not create any changes in the readings with the scope option.

5. Conclusion

The magnet field from the magnets that will be used in the field on the satellite will not be stronger than the one tested with in this test. Since the field did not disturb the cables, it is safe to have them in the payload of the satellite.

Leakage test

Test ID: SOT-TR-006-LE. Leakage test report	
Responsible: Fredrik Fossan-Waage	Test date: 2021-03-13
Report Authors: Fredrik Fossan-Waage	
Attending: Young-In Falck, Fredrik Fossan-Waage	
Purpose of test: Verify that the mechanical structure is water resistant, or that the leakage is negligible.	
Test summary: The cylinder frame was filled completely with water, then filled with 50ml of water.	
Result summary: Leaked noticeably when filled completely with water, but nothing when filled with 50ml.	

Test conclusion: The amount of fluid is very small, and the fluid smears itself out on the surface inside of the cylinder. Therefore it will smear itself out instead of leaking out. The mechanical design is waterproof enough.

Issues and weaknesses with the test:	
---	--

1. Introduction

The ferrofluid experiment must not leak and disturb the rocket's electronics. The fluid will be contained in a separate box, which in itself shall be watertight. However, if it leaks, it should not leak out of the satellite. Therefore we want to test how the satellite frame handles leaks. The test was done with the screwable lid mounted on the bottom.

2. Method

2.1 Which tests are conducted?

2.1 Test #1

Test description:	Test: Fill the cylinder completely with water and see if it leaks.
Test rationale:	Filling it with water simulates pressure from the fluid if it leaks during 15g.
What are we looking for:	As little leakage as possible.
How is data measured:	Visually and measure the amount of water.

2.2 Test #2

Test description:	Test: Fill the cylinder with 50ml and test the leakage
Test rationale:	This is closer to the realistic amount of ferrofluid that is going to be used.
What are we looking for:	As little leakage as possible.
How is data measured:	Visually.

2.3 Test #3

Test description:	Test: See how a small amount of ferrofluid behaves freely in the cylinder
Test rationale:	We want to see how freely moving ferrofluid behaves in the cylinder, and test if it sticks to the inside of the cylinder.
What are we looking for:	See how ferrofluid behaves.
How is data measured:	Visually.

3. Procedure

Step	Description	Comments
1	Fill the cylinder completely.	
2	Fill the cylinder with 50ml.	
3	Apply a few drops of ferrofluid on the bottom lid of the cylinder.	

4. Results

4.1 Test #1

The bottom leaked approximately 100ml in the span of 2 minutes. This is more than expected, and should ideally be less. However, this was done with very much more fluid than what is actually going to be used.

4.2 Test #2

No leak. With this amount of fluid, the fluid level was not high enough to go above the overlap of the lid.

4.3 Test #3

The ferrofluid smeared across the surface, and moved slowly when the lid was rotated and moved around. This is because the fluid has a high viscosity.



5. Conclusion

Because of the ferrofluid's high viscosity, it smears across the bottom, and moves slowly. Also since there is a low amount of fluid, we are certain that it will not leak outside of the cylinder. This is because the section of the cylinder that has threading is very wide, there is no possibility that the fluid leaks out without, because the fluid smears itself through the threading, and there will be no fluid left to leak out.

In addition, the magnet itself will also assist in keeping the fluid inside of the satellite by holding it down.

Based on this, the satellite is watertight enough.

Black Box test

Test ID: SOTR-TR-055-BB	
Black box test	
Responsible: Fredrik Fossan-Waage	Test date: 2021-03-15
Report Authors: Fredrik Fossan-Waage	
Attending: Sven Amberg, Young-In Falck, Fredrik Fossan-Waage	
Purpose of test: Give and indication on how well the black box handles impact and external force.	
Test summary: The black box was dropped from the fifth floor and smashed with a sledge.	
Result summary: The SD-card withstood both tests	
Test conclusion: The SD-card will be protected by the black box to a degree, although how much is not exact.	
Issues and weaknesses with the test:	The exact amount of force applied is uncertain. It is not possible to test the black box for forces that equal the forces during a rocket crash.

1. Introduction

The black box is a steel container that is designed to protect the SD-card from external forces. This test is meant to give us some indication on how strong it is. We do not have the tools or facilities to test the black box for the exact amount of force applied in a rocket crash, but we still wanted to conduct this test to give us a general estimate.

2. Method

2.1 Which tests are conducted?

2.1.1 Test #1

Test description:	Test: Drop the box from the fifth floor.
Test rationale:	This was the highest point we were able to drop the box from.
What are we looking for:	No harm to the SD-card.
How is data measured:	Data on Sd-card is retrievable.

2.1.2 Test #2

Test description:	Test: Smash the box with a sledge.
Test rationale:	This was the largest amount of force we were able to apply to the box.
What are we looking for:	No harm to the SD-card.
How is data measured:	Data on Sd-card is retrievable.

3. Results

3.1 Test #1

The black box was unharmed after the drop. The SD-card was not examined, since this would take more time, because we would have to reapply foam and let it harden.

3.2 Test #2

The largest wall was bent in and the lid was bent back. The welding points broke. SD-card was unharmed. Two images and a text file stored on the card were unaltered.



Before and after.

4. Conclusion

This test is not exact enough to give any hard evidence that the black box will withstand the forces from the impact. However, it makes us more certain that the SD-card will survive a crash landing. To give additional resilience, additional welding will be done to give extra strength.

G-force test

Test ID: SOT-TR-004-GF G-force test report	
Responsible: Fredrik Fossan-Waage	Test date: 2021-03-15
Report Authors: Fredrik Fossan-Waage	
Attending: Young-In Falck, Fredrik Fossan-Waage	
Purpose of test: Verify that the mechanical structure can handle the acceleration, up to 15g.	
Test summary: Components were weighted with 20 times their own weight, to simulate the acceleration from the rocket and stress from the vibration.	
Result summary: All the components handled the weight.	
Test conclusion: All components handle the weight corresponding to the acceleration.	
Issues and weaknesses with the test:	

1. Introduction

The purpose of the test is to verify that the mechanical components can handle acceleration up to 15 g. This will be done by weighting the components with a weight that corresponds to 20 times their own weight. The reason we test with 20 times instead of 15 is because we want a safety margin, considering vibrations may cause some additional stress.

2. Method

2.1 Setup

The components that will be tested are:

- Battery support component.
- Interior wall with Raspberry Pi and SenseHat.
- Fastening points from the threaded rods to the lid.

The interior wall for the OBC and EPS will not be tested, since these components are light and their mass centers are fastened close to the wall.

Although the Raspberry Pi and SenseHat will be tested, since this component is slightly heavier than the EPS and OBC, and since the Raspberry Pi and Sense Hat will be mounted on top of each other, the mass center will be further away from the interior wall.

The fastening points will be tested, although the weight should theoretically rest on the nuts that fasten the rods to the bottom plate. However, if there is a failure during assembly, and the nuts do not touch the bottom completely, the rods have to be able to hold the weight.

No test will be done for the small battery package, because it is lighter than the large package, and has the same battery holder plate. If the large package can take the weight, so can the small.

Component	Weight of component mounted on it (grams)	Weight of component mounted on it x 20 (grams)
Battery support	90	1800
Interior wall with Raspberry Pi and SenseHat.	75	1500
Fastening points from the threaded rods to the lid.	1260	2520

2.2 Which tests are conducted?

2.2.1 Test #1

Test description:	Test: Apply weight to battery supports with weight that corresponds to 20 times the weight of 2 batteries.
Test rationale:	Verify that the supports can hold the weight of components under 16g. This is specially important for the battery holders, considering that the batteries are the heaviest components.
What are we looking for:	Battery supports can hold 2 batteries under 20 g.
How is data measured:	Visually, parts remain in place.

2.2.3 Test #2

Test description:	Test: Apply weight to the interior walls with a weight that corresponds to 20 times the weight of the Raspberry Pi and SenseHat..
Test rationale:	Verify that the walls are mechanically strong enough to hold the weight of components under 16g.
What are we looking for:	Walls can hold Raspberry Pi and SenseHat under 16g.
How is data measured:	Visually, parts remain in place.

2.2.4 Test #3

Test description:	Test: Weight the threaded rods that are fastened to the upper lid.
Test rationale:	The lid carries the weight of the inner structure. The weight is also held by the lower plate that rests against the lid, so the upper lid will not hold all the weight of the inner structure, but we will test it for the full weight for the inner structure nonetheless. This is because we want to be sure that it can hold the whole weight, in case the weight distribution is not even.
What are we looking for:	Lid can hold the weight of the inner structure under 16g.
How is data measured:	Visually.

3.5 Procedure

Step	Description	Comments
1	Calculate weight for component	
2	Weigh items to correspond weight to 20g.	
3	Place weight instantly on components, to simulate an instant increase in acceleration to 20g.	Verify that components do not move.

4. Results

4.1 Test #1

The large battery package was mounted on rods, with the battery holder plate underneath. The package held the weight.

4.2 Test #2

The Raspberry Pi and Sensehat were mounted on top of each other to a vertical wall and fastened with screws. They held the weight.

4.3 test #3

Two round horizontal plates were assembled with rods between them, with nuts on both ends. Tightening nuts were used on the lower plate, and the upper had ordinary nuts. This was done for the sake of making the time for preparing the test shorter.

The structure held 25 kg. Since it held the weight with ordinary nuts on the upper plate, it will also do so when we use tightening nuts.



Weight was added to two backpacks, and strapped onto the structure. The structure was then lifted off the ground.

6. Conclusion

The components will handle the g-force.

C. Hazard analysis

Hazard Analysis

Introduction

This appendix addresses the hazards that pose a potential danger to personnel related to material handling, pre-launch procedures, hazards in flight, and transportation and storage of propellant. Risks to mission success can be found in the Risk Assessment Appendix D.

The scale used here to indicate the risk level in this appendix consists of five levels: Very low - Low - Medium - High - Very high. Risk is the combination of perceived likelihood and consequence.

Category	Hazard	Possible cause	Initial risk	Mitigation approach	Residual risk
Material handling	Ferrofluid - will be used in the payload. Can cause eye and skin irritation. Can catch fire.	Incorrect handling	Low	Personnel will wear protective gloves and eyewear when handling the ferrofluid. The ferrofluid will only be interacted with by personnel during assembly, when it is applied to the ferrofluid container. The ferrofluid will be contained in safe storage for transport. The fluid will be kept away from any open fire.	Very low
	Magnets - will be attached to the cylinder frame in the payload. Potential pinching of fingers between the magnets and the payload.	Incorrect handling	Very low	The magnets will be kept away from the payload until the ferrofluid container is inserted, and handled with caution.	Very low

	Carbon Fiber - Can cause irritation to eye, skin, throat and nasal passages.	Incorrect handling	Low	Personnel will wear protective gloves and eyewear when handling the carbon fibre.
	CO₂-canisters - unexpected release can cause injury	Incorrect handling	Low	Canisters will be stored out of direct sunlight and away from other sources of direct heat. Will be stored in an appropriate container during transport.
	Epoxy - Can cause eye and skin irritation	Incorrect handling	Low	Personnel will wear protective gloves and eyewear when handling the epoxy
	Batteries - can explode due to close proximity with a heat source, or due to short circuiting, causing injury	Incorrect handling	Low	Will be stored dry and out of direct sunlight and away from other sources of direct heat. Will be stored in an appropriate container during transport.
	Propellant - can irritate eyes and the respiratory tract. Accidental ignition can cause serious injury	Incorrect handling	Low; higher risk due to the potential of serious injury, but the propellant is very stable and from a well known manufacturer. The probability of accidental ignition is very low	The propellant will be stored in its original packaging until assembly. The propellant will be handled according to safety guidelines, manufacturer's instructions for use, and pre launch checklist. It will not be stored with combustibles or close to heat sources that might cause an ignition.

	Microwaves - Radio transceivers emit strong electromagnetic waves around them. Being too close can cause damage to the body in different ways.	Standing too close to strong radio equipment	Low	The transceiver in the rocket has a minimum safety distance at 0.5 meters when at max power. The ground station transceiver has a minimum safety distance of 2 meters in front of the transceiver, and 0.5 meters from the other sides. By keeping the correct safety distance from this equipment personnel should be completely safe.	Very low
Pre-launch	Rocket falls off launch rail and causes injury	Launch rail was not properly assembled or is damaged	Low	Launch rail will be inspected before launch to ensure everything is secured in place and there is no damage done that might cause the rail to let go of the rocket, tilt or fall over.	Very low
		Rocket was not properly secured to launch rail	Low	The rail and rocket will be inspected to ensure that the fasteners are in working order. After fastening the rocket, there will be a last check to ensure the rocket stays in place.	Very low
	Fuel grain ignites after the igniter is installed, causing injury to personnel	Personnel fails to check propellant for cracks and damage	Low: the propellant is very stable and from a well known manufacturer. The probability of accidental ignition is very low	A routine check of the fuel grain will be done before it's inserted in the rocket.	Very low
		The propellant comes in contact with a source of heat or static		All handling of the propellant pre launch will be done according to safety guidelines, manufacturer's	

		discharges		instructions for use, and the checklist. It will not be stored with combustibles or close to heat sources that might cause an ignition.	
		Igniter is not installed correctly	Medium; the combination of the igniter and propellant pose a higher risk than the propellant by itself	Correct handling and installation of igniter while following all safety regulations	Low
	Accidental firing of the Hawks during preparations causing injury	Safety pins have not been inserted properly	Low	The Hawks are to be armed at the last moment possible to minimize the risk of it accidentally going off. Double check the safety pin by several people on the team.	Very low
Storage and transportation of propellants	Storage - potential of accidental ignition which can lead to damage on property and/or personnel		Low	Storage will be handled by the vendor until the competition, and will be delivered on site. It will be stored in its original packaging until assembly.	Very low
	Transportation - potential of accidental ignition which can lead to damage on property and/or personnel		Low	Transportation will be handled by the vendor until the competition, and will be delivered on site.	Very low
Flight	The rocket touches the ground at a higher speed than anticipated, in one or multiple	Scenarios mentioned below are further discussed in Appendix D Risk assessment.	Low	Preflight checklist ensure that: i.Joints are tight before launch. ii.Batteries powering the avionics system are fully charged before	Very low

segments, and the debris causes injury to property and/or personnel	The drogue chute is not deployed		launch.	
	The main chute is not deployed	Medium	Preflight checklist ensure that: i.Joints are tight before launch. ii.Batteries powering the avionics system are fully charged before launch.	Low
	Cords and chutes are entangled.	Medium	Wrapping the chords with the “non-tied fishtail braid” is a way to ensure a clean unraveling of the chords and minimize the risk of entanglement. Packing the chutes in a protective deployment bag. Swivel link attached to the chords to rotate alongside the rotation of the rocket.	Low
	The rocket shreds	Medium	The rocket will not be launched if there is a lot of wind. The mechanical structure is dimensioned to withstand forces at max Q and the release forces from parachutes.	Low
	Rocket strays from nominal flight path and endangers property and/or	Unstable launch rail	Medium	Launch rail and rocket will be inspected before launch to ensure everything is secured in place and there is no damage done that might
	Fins separate from rocket or flutters,	Medium		

	personell	causing the rocket to be unstable		affect the rocket's trajectory.	
		Damage to the rocket body causing instability in flight	Medium	The rocket will not be launched if there is a lot of wind.	
117	The rocket explodes during launch or close to the ground, the debris causing damage to property and/or personnel	Cracks in the propellant	Medium; higher risk due to the potential of serious damage, but the propellant and casing is from a well known manufacturer and the probability of accidental ignition is low	Visual inspection of casing and fuel grain during final assembly to ensure there is no damage.	Low
		Damage to the casing		Commercial casing and fuel grain with proven reliability, low probability of wrong installation if instructions are followed	
		Propellant breaks off in chunks during flight, blocking nozzle			
		Incorrect installation of casing and/or fuel grain			
		Motor mount failure			
		Overpressurization		Follow the instructions for motor assembly, inspect the motor casing threads for damage or wear, prior to assembly and adhere to the recommended safety distance during launch.	

D. Risk assessment

Risk Assessment

Introduction

The following sections present the completed set of risks to mission success, as well as the mitigation approaches. Severity, and failure probability after mitigation, are evaluated for every risk on a scale from one to three. The meaning behind these numbers are described in “European Rocketry Competition Rules & Requirements”, table 8 and table 9. Critical rating is the resulting product of these two evaluations. The risks are sorted according to the phases described in Section III, Mission Concept Overview. Risks that are present in multiple phases, are only described in the first phase where it occurs. Several risks are mitigated by pre-launch procedures, which are described in detail in Appendix V.E Assembly, Preflight and Launch Checklists. Risks that are related to health and safety are stated in Appendix V.C Hazard analysis.

Propulse Risk Analysis and Mitigation						
Mission Phase	Failure Mode	Possible Cause	After mitigation		Mitigation approach	Critical rating
			Mishap Severity	Failure probability		
Initial Arming	Battery overheating while waiting for the launch signal.	Excessive heating due to climate circumstances	2	1	Store batteries appropriately beforehand. Use thermal blanket to protect rocket from sunlight heating, when relevant.	2
	Loose wiring, bad connection.	Assembly mistake	3; Could result in the avionics system not being armed	1; Will most likely be able to verify this before launch	Follow the assembly checklist. Rehearse pre-launch procedures.	3
		Bad wiring			Verify connections with voltmeter.	

	Payload does not receive or respond to launch signal	Bad wiring	2; If the payload does not receive the launch signal, it will never exit idle mode, and by that never start recording any data from the experiment.	1	The cable connections will be tested by checking the resistance between them, which lowers the risk of not receiving the signal. Payload arming thoroughly tested.	2
	Arming switch circuit fails	The wires get cut due to vibrations and sharp edges when handling the rocket	3; the system connected to the circuit would fail, resulting in an abort of the launch.	1	The metal where the wires pass through is rounded, with no sharp edges.	3
	Low/no power delivered to the avionics system	PSU fails to deliver enough power	3; the avionics would malfunction, resulting in no recovery activation.	1	There is more battery capacity than needed (approximately 1 hour of max. power draw). Extensive testing of the PSU should prevent failure.	3
		Batteries are discharged			Checking the batteries and wires during assembly.	
		Bad wires				
	Loss of communication to ground station	Software error	2; Won't be able to send the arming signal, thus the radio transmitter won't turn on until	1; FSM will ensure that the avionics gets armed	FSM can jump from idle to armed if launch is detected, allowing the rocket to perform its main function, regardless of contact to ground station.	2

			powered flight. In this case the sensor data is still collected, and the FSM is working.		The sensor data is also saved on two SD cards.	
		Signal corruption due to loose/bad wires			Check wiring with voltmeter	
Final arming	The pressure separation system is released pre-launch	State detection error	3	1	Arming the hawk at the last moment	3
		Short circuit			Double check wires	
	Loss of communication with COTS GPS	Low battery charge or bad connection to GPS payloads or tracker	1; COTS system. But failure will require an abort of launch.	1	Testing systems beforehand, and making sure batteries are charged prior to launch.	1
	Payload runs out of battery	Not enough batteries, power drain is too high	3	1	The battery capacity has been tested thoroughly and power capacity is over dimensioned. It is possible to make the payload return to idle mode to save battery.	3
	Payload does not receive or respond to launch signal	Bad wiring	2; If the payload does not receive the launch signal, it will never exit idle mode, and by that never start recording any	1	The cable connections will be tested by checking the resistance between them, which lowers the risk of not receiving the signal.	2

			data from the experiment.		The logic that responds to the signal is thoroughly tested.	
Lift off	Motor (IAE.M) explodes during launch	Electronic shortage in ignition system	3; Seeing as this can be hazardous to both rocket performance and bystanders.	1; Motor is built professionally and securely and likely will not be harmed during shipping. The only chance of this happening is due to a production fail.	Follow pre-launch procedures.	3
		Production failure from Cesaroni. Motor overpressurized.				
	Failure to ignite propellant	Production failure from Cesaroni.	1; Should this hazard occur, it will not pose a serious threat. Will need time to re-arm.	1	Follow pre-launch procedures.	1
	Delay between launch and ignition “Hang fire”	Incorrect mounting of the rocket to the launch rail	1; Using the ignition system provided by Cecaroni sets this hazard down to low risk	1	Follow pre-launch procedures.	1

		Malfunctioning of the fuse				
	Motor (IAE.M) goes through the motor mount (IC.MM)	Motor mount cannot withstand forces from rocket	3; Will destroy the lower parts of the rocket (motor mount, possibly fins and lower fuselage).	1	Run FEM analyses[Appendix V.I].	3
Powered flight	Failure/breakage of forward airframe	High AoA due to wind and other aerodynamic forces	3	1	Looking at technical reports from other student rocket teams with successful flight. Comparing the thickness of our airframe with theirs. If there is too much wind, the launch will be postponed.	3
	Failure/breakage of fins	Shock wave leads to high pressure on fins	3	1	Used both screws (F 35 and F 36 [Appendix V.K]) and adhesive between fins and fin brackets, and also between fin brackets and aft airframe, for redundancy purposes.	3
	Unstable flight	Fin fluttering due to loose bolts and/or weak fibre layup	3	1	Make sure bolts are pre-strained before launch. Analysis done on fin fluttering shows that fin flutter will not occur [II.D.3.Fin fluttering].	3

	Under stable	3	1	According to simulations done in both OpenRocket, RASAero II and CFD, the SM off-rail is not under stable according to DTEG 8.3 Ascent Stability standards [II.D.2.Stability Margin].	3
	Turbulence due to the transonic region	3	1	According to simulations done in OpenRocket, the rocket spends less than 0.5 seconds in the transonic region, which means there is not much time for turbulence to generate.	3
	Reaching the eigenfrequency of the rocket	3	1	Have conducted a frequency analysis [II.D.3.Frequency analysis].	3
	Boattail starts burning	High temperature zone on the inside of the boattail due to the plume from the motor	3	Insert insulating layer of fiberglass on inside of boattail	3
	Rocket won't reach as high as anticipated	Error in calculations and simulations.	1	2; Cannot be completely certain of how different factors affect apogee. Get an estimate through previous testing and OpenRocket.	2

	Trajectory angle affected by weather circumstances					
Rods not able to withstand stress from payload	Payload mass poorly distributed or too heavy	2; Could break the rods and ruin the structure, making the rocket unstable and unsafe.	1	Calculate the forces the rods are able to withstand [Appendix V.I]	2	
Forces impacting angle of attack	Slanted rocket fins, camera placement, launch lugs, etc. affecting aerodynamic forces	2; Unsure of the weather and environmental factors to be present during the competition.	2	Scrub launch in case of bad weather.	4	
FSM transitions fail, either by happening too early, to the wrong state, or not at all, resulting in recovery activation at the wrong time.	FSM software failure	2; could result in recovery activation and release of the main chute too early, but the COTS flight computer ensures this won't happen too late.	1; Testing of all software should make this unlikely.	The COTS flight computer ensures that the recovery activation happens even if our software fails. We also test the FSM with multiple functions for changing states	2	
	Bad sensor data from barometers due to defect sensors or communication failure, giving the Kalman filter unusable data.			The three sensors with initial filtering should ensure that the Kalman filter always gets some usable data. The PCBs are also produced by reputable manufacturers, minimizing the chance of bad connections. Extensive testing of the software for		

				sensor reading should ensure we detect any mistakes.	
	Kalman filter software not working or giving wrong predictions.			Extensive testing of the software should make it possible to iron out all errors.	
Early separation, therefore early release of drogue chute	FSM apogee detection failure	3	1	Test and double check of barometers before launch	3
	Overpressure during launch causing early separation.			Shear screws are dimensioned to withstand the overpressure [Appendix VI].	3
Early release of main chute	Vibrations causing the release arm to vibrate out of position.	3	1	Extension springs are installed and connect the release arm to the main chute docking.	3
Ferrofluid leakage from the payload.	This could damage the avionics system	1	1	A test was conducted showing that the ferrofluid did not leak [Appendix V.B].	1

	The components inside the payload fall apart during high acceleration or vibration		2	2	Components will be secured by using epoxy and fasteners.	4
	Data corruption from the payload experiment		2	2	Video is recorded in one second intervals, to negate corruption.	4
	Insufficient storage space for the payload experiment	If the SD-card does not have enough storage space, the video files and sensordata will not be logged. The damage potential is severe, if we do not get all the data from the flight.	3	1	It has been verified through testing that the SD-card can film and measure data for a long enough period.	3
	Vibrations can make the video file from the payload experiment blurred	Vibrations will likely cause the camera to shake, and if the ferrofluid container shakes at a different	2	2	To avoid this, the inner structure will be stiff, and the camera holder and ferrofluid container will be stiff to hopefully make them vibrate at the same frequency, and by	4

		frequency, the video might be blurred.			that negating some of the blurriness the vibrations may cause.	
Coastin g	Drastic change of trajectory	Over stability	3	1	According to simulations done in both OpenRocket, RASAero II and CFD on SM, the rocket is not overstable during flight according to DTEG 8.4 Over-stability standards [II.D.3.Stability Margin].	3
		Weather conditions			Scrub launch in case of bad weather.	
Drogue chute deployment	Pressure separation system fails resulting in no drogue chute deployment	A leakage in the recovery chamber making it not airtight	3	1	Using PTFE tape during assembly and adding o-rings that are made of a material with a wide temperature range (VMQ). Verified by pressure separating tests [Appendix V.B]	3
	Chute malfunctioning	Chords and chutes entangles			Swivel links are used to rotate alongside the rotation of the rocket creating a lesser probability of entanglement. Folding the chords in a “non-tied fishtail braid” to shorten the length of the shock cord inside the rocket.	

		Holes and rips in the chutes	3	1	Packing the chutes in a protective deployment bag, and a physical inspection and pull test to uncover any tears before assembly.	
Main Chute Deployment	Main chute release system error, resulting in not deploying the main chute	Low power	3	1	Double check batteries and have more power than needed for redundancy	3
		State detection error			Double check wirings and sensors.	
129	Landing	Rocket and components destroyed by landing impact	Landing speed can be higher than predicted. Angle of landing can affect the landing impact. Impact of landing can also be affected by climate circumstances (sand, grass, stone, concrete etc.).	2; Unsure of how fast the landing speed will be. Could make a big impact.	2 The landing speed is calculated in Appendix VI, <i>Parachute trajectory calculations</i> . The structure is dimensioned after impact forces calculated in Appendix VI, <i>Impact force calculation</i> . A blackbox is used to protect the most important data [Appendix V.N]. Trapezoidal shape on fins reduces the chance of breakage [II.D.3.Fin design].	4

					Have spare parts in case of damage on fins after landing.	Orange
Blackbox breaks upon high impact	Bad design	2; the sensor data should also be saved on the ground station.	1		<p>Sturdy construction to ensure the blackbox doesn't break even if falling at terminal velocity.</p> <p>All data is also sent simultaneously to the ground station.</p>	2
Major damage is imposed on the payload	During a potential crash-landing, the payload could be severely damaged.	2	1		<p>To avoid this, the payload structure is sturdy and made of steel. We also save all the data on a black box, to make sure no data gets lost. This means that even if our sensors and other components get destroyed during a crash, the data retrieved from the sensors and camera will survive.</p>	2

E. Assembly, Preflight and Launch checklists

Assembly checklists

Recovery sub-assembly

Step	Action	Description	If not nominal	Tools required	Fasteners	Check
1	1.1	Fasten the two Main chute release dockings together with three spacers between the two parts.	Use backup fastners	Screwdriver	F.31	FALSE
	1.2	Insert the two fastners into the lower holes of the Main chute release dockings.	Use backup fastners, and screw fastner in	---	F.23	FALSE
	1.3	Fasten the Upper release arm to the Main chute release docking using ring shims on each side.	Use backup fastners	Wrench	F.27	FALSE
	1.4	Fasten the Lower release arm to the Main chute release docking using ring shims on each side.	Use backup fastners	Wrench	F.25	FALSE
	1.5	Fasten the black MCRS servo motor to the Main chute release docking using one of the servo mounts. Make sure the pivot point is furthest from F.23.	Use backup fastners, fasten from the bottom	Screwdriver	F.24	FALSE
	1.6	Validate that the servo motor rotates CW, seen from the bottom of the servo	Check servo orientation and chech wiring. Redo step 1.5	---	---	FALSE
	1.7	Fasten the white MCRS servo motor to the other Main chute release docking using the other servo mounts. Make sure the pivot point is furthest from F.23.	Use backup fastners, fasten from the bottom	Screwdriver	F.24	FALSE
	1.8	Validate that the servo motor rotates CCW, seen from the bottom of the servo	Check servo orientation and chech wiring. Redo step 1.5	---	---	FALSE
	1.9	Fasten one spacer on each side of the lower release arm in the lower hole.	Use backup fastners	Screwdriver	F.40	FALSE
	1.10	Screw the long spring attachment into the lower release arm.	Use backup spring attachment	---	---	FALSE
	1.11	Screw the short spring attachment into the Main chute release dockings.	Use backup spring attachment	---	---	FALSE
	1.12	Connect the extension spring to the long and short spring attachments.	Use backup extension springs	---	---	FALSE
2	2.1	Fasten the fitting to the Hawk body, wrapped in PTFE tape. Make sure the female points oppsite to the Hawk bodies larger hole.	Wrap in more PTFE	Wrench	---	FALSE
	2.2	Fasten the Hawk body to the Hawk plate	Use backup fastners	Screwdriver	F.31	FALSE
	2.3	Arm the internal spring	Re-arm spring	Special tools, umbraco key	---	FALSE
	2.4	Insert the safety pin	Re-arm spring	---	---	FALSE
	2.5	Fasten the Hawks servo motor to the recovery plate	Use backup fastners	Screwdriver	F.41	FALSE
	2.6	Make sure the servo arm points towards the Hawk body	Rotate to correct position	---	---	FALSE
	2.7	Wrap one of the hose in PTFE tape and screw it into the brass fitting	Wrap in more PTFE	Wrench	---	FALSE
	2.8	Repeat step 2.1 trough 2.7 for the other Hawk	---	---	---	FALSE

Upper threaded rod sub-assembly

Step	Action	Description	If not nominal	Tools required	Fasteners	Check
1	1.1	Fasten the upper threaded rod to the (payload) bulkhead, at the bottom of the rod using 2 M8 nuts	---	---	---	
	1.2	Fasten the radionor antenna to the radionor plate.	Use backup fastener or plate	Umbrako key	F.1	
	1.3	Fasten the Sensorboard + PSU to the Sensorboard + PSU plate	Use backup fastener or plate	Umbrako key	F.2	
	1.4	Put the video encoder into the video encoder housing, and fasten the video encoder housing to the video encoder plate.	Use backup fastener, plate or housing	Umbrako key	F.3	
	1.5	Fasten the Altimax & COTS GPS to the Altimax + COTS GPS plate	Use backup fastener or plate	Umbrako key	F.4, F.5	
	1.6	Fit the lower plate to the upper threaded rod, all of the plates mentioned above and the middle plate onto the upper threaded rod, using 4 M8 nuts	Use backup plate	---	---	
	1.7	Place the COTS GPS battery in the COTS GPS battery housing, and mount it to the back of the radionor plate.	Use backup fastener, plate or housing	Umbrako key	F.6	
	1.8	Place the Altimax battery in the Altimax battery housing and mount it to the Altimax battery plate.	Use backup fastener, plate or housing	Umbrako key	F.7	
	1.9	Mount the black box to the black box plate	Use backup fastener or plate	Umbrako key		
	1.10	Place the plates from step 1.7 and 1.8 on the middle plate. Then place the lower disk bulkhead on top of the two plates, using 1 M8 nut	Use backup plate	---	---	
	1.11	Slide the battery holder, then the upper disk bulkhead onto the upper threaded rod, and fasten them using 4 M8 nuts.	Use backup battery holder	---	---	
2	2.1	Route the power cables to/from the upper avionics mount and the battery holder	---	---	---	

Lower threaded rods sub-assembly

Step	Action	Description	If not nominal	Tools required	Fasteners	Check
1	1.1	Mount the recovery bay camera with camera mount to the recovery plate, and route the cable through the recovery plate.	Use backup fasteners	Umbrako key	F.34, F.35	
	1.2	Mount the pre-assembled MRS, and route the cable through the recovery plate	Use backup fasteners	Umbrako key	F.23	
	1.3	Fasten the U-bolt to the recovery plate, using 4 5/16"-18 nuts	---	---	---	
	1.4	Mount one camera with camera mount and one hawk plate with assembled hawk to two of the threaded rods.	Use backup fasteners	Umbrako key	F.13	
	1.5	Repeat the last step with the other two lower threaded rods.	Use backup fasteners	Umbrako key	F.14	
	1.6	Lead the tubes from the hawks and through the recovery plate	Use backup hose	---	---	
	1.7	Fasten the lower threaded rods to the recovery plate, using 8 M6 nuts	---	---	---	
	1.8	Fasten the lower threaded rods to the (payload) bulkhead, using 8 M6 nuts	---	---	---	
2	2.1	Cable/tube routing	---	---	---	

Cabling sub-assembly (TBD)

Stetind master assembly

See Appendix V.S for payload sub-assembly.

Assembly	Action	Description	If not nominal	Tools required	Fasteners	Check
1 - Upper half	1.1	Assure that the upper threaded rod sub-assembly is assembled	---	---	---	
	1.2	Assure that the lower threaded rods sub-assembly is assembled	---	---	---	
	1.3	Assure that the recovery sub-assembly is assembled	---	---	---	
	1.4	Assure that all needed cableing are finished in the sub-assemblies	---	---	---	
	1.5	Assure that the payload sub-assembly is assembled.	---	---	---	
	1.6	Fasten the upper threaded rod sub-assembly to the payload via the bulkhead.	Use backup fasteners	Umbraco key	F.19	
	1.7	Fasten the lower threaded rod sub-assembly to the payload via the bulkhead on the other side of the payload.	Use backup fasteners	Umbraco key	F.20	
	1.8	Cabling	---	---	---	
	1.9	Lie the upper airframe horizontally down on a support structure (e.g. tabel) in waste height.	---	---	---	
	1.10	Fit the now assembeled inner structure of the upper half into the forward airframe	---	---	---	
	1.11	Fasten the upper threaded rod to the middle part of the nosetip, using 1 M8 nut.	---	---	---	
	1.12	Screw the upper part of the nose tip to the middle part of the nose tip.	---	---	---	
	1.13	Screw the bulkheads on each side of the payload to the forward airframe, via the bulkhead rings.	Use backup fasteners	Screw driver	F.15, F.16	
	1.14	Fasten the recovery plate to the upper coupler / fuselage	Use backup fasteners	Screw driver	F.22	
	1.15	Fasten one of the two launch rail lugs to the upper coupler.	Use backup lug	Screw driver	F.	
	1.16	Fit the camera covers to the holes on the upper coupler / fuselage	---	---	---	
2 - Lower half	2.1	Lie the aft airframe down on a support structure (e.g. tabel) in waste height close to the upper half, so that work easily can be done in the coupler section.	---	---	---	
	2.2	Screw off the boat tail from the boat tail centering ring.	---	---	---	
	2.3	Loosen and remove eye-bolt.	---	---	---	
	2.4	Remove the motor casing from the rocket, and remove the nozzle.	---	---	---	
	2.5	Fit the solid rocket motor grain into the motor casing, and refit the nozzle.	---	---	---	
	2.6	Fasten all fin brackets to the fuselage.	Use backup fasteners	Screw driver	F.41	
	2.7	Fasten one of the two launch rail lugs to the motor centering ring / fuselage.	Use backup lug	Screw driver	F.	
	2.8	Slide the motor casing into the aft airframe, from the bottom.	---	---	---	
	2.9	Secure the motor casing to the motor mount with the eye-bolt.	---	---	---	
	2.10	Screw on the boat tail to the boat tail centering ring.	---	---	---	
	2.11	Fasten the fins to the fin brackets.	Use backup fasteners	Umbraco key	F.40	
	2.12	Apply dry lube to the surface of the lower coupler, where it will overlap with the upper coupler	Clean off and apply again	---	---	
3 - Coupler section	3.1	Connect the Y shock chord to the U-bolt in one end, to the MRS-system in the other end.	---	---	---	
	3.2	Connect the straight shock cord to the eye-bolt.	---	---	---	
	3.3	Pack the main chute, and then the drouge chute into the upper coupler.	Unpack and try again	---	---	
	3.4	Pack the shock cords into the upper coupler.	Unpack and try again	---	---	
	3.5	Mate the upper and lower halves	---	---	--	
	3.6	Fasten the coupelers together. Wrap the shear screws with PTFE-tape to the shear screws before fastening	Use backup fasteners	Screw driver	F.11	

Preflight checklist

T-[hh:mm:ss]	Location	Action	Description	Check
T-???:???:??	1 - BEFORE assembly area	1.1	Bring equipment, tents, chairs, water from hotel	
		1.2	Charge batteries	
		1.3	Check SD-cards formatted correctly	
		1.4		
T-???:???:??	2 - Assembly Area	2.1	Set up tent and working station in assembly area	
		2.2	Check battery charge	
		2.3	Assemble rocket - see assembly master	
		2.4	arm all systems	
		2.1	test electronics functionallity, radio connection, payload connection, gps connection	
		2.2	dis-arm all systems	
		2.3	launch readiness review	
T-00:45:00	3 - On vehicle	3.1	Transport rocket to launch pad	
		3.2	Initiate contact with Ground station through phones/radio	
T-00:30:00	4 - On Pad	4.1	Install rocket on pad	
		4.2	Grease rail lugs	
		4.3	Avoid pointing rocket towards rocket assembly or launch areas while loading rocket on the rail.	
		4.4	Erect launch rail to correct angle	
		4.5	Confirm contact with ground station	
T-00:25:00	5 - Launch Pad	5.1	Non-essential personell leave launch pad!	
		5.2	Remove camera tape	
		5.3	Arm Featherweight GPS (dir1)	
		5.4	ARM COTS FC system (dir2)	
		5.5	ARM SRAD FC system (dir3)	
		5.6	Confirm all systems armed	
		5.7	Verify ground station contact with rocket	

Launch checklist

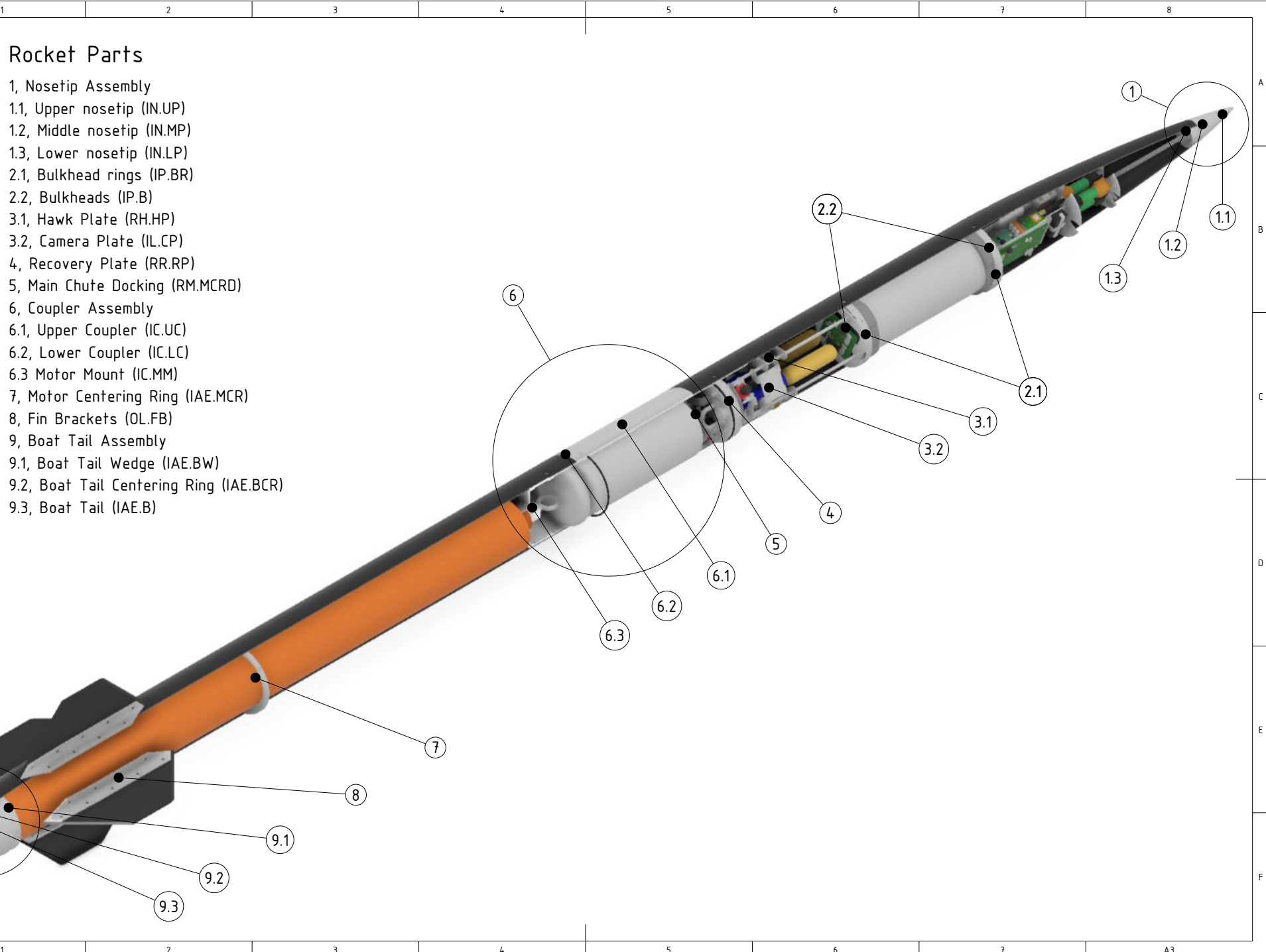
T-[hh:mm:ss]	Location	Action	Description	Check
T-00:20:00	1- Ground Station	1.1	Ground station confirms rocket is still in idle state	FALSE
T-00:20:00	2 - Launch pad	2.1	Ask Range Manager for permission to install motor igniters	FALSE
		2.2	Remove nozzle cap	FALSE
		2.3	Install motor igniters	FALSE
		2.4	Leave igniters shunted for Range Manager to be present while connecting firing line, or perform it him/herself.	FALSE
		2.5	Verify firing line is not "hot" before connecting to igniters, by touching the leads together and checking for sparks	FALSE
		2.6	Ensure all non-essential personell have evacuated the launch pad	FALSE
		2.7	Connect firing line to igniters	FALSE
		2.8	Coordinate continuity check with the launch control unit.	FALSE
		2.9	All personnell leave launch pad!	FALSE
T-00:15:00	3 - Assembly Area	3.1	Measure wind and prepare lookup table with respect to simulation closest to actual wind	FALSE
T-00:05:00	4 - Launch Pad	4.1	Ground station sends arming signal to rocket	FALSE
T-00:01:00		4.2	Possible HOLD due to weather, wind and unforseen conditions	FALSE
T-00:00:10		4.3	Countdown initiated	FALSE
T-00:00:00		4.4	Launch	FALSE
T+00:00:25		4.5	Apogee	FALSE
T+00:02:00		4.6	Landing	FALSE

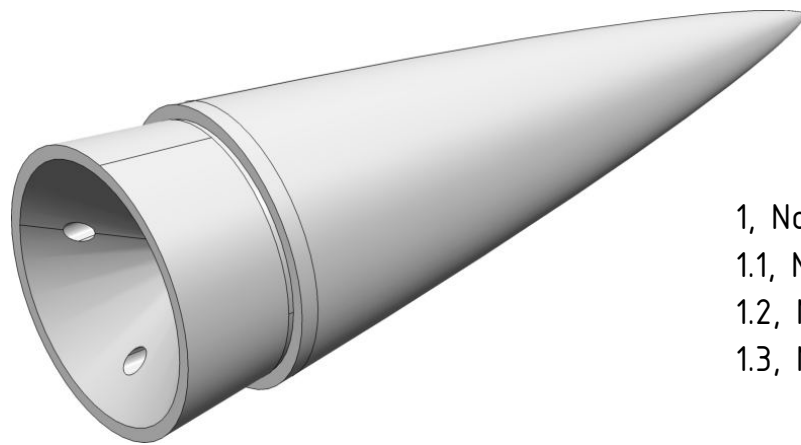
Off-Nominal checklist

Location	Action	Description	Check
Launch Pad	1	Consult situation with Range Manager	FALSE
	2	Disconnect firing line from igniters	FALSE
	6	Carefully lower launch rail	FALSE
	3	Igniter shunted and removed	FALSE
	4	Safety pins inserted back in to the Hawks	FALSE
	5	Turn power switch (left) CW	FALSE
	7	Remove rocket from rail	FALSE
	8	Tape structure holes	FALSE
Ground Station	9	Stop data recording	FALSE
Assembly Area	10	Disassemble the rocket and remove the FWD airframe	FALSE
	11	Turn payload of	FALSE

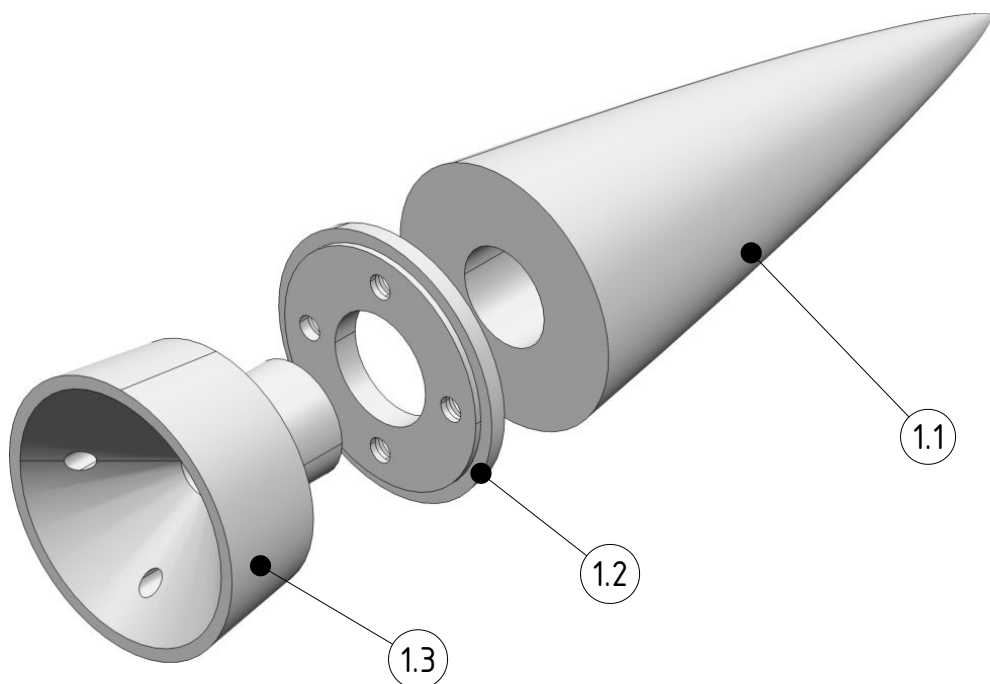
Postflight checklist (TBD)

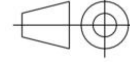
F. Engineering drawings

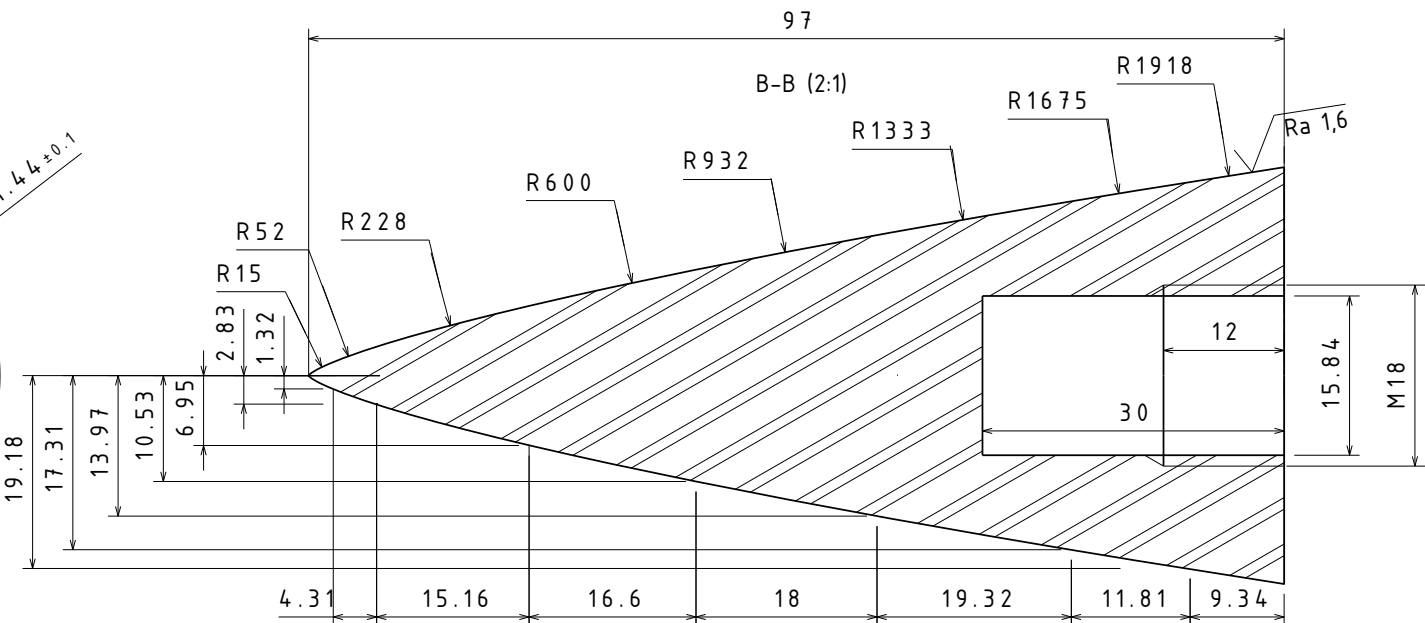
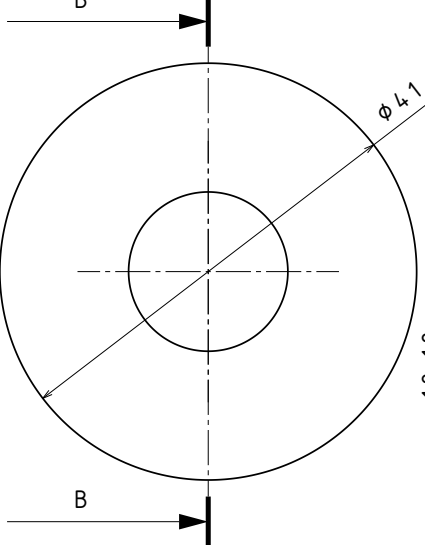




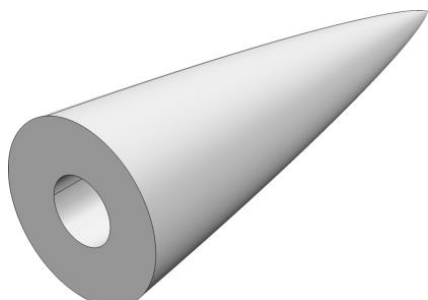
1, Noisetip Assembly
1.1, Noisetip Upper
1.2, Noisetip Middle
1.3, Noisetip Lower



Part name / Component ID / Drawing number: Noisetip Assembly / IN. / 1	Designed by: Erik Trydal / 12.04.2021
Roughness: Ra = 3,2 unless otherwise specified	Approved by: Ask Hovik / 13.04.2021
Material: Aluminium	Technical Reference: Erik Trydal / 99318700
Tolerance: For non-specified tolerances, use NS-ISO 2768-1 Middels	 Sheet: 1/4
	Paper size: A4 Scale: 1:1
	Date: 15.04.2021 Version: 1



Isometric View (1:1)



Part name / Component ID / Drawing number:
Upper Nosetip / IN.UP / 1.1

Designed by:
Erik Trydal

Roughness:
Ra = 3.2 unless otherwise specified

Approved by:
Steven Xu

Material:
Aluminium 7075-T6

Technical Reference:
Erik Trydal, 99318700

Tolerance:
For non-specified tolerances, use NS-ISO 2768-1 Fin

Sheet:
2/4



Paper size:
A3

Scale:
2:1

Date:
28/04/21

Version:
5

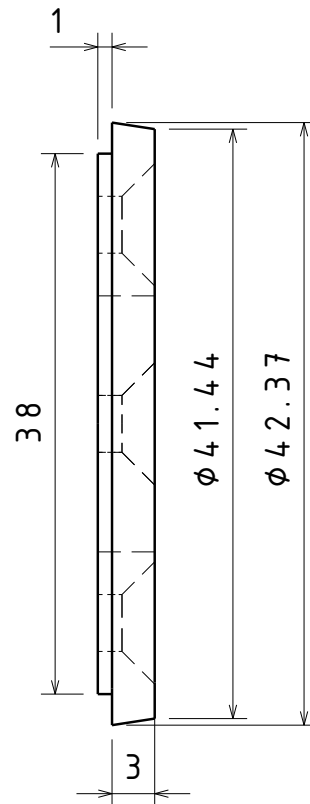
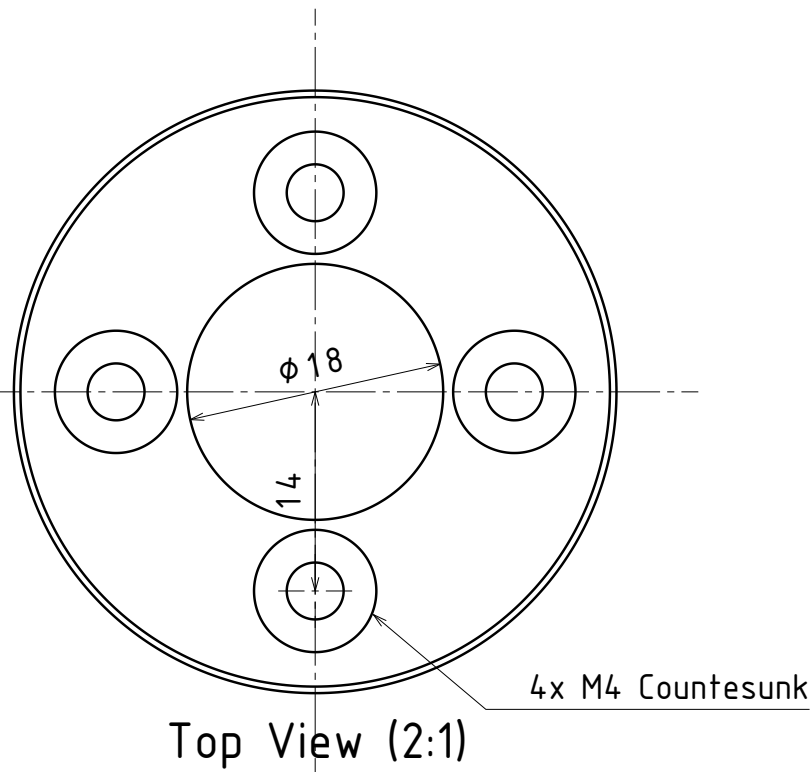
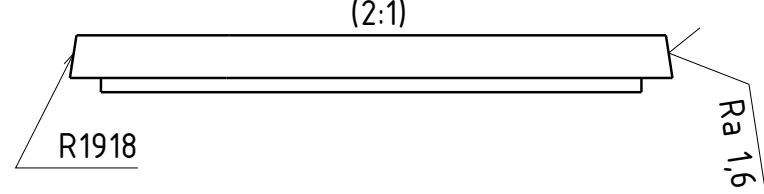
1

2

3

4

A



Side View (2:1)

Part name / Component ID / Drawing number:
Middle Nasetip / IN.MP / 1.2

Designed by:
Erik F. Trydal/23.01.2021

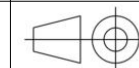
Roughness:
 $Ra = 3,6$ med mindre annet er oppgitt

Approved by:
Ask Haugerud Hovik

Material:
6061-T6 aluminium

Technical Reference:
Erik Trydal, 99318700

Tolerance:
Toleranser for ikke-toleransesatte mål NS-ISO 2768-1 Fin

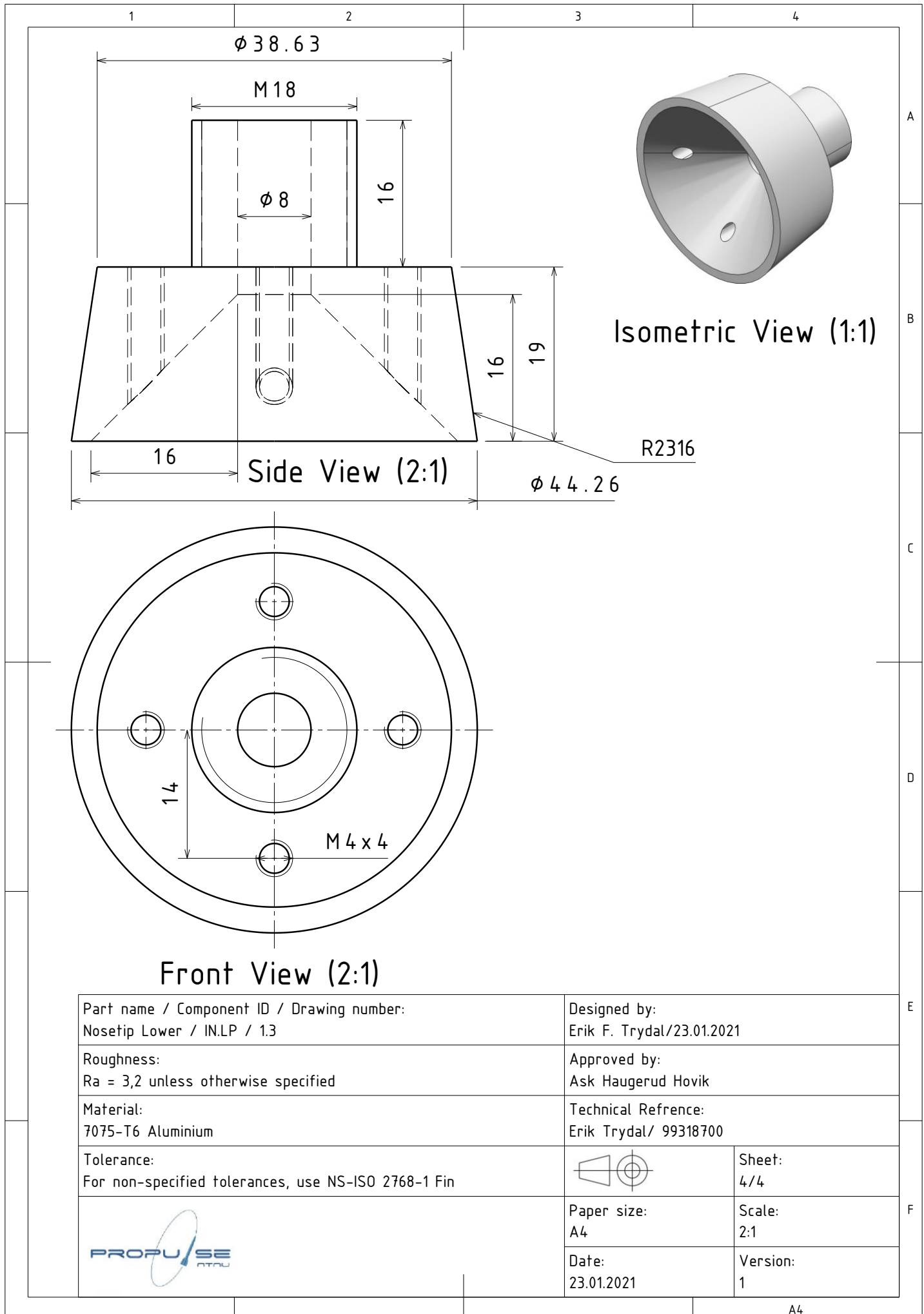


Sheet:
1/1

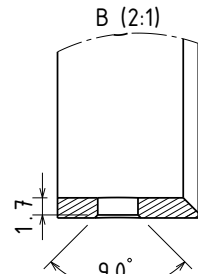
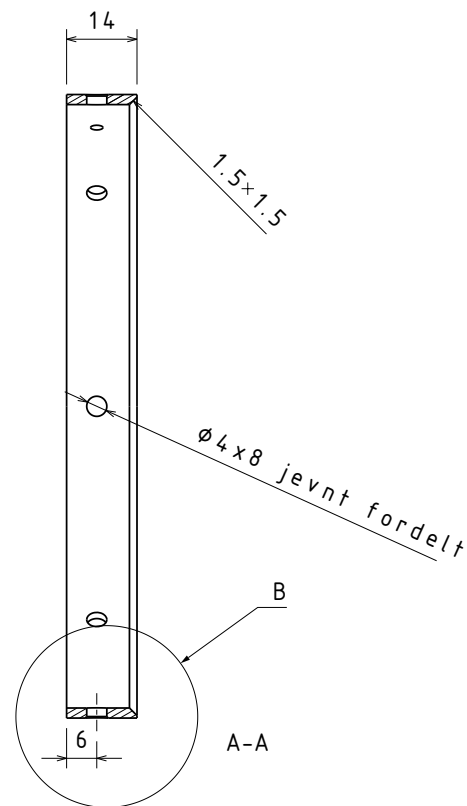
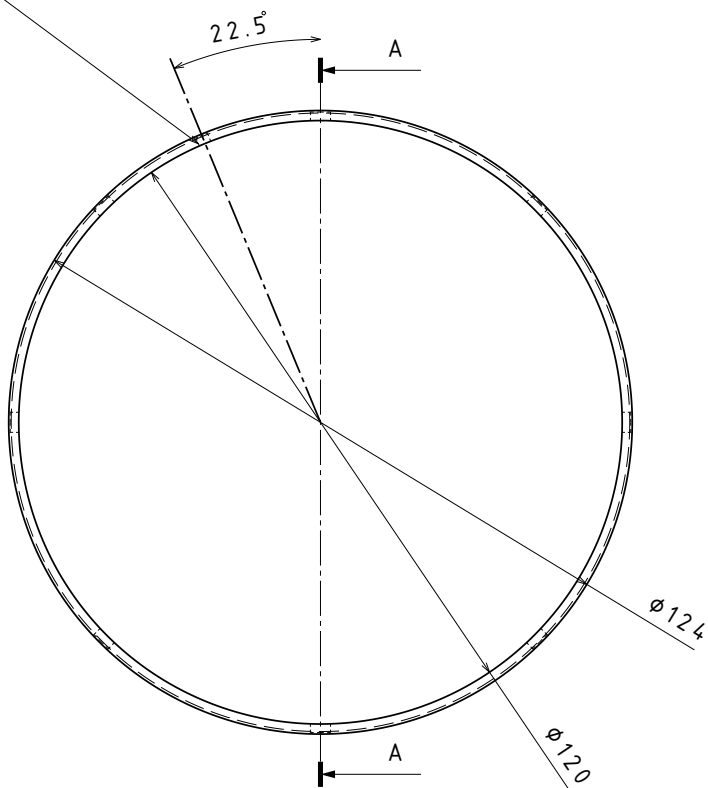


Paper size:
A4
Date:
23.01.2021

Scale:
2:1
Version:
1



M3. Ligger på inje med de andre hullene



Part name / Component ID / Drawing number:
Stetind Bulkhead Ring / IP.BR / 2.1

Designed by:
Erik Trydal/16.02.2021

Roughness:
 $R_a = 3.2$ unless otherwise specified

Approved by:
Steven Xu/03.03.2021, Ask Hovik

Material:
Any aluminium

Technical Refrence:
Ask Hovik, 90593845

Tolerance:
For non-specified tolerances, use NS-ISO 2768-1 Middels

Sheet:
1/1

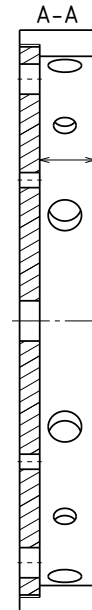
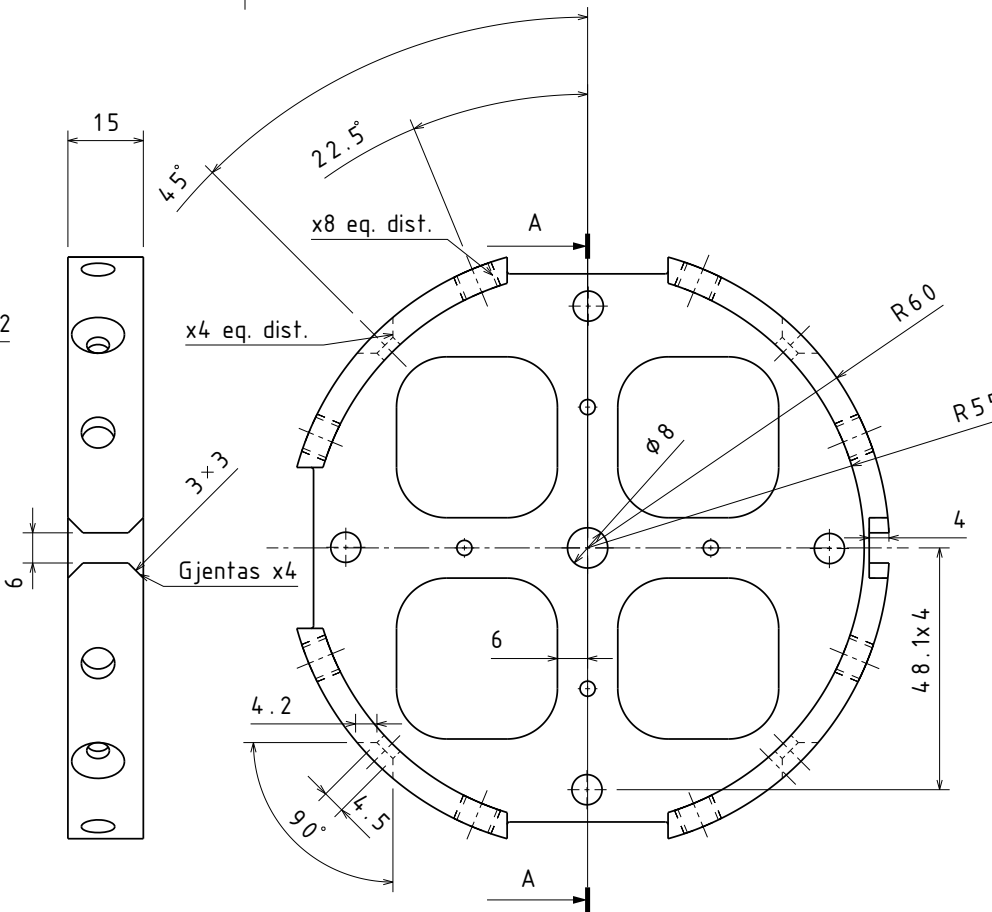
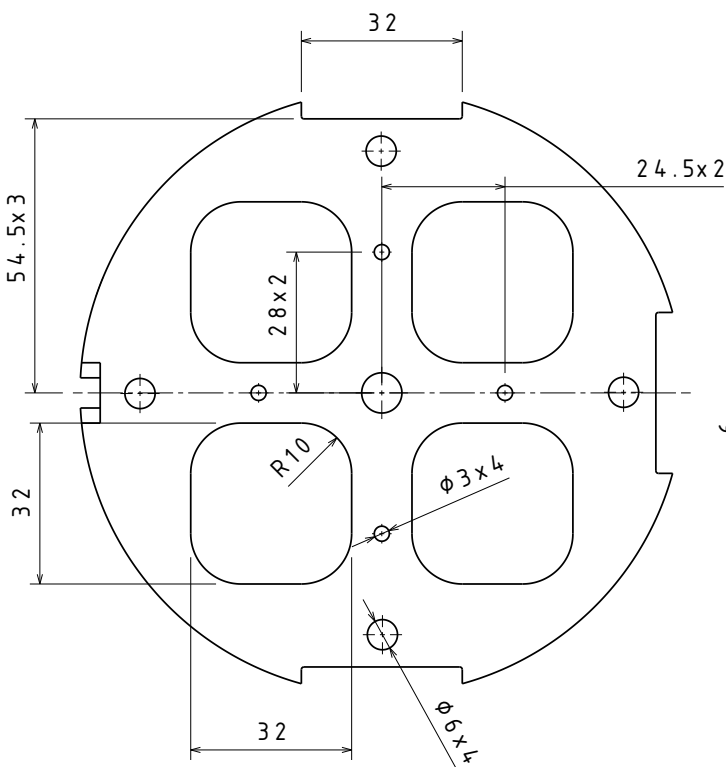
PROPUSE
nrmu

Paper size:
A3

Scale:
1:1

Date:
16.02.2021

Version:
1



Isometric View
(1:2)

Part name / Component ID / Drawing number:
Bulkhead / IP.B / 2.2

Designed by:
Erik Trydal

Roughness:
 $R_a = 3.2$ unless otherwise specified

Approved by:
Ask Hovik

Material:
Aluminium 6082-T6

Technical Refrence:
Ask Haugerud Hovik, 90593845

Tolerance:
For non-specified tolerances, use NS-ISO 2768-1 Middels

Sheet:
1/1

Paper size:
A3
Scale:
1:1
Date:
25/03/21
Version:
2

1 2 3 4 5 6 7 8

A

B

C

D

E

F

A

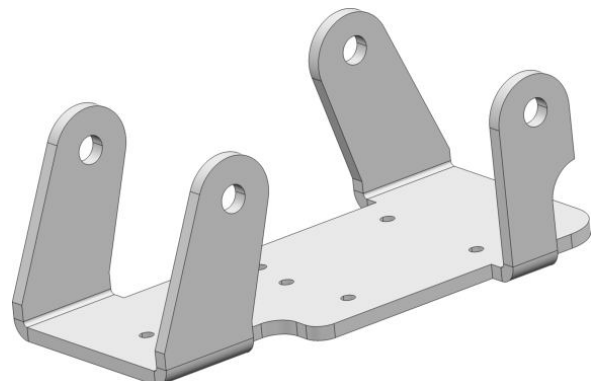
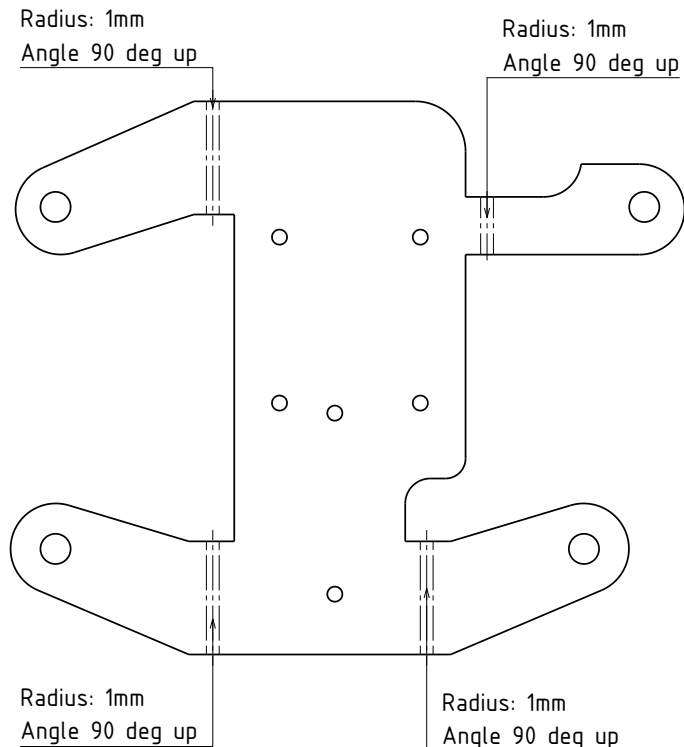
B

C

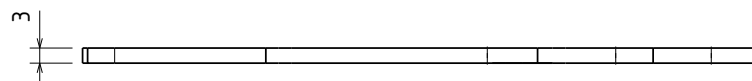
D

E

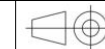
F



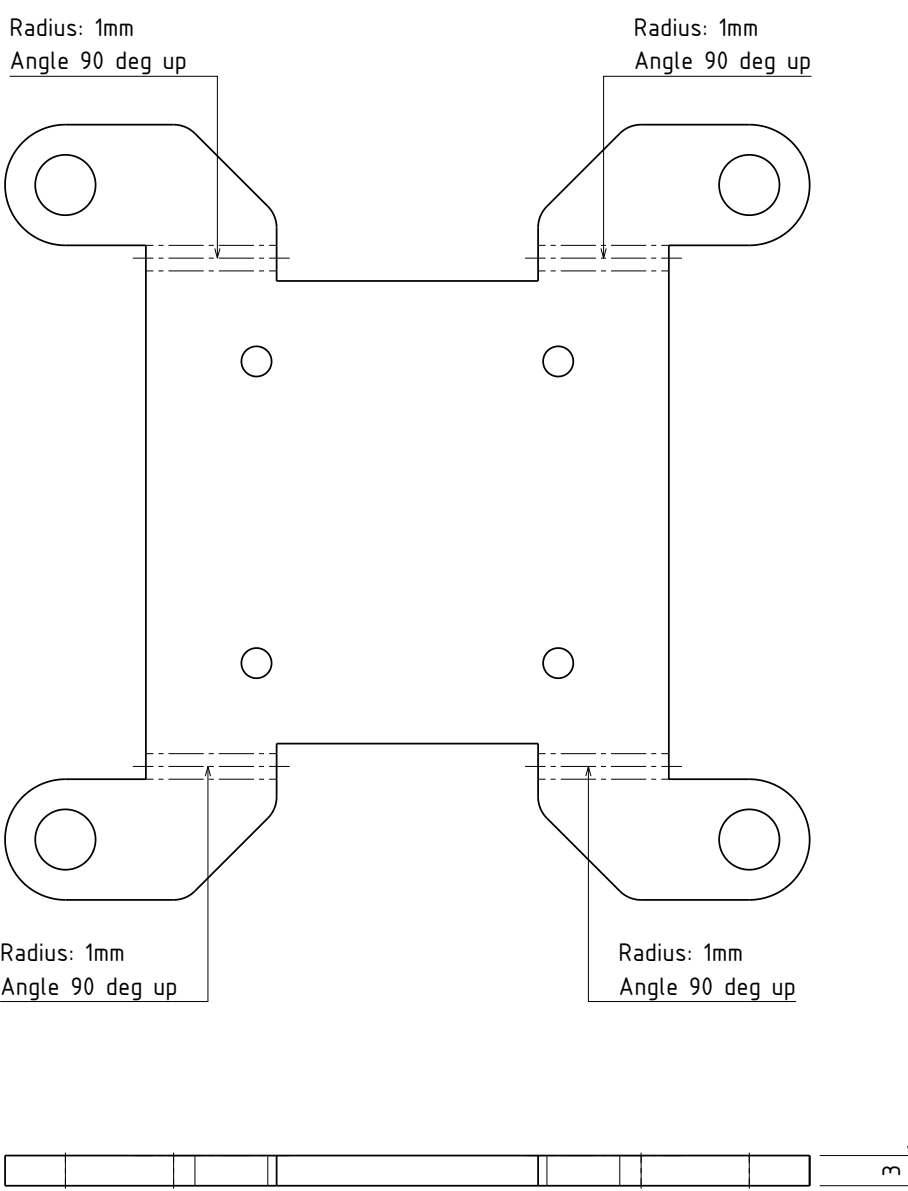
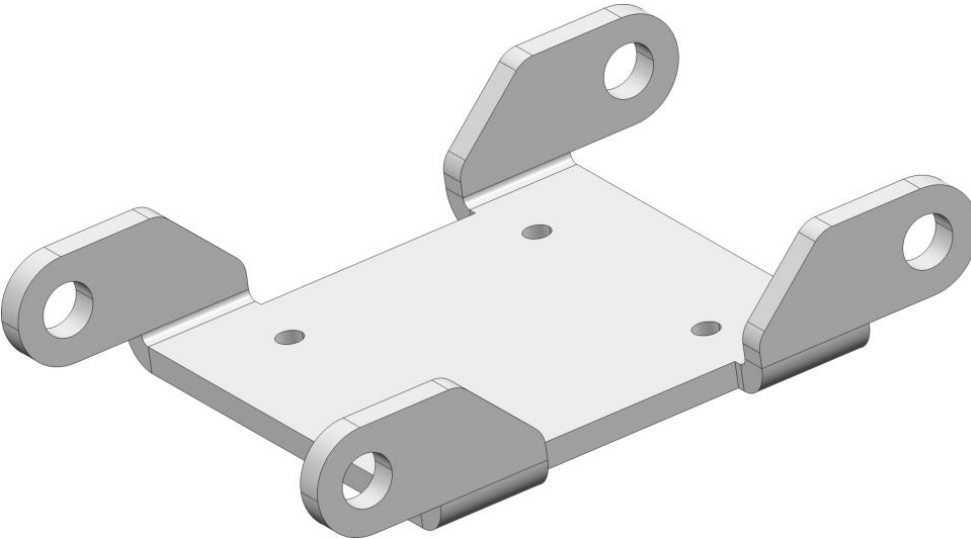
Isometric view
1:1

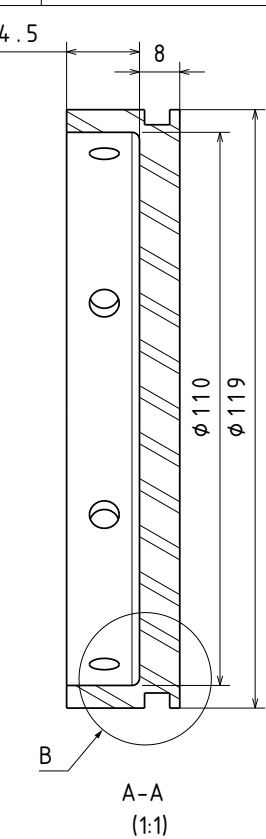
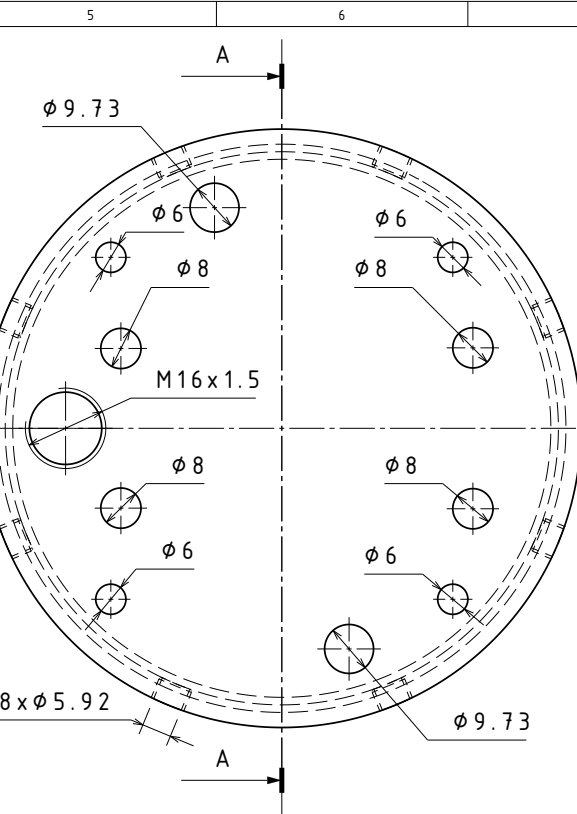
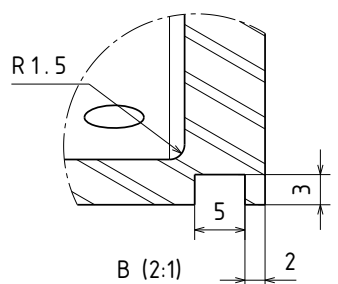
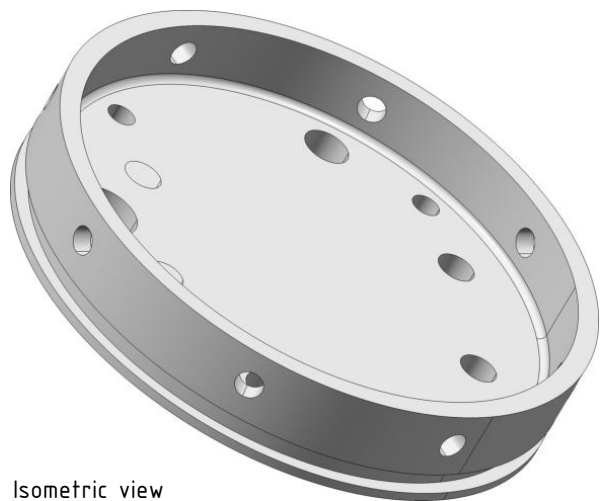
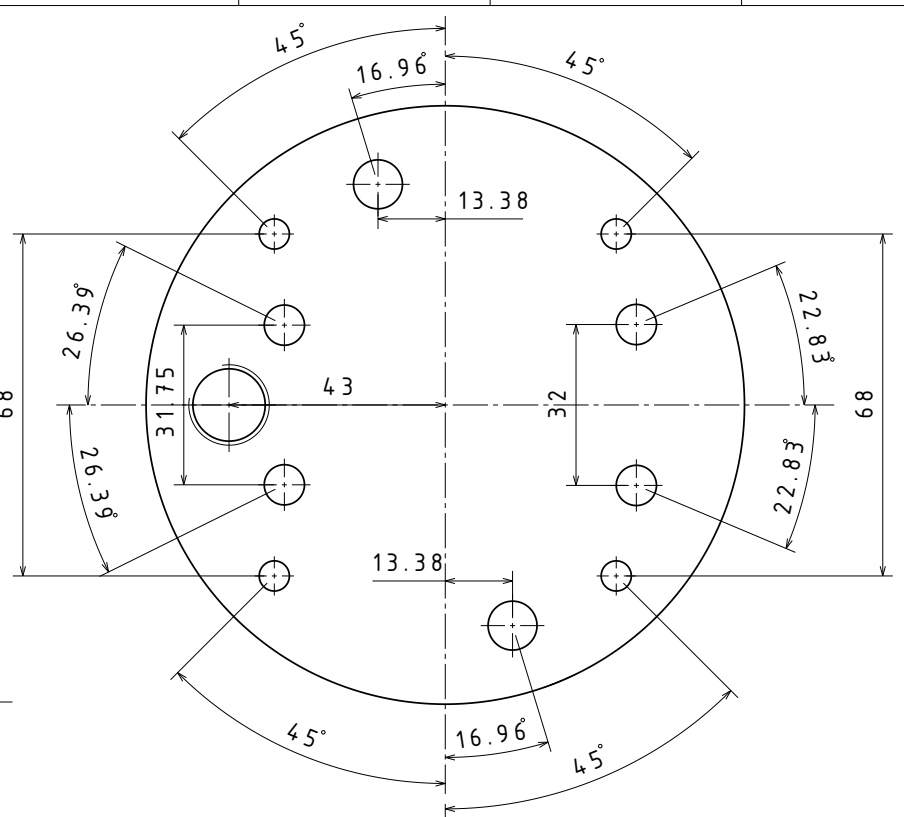


Production method watercutting. Refer to DXF for cutting path

Part name / Component ID / Drawing number: Hawk plate / RH.HP / 3.1	Designed by: Vebjørn G. Bratlie
Roughness: Ra = 3.2 unless otherwise specified	Approved by: Ask Hovik
Material: Aluminium	Technical Refrence: Vebjørn G. Bratlie, 94 88 51 67
Tolerance: For non-specified tolerances, use NS-ISO 2768-1 middels	 Sheet: 1/1
	Paper size: A3 Scale: 1:1
	Date: 18.04.2021 Version: 2

1 2 3 4 5 6 7 A3

1	2	3	4	5	6	7	8												
A							A												
B							B												
C							C												
D							D												
E							E												
F							F												
																			
<p>Production method watercutting. Refer to DXF for cutting path.</p>				<table border="1"> <tr> <td>Part name / Component ID / Drawing number: Camera Plate / ILCP / 3.2</td><td>Designed by: Vebjørn G. Bratlie/08.03.2021</td></tr> <tr> <td>Roughness: Ra = 3.2 unless otherwise specified</td><td>Approved by: Erik Trydal / 03.05.2021</td></tr> <tr> <td>Material: Aluminum</td><td>Technical Refrence: Vebjørn G. Bratlie/ 94 88 51 67</td></tr> <tr> <td>Tolerance: For non-specified tolerances, use NS-ISO 2768-1 Middels</td><td> Sheet: 1/1</td></tr> <tr> <td></td><td>Paper size: A3 Scale: 2:1</td></tr> <tr> <td></td><td>Date: 03.05.2021 Version: 1</td></tr> </table>				Part name / Component ID / Drawing number: Camera Plate / ILCP / 3.2	Designed by: Vebjørn G. Bratlie/08.03.2021	Roughness: Ra = 3.2 unless otherwise specified	Approved by: Erik Trydal / 03.05.2021	Material: Aluminum	Technical Refrence: Vebjørn G. Bratlie/ 94 88 51 67	Tolerance: For non-specified tolerances, use NS-ISO 2768-1 Middels	 Sheet: 1/1		Paper size: A3 Scale: 2:1		Date: 03.05.2021 Version: 1
Part name / Component ID / Drawing number: Camera Plate / ILCP / 3.2	Designed by: Vebjørn G. Bratlie/08.03.2021																		
Roughness: Ra = 3.2 unless otherwise specified	Approved by: Erik Trydal / 03.05.2021																		
Material: Aluminum	Technical Refrence: Vebjørn G. Bratlie/ 94 88 51 67																		
Tolerance: For non-specified tolerances, use NS-ISO 2768-1 Middels	 Sheet: 1/1																		
	Paper size: A3 Scale: 2:1																		
	Date: 03.05.2021 Version: 1																		
1	2	3	4	5	6	7	A3												



Part name / Component ID / Drawing number:
Recovery plate / RR.RP / 4

Designed by:
Erik Trydal

Roughness:
 $Ra = 3.2$ unless otherwise specified

Approved by:
Ask Hovik

Material:
Aluminum 6082-T6

Technical Reference:
Ask Haugerud Hovik, 90593845

Tolerance:
For non-specified tolerances, use NS-ISO 2768-1 middels

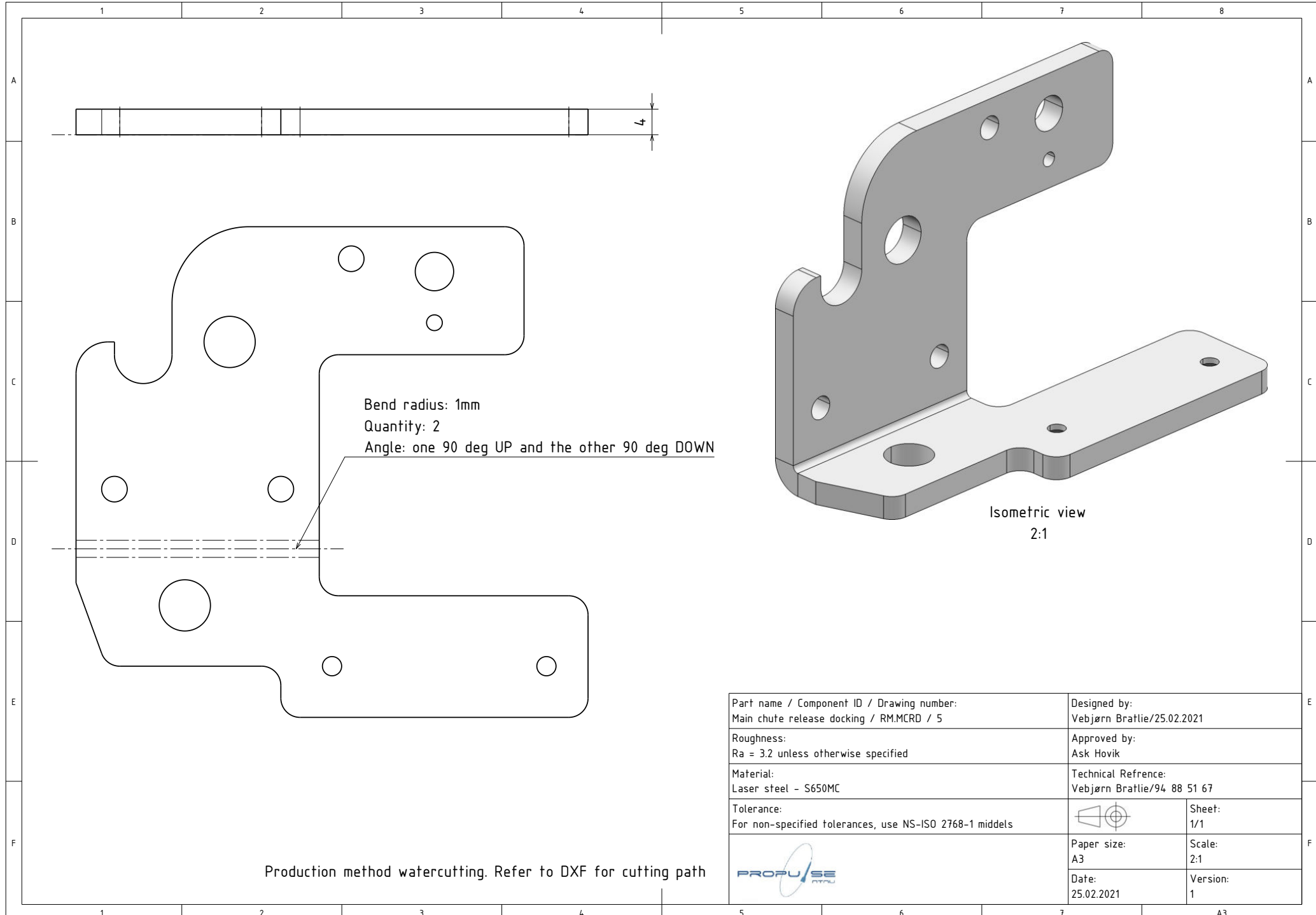
Sheet:
1/1

Paper size:
A3

Scale:
1:1

Date:
04.05.2021

Version:
3

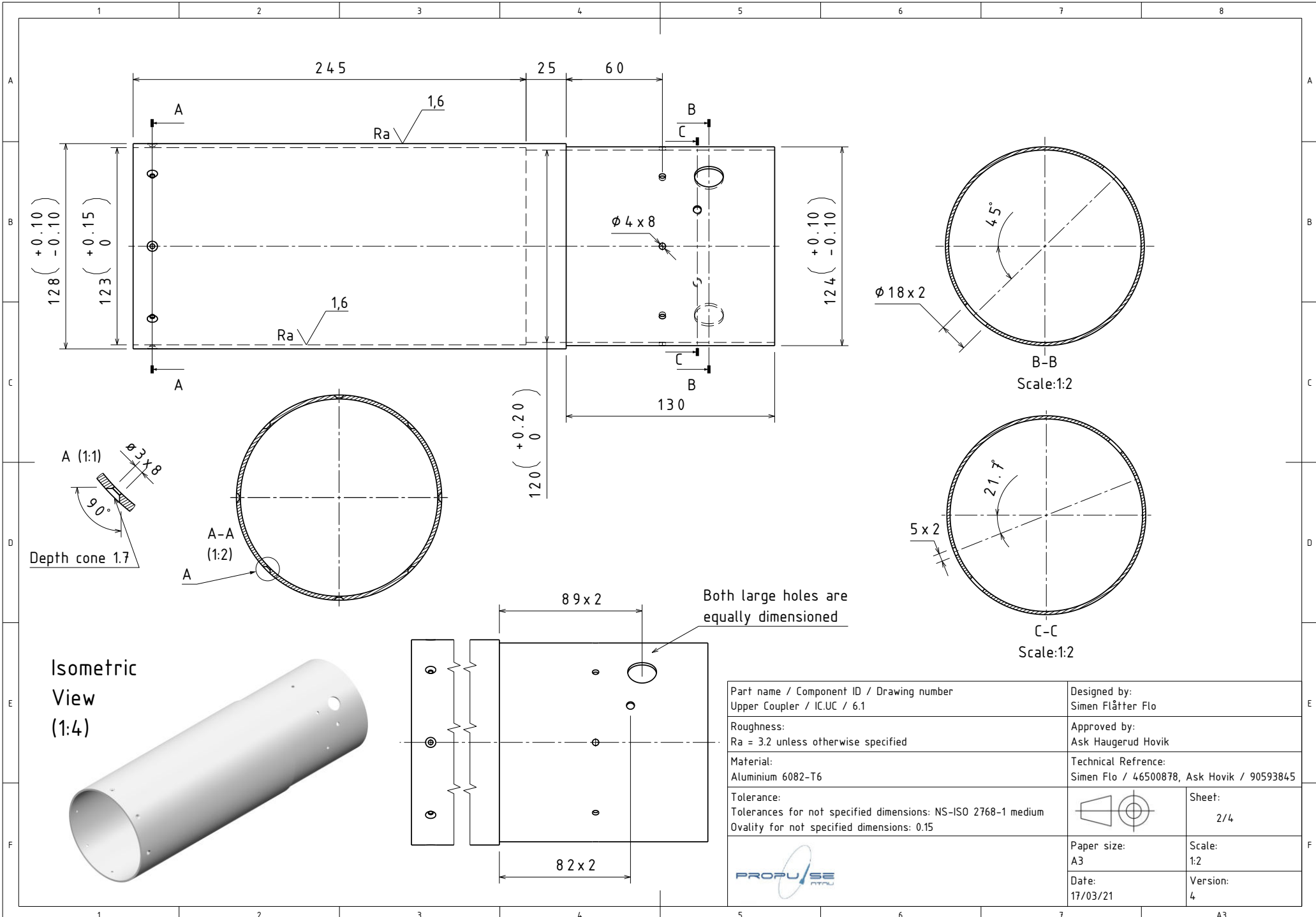


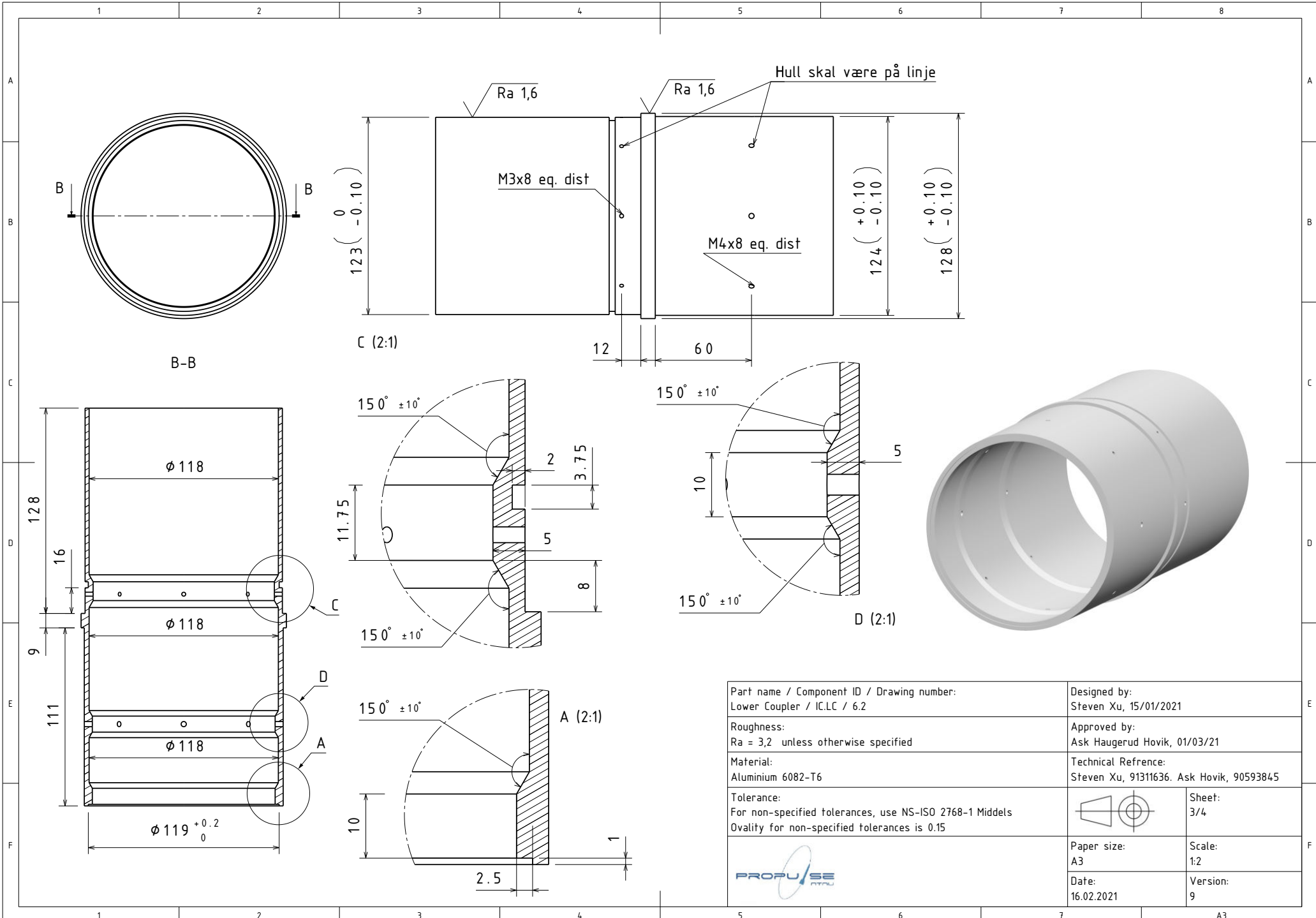
1	2	3	4	5	6	7	8
A							A
B							B
C							C
D							D
E							E
F							F
1	2	3	4	5	6	7	A3

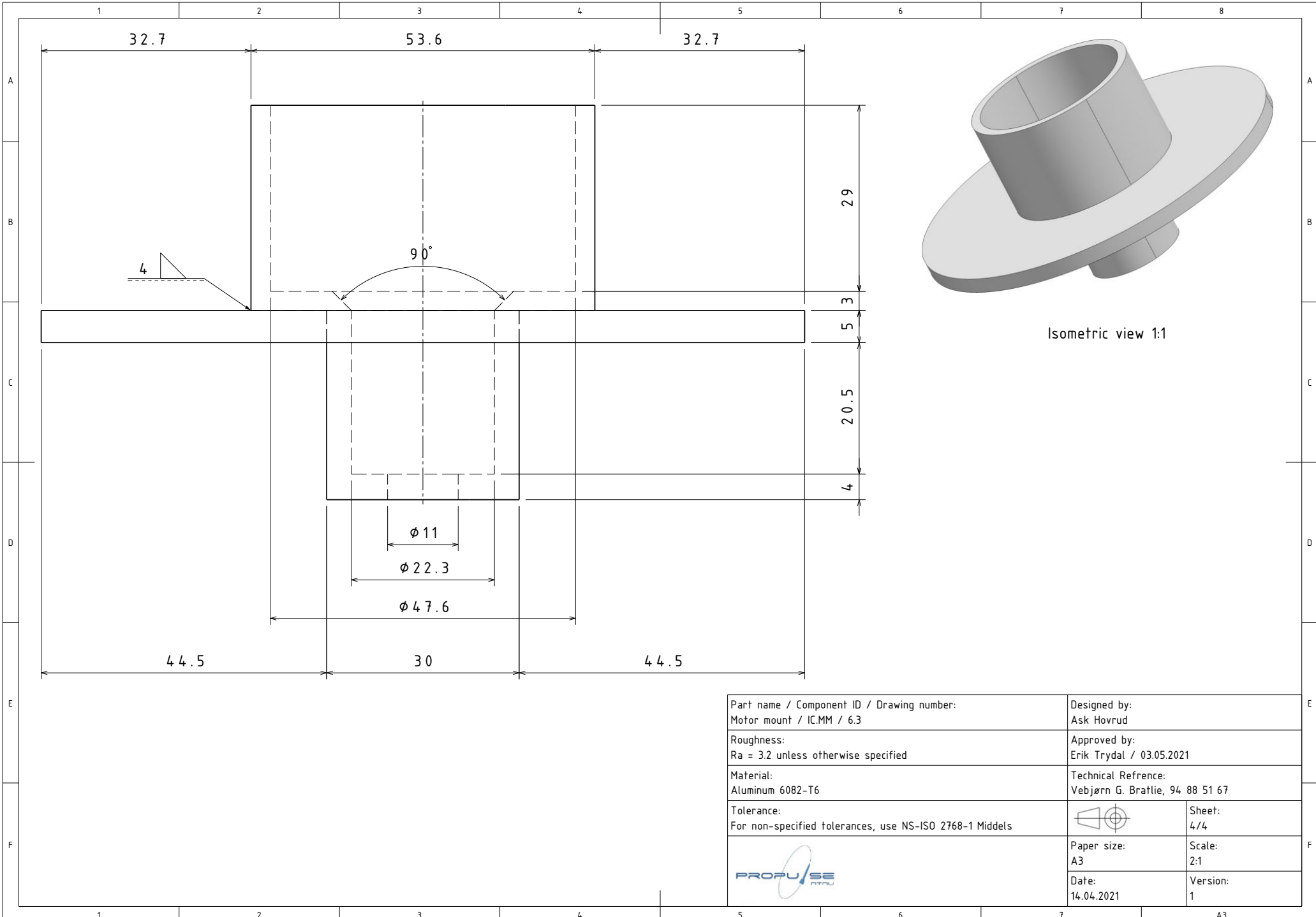
6, Coupler Assembly
6.1, Upper Coupler
6.2, Lower Coupler
6.3, Motor Mount

3

Part name / Component ID / Drawing number: Coupler Assembly / IC. / 6	Designed by: Erik Trydal/15.01.2021
Roughness: $R_a = 3,2$ unless otherwise specified	Approved by: Ask Haugerud Hovik
Material: 6061-T6	Technical Refrence: Ask Haugerud Hovik, 90593845
Tolerance: For non-specified tolerances, use NS-ISO 2768-1 Middels	Sheet: 1/4
	Paper size: A3
	Scale: 1:2
	Date: 03.05.2021
	Version: 5

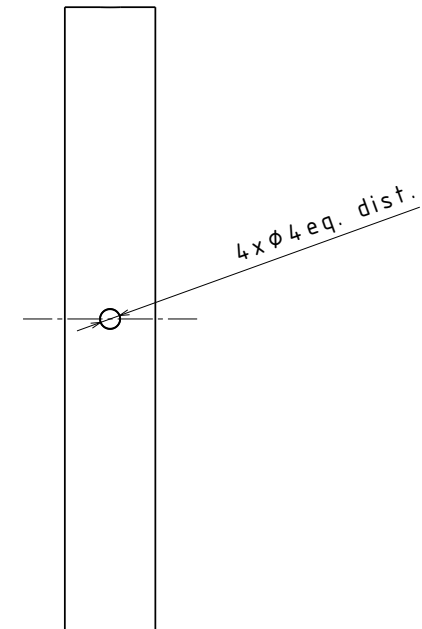
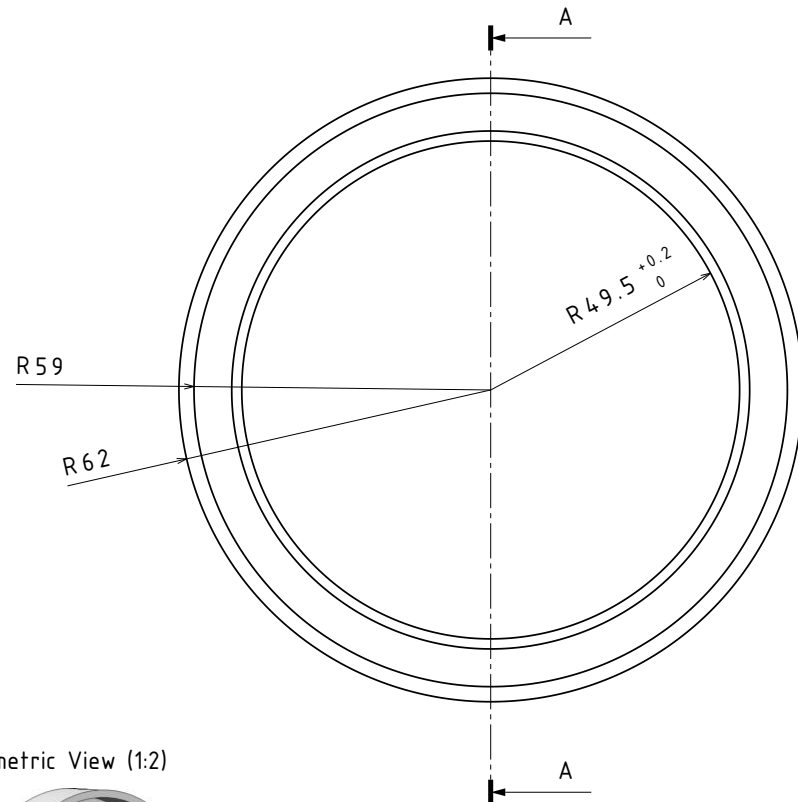
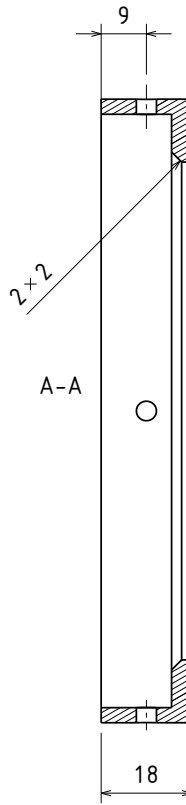






1 2 3 4 5 6 7 8

A A
B B
C C
D D
E E
F F



Part name / Component ID / Drawing number
Motor centering ring / IAE.MCR / 7

Designed by:
Steven Xu / 03.03.2021

Roughness:
 $R_a = 3.2$ unless otherwise specified

Approved by:
Ask Hovik, 23/06/21

Material:
Aluminium 6082-T6

Technical Reference:
Ask Hovik, 90593845

Tolerance:
Tolerances for non-specified dimensions: NS-ISO 2768-1 middels

Sheet:
1/1


PROPUSE

Paper size:
A3

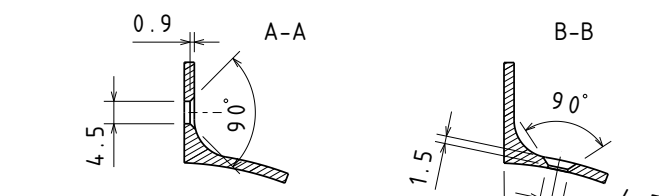
Scale:
1:1

Date:
23.06.2021

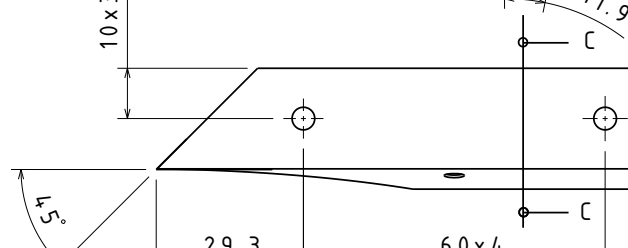
Version:
3

1 2 3 4 5 6 7 A3

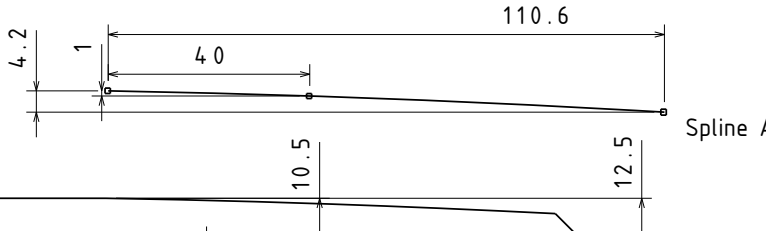
Part information		
Part name	Sheet	Quantity
Fin Bracket	1/1	4
Fin Bracket MIRROR	1/1	4



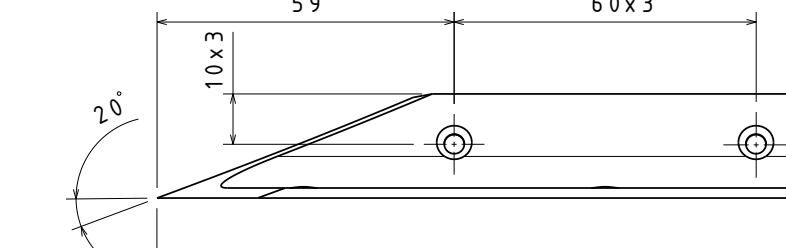
B-B



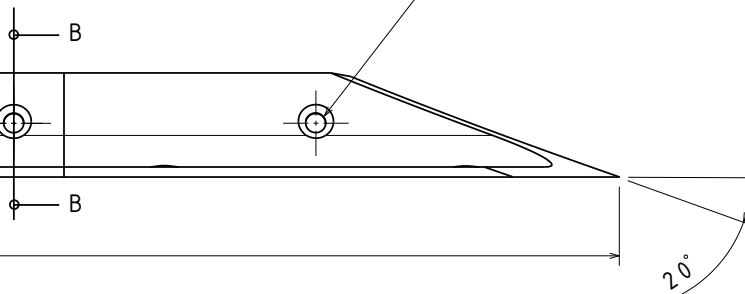
Back view



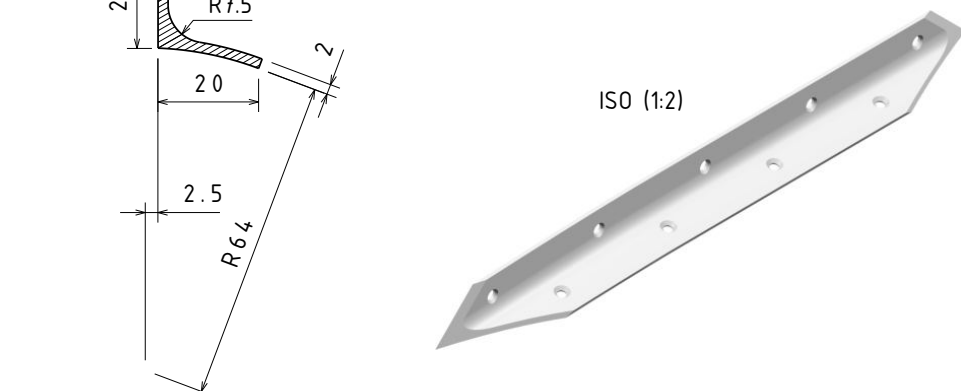
Spline A



Top view



Outer hole 2.1 deg angle from normal



ISO (1:2)

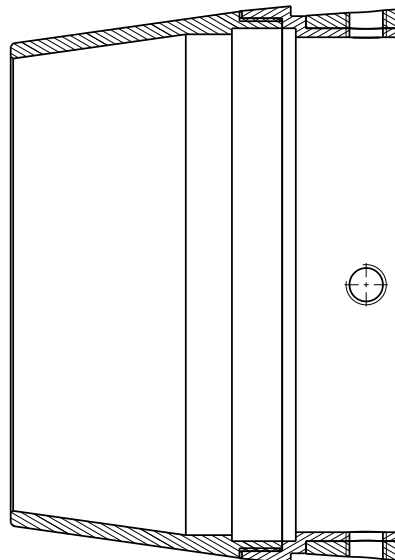
Kommentar: Legg merke til at det trengs 8 braketter for å feste alle finnene. Og halvparten av dem må være SPEILVENDT i forhold til denne tegningen

Part name / Component ID / Drawing number: Fin Bracket / OL.FB / 8	Designed by: Ask Haugerud Hovik, +47 90593845	
Roughness: Ra = 3.2 unless otherwise specified	Approved by: Erik Trydal / 03.05.2021	
Material: Aluminium 6082-T6	Technical Reference: Fabian Etzen, +47 94166454	
Tolerance: For non-specified tolerances, use NS-ISO 2768-1 Middels		Sheet: 1/1
	Paper size: A3	Scale: 1:1
	Date: 28/02/21	Version: 1

1	2	3	4	5	6	7	8			
A	B	C	D	List of parts in assembly						
				Part name		Sheet		Quantity		
				Boat tail centering ring		2/4		1		
				Boat tail centering ring wedge		3/4		1		
				Boat tail		4/4		1		

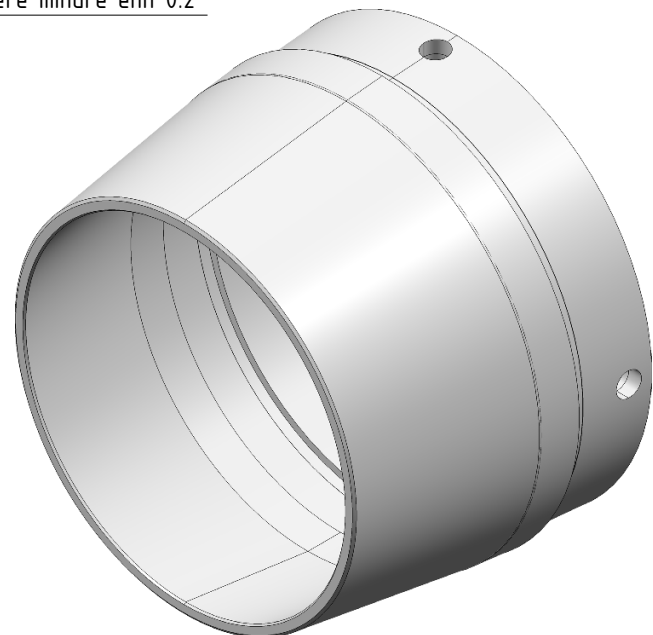
Hull i ring og wedge skal matche

Diameter skal matche. Forskjellen i diameter burde være mindre enn 0.2

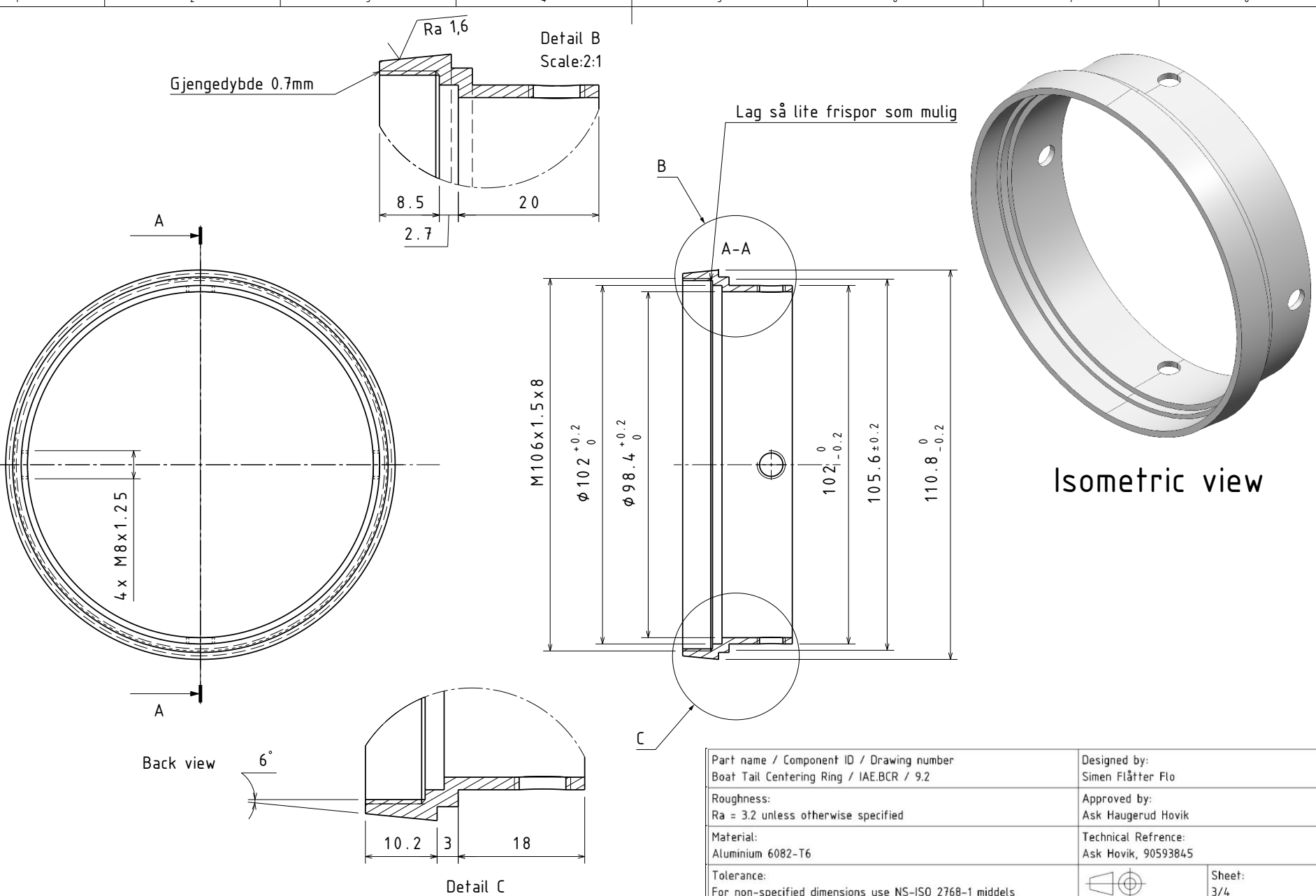


Sectioned view

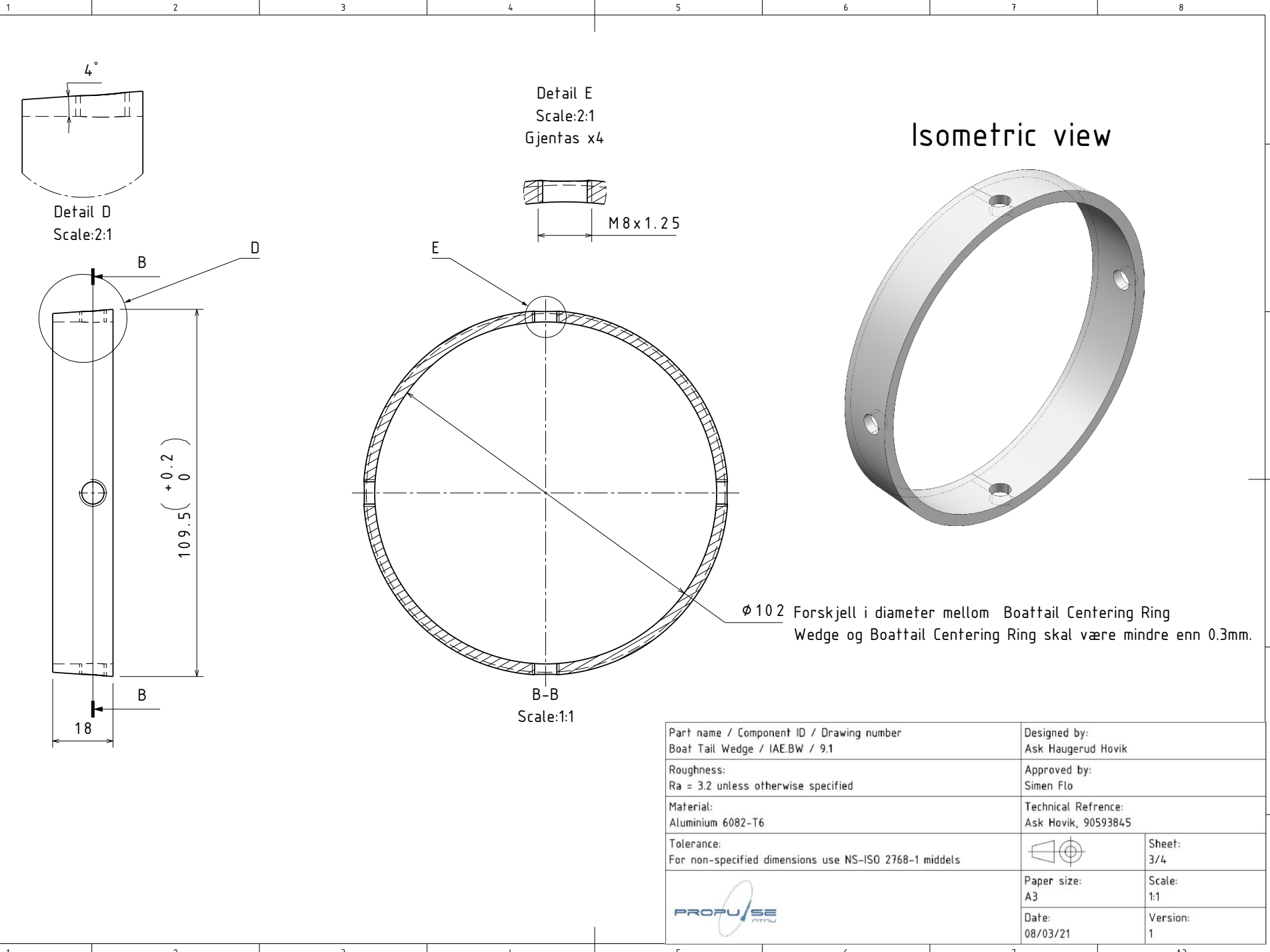
Isometric view

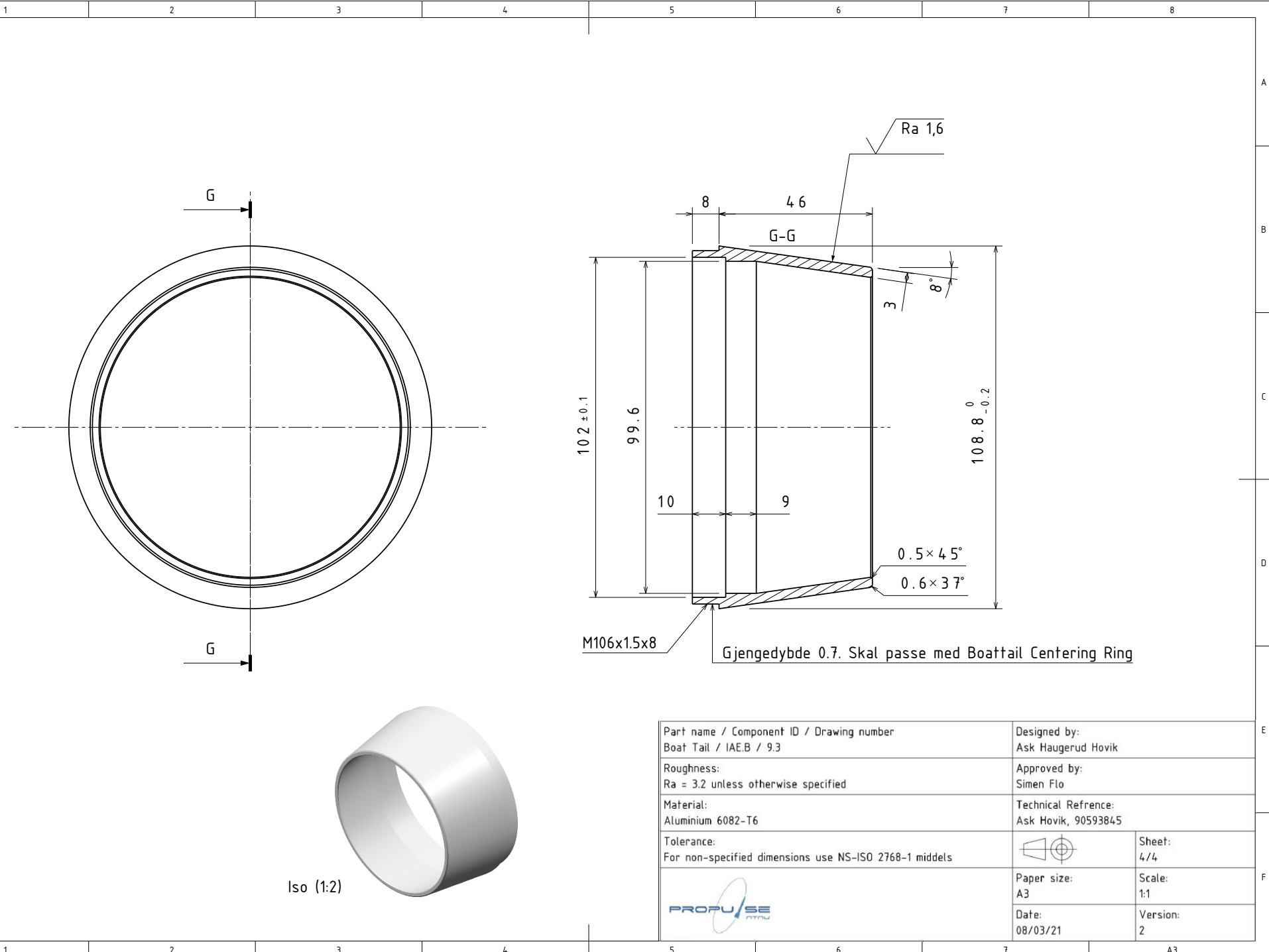


Part name / Component ID / Drawing number Boat Tail Assembly / N/A / 9	Designed by: Ask Haugerud Hovik
Roughness: $R_a = 3.2$ unless otherwise specified	Approved by: Erik Trydal
Material: Aluminium 6082-T6	Technical Reference: Ask Hovik, 90593845
Tolerance: For non-specified dimensions use NS-ISO 2768-1 middels	Sheet: 1/4
	Paper size: A3
	Scale: 1:1
	Date: 08/03/21
	Version: 1



Part name / Component ID / Drawing number Boat Tail Centering Ring / IAE.BCR / 9.2	Designed by: Simen Flåtter Flo
Roughness: Ra = 3.2 unless otherwise specified	Approved by: Ask Haugerud Hovik
Material: Aluminium 6082-T6	Technical Refrence: Ask Hovik, 90593845
Tolerance: For non-specified dimensions use NS-ISO 2768-1 middels	 Sheet: 3/4
	Paper size: A3 Scale: 1:1
	Date: 08/03/21 Version: 3

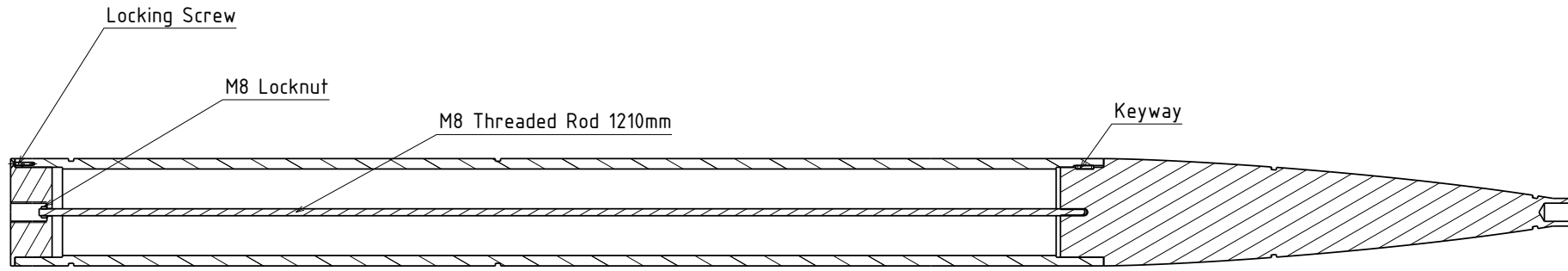




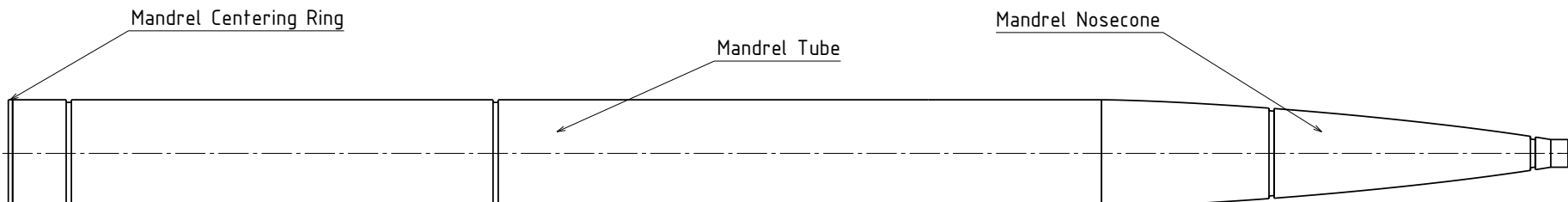
1	2	3	4	5	6	7	8
---	---	---	---	---	---	---	---

List of parts in assembly

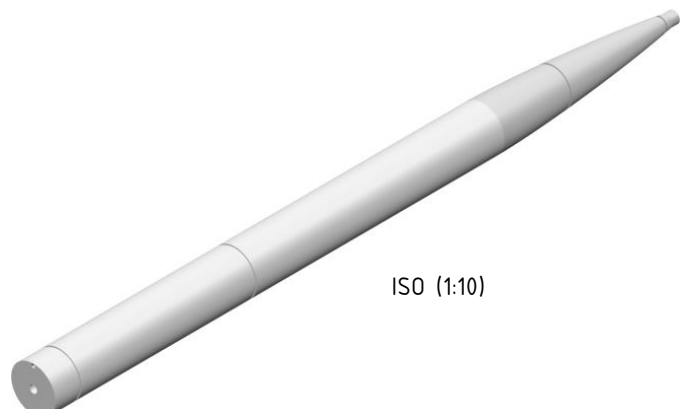
Part name	Sheet	Quantity
Mandrel Nosecone	2/4	1
Mandrel Tube	3/4	1
Mandrel Centering Ring	4/4	1



Section view



Side view



ISO (1:10)

Part name: Mandrel Assembly	Designed by: Ask Haugerud Hovik, 22/02/21
--------------------------------	--

Roughness: $R_a = 3,2$ med mindre annet er oppgitt	Approved by: Henrik Øvrebo, 22/02/21
---	---

Material: Aluminium	Technical Reference: Ask Haugerud Hovik, 90593845
------------------------	--

Tolerance: Toleranser for ikke-toleransesatte mål NS-ISO 2768-1 middels	Sheet: 1/4
--	---------------

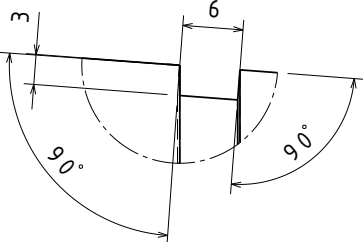
	Paper size: A3	Scale: 1:5
	Date: 22/02/21	Version: 3

1	2	3	4	5	6	7	A3
---	---	---	---	---	---	---	----

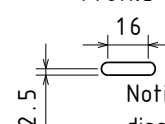
1	2	3	4	5	6	7	8
---	---	---	---	---	---	---	---

List of parts in assembly		
Part name	Sheet	Quantity
Mandrel Nosecone	2/4	1
Mandrel Tube	3/4	1
Mandrel Centering Ring	4/4	1

Repeated detail A (2:1) x2

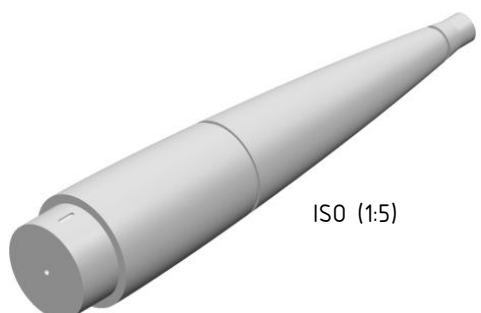
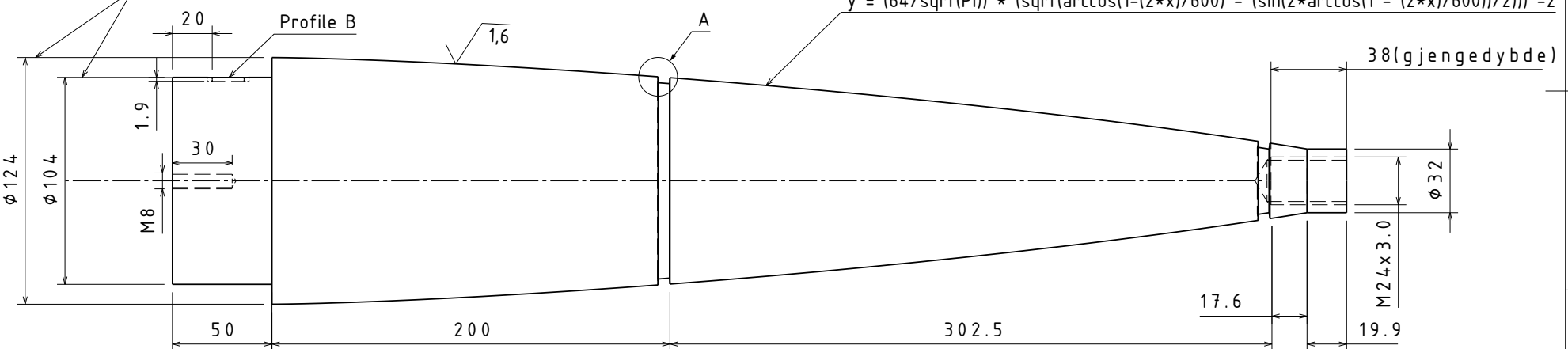


Profile B



Notis: Det er ikke viktig å bruke
disse størrelsene på nøkkelen (keyway).
Dere kan bruke en nøkkel dere har.

Diameter skal matche diameter på Mandrel Tube



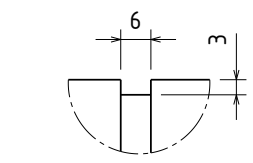
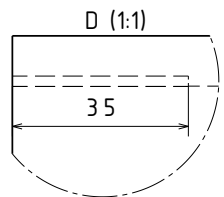
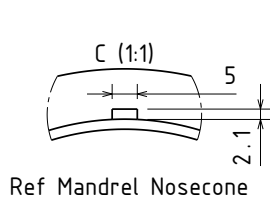
ISO (1:5)

Part name: Mandrel Nosecone	Designed by: Ask Haugerud Hovik, 22/02/21
Roughness: $R_a = 3,2$ med mindre annet er oppgitt	Approved by: Henrik Øvrebø, 22/02/21
Material: Aluminium	Technical Reference: Ask Haugerud Hovik, 90593845
Tolerance: Toleranser for ikke-toleransesatte mål NS-ISO 2768-1 middels	Sheet: 2/4
	Paper size: A3
	Scale: 1:2
	Date: 22/02/21
	Version: 3

1	2	3	4	5	6	7	8
---	---	---	---	---	---	---	---

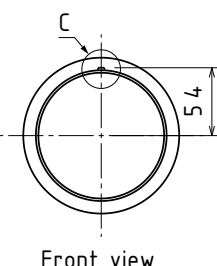
List of parts in assembly

Part name	Sheet	Quantity
Mandrel Nosecone	2/4	1
Mandrel Tube	3/4	1
Mandrel Centering Ring	4/4	1



Repeated detail B (1:1) x2

Ref Mandrel Nosecone



Front view

124 ($+0.05$ -0.05)

104

55
69.8

D

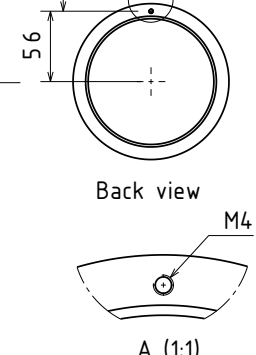
B

Ra 1.6

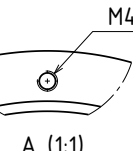
119.2
126.0

Max 100

55
2.2
10.4



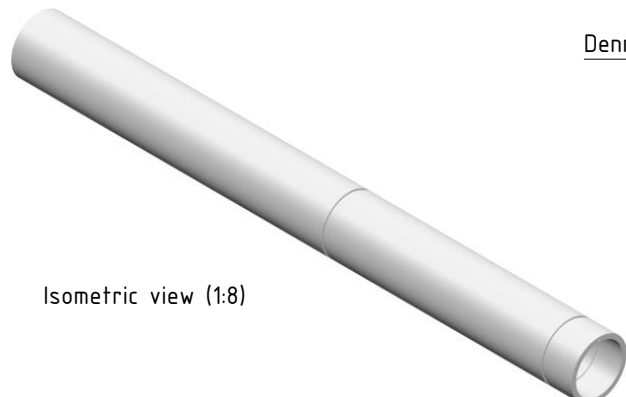
Back view



A (1:1)

Denne diametren er ikke viktig så lenge den passer med Mandrel Nosecone

Denne diametren er ikke viktig så lenge den passer med Mandrel Centering Ring



Isometric view (1:8)

Part name: Mandrel Tube	Designed by: Ask Haugerud Hovik, 16/11/20
Roughness: Ra = 3.2 med mindre annet er oppgitt	Approved by: Henrik Øvrebo, 22/02/21
Material: Aluminium	Technical Reference: Ask Haugerud Hovik, +4790593845
Tolerance: Toleranser for ikke-toleransesatte mål NS-ISO 2768-1 middels	Sheet: 3/4
	Paper size: A3
	Scale: 1:4
	Date: 15/02/20
	Version: 4

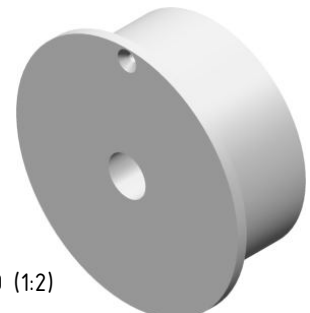
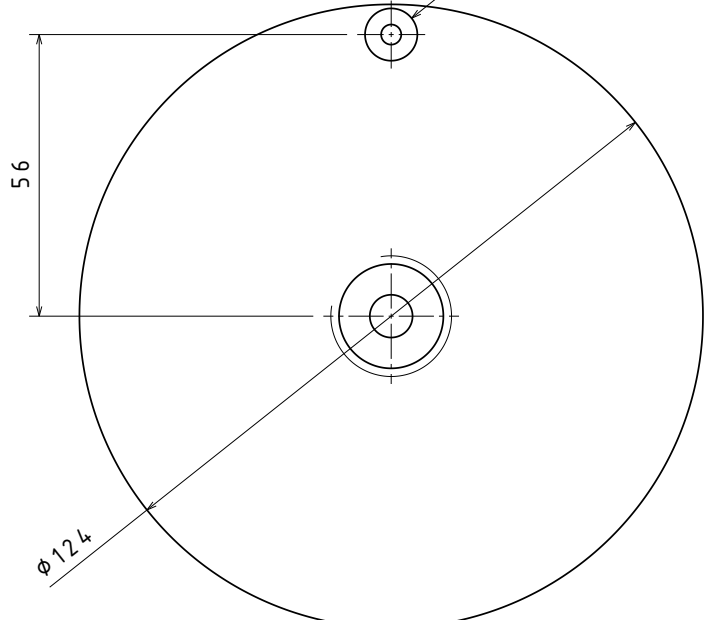
1	2	3	4	5	6	7	A3
---	---	---	---	---	---	---	----

Plasseringen på gjenge ikke viktig, så lenge det passer med korresponderende hull på Mandrel Centering Rng

1	2	3	4	5	6	7	8
---	---	---	---	---	---	---	---

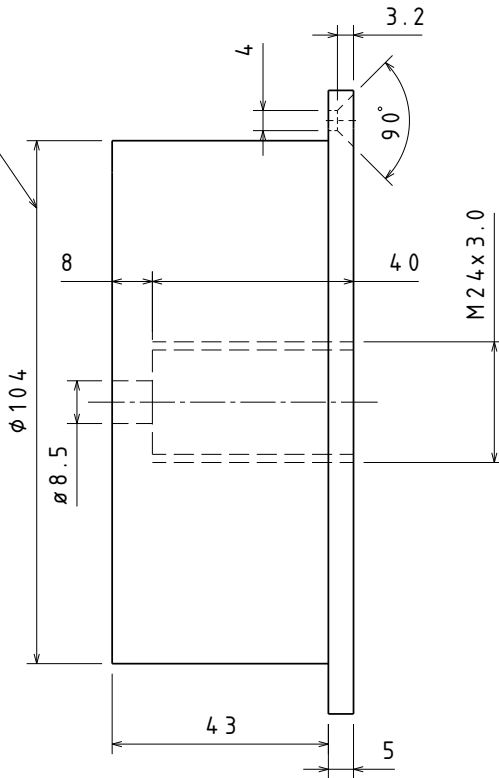
Denne diametren må matches til diameteren på Mandrel Tube

Plasseringen på hull ikke viktig, så lenge det passer med korreseponderende hull på Mandrel Tube



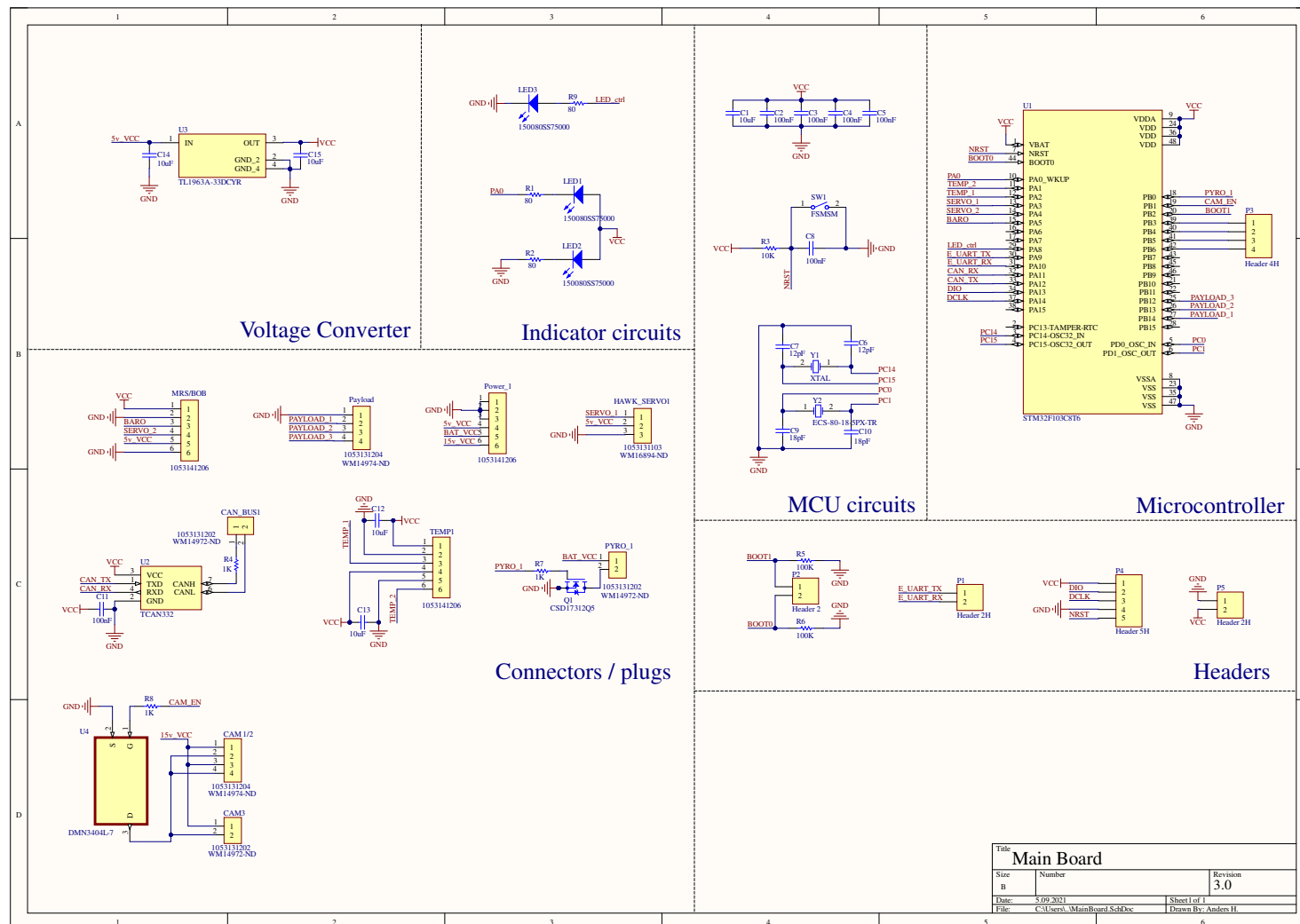
ISO (1:2)

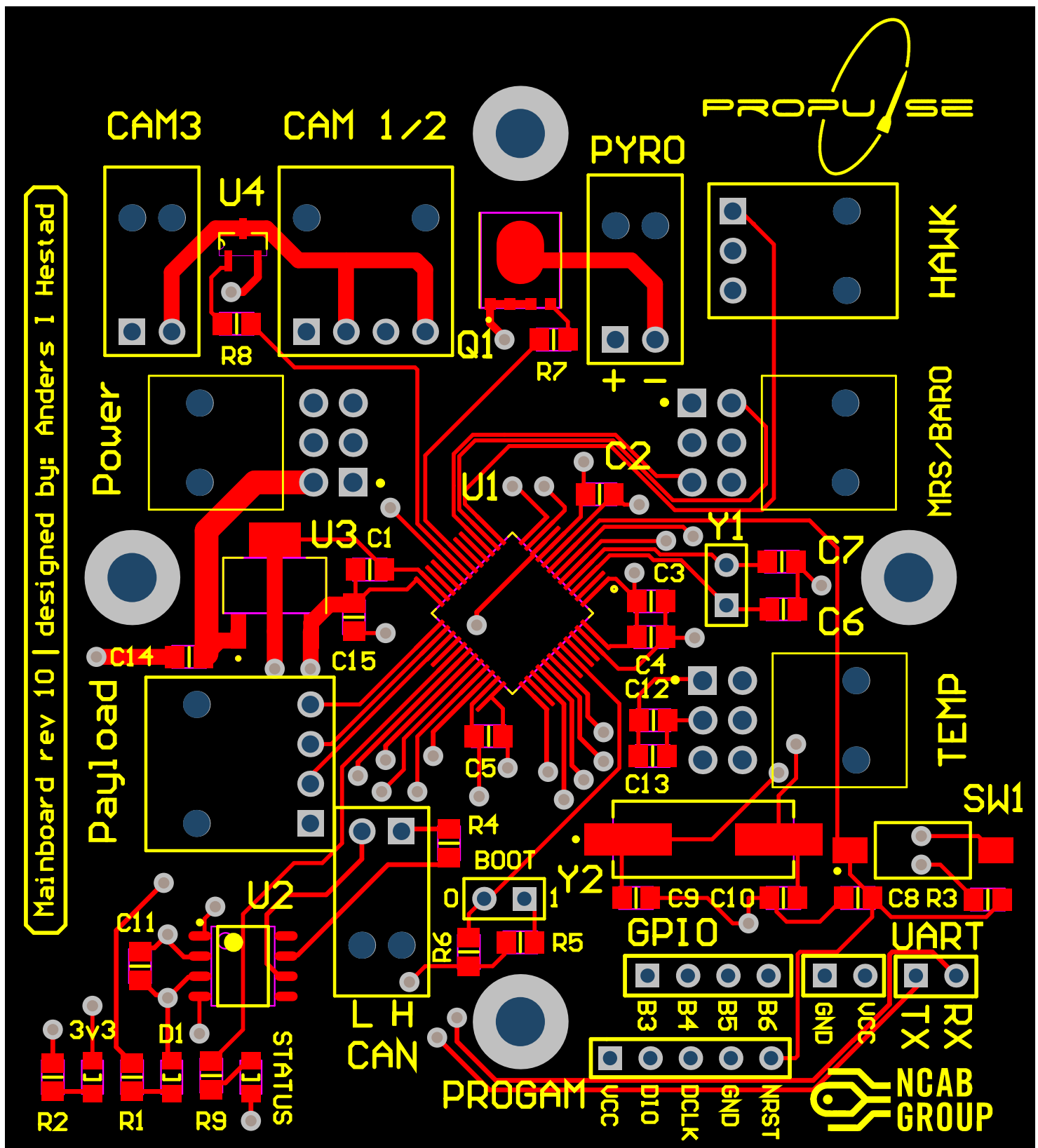
List of parts in assembly		
Part name	Sheet	Quantity
Mandrel Nosecone	2/4	1
Mandrel Tube	3/4	1
Mandrel Centering Ring	4/4	1



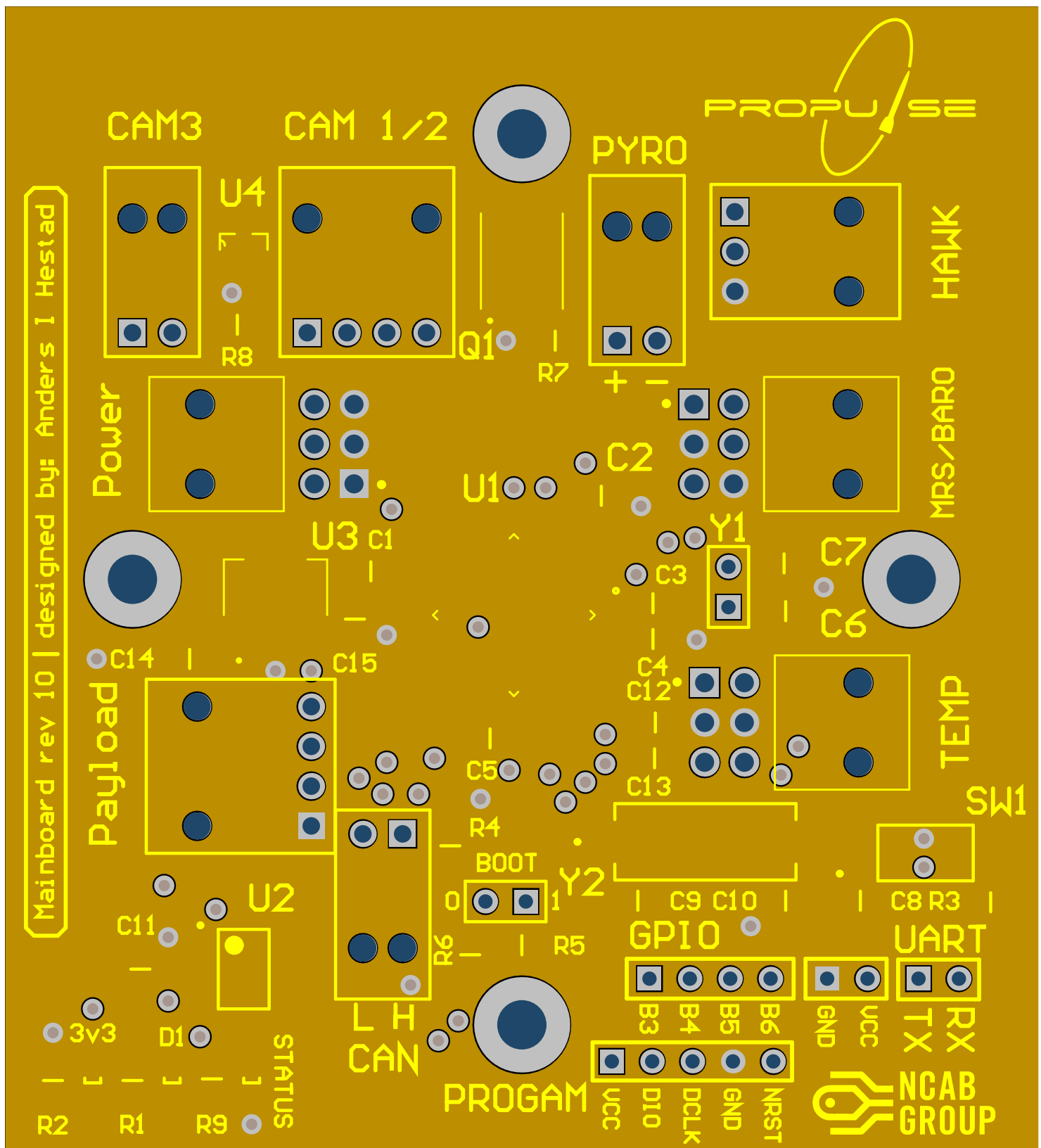
Part name: Mandrel Centering Ring	Designed by: Ask Haugerud Hovik, 22/02/21
Roughness: $R_a = 3.2$ med mindre annet er oppgitt	Approved by: Henrik Øvrebo 22/02/21
Material: Aluminium	Technical Reference: Ask Haugerud Hovik, 90593845
Tolerance: Toleranser for ikke-toleransesatte mål NS-ISO 2768-1 middels	Sheet: 4/4
	Paper size: A3
	Scale: 1:1
	Date: 22/02/21
	Version: 3

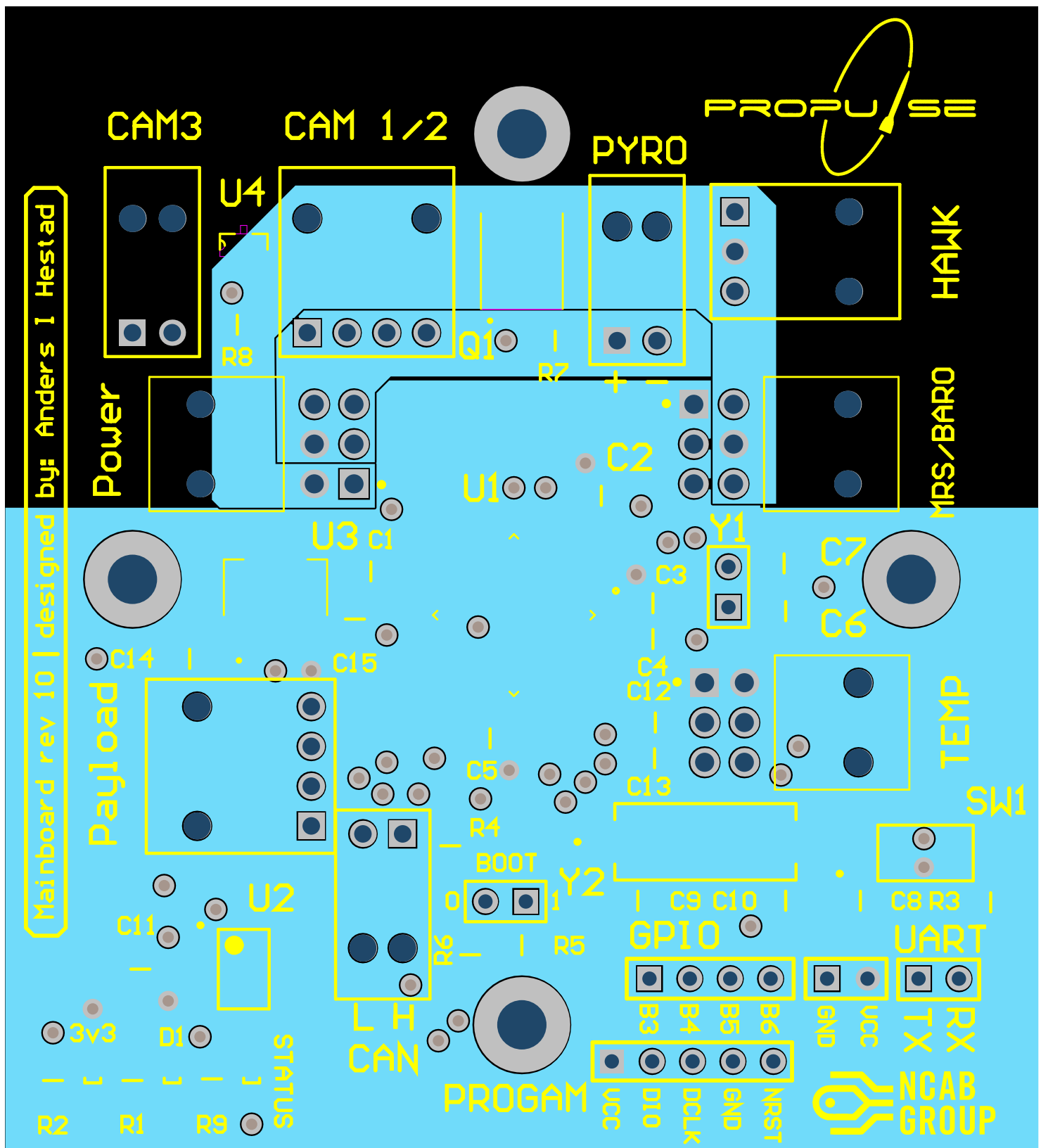
1	2	3	4	5	6	7	A3
---	---	---	---	---	---	---	----



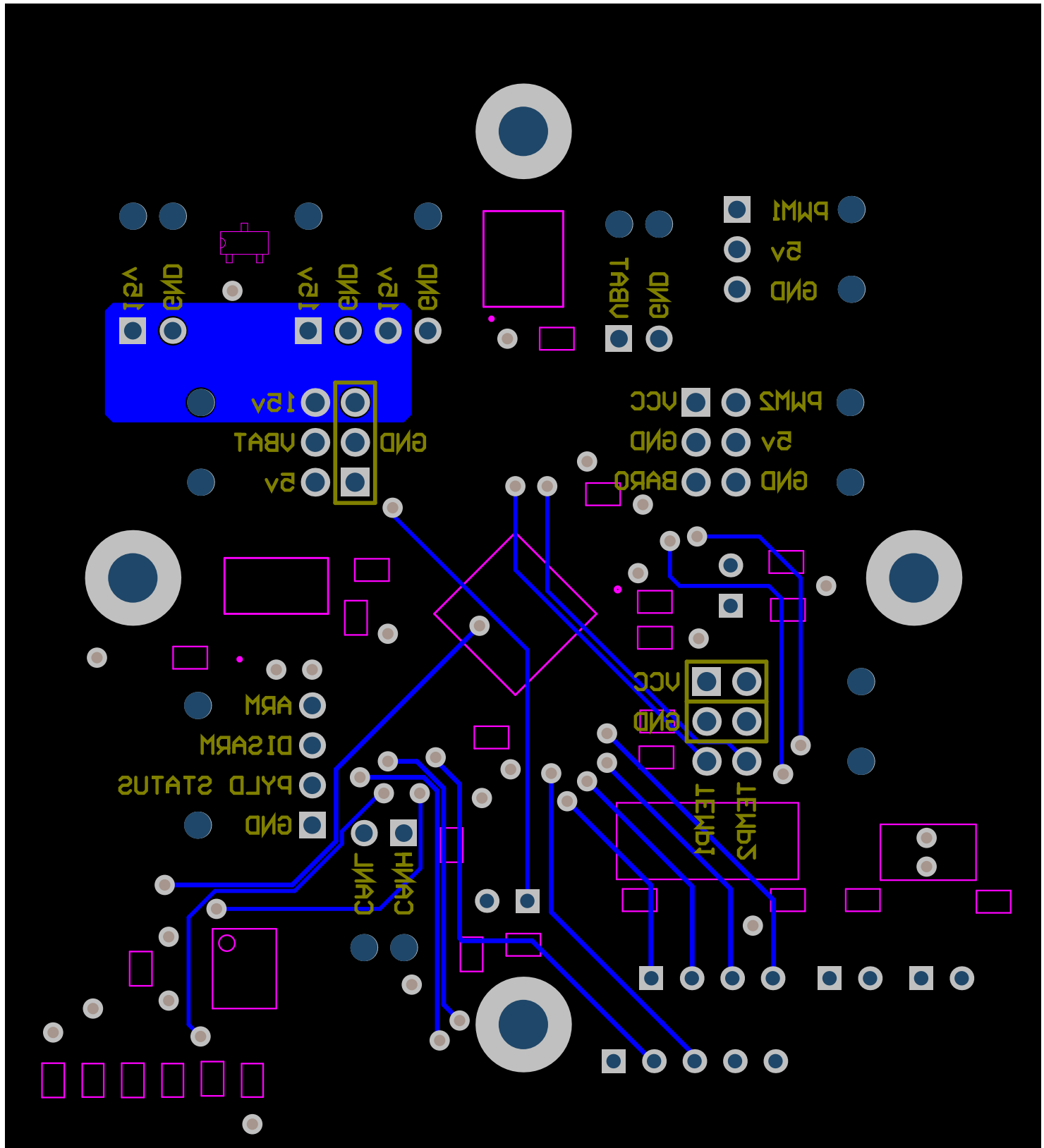


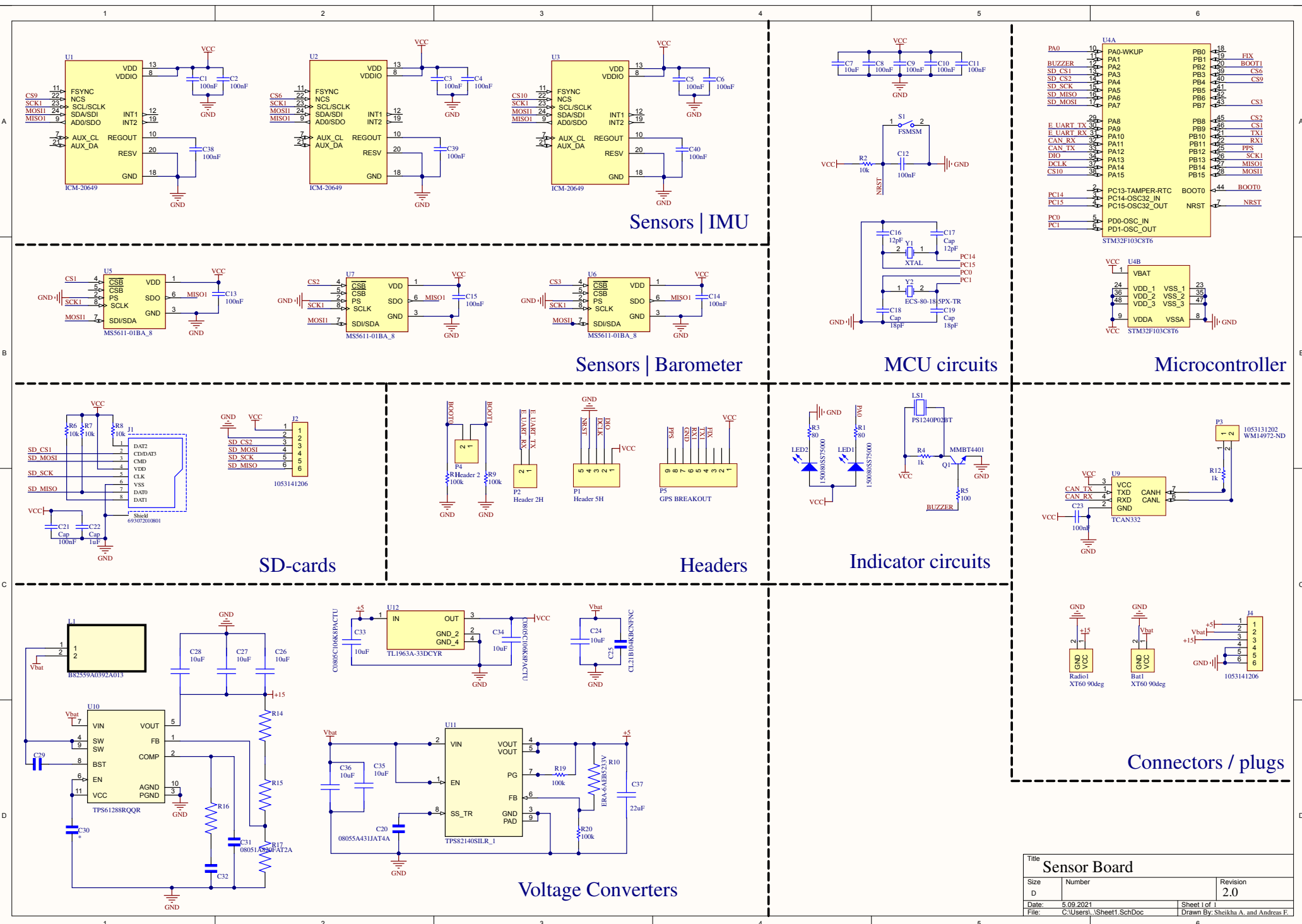
Main Board PCB GND layer



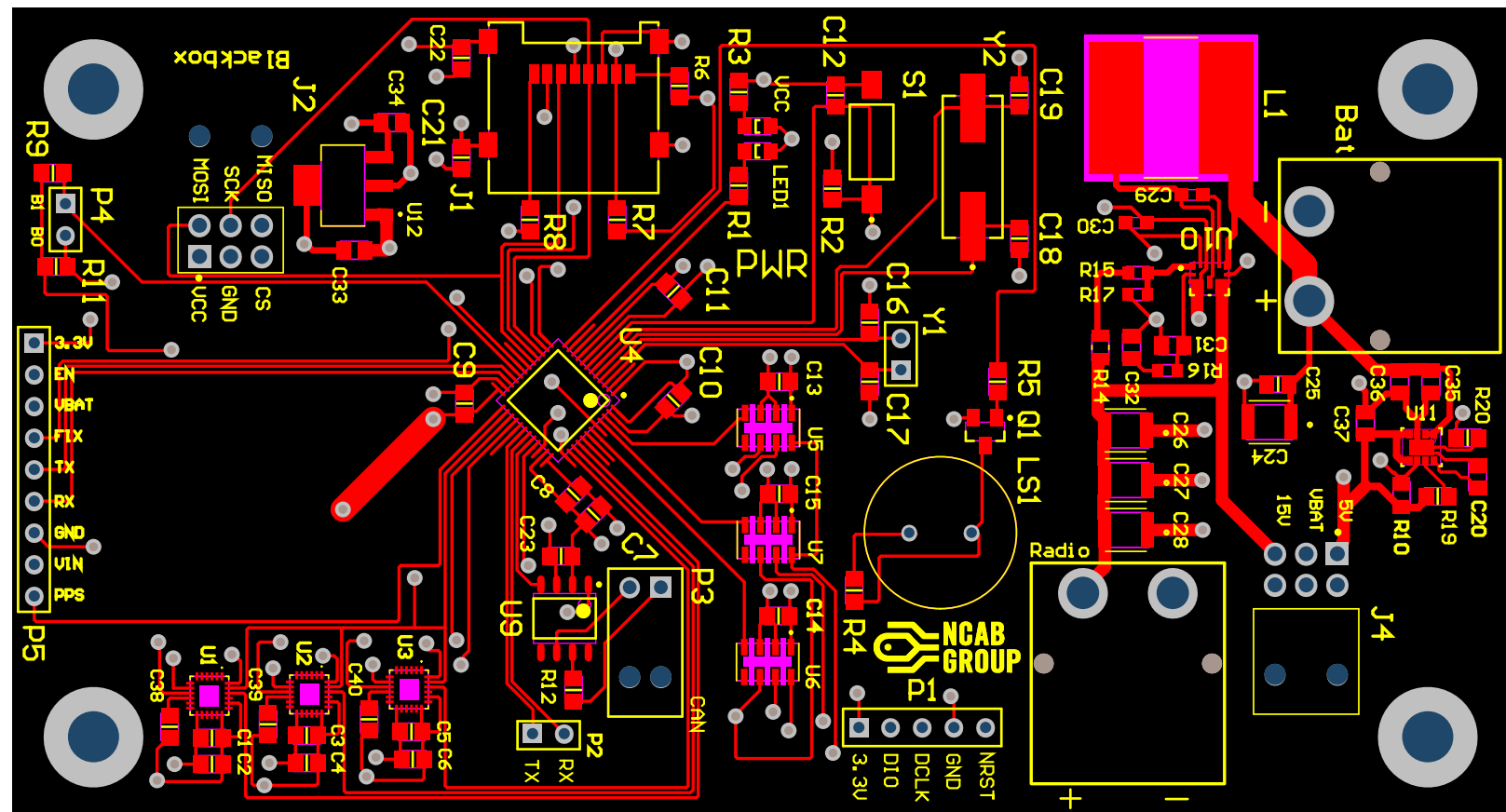


Main Board PCB Bottom layer

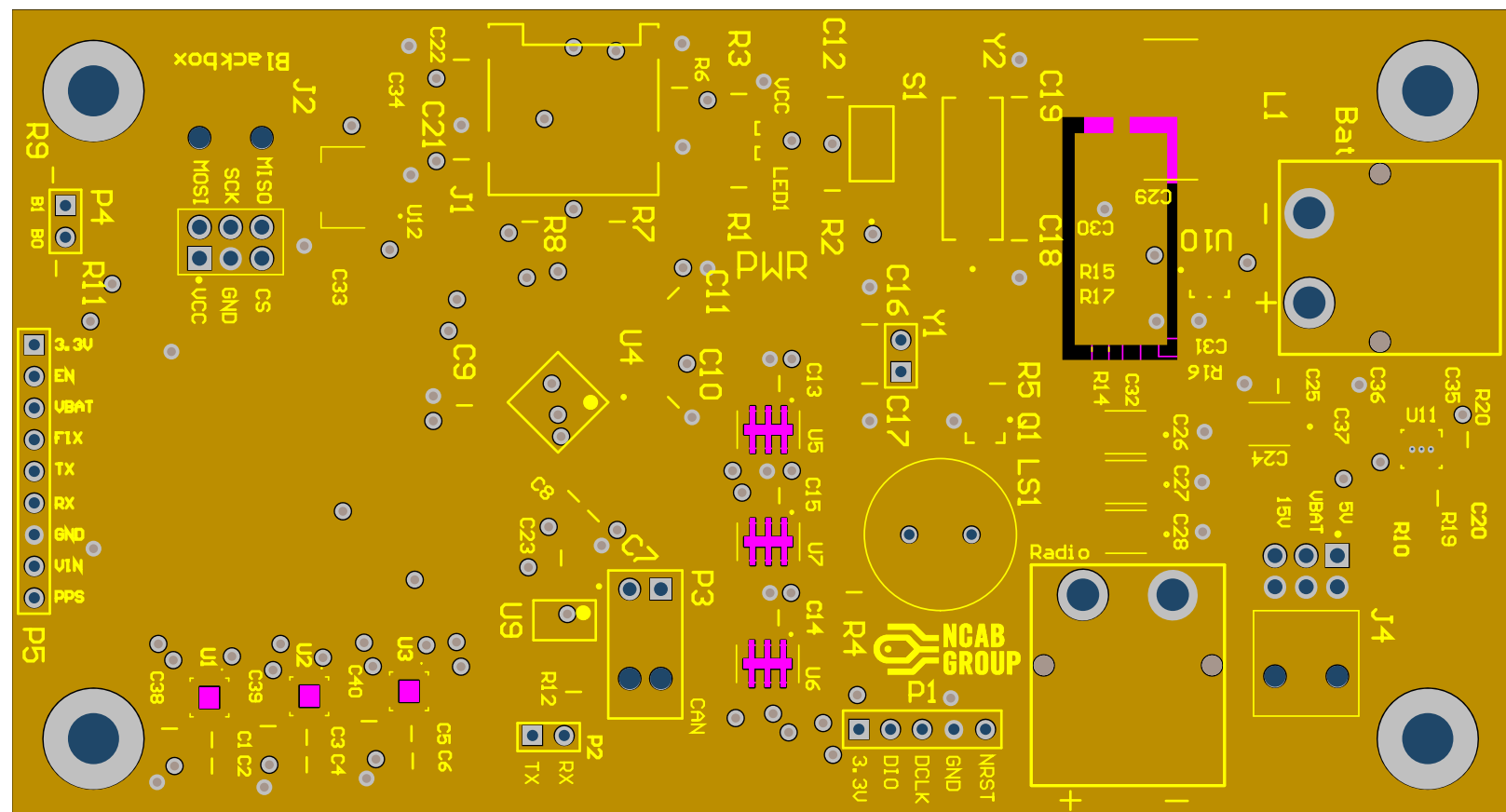




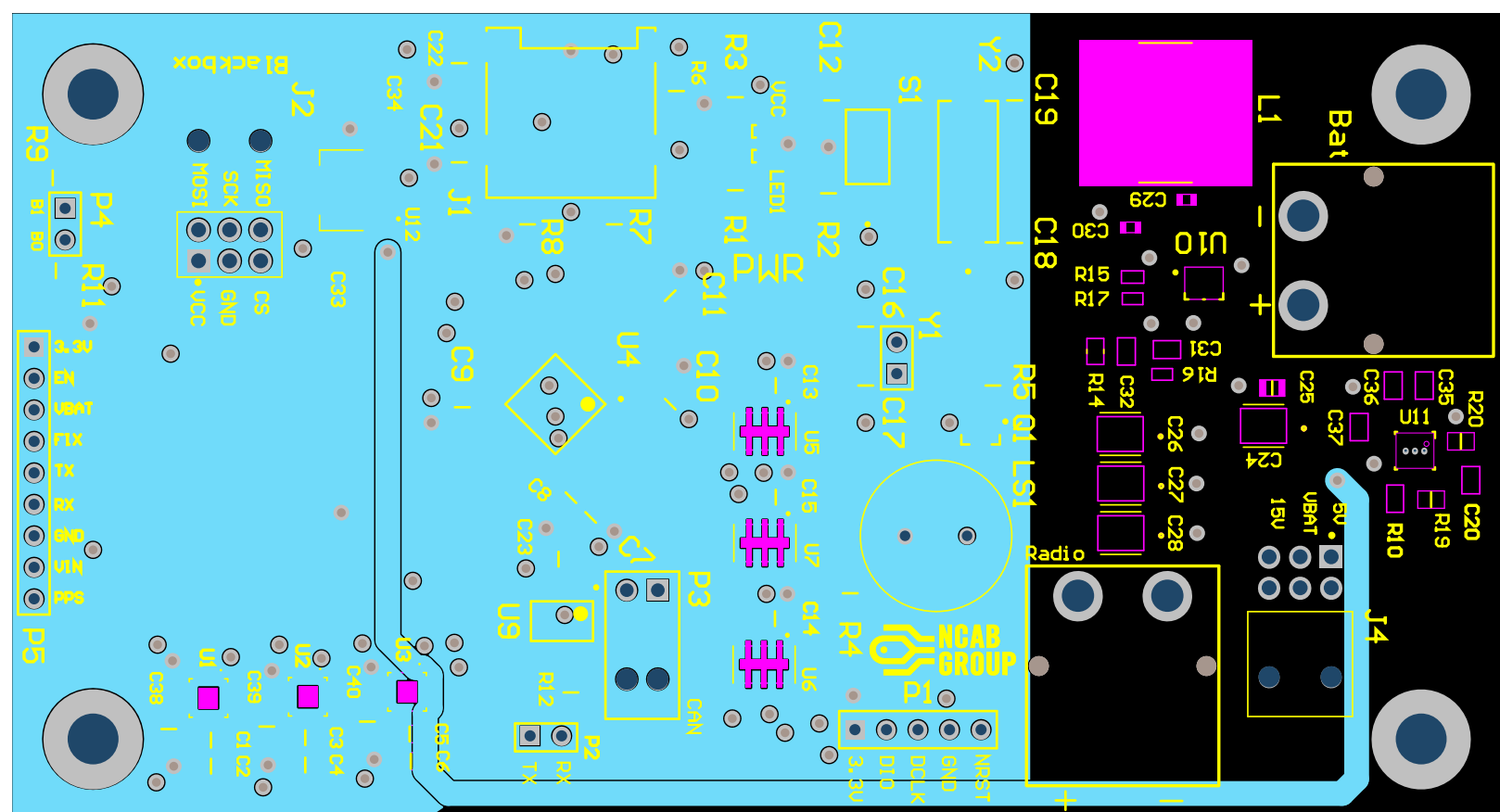
Sensor Board PCB Top layer



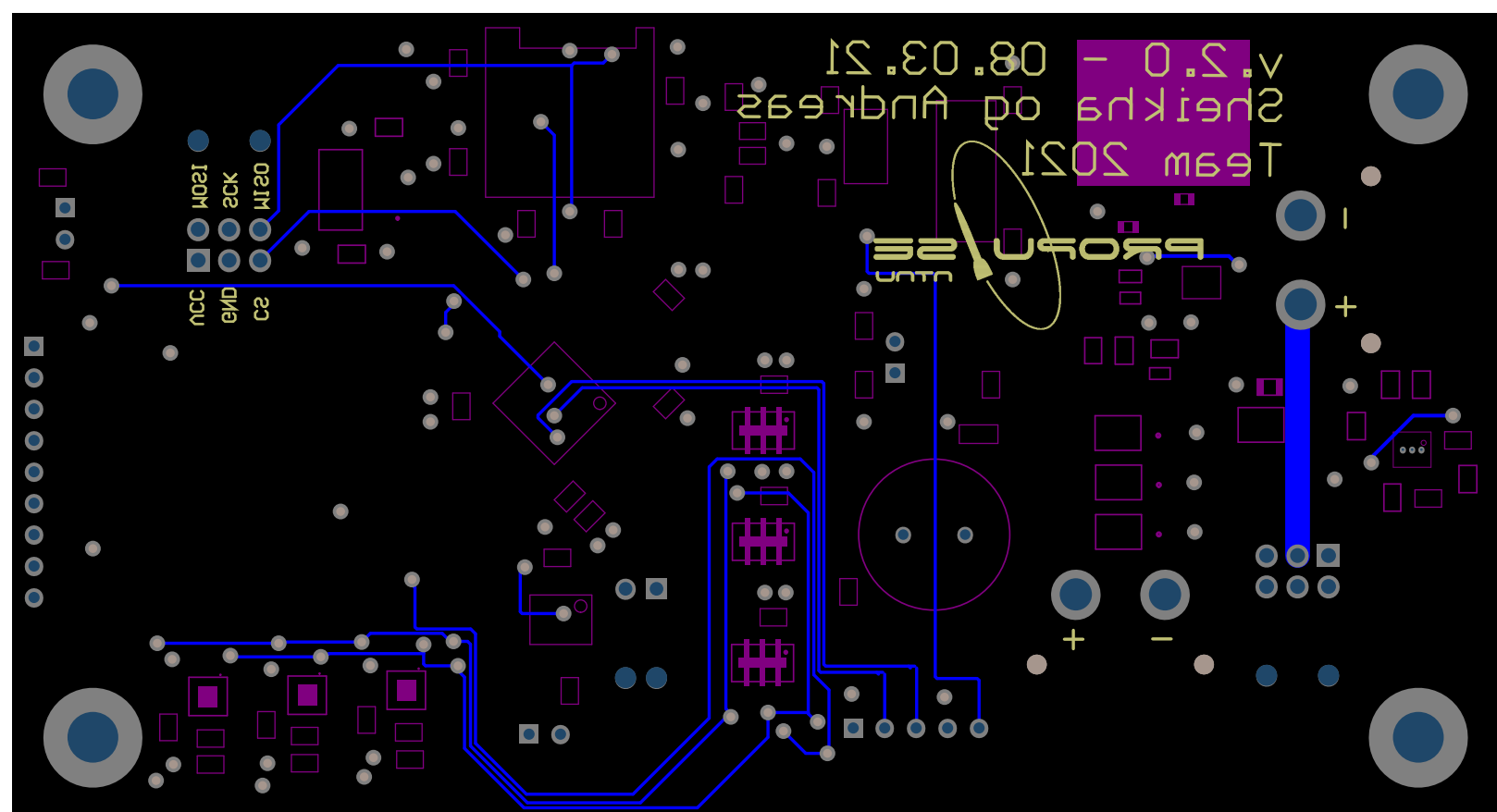
Sensor Board PCB GND layer



Sensor Board PCB PWR layer



Sensor Board PCB Bottom layer



G. Aerodynamics

Aerodynamics

This document will elaborate on the theory and methods that have been applied to achieve the results presented in section II.C and II.D in the main report, as well as discussion around error and uncertainty.

Table of contents

Equations	1
Uncertainties	3
Aerodynamic Coefficients	6
Introduction to Computational Fluid Dynamics (CFD)	9
Static Pressure Distribution	11
Mach Contour and Shock Angle Presentation	14
Thermal Evaluation	16
Turbulence Intensity Evaluation	19

Equations

Here the relevant force equations are presented, followed by an outline for how to obtain the drag, lift and moment coefficients presented in each equation and their relevance. Then, a comparison between solutions for drag and lift coefficient, obtained from CFD and RASAero II will be presented graphically.

In aerodynamics, the dimensional quantity called the freestream dynamic pressure, can be expressed as:

$$q_{\infty} = \frac{1}{2} \rho_{\infty} V_{\infty}^2 \quad (1.1)$$

where the freestream variables q_{∞} and V_{∞} are density and velocity, respectively. The air density in the incompressible regime was set to standard atmospheric condition, and the compressible regime was selected to adhere to the ideal gas law.

The drag equation has been used to evaluate the drag force exerted on the rocket, which is [7]:

$$F_D = C_D A q_\infty \quad (1.2)$$

where A is the reference area representing the largest cross-sectional area of the airframe tube section, and C_D is the drag coefficient.

The equation for the lift force is almost equal to the drag force equation, and are expressed as [7]:

$$F_L = C_L S q_\infty \quad (1.3)$$

where C_L is the lift coefficient, and S is a reference area pertaining to the relevant geometry, which here has been selected to be the planform area of the fin section. See Figure (1.1) for illustration of this distinction.

The moment at CG can be calculated using the moment equation as [7]:

$$M_{LE} = C_M S l q_\infty \quad (1.4)$$

where l is a reference length, which has been selected to represent the mean chord length, c , of the fin, and C_M is the moment coefficient.

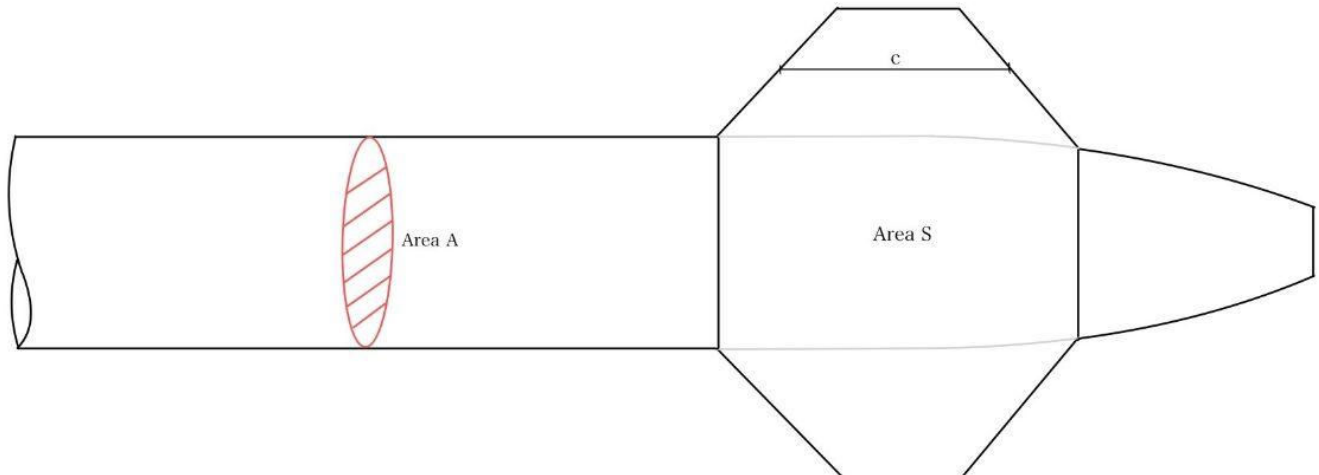


Figure 1.1: Overview of reference area A, and S.

The equation for drag coefficient, lift coefficient and moment coefficient are represented through equation 1.6-1.8 [7]:

$$C_D = \frac{F_D}{q_\infty A} \quad (1.6)$$

$$C_L = \frac{F_L}{q_\infty S} \quad (1.7)$$

$$C_M = \frac{M_{LE}}{q_\infty Sl} \quad (1.8)$$

Where F_D , F_L and M_{LE} is the drag force, lift force and moment respectively.

Uncertainties of calculations

This section presents the methods used to simulate the rocket's flight trajectory, estimate flight stability, as well as the accuracy of the corresponding results thereof.

Comparison between OpenRocket and RASAero II:

OpenRocket applies aerodynamic theories related to the incompressible and subsonic region, and simplified, empirical methods to approximate aerodynamic effects in the transonic and supersonic region. It is therefore important to keep in mind the error related to the results gained within the two latter flight regions.

OpenRocket enables comparing experimental flights with flight simulation data. The first experimental model rocket used by Sampo Niskanen (the developer of Open Rocket) was a 560 mm long, 29 mm diameter rocket with two different motors. The nose cone was selected to be 100 mm long with a Tangent Ogive shape. The fin design was trapezoidal in shape, and the expected max velocity was within Mach = 0.2, making both experimental flight tests within the incompressible regime. The results were an overprediction of altitude, yielding 16 % for an apogee of 74.4 m and 7% for an apogee of 161.4 m.

Further conclusions is a 10% accuracy prediction for both the drag coefficient (C_D) and the center of pressure location (C_p) within the subsonic region. Whereas no conclusion was drawn for all three

parameters, hereby C_p , C_D and C_N , for the supersonic region. However, Sampo Niskanen states that the expected accuracy should be reasonable up to Mach 1.5.

RASAero II is mainly focused on the aerodynamic effects on rockets. The program also has the additional use of flight trajectory simulation similar to OpenRocket. However, to use this feature, one needs to implement the correct rocket engine and flight characteristic parameters, such as the location of center of mass (C_G). The program does not have the feature of implementing design parameters for each part of the rocket, such as mass, surface roughness and component thickness. Thus, limiting the program when compared to OpenRocket. In addition, the program is not open-source software, which restricts access and therefore it is difficult to gain knowledge about how the program works and how it is built.

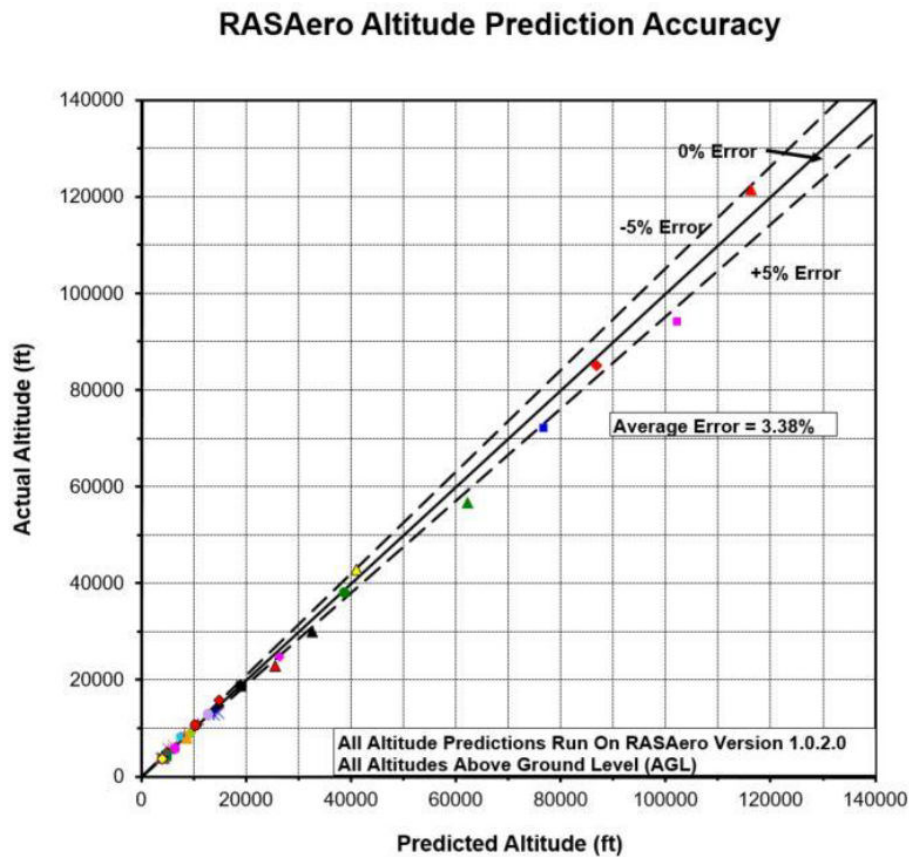


Figure 1.2: Comparison of predicted altitude from RASAero II against experimental flights data records.

Experimental flights have been used to predict both relevant and average altitude accuracy for the software. Lines of relative error of $\pm 5\%$ have been drawn in the chart as seen from Figure 1.2. Most of the compared data are experimental flights reaching up to 30 000 feet where the predicted error is significantly low compared to experimental flights up to almost 120 000 feet. The overall average

error has been estimated to be 3.38% and the highest estimated error is just above 5% [22], making RASAero II significantly more accurate compared to OpenRocket. Moreover, no predicted value for the accuracy of the CP location was found. However, a RASAero II graphical comparison with ARCA sounding rocket with additional wind tunnel data has been done for the CP location.

The wind tunnel data are for the NASA TN D-4013 and NASA TN D-4014. The difference between the two models is the length, whereas the first model is 1.04 m and the second is 1.36 m [23].

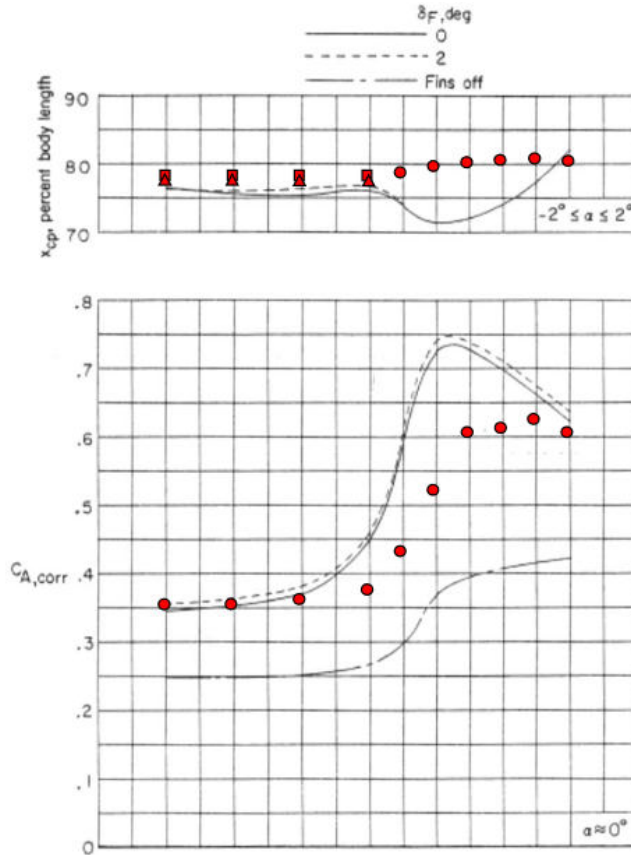


Figure 1.3: C_p (top) and drag coefficient (bottom) comparison between RASAero II (red marks) and NASA TN D-4014 between Mach 0.6-1.2. Triangle indicates Rogers Modified Barrowman method, square indicates Barrowman's method and circles indicates transonic-supersonic prediction [23].

A comparison between experimental data on NASA TN D-4014 and RASAero II numerical results can be found in the upper graph from Figure 1.3. RASAero II predicts C_p well with minor deviations between Mach 0.6 and 0.9. However, for the transonic region, a significant deviation can be observed [23]. This is expected as the numerical uncertainty increases significantly in the transonic region [6].

Furthermore, for Mach numbers greater than 1, there are insignificant deviations on predicted C_p location when compared with data from NASA TN models [23].

The lower graph in Figure 1.3 is a comparison of the drag coefficient where $C_{A,corr}$ denotes the axial force coefficient corrected for base pressure difference relative to the freestream static pressure. Here, a significant deviation can be observed between Mach 0.9 and 1.2 which is identical the case for C_P prediction. However, for the prediction before Mach 0.9, where the comparison is not shown in Figure 1.3 for $Mach > 1.2$, shows that RASAero II predicts C_D well and with insignificant error.

A comparison between the CFD results and results from RASAero II can be seen from Figure 1.4.

As RASAero II predicted the aerodynamic aspect of the rocket with minor errors compared to OpenRocket, it was decided to use the program in combination with CFD to derive meaningful data on the aerodynamic characteristics of the rocket.

Finally, all of the outer structural components were designed and iterated in combination with flight simulations to find the optimal aerodynamic design. The task was then to find critical points and events in the flight profile, to find the localized stability of the rocket. The critical points were determined using both the CG location from OpenRocket and CP location from RASAero II. These results were then compared with results from CFD using ANSYS fluent.

Aerodynamic Coefficients

The aerodynamic coefficients are used to predict different aerodynamic aspects of the flow field and the interaction between the moving fluid and the rocket design. The coefficients have been used to compare values from CFD against values from RASAero II. This is a validation technique to see how well the CFD solutions are relative to the more approximated values from RASAero II.

The coefficients are strongly dependent on the Reynolds number, Mach number and the angle of attack (AoA), being generally expressed as [7]:

$$C_i = f(Re, M_\infty, \alpha), \quad (1.9)$$

where $i \in \{D, L, M\}$ and denotes drag, lift and moment, respectively. Re is the Reynolds number, M_∞ is the upstream Mach number and α is the AoA.

The general equation for drag coefficient and lift coefficient are represented by [7]:

$$C_i = \frac{F_i}{q_\infty A_{ref}}, \quad (2.0)$$

where A_{ref} is a reference area.

The coefficients are typically determined through both numerical analysis, such as CFD, and by experiments, e.g. using wind tunnels. Unfortunately, no wind tunnel was available this year during the project, meaning only CFD simulations, RASAero II, and OpenRocket, were available to estimate the coefficients. The drawback by not using a wind tunnel is that the numerical simulations generally have discernible errors and several assumptions are made, which ultimately can lead to wrong interpretation of the data and conclusions. Despite this, as mentioned above, the predicted accuracy on the coefficients obtained from RASAero II is determined to be adequate for the purpose of this project. Therefore, results on drag coefficients derived from CFD have been compared with values from RASAero II and can be viewed in Figure 1.4 below.

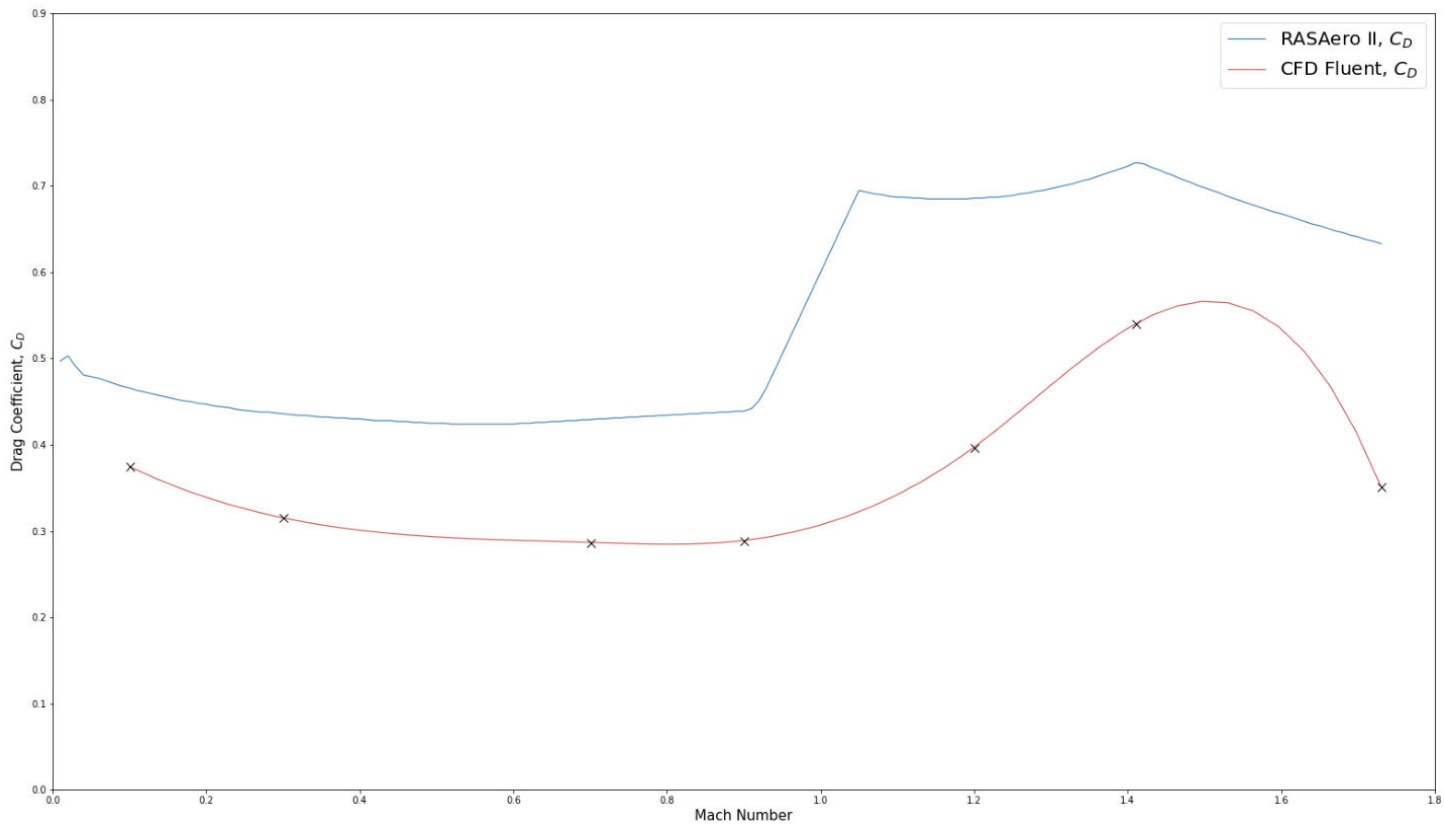


Figure 1.4. Drag coefficient (C_D) comparison between RASAero and CFD.

From aerodynamic theory, the drag coefficient is expected to decrease in the subsonic region as the freestream pressure decreases. As the rocket enters the transonic region, the drag coefficient is then expected to increase as shock waves start to form around the rocket body [7]. Both of these physical effects have been captured by numerical solutions from both simulation programs, as seen in Figure 1.4 above. However, the difference is that RASAero II predicts a more rapid increase, whereas CFD results predict this increase to happen with a broader range of Mach numbers. What is the most accurate estimate is hard to tell as this is strongly dependent on the geometry of the rocket and the physical flow field around it. Numerical simulations from both programs predict almost the same maxima for the drag coefficient, which is around Mach 1.4 - 1.5. Thus the highest drag on the rocket is

expected around this region. Furthermore, it can be observed that smaller value for C_D was obtained from the CFD simulations compared to RASAero II, where the largest deviation happens around Mach 1.1. Which one is the most correct is also hard to tell. However, as shown in the section above, RASAero II predicts the drag coefficient with minor to insignificant error compared to experimental flights.

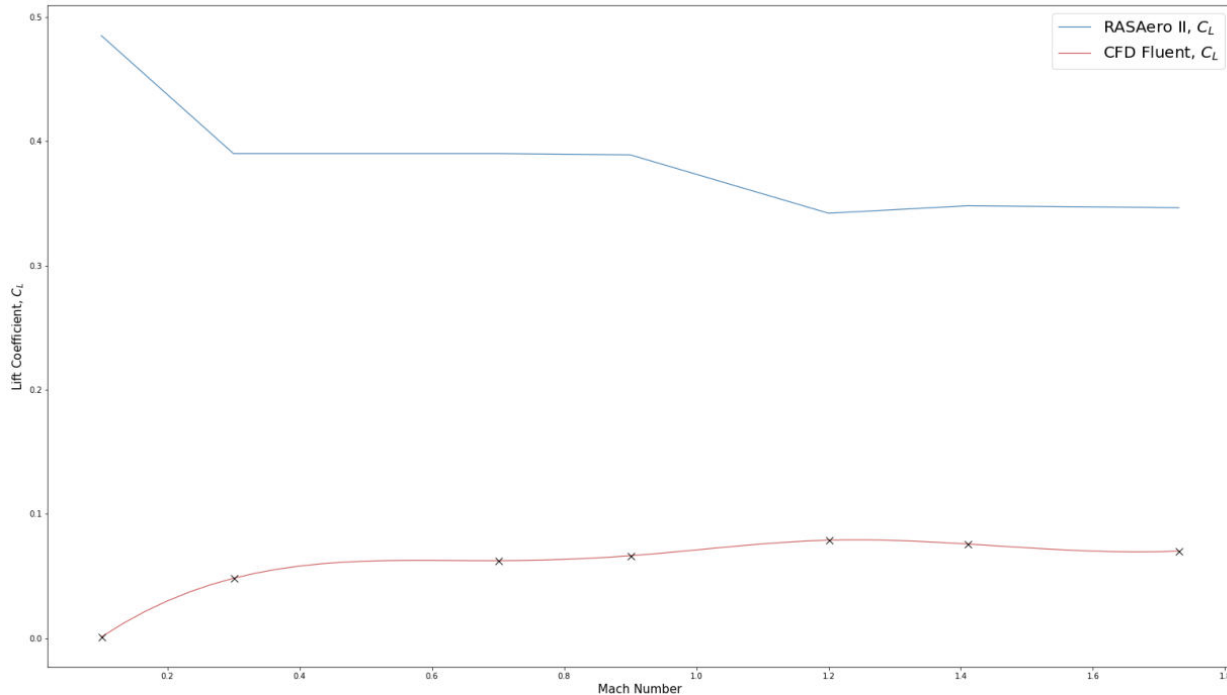


Figure 1.5. Lift coefficient (CL) comparison between RASAero II and CFD. Measured for 2° AoA.

The lift coefficient is determined by integrating both the pressure and the shear force over the outer surface of the rocket. However, as the shear force is working tangentially and the pressure is normal to the surface, this leads to a strong dependence on the pressure field as the lift force acts in the normal direction. The value for C_L obtained is therefore directly proportional to the numerical integration of the pressure field around the object, here considering the fins.

Figure 1.5 shows that RASAero II and the results from CFD deviates significantly from each other. As RASAero II is not an open source program, it is hard to tell which empirical method is used to derive the lift coefficient and the related numerical error. As for the CFD results, the accuracy is strongly dependent on the mesh quality obtained around the fins. The final mesh quality is presented in Table 1 in the next section. However, no conclusion could be drawn from either one of the two numerical solutions obtained in Figure 1.5.

Introduction to Computational Fluid Dynamics (CFD)

This is only a brief introduction into the CFD simulation used in this project. A simple presentation of the assumptions and the simulation setup will be presented. The topic on discretization of the domain is left out for the simplicity of this report.

Ansys Fluent R2021 was used to derive numerical solutions on flow analysis of the rocket, where a 3D cylindrical fluid domain was implemented around the rocket. Two different fluid domains were used: one pressure-farfield domain for the compressible sub- and supersonic regions; and one velocity-inlet/pressure-outlet domain for incompressible flow up to Mach 0.3. After creating the fluid domain, two separate meshes were made using Hexahedral dominant mesh topology. The pre-estimated target cell value for the incompressible domain was 4 200 000 and 2 500 000 for the compressible domain. See Table 1 for an overview of the measured cell number and mesh quality for both domains. The optimal values for Orthogonal Quality and Aspect ratio were set to 1 and 20, respectively. Equal mesh results were obtained for the compressible domain, except for the Aspect ratio of 50. This is expected as the domain is smaller compared to the incompressible domain. The above mentioned values as well as the values presented in Table 1 were determined to be reasonable and within the desired accuracy.

Table 1. Discretization for each simulation domain

Mesh Domain	# of Cells	Max. Aspect Ratio	Min. Orthogonal Quality	Max Skewness
Incompressible regime	4 279 878	73	0.20	0.58
Compressible regime	2 771 789	50	0.20	0.58

It was decided to use the same domain-setup for all simulations, except for the incompressible lift-off analysis. This is to save computational time as each simulation shares the same solver domain which can be done by connecting each tool box in ANSYS together in a tree-branch setup.

Incompressible Air

The incompressible regime assumes a constant density profile as the temperature varies linearly with altitude inside the troposphere. Here, the density was estimated using an exponential approximation of the International Standard Atmosphere (ISA) model, which is determined by equation 2.1 below [24].

$$\rho(z) = \rho_0 e^{-(\frac{gMz}{RT_0} - \frac{Lz}{T_0})} \quad (2.1)$$

where, ρ_0 is the standard atmospheric density, g is the universal gravitational constant, M is the molar mass of air, $L = 0.0065 \text{ K/m}$ is a temperature lapse rate, R is the universal gas constant, T_0 is the sea level standard temperature and z is the altitude.

Compressible Air

For the compressible regime, the pressure-far field domain was used where the density model was set to follow the ideal gas law. For each of the critical points, both the pressure and temperature have been estimated using the ISA model.

The viscosity model used was the $k - \omega$ SST with viscous heating and curve correction, which is the preferred model for external aerodynamic cases [25]. The turbulence intensity is generally considered to be low ($\leq 1\%$) and was determined by equation 2.2 as a function of Reynolds number, Re .

$$I = 0.16 (Re_L)^{-\frac{1}{8}} \quad (2.2)$$

Furthermore, the Sutherland viscosity was selected for the fluid (air) and energy was activated for the analysis. The solver is coupled for the pressure-velocity coupling, with second order upwind for both energy, turbulence kinetic energy, density, and momentum. In addition to this, the solvers are using double precision which requires more computation time; however, this will improve the numerical accuracy considerably.

Static Pressure Distribution

From the contour plot shown by Figure 1.6, the highest pressure regions are at the nose tip and the leading edge of all four fins. A low pressure region can be observed behind the nose cone transition, behind the leading edge of the fins and at the von Kármán transition at the base of the rocket. This is due to an accumulation of the stream which will lead to decrease in pressure.

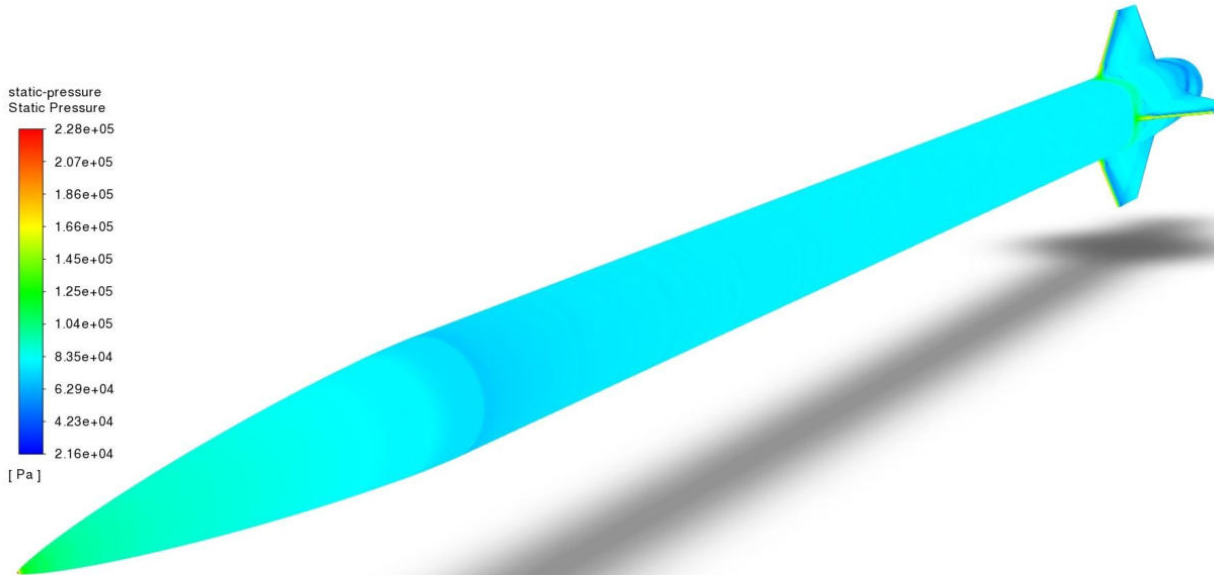


Figure 1.6: Static pressure overview of the entire rocket surface. At Mach 1.73 with 0° AoA.

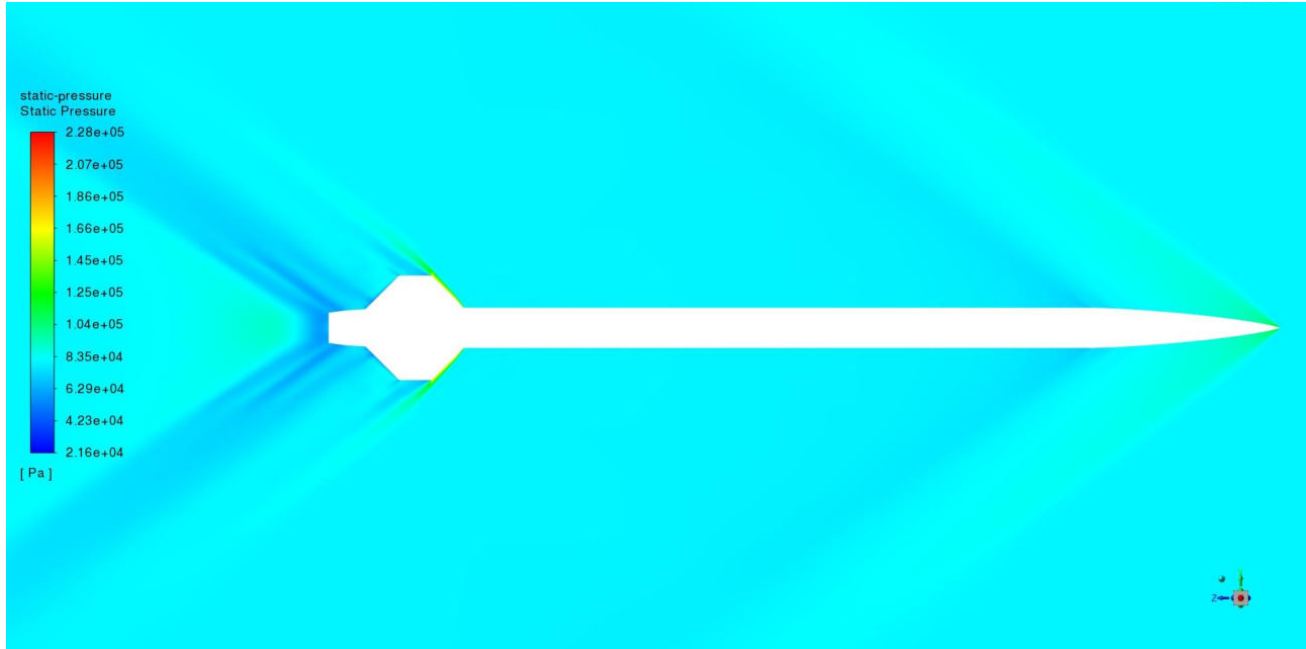


Figure 1.7: Static pressure field around the rocket body. At Mach 1.73 with 0° AoA.

Lift forces are generated due to pressure difference and viscous shear force. However, as the skin friction force acts normal to the direction of lift, the viscous effects are negligible when estimating the lift.. Figure 1.8 and Figure 1.9 display the static pressure on the fins at Mach 1.73 with $\alpha = 0^\circ$ and $\alpha = 7^\circ$, respectively.

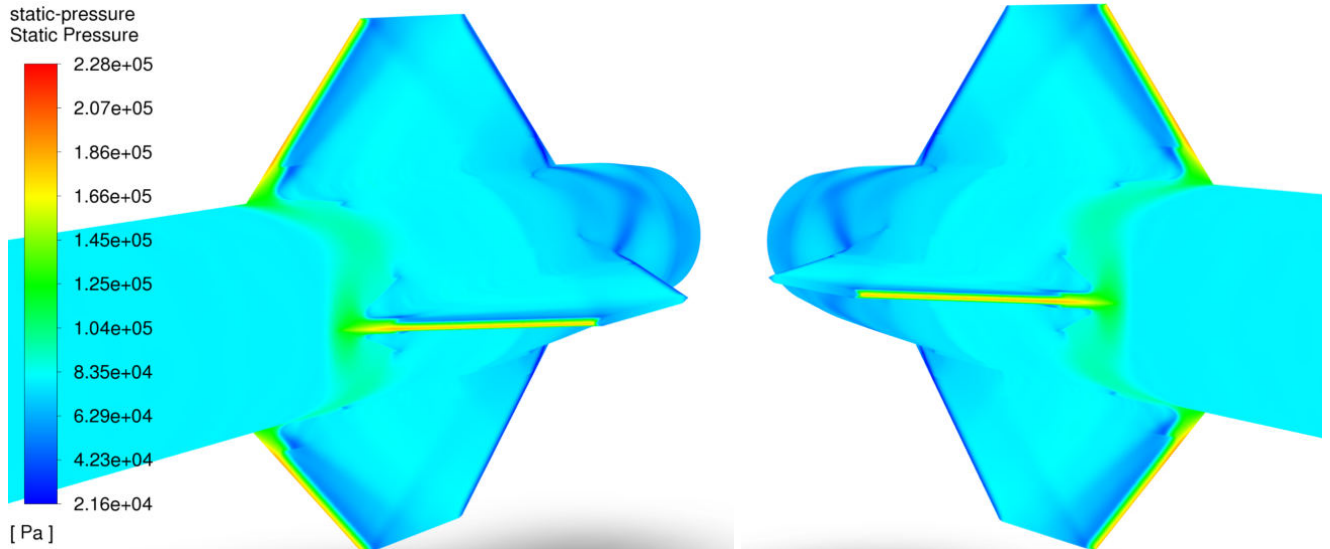


Figure 1.8: Static pressure field around the fins, measured at Mach 1.73 with 0° AoA.

From Figure 1.8, a uniform pressure distribution on the fins can be observed, where no lift is generated. Here the stagnation pressure at the leading edge (LE) is measured to a maximum value of 190.6 kPa.

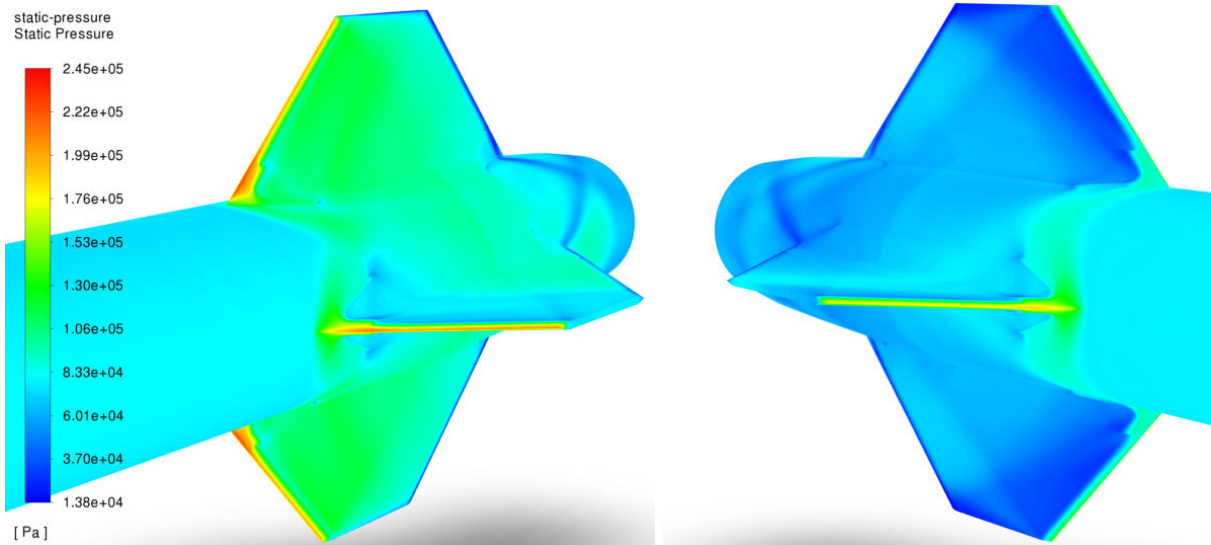


Figure 1.9: Static pressure field around the fins, measured at Mach 1.73 with 7° AoA.

As seen from Figure 1.9, there is now a nonuniform pressure distribution around the fins. The pressure is higher at the right hand side compared to the left side, thus resulting in a lift force. The highest stagnation pressure is measured to 229.3 kPa, which is shifted slightly to the right of the LE as a result of the chosen AoA of 7°. Seen in both Figure 1.8 and Figure 1.9, the angled lines on the aft tube indicate low pressure regions which implicates propagation of expansion fans. Additional observations

can be made from Figure 1.7, where the flow accelerates at the trailing edge of the fins and in the vicinity of the von Kármán base section. Figure 2.0 presents the pressure distribution around the nose cone, where the measured stagnation pressure is 228 kPa located at the nose tip. The highest measured stagnation pressure is 245.44 kPa at 7° AoA which is 16.1 kPa more than the highest measured stagnation pressure on the fins.

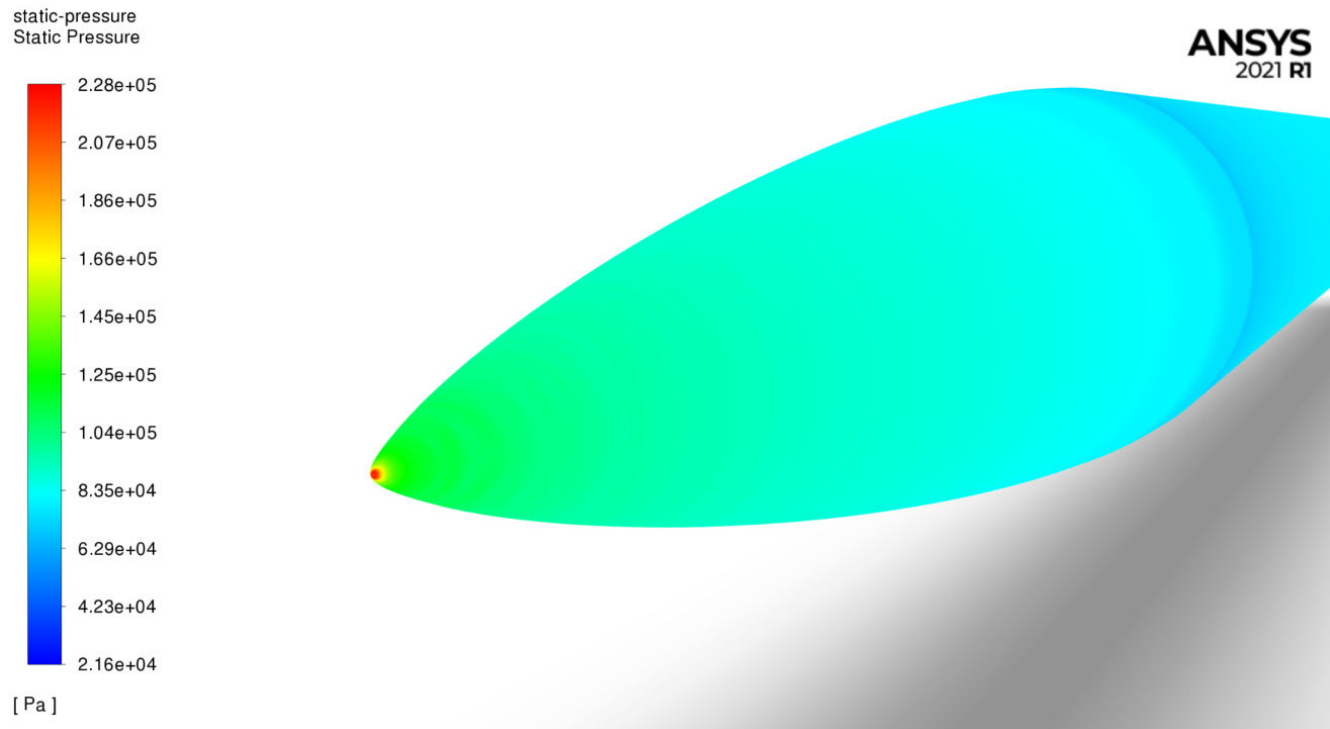


Figure 2.0: Static pressure distribution on the nose cone. Red contour mark on the nose tip indicates stagnation pressure. Measured at Mach 1.73 with 0° AoA.

Mach Contour and Shock Angle Presentation

This section presents the results obtained for the shock angle with respect to increasing Mach number.

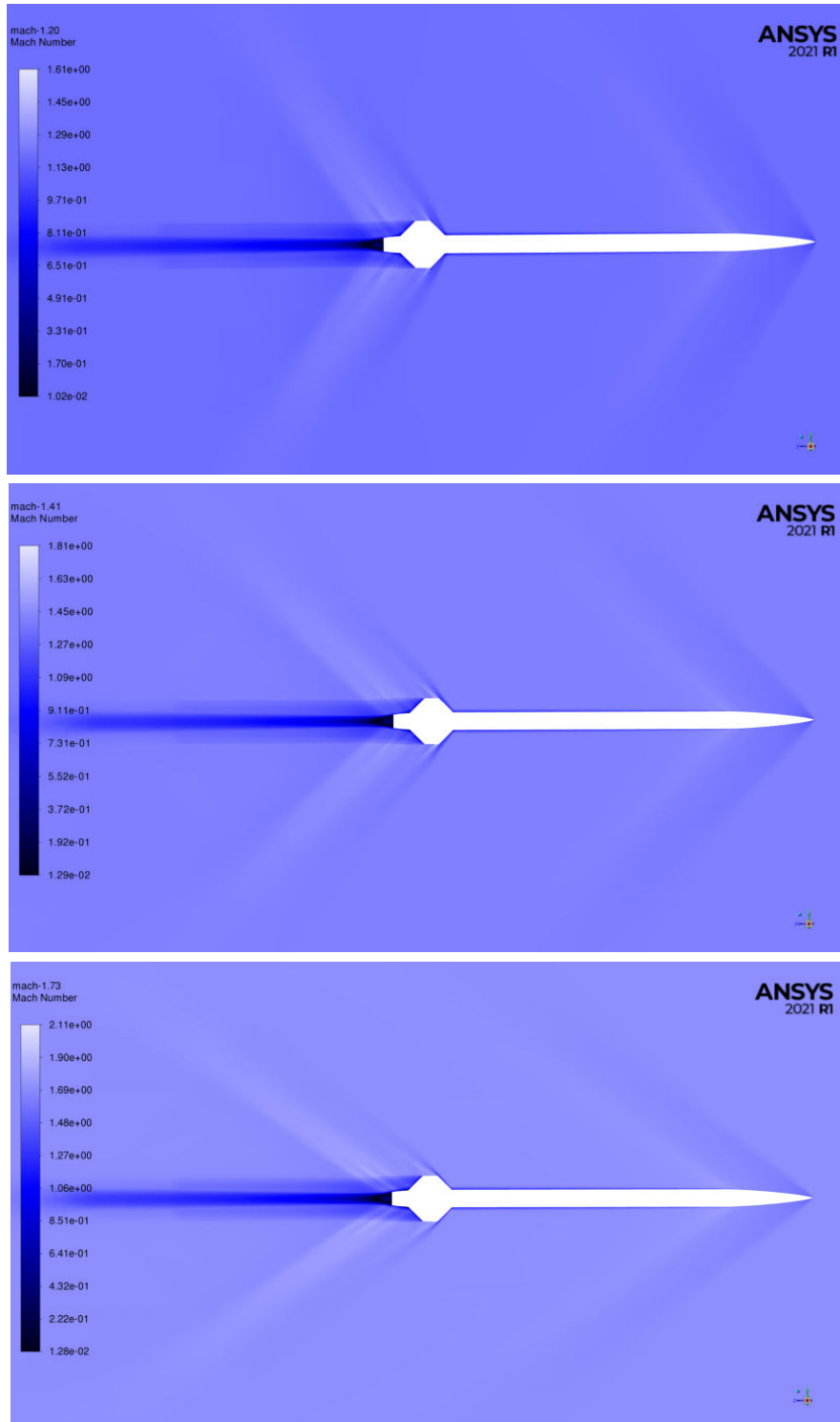


Figure 2.1: Mach angle comparison ranging at Mach 1.20, 1.41 and 1.73, respectively.

As seen in Figure 2.1, the Mach angle tends to decrease with increasing Mach number. These results imply that the numerical solutions with respect to the supersonic velocity field are numerically correct. See Table 2 for simulated Mach angles, μ . The Mach angle may be expressed as

$$\sin \mu = \frac{1}{M_\infty} \quad (2.3)$$

The top figure of Figure 2.1 shows that the Mach angle at Mach 1.2 is higher than the sweep angle of the fins. However, at Mach 1.41, shown in the center, the angle μ is smaller than the sweep angle of the fins, $\Lambda = 45^\circ$, which leads to an increase in wave drag. To overcome this, the sweep angle could be decreased, however, this again would affect the location of C_p . Due to constraints, such as location of C_g and design and mounting point of the fin brackets, changing the sweep angle was not achievable without deteriorating the stability of the rocket. Hence, the sweep angle was set to 45 degrees with an acceptable loss in kinetic energy due to an increase in wave drag.

Table 2. Calculated Mach angles for simulated Mach numbers

Mach Number, M	Mach Angle, $\mu [^\circ]$
1.2	56.5
1.41	45.2
1.73	35.3

Thermal Evaluation

Throughout the rocket's ascent, the rocket hull is expected to be exposed to high surface temperatures that are mainly due to viscous skin friction. The material properties such as ultimate tensile yield strength, is strongly dependent on the temperature, and is important for understanding the structural integrity of the rocket. Furthermore, there are two key elements that will determine the criticality of the surface temperature: 1) the duration of which the surface is exposed to such high temperatures; and 2) the heat transfer rate. The duration of exposure is determined to be less than 6.5 seconds which is based on the engine burn time.

When the rocket is in the incompressible region, the boundary layer growth is expected to be positive [26], and depends on the Reynolds number [7]. Boundary layer growth with adverse pressure gradient will lead to a turbulent boundary layer which will increase the heat transfer coefficient. This is due to the good mixing in the turbulent stream which has a cooling effect on the surface temperature [26]. However, as the rocket enters the transonic and supersonic region, the Reynolds number will increase, resulting in a decreasing boundary layer [7]. As the boundary layer gets thinner, the heat transfer

coefficient will decrease, resulting in a lower surface heat flux. The surface temperature will therefore increase with higher Mach number.

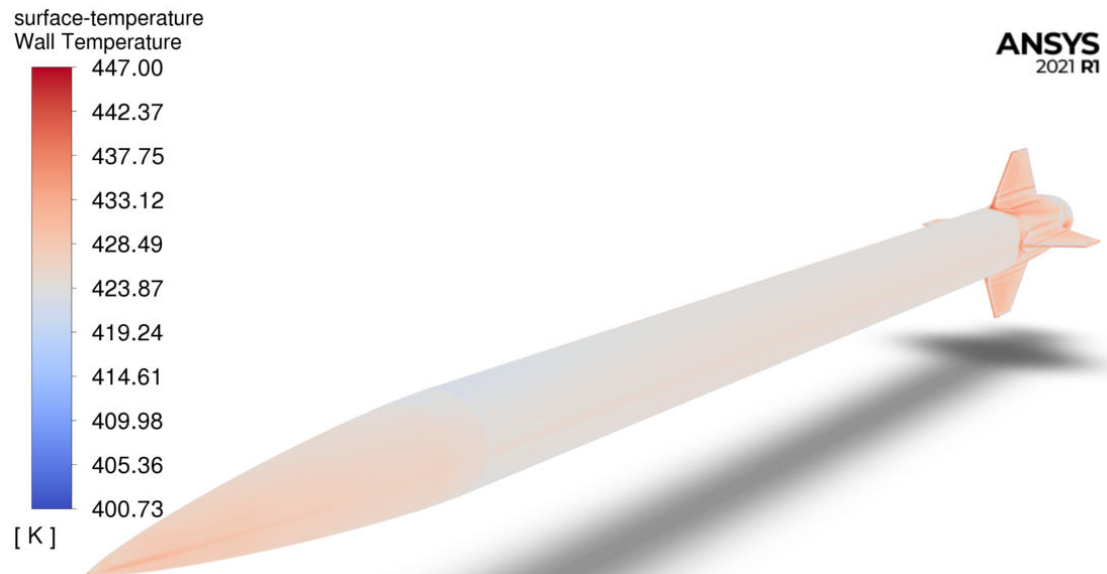


Figure 2.2: Surface temperature measured by CFD at Mach 1.73 with 7° AoA.

In the limited time frame in the project, unfortunately no calculations were made on the heat transfer coefficient throughout the rocket ascent phase. However, a preliminary temperature analysis has been performed with the goal of finding the highest surface temperature that might be expected. The results are displayed below in Figure 2.3 and 2.4 where the highest measured value is found on the fins upper edge due to stagnation condition. This value was measured to 447 K, followed by a high surface temperature measured at the lower part of the LE, yielding a temperature of 436.8 K, as seen in Figure 2.4. These results are found at Mach 1.73 which is expected to occur 5 seconds after launch rod clearance. As the heat transfer rate is unknown, the highest measured temperature ($T_{crit} = 447 K$) was taken to be the overall average critical value. See Section II.3 *Airframe manufacturing* and Section II.3 *Fin manufacturing* for more details.



Figure 2.3: Surface temperature measured on the nose cone, at Mach 1.73 with 7° AoA.

The average surface temperature on the rocket at Mach 1.73 can be taken to be around 424 K, as shown in Figure 2.2. A small increase in temperature is indicated along the side of the nose cone and at the nose tip. This is due to the stagnation condition when the rocket is inclined by 7° AoA. A close-up of this is shown in Figure 2.3.

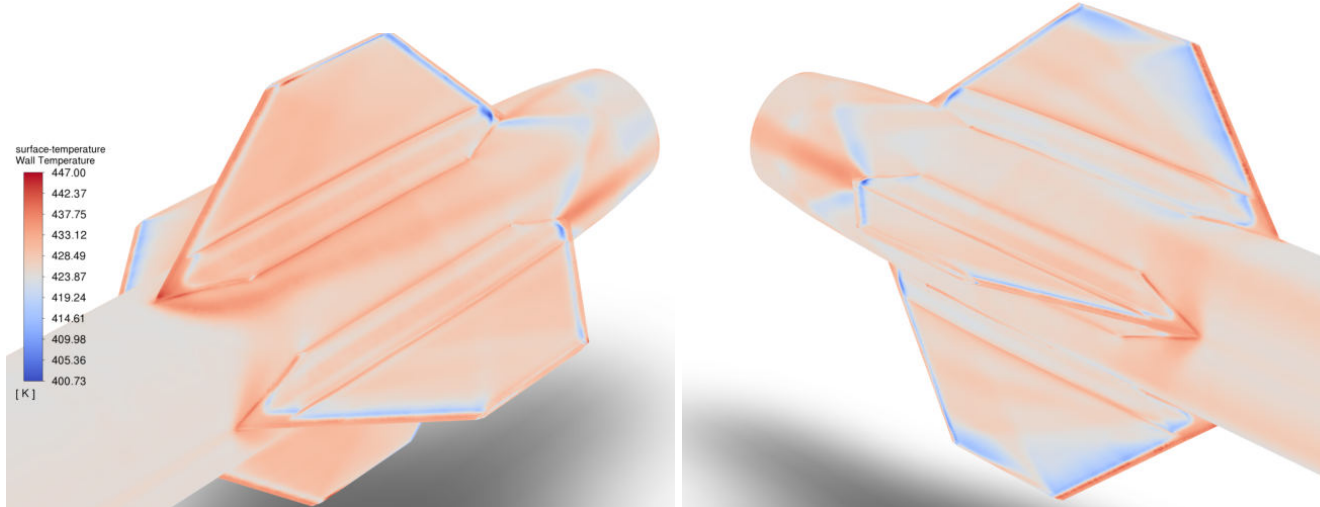


Figure 2.4: Surface temperature distribution on the fins, at Mach 1.73 with 7° AoA.

From Figure 2.4, it can be observed that high temperatures exist at the lower point of the LE, as well as on the upper edge of the fin. The blue color indicates a lower surface temperature as the flow accelerates over the LE of the fins. As the pressure decreases, the flow is likely to separate from the fin surface, leading to wake generation and a turbulent region. As stated earlier, turbulent mixing will decrease the surface temperature as the heat transfer increases, which is captured by the numerical simulation results. Moreover, the same effects from the expansion fans at the base of the von Kármán section can also be observed, analogous to a decrease in temperature. All the above mentioned

observations show that the simulation results are both numerically consistent and accurately predict the theoretical solutions.

Turbulence Intensity Evaluation

Along the forward part of the airframe, the flow will eventually at some point become turbulent due to an adverse pressure gradient, leading to flow transitioning from a laminar boundary layer to a turbulent boundary layer. This will increase the shear stress and the skin friction drag. Another effect of the turbulent layer is the influence on the fins' operating condition. Qualitative design choices regarding the nose cone length have been made to minimize the turbulence by having the transitional point located closer to the fins' position. Also having a longer nose cone reduces the generation of expansion waves in the transonic and supersonic region as the gradient of the von Kármán curve becomes smoother. Additionally, flow separation may happen due to the von Kármán shape at the aft section or next to the boat tail, resulting in increased pressure drag and formations of turbulent eddies that will grow while traveling downstream. The slope of both the aft section and the boat tail have been carefully selected to minimize the magnitude of the adverse pressure gradient and therefore extend the point of flow separation further back.

The sections below with combined figures presents the results gathered using CFD to model the turbulent region around the rocket's airframe. This numerical study enables better understanding about the degree of severity that the nose cone has on the flow field in the vicinity of the fins', and to locate the boundary layer along the rocket's body. It is worth mentioning that the near wake region behind the rocket will not manifest itself as presented in the figures below while the rocket ascends towards its maxQ, which is mainly due to the nozzle plume released from the rocket engine. However, the observations in figures below will be expected right after engine burnout and during cruise phase towards apogee. Due to technical difficulties and lack of design information from the manufacturer of the nozzle geometry, no simulations with a running engine were achieved.

The first six sections of figures will present the turbulence intensity measurements from these selected Mach regions; $M \in \{0.3, 0.7, 0.9, 1.2, 1.41, 1.73\}$, all with AoA of 2° , followed by a close up comparison of the turbulent boundary layer along the rocket. This is to estimate the boundary layer growth throughout the flight profile, and how the turbulent layer behaves in most parts of the ascending phase.

Individual results on turbulence intensity have three views for each figure. All three views show the turbulence intensity in percent. The upper view shows an overview of the rocket and its near wake region, followed by a close-up view of the turbulent boundary layer from the nose tip to LE of the fins. Finally, the lower view shows a rear view of the wake turbulence around the entire rocket body including the fins, showcasing the cross flow.

Remark: *The launch lug will impose a far greater turbulent boundary layer than compared to the presented solution below. However, this has not been further analyzed, as the launch lugs are not a design component and are therefore constrained without option for further optimization. The placement of the launch lugs will therefore not be determined from flow analysis, but from mechanical analysis and structural design decisions.*

Turbulence Intensity measured at Mach 0.3, $\alpha = 2^\circ$: View 1, overview. View 2, side view. View 3, back view.

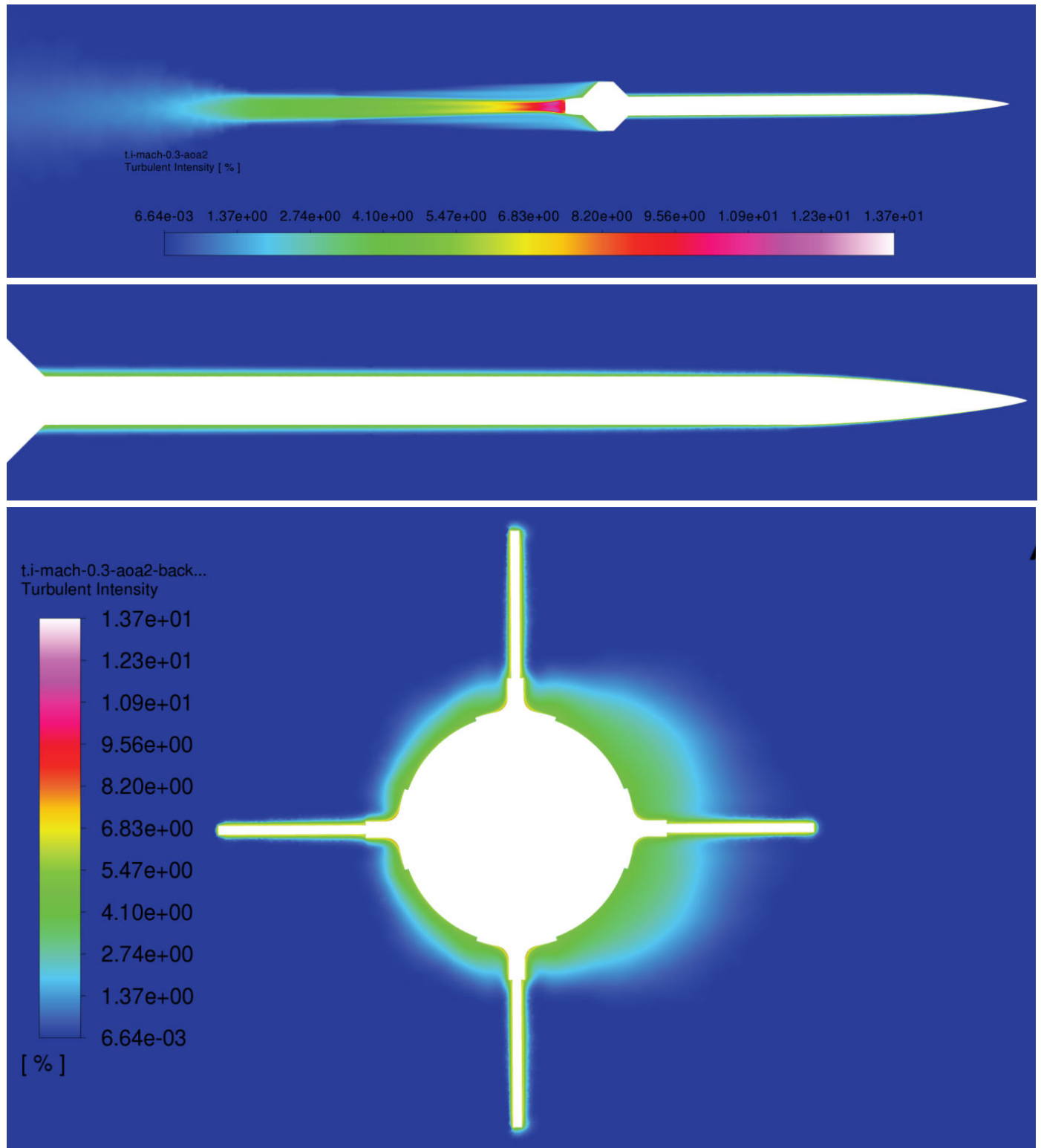


Figure 2.5: Turbulence intensity contour at Mach 0.3 with 2° AoA.

Turbulence Intensity measured at Mach 0.7, $\alpha = 2^\circ$: View 1, overview. View 2, side view. View 3, back view.

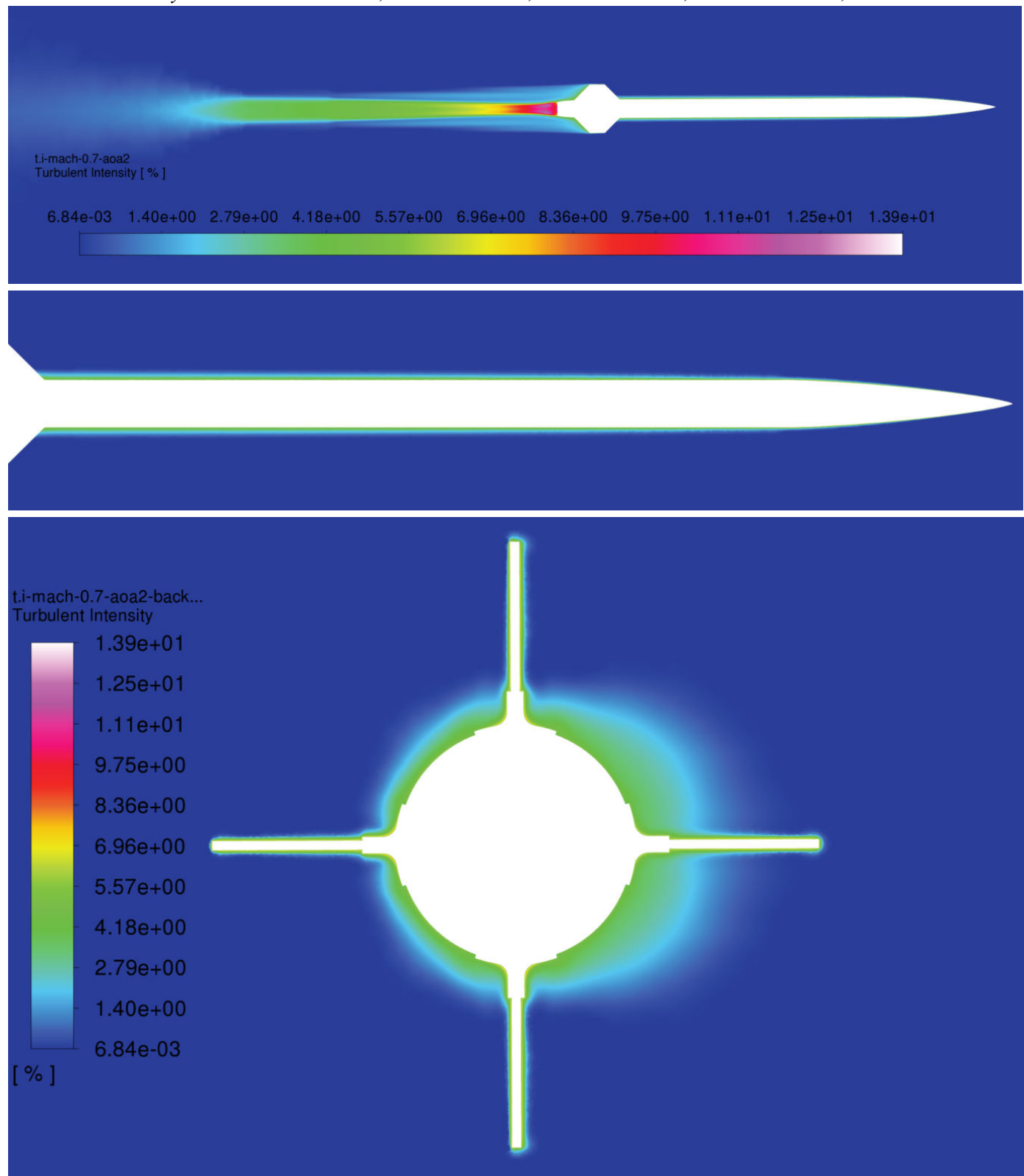


Figure 2.6: Turbulence intensity contour at Mach 0.7 with 2° AoA.

Turbulence Intensity measured at Mach 0.9, $\alpha = 2^\circ$: View 1, overview. View 2, side view. View 3, back view.

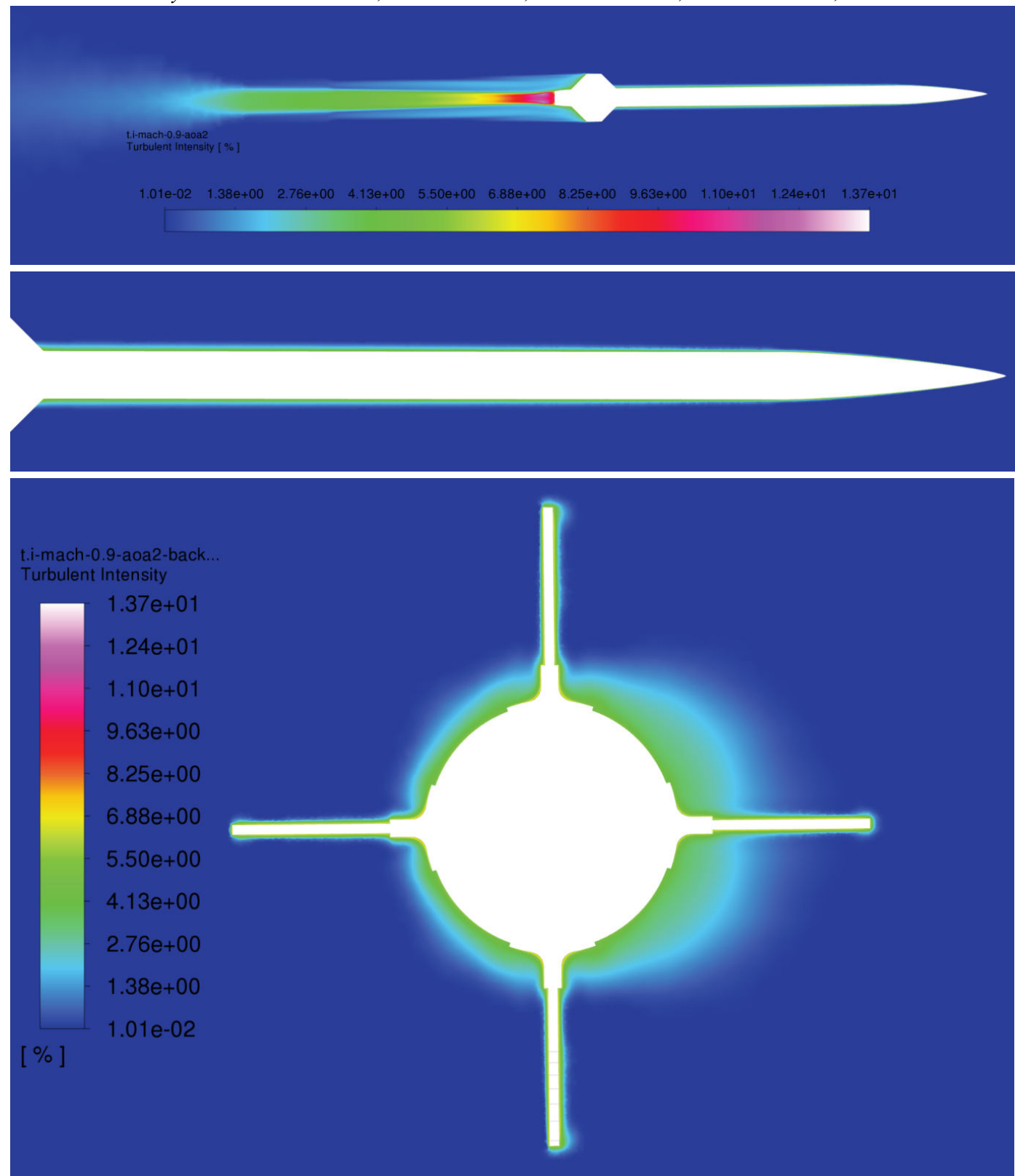


Figure 2.7: Turbulence intensity contour at Mach 0.9 with 2° AoA.

Turbulence Intensity measured at Mach 1.2, $\alpha = 2^\circ$: View 1, overview. View 2, side view. View 3, back view.

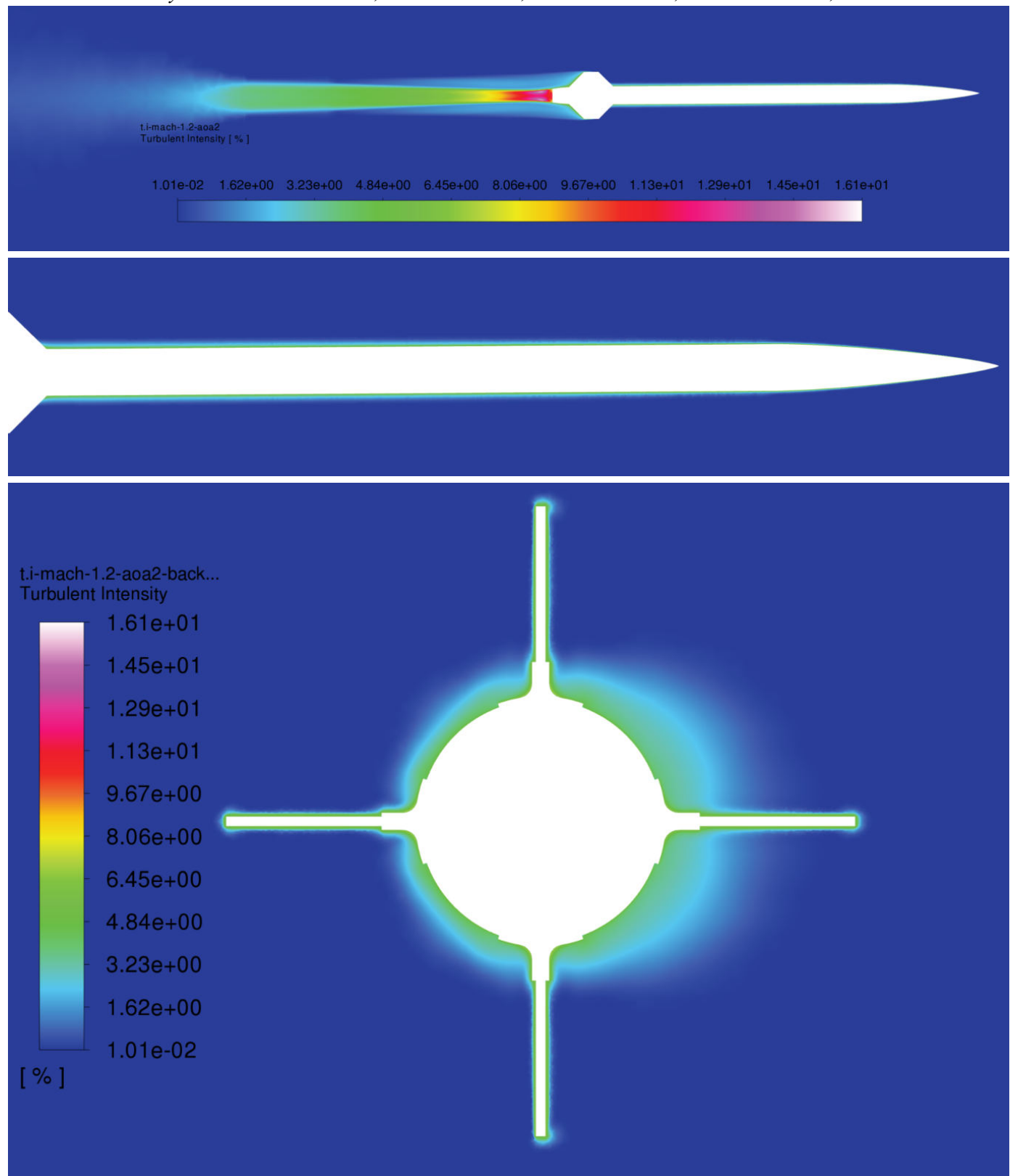


Figure 2.8: Turbulence intensity contour at Mach 1.2 with 2° AoA.

Turbulence Intensity measured at Mach 1.41, $\alpha = 2^\circ$: View 1, overview. View 2, side view. View 3, back view.

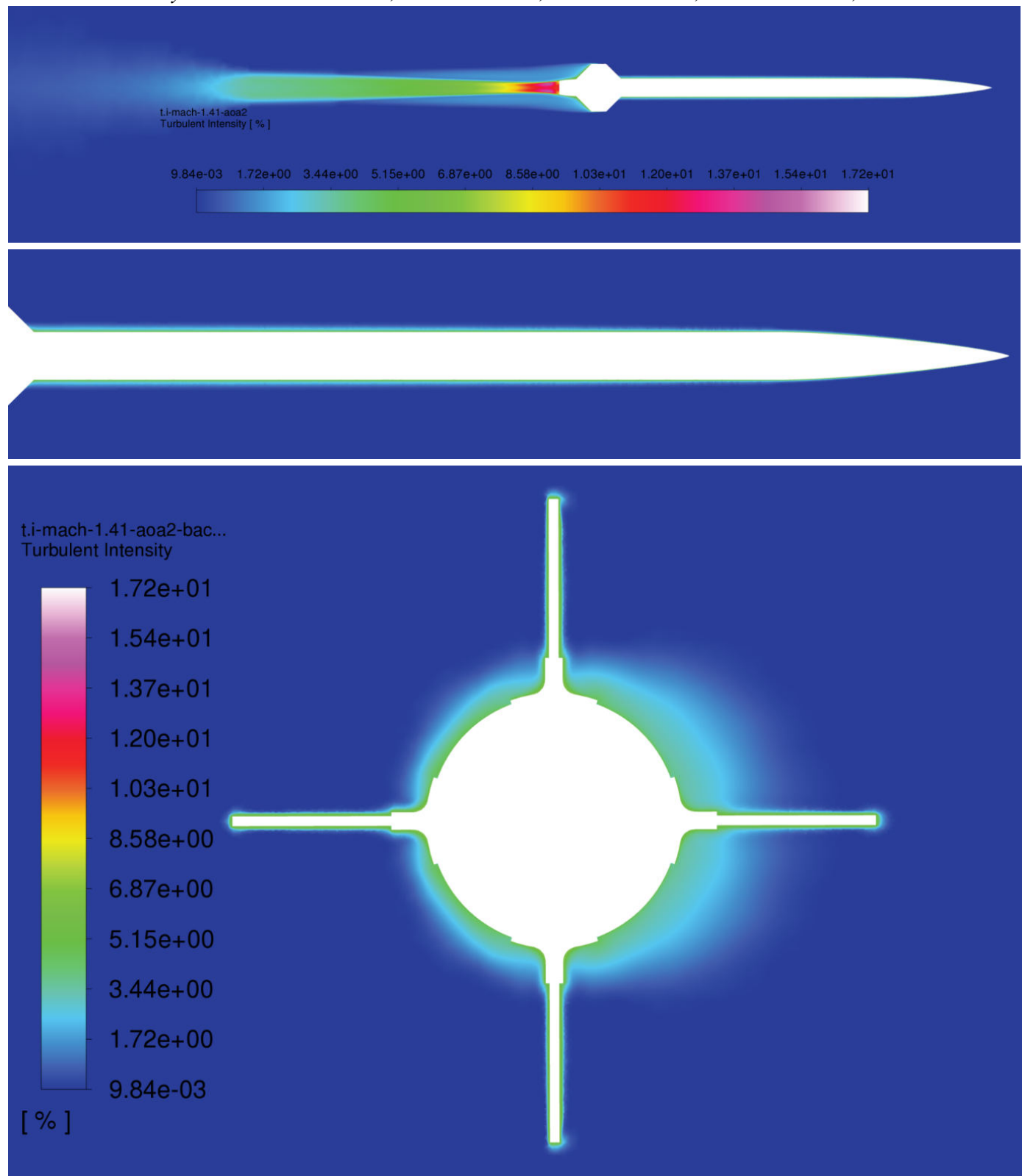


Figure 2.9: Turbulence intensity contour at Mach 1.41 with 2° AoA.

Turbulence Intensity measured at Mach 1.73, $\alpha = 2^\circ$: View 1, overview. View 2, side view. View 3, back view.

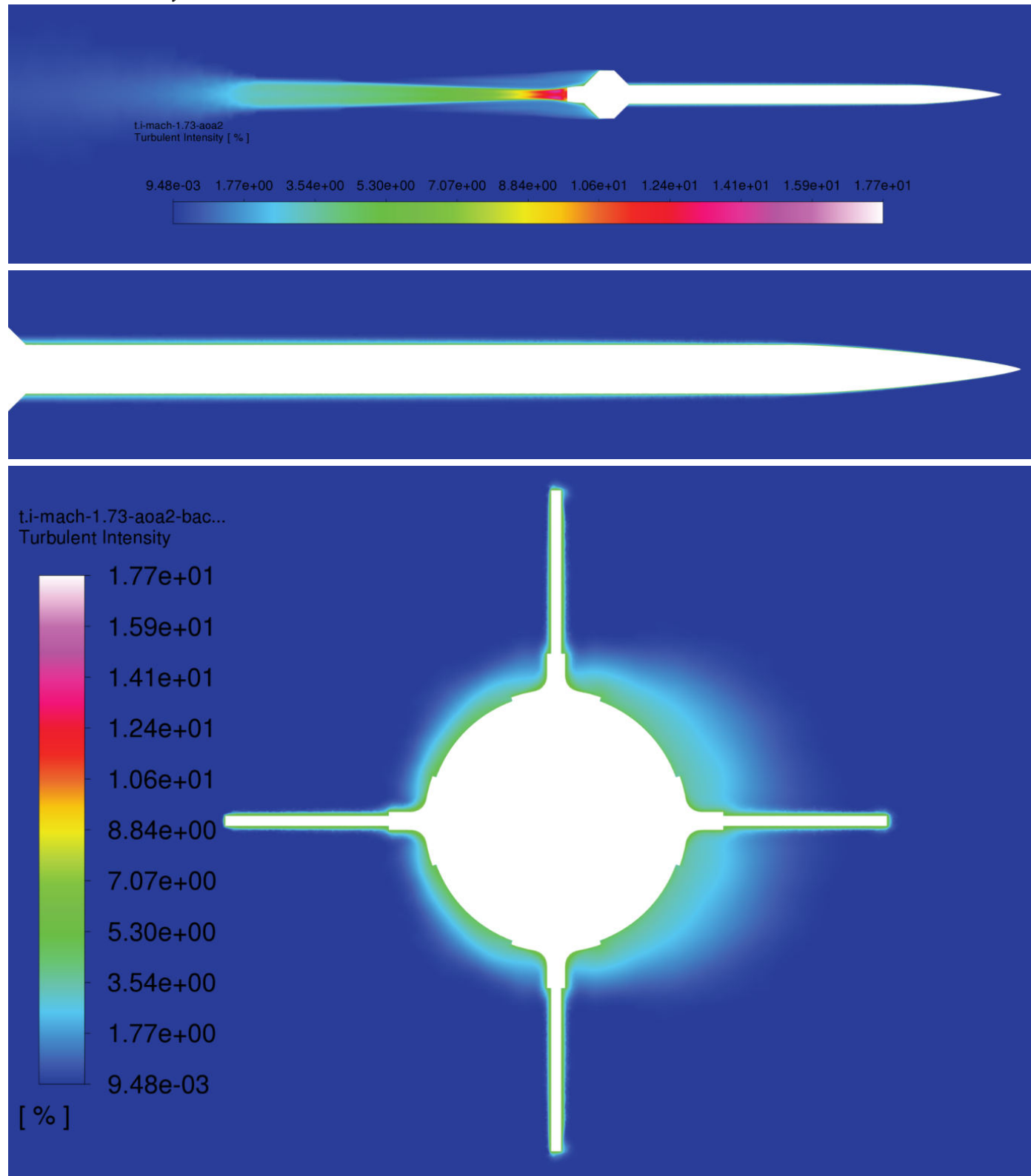


Figure 3.0: Turbulence intensity contour at Mach 1.73 with 2° AoA.

Turbulence comparison along upper side of airframe tube, with $M \in \{0.3, 0.7, 0.9, 1.2, 1.41, 1.73\}$:

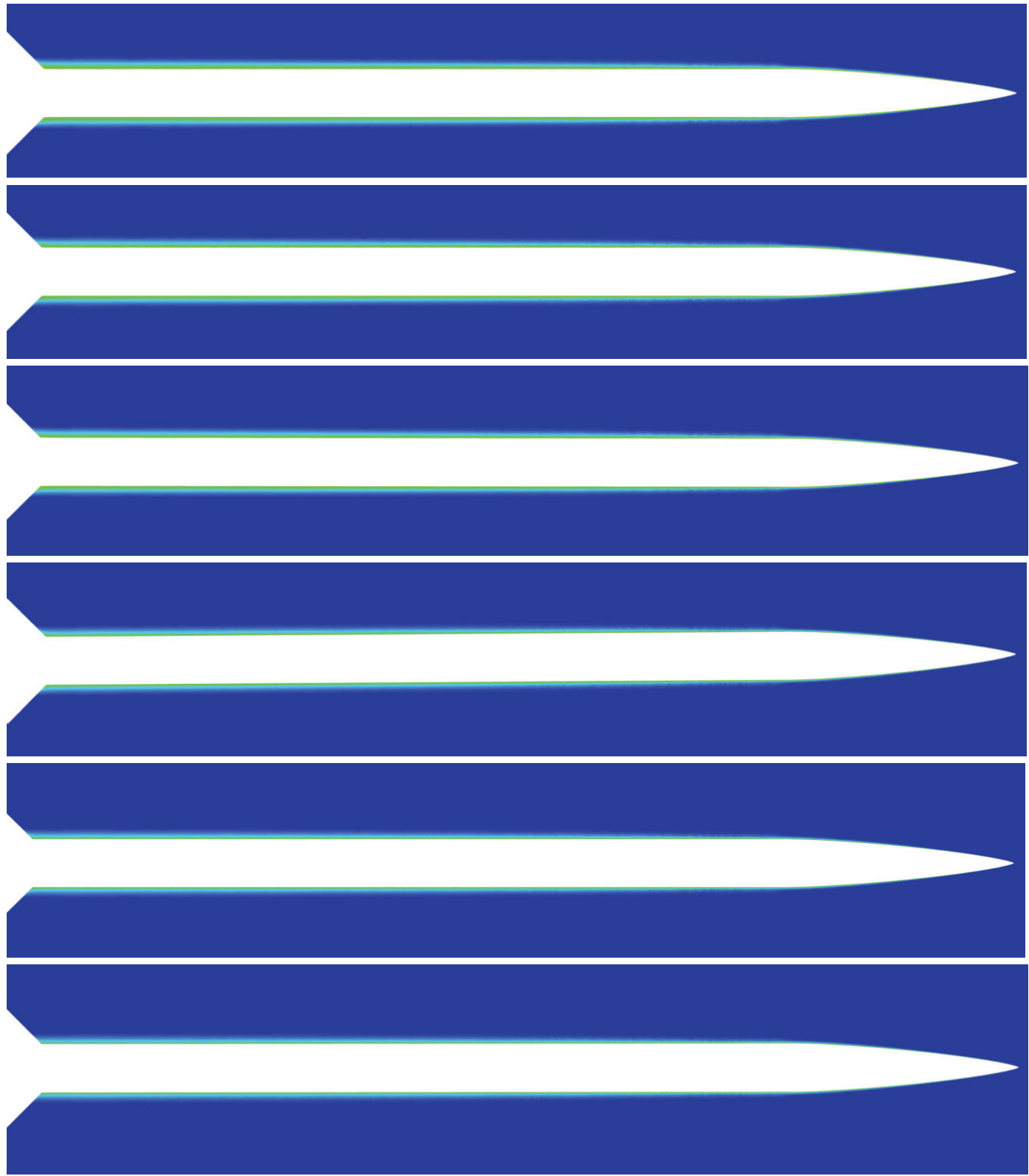


Figure 3.1: Turbulent boundary layer comparison with increasing Mach number. (Sideview)

Turbulence comparison along the side of the airframe tube, with $M \in \{0.3, 0.7, 0.9, 1.2, 1.41, 1.73\}$:

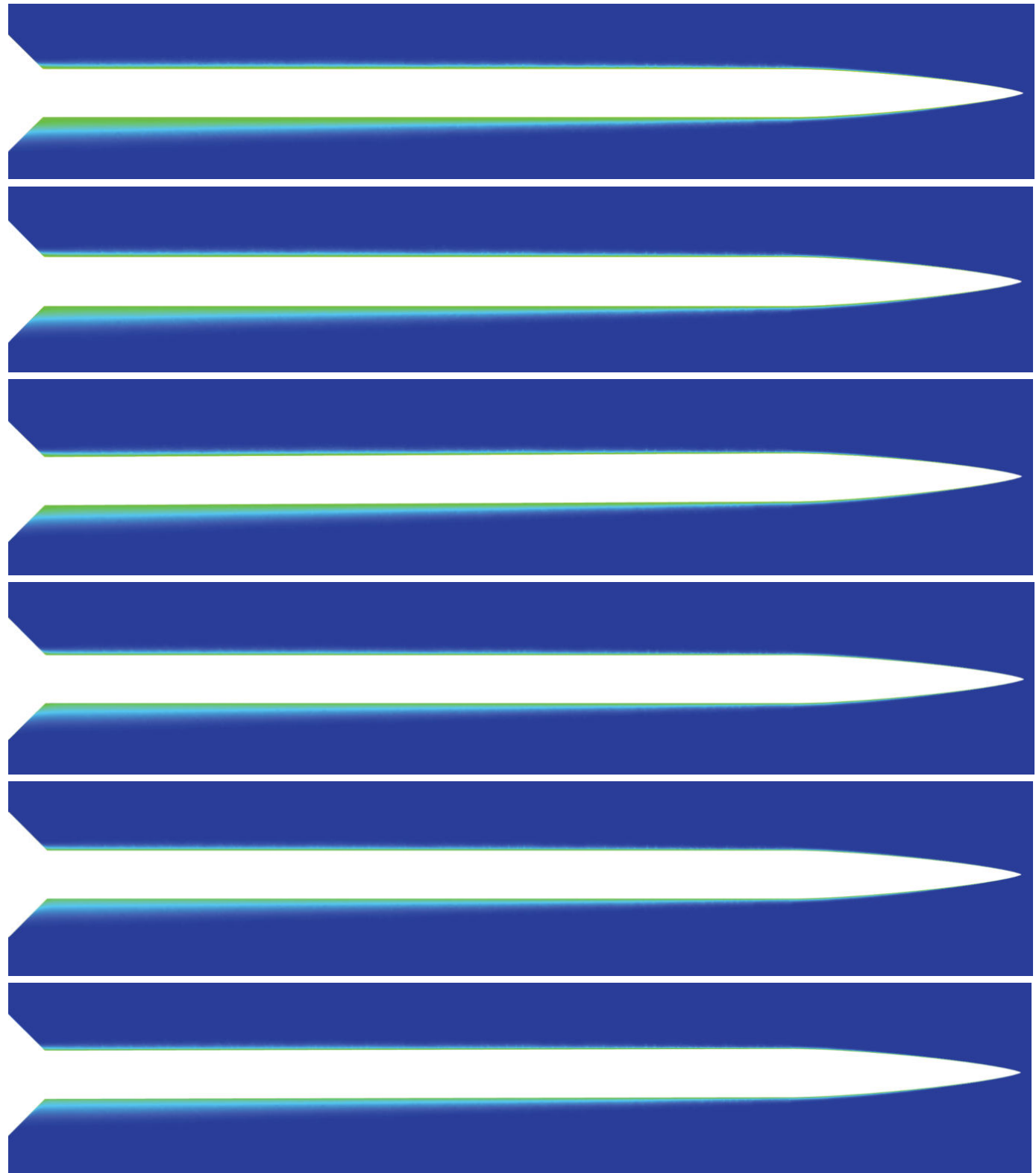


Figure 3.2: Turbulent boundary layer comparison with increasing Mach number and cross flow. (Topview)

Comparing the first view for Figure 2.5 - 3.0, it can be seen that the near wake decreases with increasing Mach number as it propagates downstream of the rocket. Here, it is evident that the distance it takes for the flow to recover from the turbulent and unstructured flow pattern decreases and gets shorter as the Mach number increases. Additionally, the width of the wake tends to decrease for larger freestream velocity. This is a correct solution as the turbulent kinetic energy will dissipate faster due to increasing freestream velocity closer to the upper wake layers. It can also be observed that the dissipation length of the wake turbulence from the fins decreases as the surrounding freestream velocity increases. Lastly, the latter mentioned dissipation length can be taken to be significantly smaller than the near wake dissipation length. This could indicate that the chosen fin design produces minimal turbulence and will not be a significant contribution to the rocket's loss in kinetic energy towards apogee.

By comparing the center view for Figure 2.5 - 3.0 and by looking at the comparison presented in Figure 3.1, it can be observed that the turbulent boundary layer decreases with increasing Mach number. This agrees well with the theory discussed earlier in the section on *Thermal Evaluation*. Another important observation from Figure 3.1 is that the overall boundary layer growth can be taken to have a minor effect on the operating conditions of the fins. This conclusion can also be drawn from the results obtained in Figure 3.2 where the boundary layer grows as a result of the cross flow, however, the boundary layer height is negligible compared to the fins height.

The most interesting view is the third view presented by Figure 2.5 - 3.0, showing the wake turbulence due to cross flow. It can be observed that the area of high turbulence at the right side of the rocket body tends to decrease for increasing freestream velocity. This was also the case for the wake turbulence generated by the fins, and is expected as the viscosity of gases is strongly dependent on the temperature and increases with lower temperature. As the rocket ascends towards maxQ , the temperature is estimated to fall from approximately 20°C to 3°C when the rocket reaches maxQ , recalling that the boundary layer is strongly dependent on the Reynolds number which again is inversely proportional to the viscosity. With that in mind, as the viscosity decreases, the Reynolds number will increase and the final result is that the boundary layer will decay. It can therefore be assumed that the numerical results are correct in the physical sense.

The boundary layer height in the subsonic and supersonic region can be assumed to be insignificant as the observed height will not influence the operating condition of each of the fins. However, as seen in Figure 2.5 - 3.0, the turbulence intensity due to the airframe tube section in cross flow is significantly larger than that generated by the fins. This will be the major contributing factor for the loss of the rocket's kinetic energy in the actual cruising phase. The fins also have negligible effects in the loss of kinetic energy, and have been determined to have optimal design when considering wake generation.

H. Constraints and requirements appendix

These requirements are imposed by the team, and are in addition to the requirements stated in “Rules and Requirements” as well as “Design test evaluation and guide”. All requirements prefixed with “S” indicate that the requirement is “Self imposed”.

S1. Avionics

S1.1 Functional requirements

- S1.1.1 Must be able to send activation signals to recovery systems at correct time in flight
- S1.1.2 Must have state estimation for correctly predicting recovery signal timing
- S1.1.3 Must be able to handle data input, processing, storage and output
- S1.1.4 Must be able to safely log data
- S1.1.5 Must have data filtering for sensors (kalman filter)
- S1.1.6 Should be able to send live data from rocket to ground station during flight

S1.2 Performance

- S1.2.1 Should be able to set up and verify avionics system status on launch pad within 10 minutes
- S1.2.2 Should be able to wire up, assemble and perform initial verification on avionics systems within 2 hours

- S1.2.3 Should be able to run diagnostics on the system remotely from ground station
- S1.2.4 Should have feedback on system status (Audio, Lights etc.)
- S1.2.5 Should be a reusable system
- S1.2.6 Should be able to collect accurate flight data during harsh acceleration/pressure changes

S1.3 From other systems and the board

- S1.3.1 Must physically fit inside the rocket body
- S1.3.2 Must be able to handle rapidly changing temperature and pressure
- S1.3.3 Must be able to handle high G-forces and vibrations
- S1.3.4 Must have a blackbox like solution for safe data storage
- S1.3.5 One of the flight computers must be SRAD so that our members gain engineering experience.
- S1.3.6 Must collect data for use in later analysis and development, or for troubleshooting in case of failure.

- S1.3.7 Must be produced with the equipment available, and within budget.

- S1.3.8 Should weigh less than 1 kg

- S1.3.9 Placement and dimensions of components are restricted by other system components

- S1.3.10 Must be able to activate recovery systems

- S1.3.11 Must be capable of operating four servo motors

- S1.3.12 Must be validated through tests and/or analyses within 15. September 2021.

- S1.3.13 Must activate the separation system within 11 seconds.

S1.4 Environmental factors

- S1.4.1 Should have battery life to stay powered on the launch pad for minimum 1 hour

- S1.4.2 Should have battery life to stay powered for at least 30 min after launch

- S1.4.3 Must survive temperatures ranging from -40°C to 40°C

- S1.4.4 Must survive desert conditions (temperatures, humidity, sand)

- S1.4.5 Must be able to withstand high percentage of humidity caused by altitude increases

S2. Recovery

S2.1 Functional requirements

- S2.1.1 The recovery system must be able to withstand the experienced forces from the drogue chute and main

- chute deployment with a safety factor of 2

S2.1.2 The release force of the main chute should not exceed 4000N

S2.2 Performance

S2.2.1 The recovery bay needs to be airtight

S2.3 From other systems and the board

S2.3.1 Recovery must use electrical components compatible with the COTS flight computer

S2.3.2 The design needs to accommodate space for a 8.6mm diameter wire to the recovery bay.

S2.3.3 The recovery system needs to be able to fit between the coupler and the payload

S2.3.4 Components need to fit within the given inner diameter of 120mm

S2.3.5 The parts must be designed in such a way that they can be produced with the equipment available, and

within budget.

S2.3.6 Must be validated through tests and/or analyses within 15. September 2021.

S2.4 Environmental factors

S2.4.1 Temperature changes affect the o-rings

S2.4.1 Pressure difference between atmosphere and the recovery bay

S3. Inner structure

S3.1 From other systems and the board

S3.1.1 The parts must be designed in such a way that they can be produced with the equipment available, and within budget.

S3.1.2 The inner structure must be rigid, and withstand forces from multiple directions.

S3.1.3 The weight of the system should not exceed 6 kg.

S3.1.4 The structure must house the Cesaroni CTI Pro98 6GXL 21062 O3400-IM P.

S3.1.5 Avionics and recovery have to be in the same part of the rocket after separation as the avionics and

recovery needs to be able to communicate and deploy the main parachute after the rocket is split in two.

S3.1.6 Communication lines between avionics and recovery needs enough room and mounting points to be placed and secured properly.

S3.1.7 The upper coupler needs to have two holes for the camera lenses and two holes for the hawk pins.

The lenses are 17,3 mm in diameter and the hawk pins are 5mm.

S3.1.8 The radio transmitting subsystems of the avionics system must be placed within a RF-transparent section of the rocket fuselage.

S3.1.9 Minimum inner diameter around the hawks cannot be less than 120mm in order for the hawks to fit inside.

S3.1.10 Secure mounting points on both halves of the rocket for the parachutes.

S3.1.11 The coupler should be airtight enough to maintain an internal pressure of at least 10 bar until the rocket

decouples.

S3.1.12 The rocket needs to withstand an impact with the ground at up to 7m/s.

S3.1.13 The mounting points need to accommodate the fiber casing such that the fiber does not tear.

S3.1.14 The inner structure must adapt to the shape of the airframe.

S3.1.15 The inner structure must be arranged in a way that accommodates a suitable center of gravity for the

rocket.

- S3.1.16 Must provide adequate space for wires for avionics.
- S3.1.17 Must provide space for small PCBs below the payload.
- S3.1.18 Must accommodate for routing wires past the payload.
- S3.1.19 Must be designed in a way that makes it efficient and simple to assemble and disassemble during pre-launch procedures.
- S3.1.20 Must be validated through tests and/or analyses within 15. September 2021.
- S3.1.21 Must be designed for ease of assembly.

S4. Outer Structure

S4.1 Functional requirements

S4.1.1 Overall Structural Integrity -

The rocket shall be constructed to withstand the operating stresses and retain structural integrity under the

conditions encountered during handling, as well as during flight.

S4.1.2 Maintain a stability margin between 1.5 and 4.75 body caliber

S4.2 Performance

S4.2.1 Need an aerodynamic design in order to reach targeted apogee.

S4.3 From other systems and the board

S4.3.1 Need a RF transparent area in the nose cone and fore tube where the radio transmitter COTS GPS is situated.

S4.3.2 The parts must be designed in such a way that they can be produced with the equipment available, and

within budget.

S4.3.3 Length and diameter must be large enough for all systems to fit inside the rocket.

S4.3.4 Must be validated through tests and/or analyses within 15. September 2021.

I. Calculations and Analysis

CALCULATIONS AND ANALYSIS

Outer structure

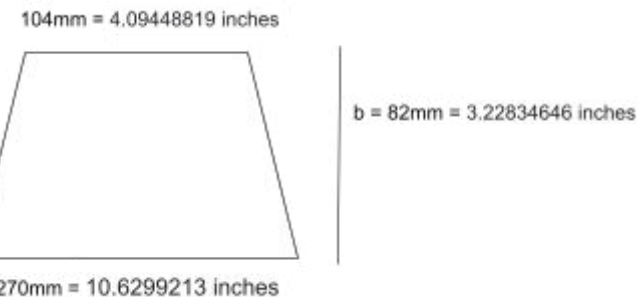
Fin fluttering

Problem statement:

Flutter boundary condition [27]. Flutter velocity prediction

As the airstream surrounding the fin increases its velocity, a pitching moment around the aerodynamic center increases as well. With the influence of a changing pressure gradient and lift generated on the fin, aeroelastic flutter can occur. This is referred to as fin fluttering.

Figure:



Assumptions and approximations:

$$T(^{\circ}\text{F}) = 59 - .00356h$$

$$P(\text{lbs}/\text{ft}^2) = 2116 \times \left(\frac{T + 459.7}{518.6} \right)^{5.256}$$

$$a = \sqrt{1.4 \times 1716.59 \times (T(^{\circ}\text{F}) + 460)}$$

Tensile strength and shear modulus relation:
G is in the range [3.5 - 5] GPa

Physical laws:

$$V_f = a \sqrt{\frac{G}{1.337 AR^3 P(\lambda + 1)}} \\ \sqrt{\frac{2(AR + 2)(\frac{t}{c})^3}{}}$$

G = shear modulus of material

Properties:

$$S = 1/2 (c_r + c_t) \cdot b \text{ surface area of the fin}$$

$$AR = b^2 / S = 0.50802, \text{Aspect ratio}$$

For carbon fiber the average poisson's ratio is in the range of 0.26 - 0.28. A poisson ratio of 0.27 was chosen.

$$\lambda = c_t / c_r \text{ Ratio between tip chord and root chord}$$

t, fin thickness

Calculations:

$$S = 1/2 (c_r + c_t) \cdot b = 27.53590515 \text{in}^2$$

$$AR = b^2 / S = 0.50802, \text{Aspect ratio}$$

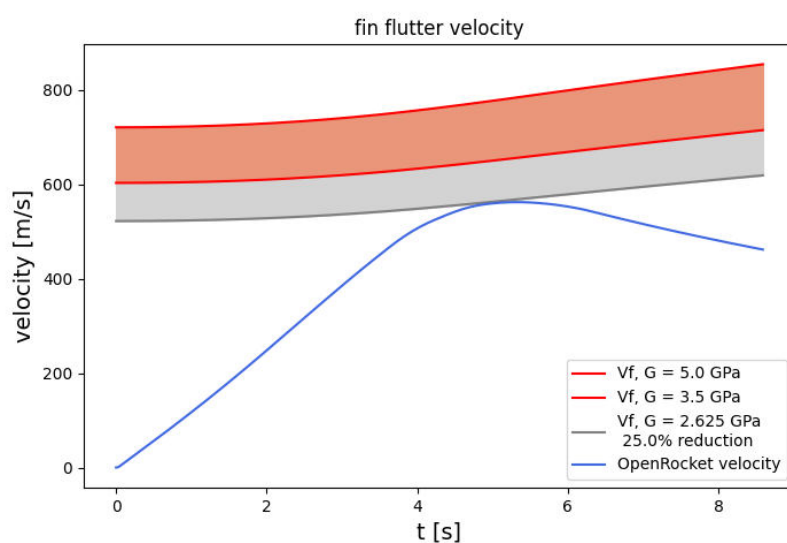
$$\lambda = c_t / c_r = 0.3851852$$

$$t = 0.196850394 \text{ in}^2$$

Reasoning, discussion and verification:

The shear modulus G plays a large part in the analysis. Since the shear modulus reduces during higher temperature and a large frictional heating is expected

As seen under the final result, the greyline is the fin fluttering when G is reduced by 25%. The red area is the flutter velocity based on the interval [3.5GPa, 5GPa].

Final results:

Inner structure

Coupler bending moment calculation

Problem statement:

To dimension the couplers properly the bending moment they experience from drag is required.

Figure:

Center of gravity: $CG = 1.796 \text{ m}$

Center of gravity, lower half: $CG_L = 2.328 \text{ m}$

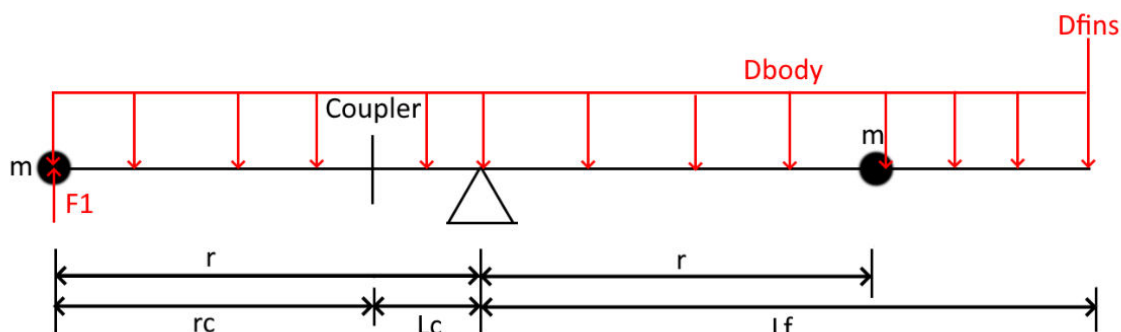
Drag force on fins: $D_{fins} = 1150 \text{ N}$ (Table 8)

Drag force on body: $D_{body} = 1336 \text{ N}$ (Table 6)

Fin-position from CG: $L_f = 0.95 \text{ m}$

Coupler distance from CG: $L_c = 0.22 \text{ m}$

All positions are from Appendix V.A



Assumptions and approximations:

It is assumed that all the mass of the rocket is concentrated in two points so that the center of gravity of the rocket acts as a fulcrum when calculating rotational inertia where the two point masses have equal distance to the fulcrum. Then the forces on the two points are split into a force induced by linear acceleration and a force induced by rotational acceleration.

Physical laws:

$$\text{Torsion from rotational acceleration: } \sum T = I \cdot \alpha \Rightarrow \alpha = \frac{\sum T}{I}$$

$$\text{Rotational inertia for a point mass: } I = m \cdot r^2$$

$$\text{Newton's 2. law: } \sum F = m \cdot a \Leftrightarrow a = \frac{\sum F}{m}$$

$$\text{Rotational acceleration to linear acceleration: } a = \alpha \cdot r$$

$$\text{Moment from force: } M = F \cdot r$$

Calculations:

Assuming the drag on the body works on half of the body:

$$F_1 = m \cdot a - m \cdot \alpha \cdot r$$

$$\Sigma T = D_{body} \cdot \frac{L}{2} + D_{fins} \cdot L$$

$$r = CG_L - CG$$

$$r_{coupler} = r - L_{coupler}$$

$$a = \frac{\Sigma F_{drag}}{m} = \frac{D_{body} + D_{fins}}{2 \cdot m}$$

$$\begin{aligned} M &= -F_1 \cdot r_{coupler} = -(m \cdot a - m \cdot \alpha \cdot r) \cdot r_{coupler} = -(m \cdot a - m \cdot \frac{\Sigma T}{L} \cdot r) \cdot r_{coupler} \\ &= -(m \cdot \frac{D_{body} + D_{fins}}{2 \cdot m} - m \cdot \frac{D_{body} \cdot L/2 + D_{fins} \cdot L}{2 \cdot m \cdot r^2} \cdot r) \cdot r_{coupler} = -(\frac{D_{body} + D_{fins}}{2} - \frac{D_{body} \cdot L/2 + D_{fins} \cdot L}{2 \cdot r}) \cdot r_{coupler} \\ &= -(\frac{D_{body} + D_{fins}}{2} - \frac{D_{body}/2 + D_{fins}}{2 \cdot (CG_L - CG)} \cdot L) \cdot (CG_L - CG - L_{coupler}) \\ &= -(\frac{1336+1150}{2} - \frac{1336/2+1150}{2 \cdot (2.328-1.796)} \cdot 0.95) \cdot (2.328 - 1.796 - 0.220) = 118.6 \text{ Nm} \end{aligned}$$

Assuming the drag works on the whole body:

$$F_1 = m \cdot a - m \cdot \alpha \cdot r$$

$$\Sigma T = D_{fins} \cdot L$$

$$r = CG_L - CG$$

$$r_{coupler} = r - L_{coupler}$$

$$a = \frac{\Sigma F_{drag}}{m} = \frac{D_{body} + D_{fins}}{2 \cdot m}$$

$$\begin{aligned} M &= -F_1 \cdot r_{coupler} = -(m \cdot a - m \cdot \alpha \cdot r) \cdot r_{coupler} = -(m \cdot a - m \cdot \frac{\Sigma T}{L} \cdot r) \cdot r_{coupler} \\ &= -(m \cdot \frac{D_{body} + D_{fins}}{2 \cdot m} - m \cdot \frac{D_{fins} \cdot L}{2 \cdot m \cdot r^2} \cdot r) \cdot r_{coupler} = -(\frac{D_{body} + D_{fins}}{2} - \frac{D_{fins} \cdot L}{2 \cdot r}) \cdot r_{coupler} \\ &= -(\frac{D_{body} + D_{fins}}{2} - \frac{D_{fins}}{2 \cdot (CG_L - CG)} \cdot L) \cdot (CG_L - CG - L_{coupler}) \\ &= -(\frac{1336+1150}{2} - \frac{1150}{2 \cdot (2.328-1.796)} \cdot 0.95) \cdot (2.328 - 1.796 - 0.220) = -64.1 \text{ Nm} \end{aligned}$$

Reasoning, discussion and verification:

It was looked at drag working on the whole body and half the body to see if there would be a significant increase in the moment if the body drag contributed to the moment. After calculating it is instead apparent that the body drag will only contribute in reducing the drag resulting in a moment between -64.1 Nm and 118.6 Nm on the coupler.

The moment generated from dynamic analysis should be significantly lower than a static analysis where the rocket is treated as a cantilever beam. Such a static analysis would result in

$$M = D_{body} \cdot L/2 + D_{fins} \cdot L = 1634 \cdot 0.95/2 + 1161 \cdot 0.95 = 1879.1 \text{ Nm}$$

It is apparent that this moment is significantly higher than the dynamic analysis and it is therefore concluded that a moment of 118.6 Nm is reasonable.

Final results:

Moment at coupler:

$$M = 118.6 \text{ Nm}$$

Upper and lower coupler

Problem statement:

As the couplers are critical components in the rocket it is important that they are dimensioned properly to ensure that the rocket remains rigid during flight. To make sure this is the case a FEA analysis was done to determine the stresses on the couplers when they are loaded.

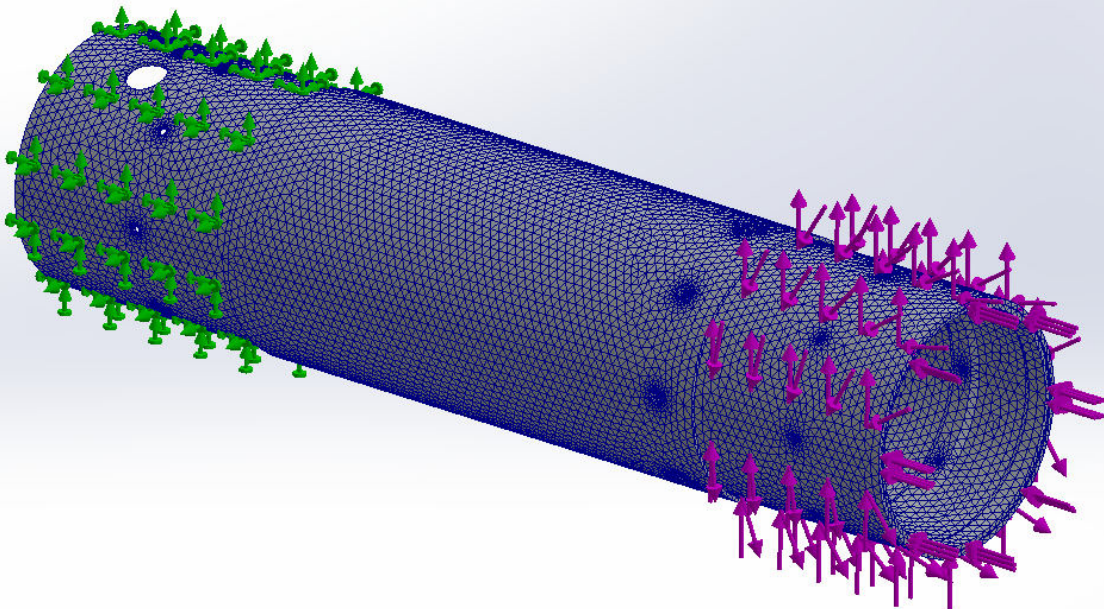
Figure:

Motor force: $F_m = 4750N$

Shear from drag: $F_d = 1336N$ (Table 6)

Bending moment from drag: $M = 118.6 Nm$ (Coupler bending moment calculation)

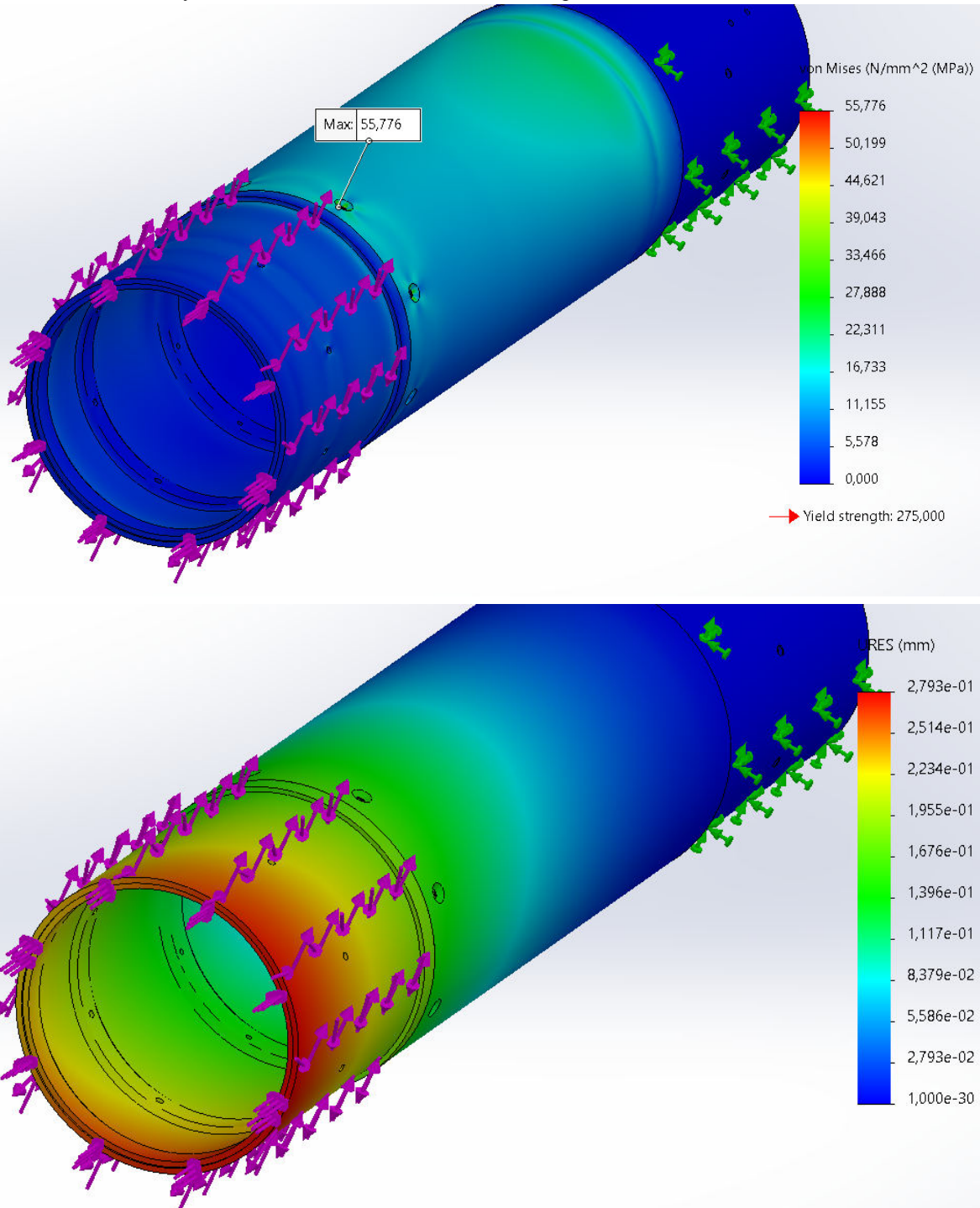
Material: 6082-T6(250 MPa yield strength)



On the image above the fixture is seen to the left on the upper coupler. On the right is the load being applied to the lower coupler. The motor force is applied on the end face and the rest is at the overlap between the coupler and airframe as these locations are where the lower coupler would receive the loads from. The couplers have a no penetration contact between them.

Reasoning, discussion and verification:

The results from the analysis are seen below. First stresses, then displacements:



It is apparent from the analysis that the couplers neither experience a high stress nor a high displacement. This shows that the couplers satisfy the requirement of being rigid as the couplers hardly have any displacement(<1mm) at maximum loads while also having a minimum factor of safety of 4.48.

Final results:

The couplers have a maximum stress of 55.8 MPa, a factor of safety of 4.48 and a displacement of 0.28mm resulting in the couplers being adequately dimensioned.

Motor mount

Problem statement:

As the motor mount is a critical component and a component that is welded it is necessary to find the stresses to make sure the motor mount is adequately dimensioned. Two versions are looked at to ensure a good thickness, one with 5mm thickness and one with 8mm thickness.

Figure:

Motor force: $F_m = 4750N$

Material: 6082-T6 (250 MPa yield strength, 220 MPa after heat treatment, 130 MPa with no heat treatment)

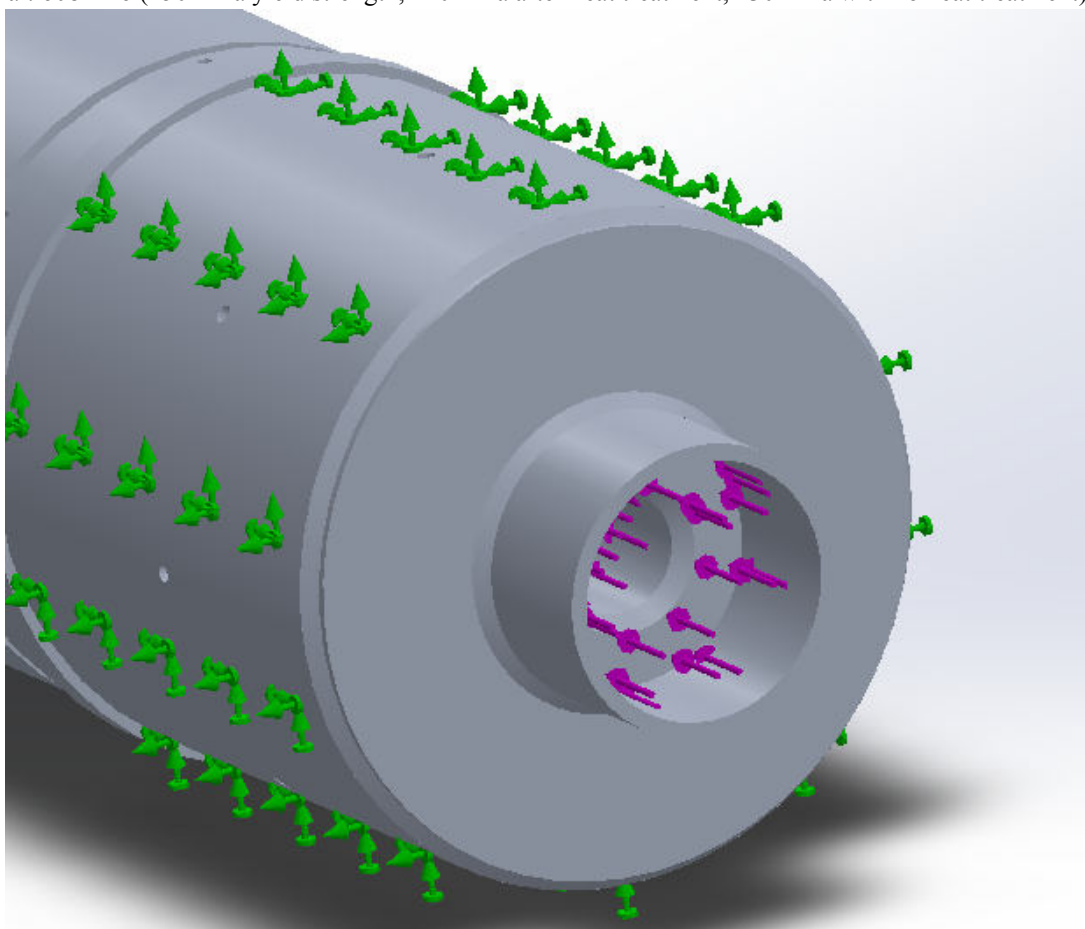


Figure 1 Fixtures and loads

As the model is an assembly bonded contact was used between the welds and the other parts, while no penetration was used between the motor mount shaft and plate.

Reasoning, discussion and verification:

Results:

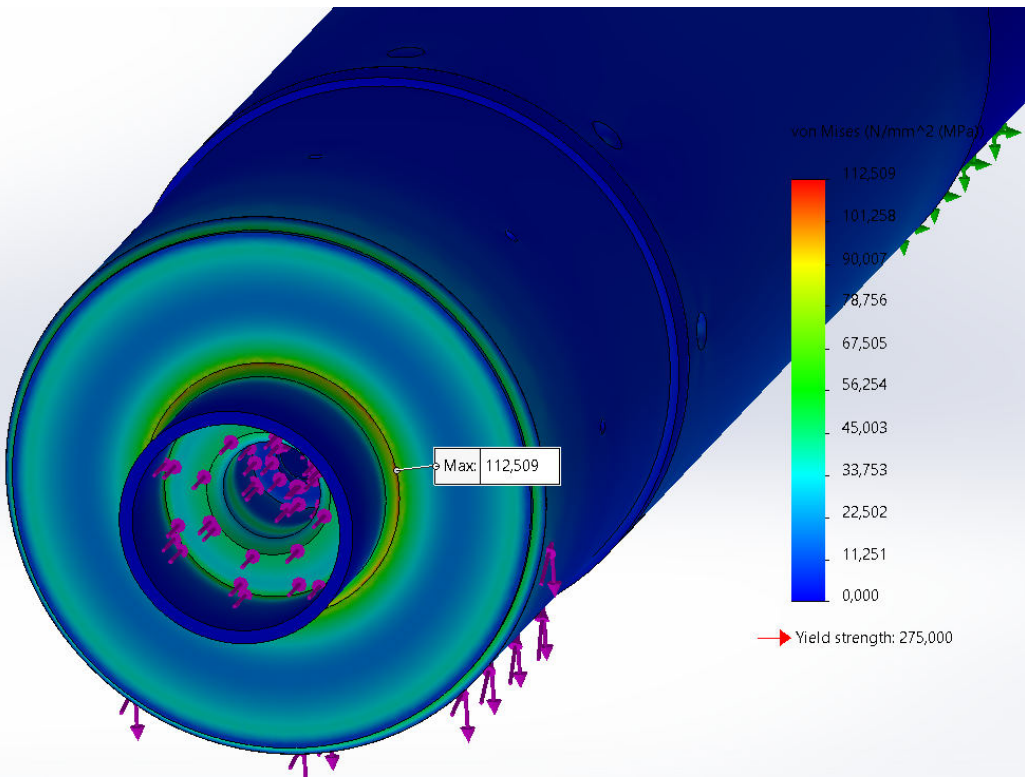


Figure 2 Thin motor mount

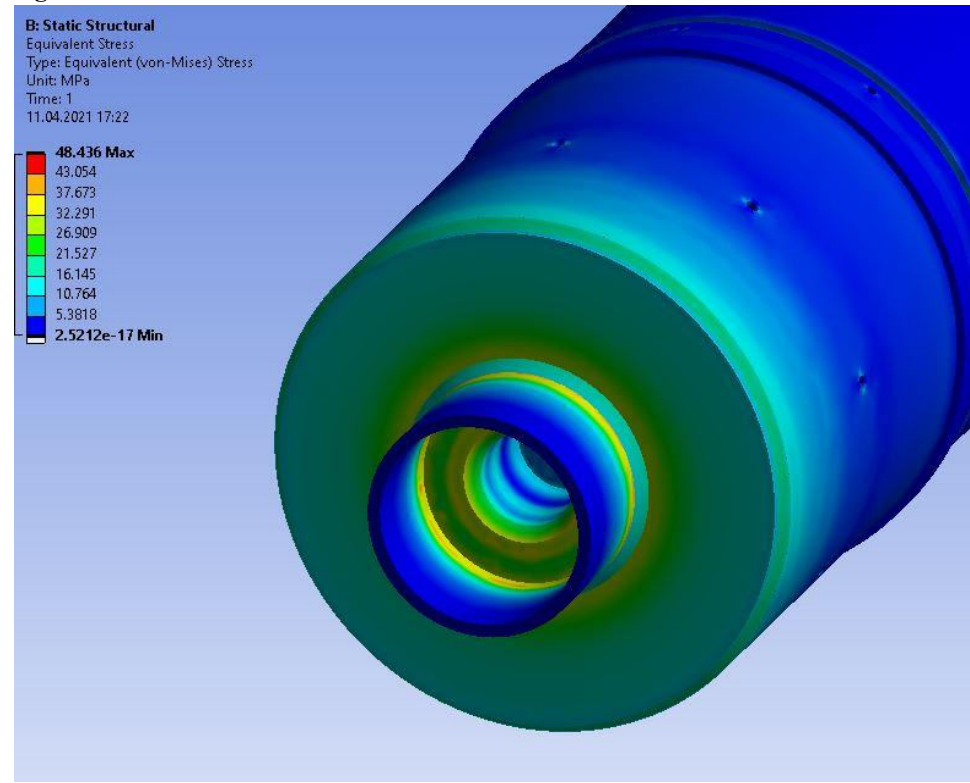


Figure 3 Thick motor mount

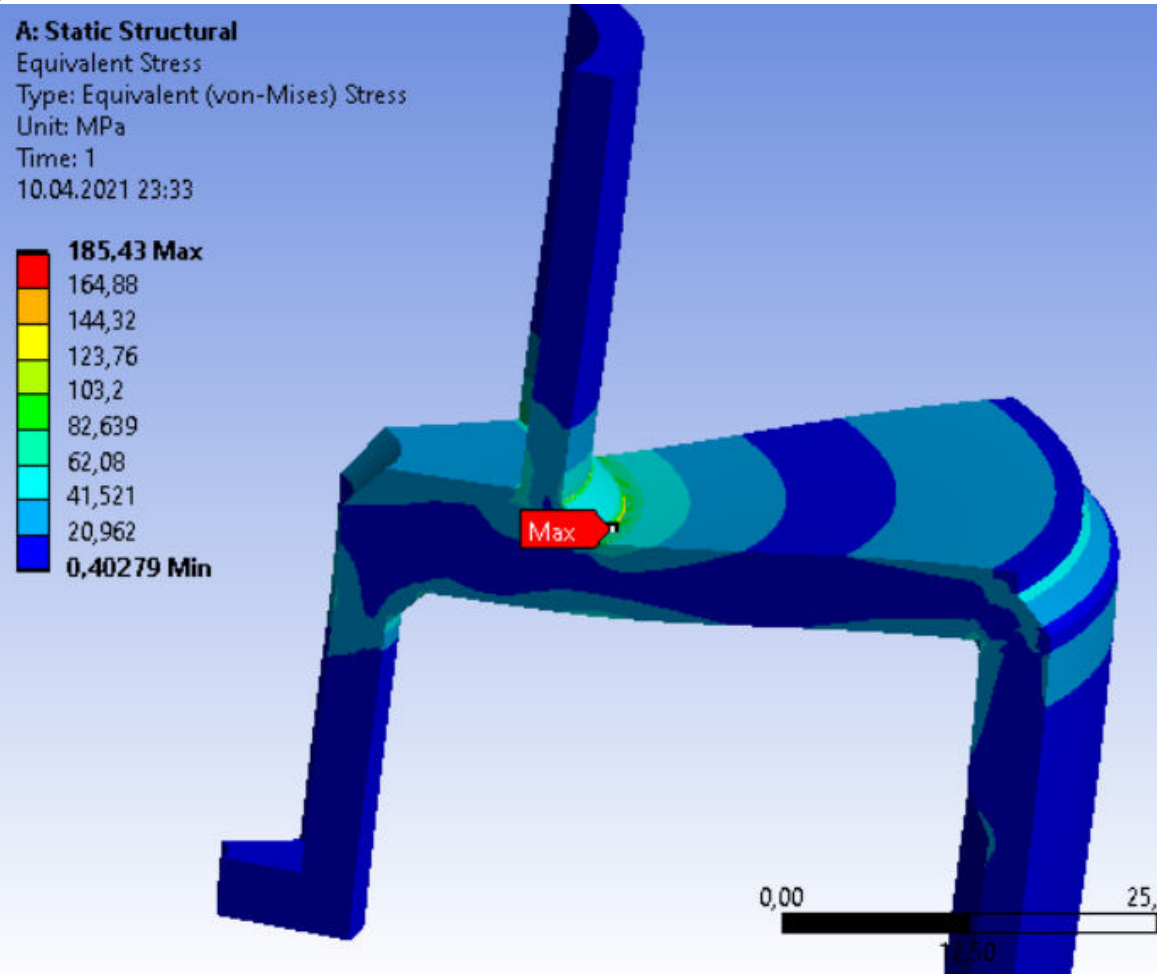


Figure 4 1/8-th of the motor mount to enable finer mesh.

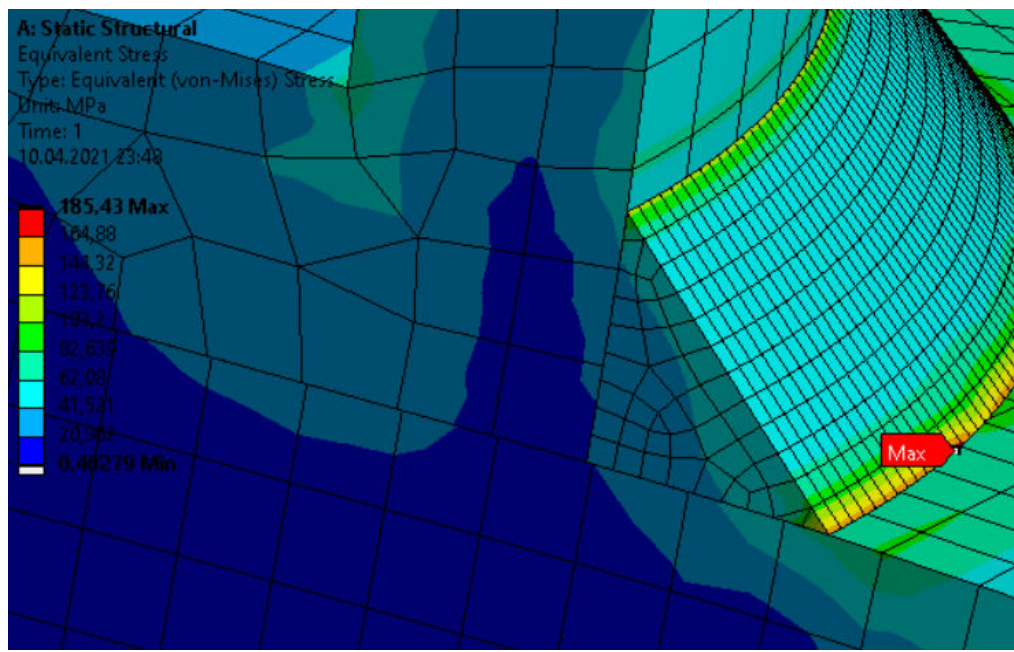


Figure 5 Closeup of 1/6-the motor mount

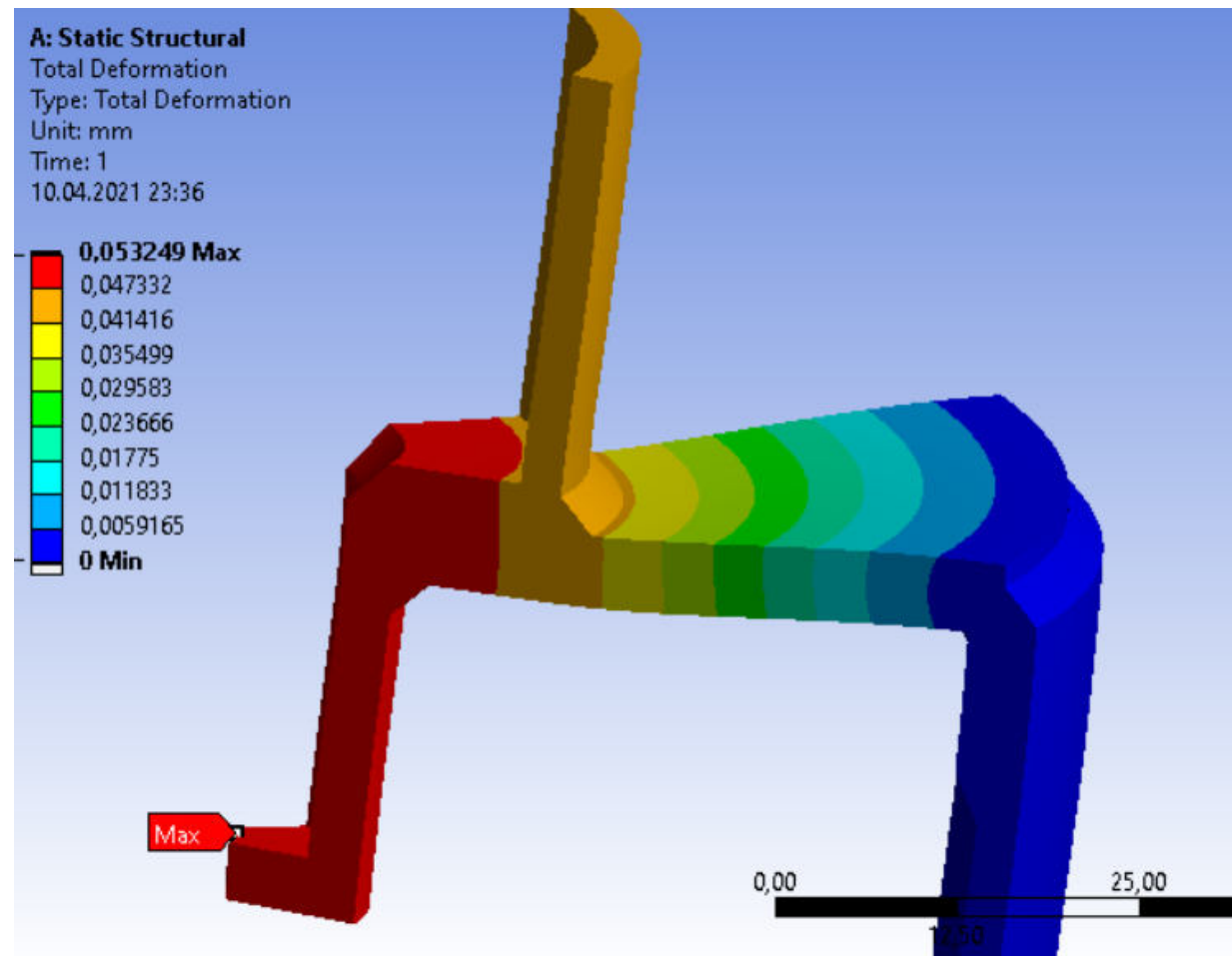


Figure 6 1/6-th model deformations

Looking at the results from the 5mm motor mount it becomes clear that the stresses are generally relatively low(<82 MPa), but at the transition from the welds to the other parts there is a clear increase. This is concluded to be because of notch stress increases as refining the mesh continues to increase these stresses. This is a known problem with corners without any radius as this means the notch effect tends to infinity as the mesh size decreases. Because of this it is concluded that the stresses in the welds does not exceed 82 MPa as is apparent in figure 5. Assuming that 82 MPa is the max stress, gives a factor of safety of 2.68 with heat treatment and 1.58 without heat treatment. This low stress is also consistent with the low deformation of 0.05mm further supporting the conclusion that the motor mount will be properly dimensioned at 5mm.

Final results:

Max stresses of 82 MPa resulting in a safety factor of 2.68 with heat treatment and 1.58 without heat treatment.

Impact force calculation

Problem statement:

To properly dimension the inner structure, the impact force when hitting the ground is an important force to take into account.

Figure:

Upper half velocity at impact: $v_{upper} = 4.38 \text{ m/s}$

Mass upper half: $m_{upper} = 12.28 \text{ kg}$

Lower half velocity at impact: $v_{lower} = 5.87 \text{ m/s}$

Mass lower half: $m_{lower} = 9.80 \text{ kg}$

Assumptions and approximations:

A stopping time of 0.02s is approximated.

The impulse formula gives the average sum of forces necessary to go from one velocity to another. When the rocket hits the ground the impact force starts at 0N and ends at ~0N. This means that the peak is higher than the average, and it is therefore assumed to have a peak value 2x higher than the average. After this is done the force from gravity is added to get the force needed to both stop the rocket and resist gravity while stopping. [28]

Physical laws:

Impulse formula:

$$J = \sum F \cdot \Delta t = m \cdot \Delta v \Leftrightarrow \sum F = \frac{J}{\Delta t} = \frac{m \cdot \Delta v}{\Delta t}$$

Calculations:

Impact force upper half:

$$\begin{aligned} F_{max\ upper} &= 2 \cdot \sum F_{upper} + F_{gravity\ upper} = 2 \cdot \frac{m_{upper} \cdot \Delta v}{\Delta t} + m_{upper} \cdot g \\ &= 2 \cdot \frac{12.28 \cdot 4.38}{0.02} + 12.28 \cdot 9.81 = 5499 \text{ N} \end{aligned}$$

Impact force lower half:

$$\begin{aligned} F_{max\ lower} &= 2 \cdot \sum F_{lower} + F_{gravity\ lower} = 2 \cdot \frac{m_{lower} \cdot \Delta v}{\Delta t} + m_{lower} \cdot g \\ &= 2 \cdot \frac{9.80 \cdot 5.87}{0.02} + 9.80 \cdot 9.81 = 5849 \text{ N} \end{aligned}$$

Reasoning, discussion and verification:

A look at the time assumption:

$$D = v_{acg} \cdot t = v_{lower}/2 \cdot 0.02 = 0.059 \text{ m}$$

A stopping time of 0.02 s results in a stopping distance of 6.2 cm. This is a possible stopping distance if the rocket hits dirt. The ground where the rocket lands is not fully known, so it could be hard or soft, but it is mostly dirt. Therefore a stopping distance of 6.2 cm seems reasonable when the rocket hits dirt.

Final results:

$$F_{max\ upper} = 5499N$$
$$F_{max\ lower} = 5849N$$

Boattail Impact Simulation

Problem statement:

As the boattail is the part that hits the ground first when descending it is important to simulate this event to ensure that the boattail does not sustain damage from the impact. The simulation should therefore find the stresses from ground impact on the boattail.

Figure:

Weight of lower half: $m = 9.5\ kg$

Impact velocity: $v = 5.87\ m/s$

Gravity: $g = 9.81\ m/s^2$

Soil stiffness: $5\ MN/m^3$

Soil depth: 200mm

Assumptions and approximations:

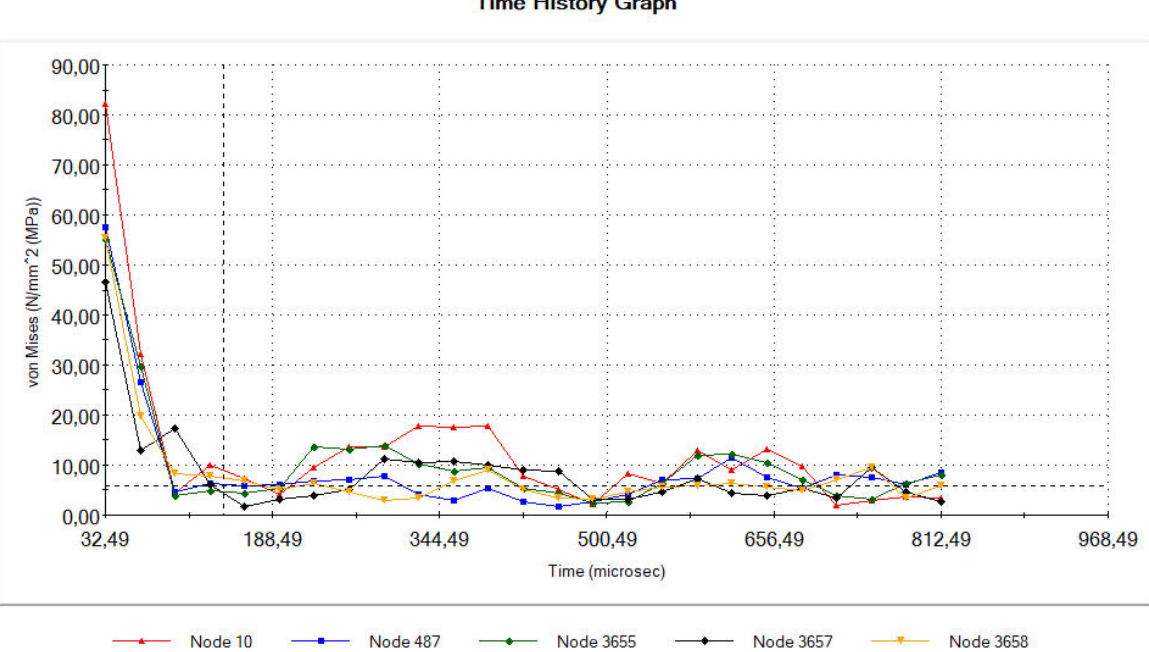
Since the ground conditions are unknown, a conservative approach was taken. Therefore the ground is assumed to be 200 mm deep before it is rigid. As the ground might not be parallel to the boattail, a simulation with impact to a plane at 15 degrees was also conducted.

Reasoning, discussion and verification:

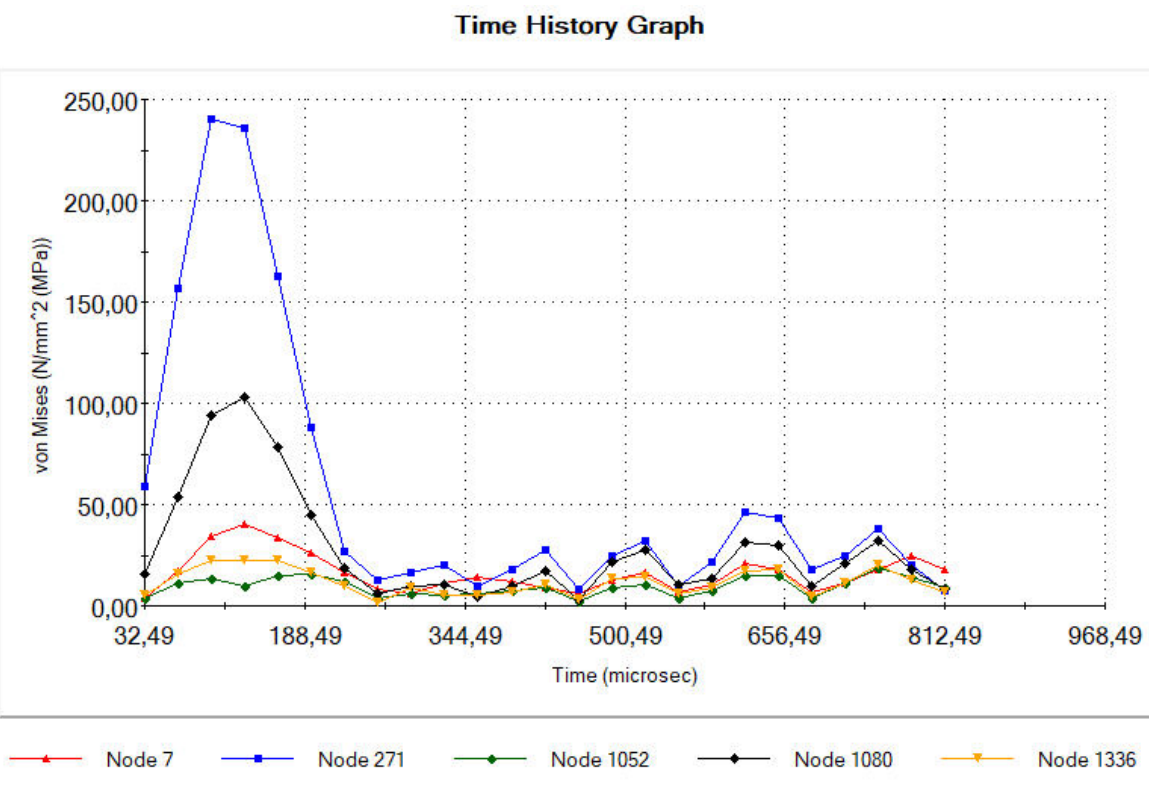
The simulation was done using Solidworks Drop Test simulation.

The nodes selected for the graphs were selected based on the location of the max stress. The max stress node was selected first, then 4 more nodes spaced equally along the length of the boattail in the axial direction.

Results(0 degrees):



Results(15 degrees):



Discussion:

A flat impact results in a max stress of 82.1 MPa which results in a FoS of 3.3. The boattail should therefore handle a flat impact without damage. With a 15 degree angle the max stress is 239.9 MPa resulting in a FoS of 1.14. This means that the boattail might sustain damage if the impact is significantly slanted. The impact analysis is also done using the stiffness of soil and not rocks. This means that the boattail will experience a higher stress if the impact location is on for example a rocky outcrop. As there is a significant chance that the boattail is damaged upon impact it might need to be replaced. Since the part is simple it is deemed acceptable to replace the boattail should it sustain damage during impact, however the boattail should be sufficiently sturdy for most impacts and a replacement should therefore not be needed for most landings.

Final results:

Max stress flat impact(0 degrees): 82.1 MPa

Max stress slanted impact(15 degrees): 239.9 MPa

Lower Threaded rods

Problem statement:

As the lower threaded rods are a mounting point for many parts it is important that they can handle the stresses imposed on them.

Figure:

Acceleration from motor(compression): $a = 147 \text{ m/s}^2$

Payload mass: $m = 4 \text{ kg}$

Impact force(tension): $F_{impact} = 5499 \text{ N}$

Size: M5

Pitch: $P = 0.0008 \text{ m}$

Length: $L = 0.31 \text{ m}$

Rods: $N = 4$

Material: Steel

Assumptions and approximations:

The rods are assumed to have no end stiffness, meaning $K = 1$ for buckling. It is also assumed that the components mounted to the rods do not give additional stiffness as well, even though they connect the rods together.

The load from the payload is split between the lower and upper threaded rods as well as the airframe. As a conservative estimate it is assumed that half of this load goes to the lower threaded rods.

The load from impact originates from the nose tip and is dispersed through the rocket. A conservative calculation of the stresses from this force is using the whole force on the 4 rods.

Physical laws:

Euler buckling: $F_{cr} = \frac{\pi^2 \cdot E \cdot I}{(K \cdot L)^2}$

Polar moment of inertia: $I = \frac{\pi \cdot D^4}{32}$

Minimum diameter for bolt: $d_{min} = d - 1.2268 \cdot P$

Calculations:**Minimum diameter for bolt:**

$$d_{min} = d - 1.2268 \cdot P = 0.005 - 1.2268 \cdot 0.0008 = 0.0040 \text{ m}$$

Euler buckling:

$$F_{cr} = \frac{\pi^2 \cdot E \cdot I}{(K \cdot L)^2} = \frac{\pi^2 \cdot 210e9 \cdot \pi / 32 \cdot (0.0040)^4}{(1 \cdot 0.31)^2} = 552 \text{ N}$$

Payload force:

$$F_P = \frac{m \cdot a}{2} = \frac{4 \cdot 147}{2} = 294 \text{ N}$$

Impact stress:

$$\sigma = \frac{F_{impact}}{N \cdot A} = \frac{5714.5}{4 \cdot \pi / 4 \cdot (0.0040 \cdot 10^3)^2} = 108.8 \text{ MPa}$$

Reasoning, discussion and verification:

Even though the forces are higher than the actual loads the threaded rods are adequate for that load. It is therefore concluded that the rods are thick enough.

Final results:**Buckling load:**

$$F_{cr} = 552 \text{ N}$$

Impact stress:

$$\sigma = 108.8 \text{ MPa}$$

Eigenfrequency

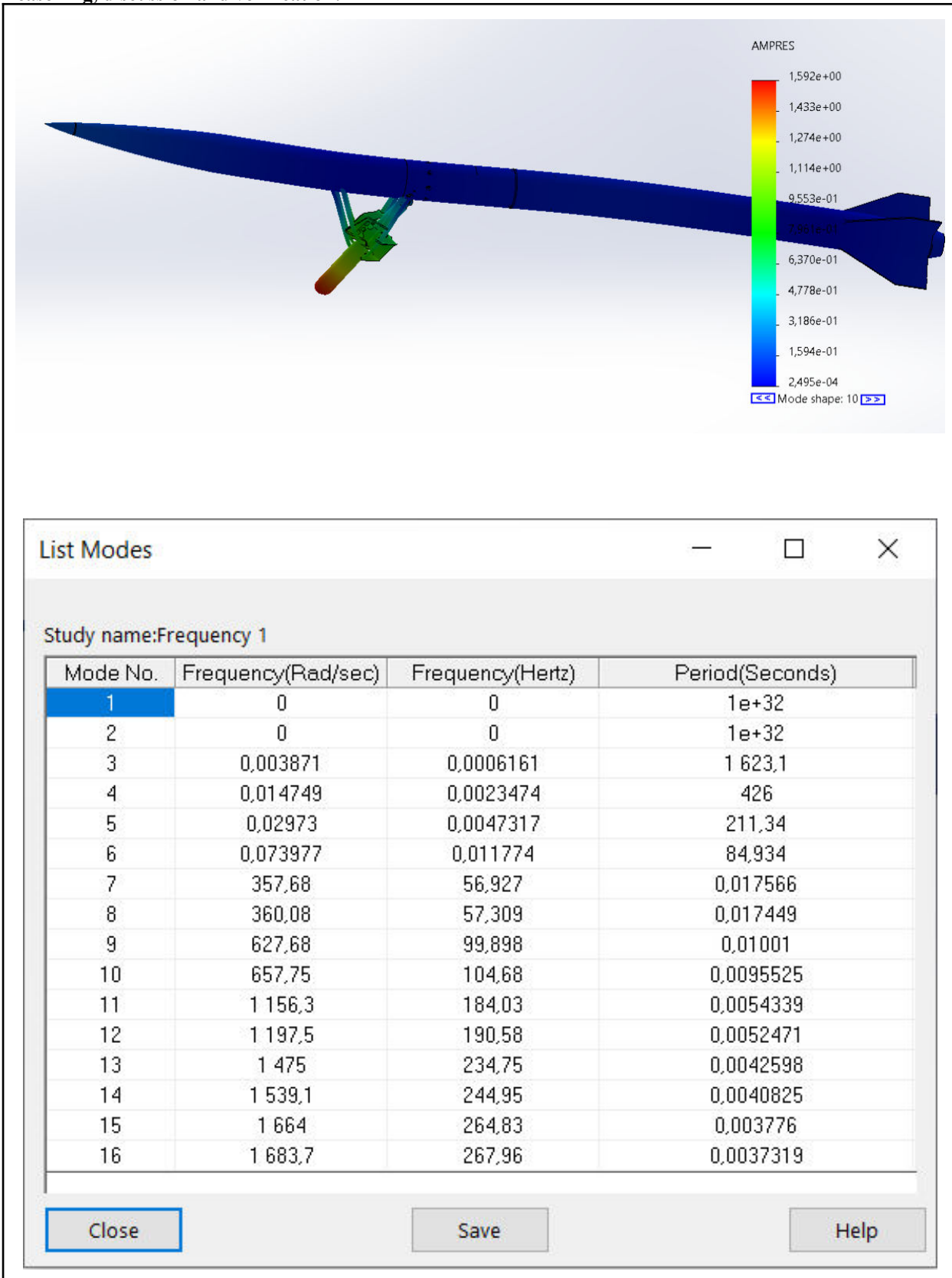
Problem statement:

The rocket vibrates during flight, it is therefore important that the rocket does not vibrate at the eigenfrequencies. A frequency analysis should therefore be done to locate the eigenfrequencies.

Assumptions and approximations:

The analysis was done in Solidworks with no fixtures. It was also done using only bonded connections, as no penetration was not possible to use. This means some connections are stiffer than in reality and the simulation therefore gives too high values.

Reasoning, discussion and verification:



In the list of frequencies it is seen that the first 6 modes are ~0 Hz. This is due to the lack of fixtures. The first mode is therefore the 7. Mode from the table.

An estimate for the highest value for what the rocket might experience during flight is considered to be 30Hz according to the Kongsberg group [29]. This means that the eigenfrequency of mode 7, which is 57 Hz can be reduced by almost 50% and still be above the highest experienced vibration. It is therefore deemed that the rocket has sufficiently high eigenfrequencies.

Final results:

Mode	Mode 1	Mode 2	Mode 3	Mode 4	Mode 5	Mode 6	Mode 7
Hertz	56.9 Hz	57.3 Hz	99.9 Hz	104.7 Hz	184.0 Hz	190.6 Hz	234.8 Hz

As these are all above 30 Hz the rocket components are deemed to be sufficiently stiff.

Recovery

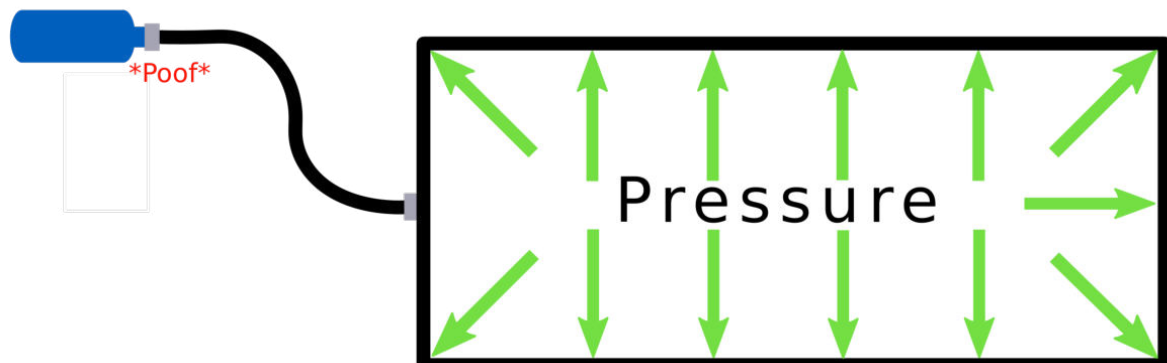
Pressure calculations

Problem statement:

Want to know the pressure force inside the packed recovery chamber, from the 3 different CO₂ canisters that the Hawk system supports, being 25g, 33g and 45g. Want to calculate using the atmosphere at apogee.

Figure:

Set up:



Assumptions and approximations:

Have assumed the temperature of the CO₂ canister is at the same temperature as the atmosphere at apogee, this will give the worst case.

Have assumed that the CO₂ has the same temperature under free expansion, as the Joule Thompson coefficient is hard to estimate due to the phase change from liquid to vapor. At -50 degrees and 1 atm [30] the Joule Thompson coefficient is positive which means there would be cooling. The assumption of no temperature change is wrong, but partially justified as the CO₂ canister will be either warmer or the same as the atmospheric temperature.

Lastly, it is assumed that the recovery chamber is airtight and that there is 1 atm inside the chamber.

Physical laws:

Van Der Waals equation:

$$(p + a \frac{n^2}{V^2}) * (V - nb) = nRT,$$

where p is the pressure, n is the mole, V is the volume, T is the temperature in kelvin, a is a correction constant for the attraction force between each particle, b is the correction constant for the volume of each particle and R is the universal gas constant.

Pressure force equation:

$$F = p * A,$$

where p is the pressure, F is the pressure force and A is the area normal to the pressure force.

Properties:

Atmospheric temperature at apogee: 217.15 K

Van der Waals constants [31]:

$$a = 0.364 \text{ Pa} * \text{m}^6/\text{mol}^2$$

$$b = 0.0427 \text{ m}^3/\text{kmol}$$

Recovery chamber volume:

4259.735cm³

Component	Compressibility	Volume	Compressed Volume
MCRS	0%	0.683 cm ³	0.683 cm ³
Main chute	30%	1483.029 cm ³	1038.120 cm ³
Drogue chute	30%	260.554 cm ³	182.388 cm ³
Shock coords	10%	293.902 cm ³	264.519 cm ³
Eyebolt	0%	9.284 cm ³	9.284 cm ³
U-Bolt	0%	7.806 cm ³	7.806 cm ³
2 Swivel links	0%	15.250 cm ³	15.250 cm ³
6 Quick links	0%	83.760 cm ³	83.760 cm ³

Calculations:

The packed volume is calculated by taking the volume of the recovery chamber and subtracting the volume times the incompressibility of each component. This gives a volume of:

$$V = 2590.315 \text{ cm}^3$$

The Van der Waals equation can be rearranged to express the pressure of the gas:

$$p = \frac{nRT}{V-nb} - \frac{n^2a}{V^2}$$

The mole amount can be found by dividing by the molecular mass of carbon dioxide.

$$n = m/M$$

Using python, the following results were obtained:

Weight	Pressure	Force
25g	3.82 bar	4250 N
33g	4.99 bar	5546 N
45g	6.68 bar	7431 N

Because the recovery chamber is airtight there will be a pressure gradient (difference from inside the rocket and outside the rocket) at apogee of approximately 0.75 atm.

This gives a pressure gradient force of: 845 N

Adding the pressure gradient to the pressure forces the final pressure forces are as follows:

Weight	Total pressure	Total force
25g + pressure gradient	4.58 bar	5096 N
33g + pressure gradient	5.75 bar	6391 N
45g + pressure gradient	7.44 bar	8276 N

Reasoning, discussion and verification:

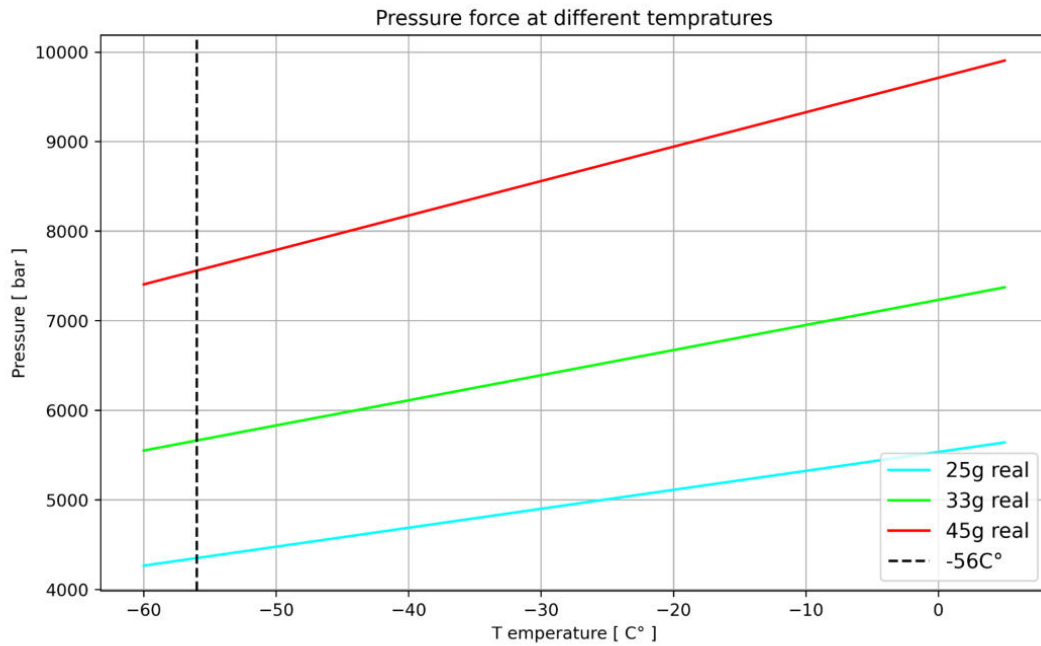
Seeing that the pressure inside the CO₂ canister is 59 bar. And, the pressures calculated are way below this, as the gas has expanded, these numbers seem reasonable.

Final results:

Expected pressure and pressure force for the different cartridges inside the recovery chamber at apogee is as follows:

Weight	Total pressure	Total Force
25g + pressure gradient	4.58 bar	5096 N
33g + pressure gradient	5.75 bar	6391 N
45g + pressure gradient	7.44 bar	8276 N

Since the temperature of the expanded gas is unknown a plot of pressure force (gas only) versus temperature was made:



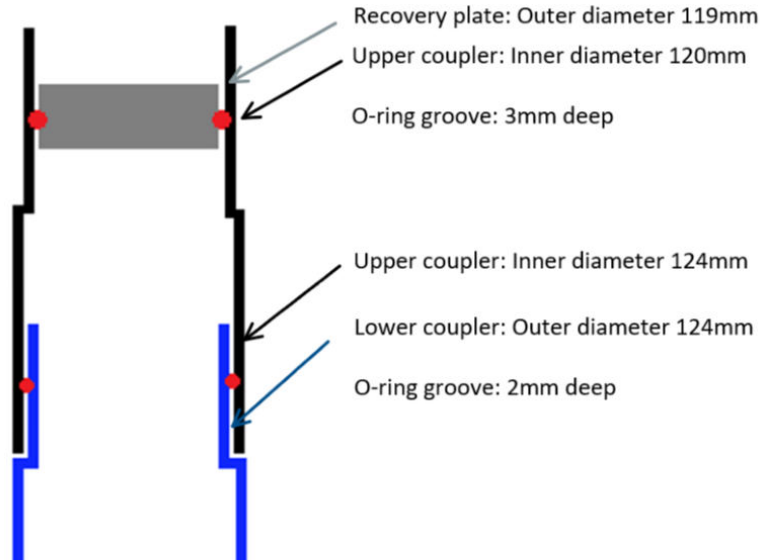
Thus the pressure gradient force makes up for the uncertainty in the temperature.

O-ring calculations

Problem statement:

Recoverybay needs to be airtight so that the pressure-separating system will have a successful separation. This requires the recoverybay to be airtight, for that o rings are used. These calculations give the best estimates for the o-ring sizes.

Figure:



Assumptions and approximations:

Because of production tolerances there will be a gap between the lower and upper coupler. Therefore, in the calculations a gap of 0.5 mm has been added. This is in the higher range considering tolerances therefore the compression of that ring is set on the lower side.

Physical laws:

Ring needs to be stretched 2 - 3% to get the best fit and minimize risk of extrusion.

Static o-ring: Compression of 30 - 40%.

Dynamic: Compression 20 - 30%.

Have used basic o-ring calculations [32].

Properties:

Needs to withstand the temperature range of what the rocket endures.

The material chosen is EPDM which is an elastomer with a temperature range of -50 °C to 150 °C.

Calculations:

Static:

$$CS: 3.5 \text{ mm} + 30\% = 3.5 \text{ mm} + 1.5 \text{ mm} = 5 \text{ mm}$$

$$ID: 113 \text{ mm} - 2.5\% = 113 \text{ mm} - 2.83 \text{ mm} = 110 \text{ mm}$$

Dynamic:

$$CS: 2.5 \text{ mm} + 20\% = 2.5 \text{ mm} + 0.5 \text{ mm} = 3 \text{ mm}$$

$$ID: 120 \text{ mm} - 2.5\% = 120 \text{ mm} - 3 = 117 \text{ mm}$$

Reasoning, discussion and verification:

The results from the calculations give an estimate of the sizes for the rings. The standard size ring closest to the results from the calculations is the size that will be purchased.

EPDM material is extremely durable and elastic, therefore below you can see that the chosen dynamic o-ring is a lot smaller than the results of the calculations! Main reasonings for this is the limited access to o ring size in this material and also opting for a smaller ring instead of a larger one to minimize the risk of extrusion.

Final results:

Static: 110 mm x 4 mm

Dynamic: 107.62 mm x 2.62 mm

These have been fitted and tested alongside the final rocket components.

Shear screws calculations

Problem statement:

The size and number of nylon 6/6 shear screws needed to prevent unintended and ensure intended separation of the rocket.

The shear strength of nylon shear screws ranges from 66.20 - 72.40 MPa [33]. Shear force to withstand is 845.2N and pressure forces from the CO₂-canisters are listed in the result table in *pressure calculations*. See *pressure calculations* for derivation of these quantities.

Figure:

Shear force: F

Shear strength nylon 6/6 shear screws: Ts

Diameter screw: d

Cross-sectional area: A

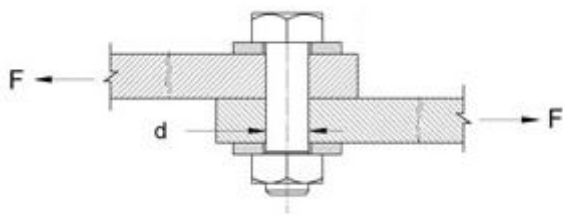


Figure from: https://www.engineersedge.com/material_science/bolt_single_shear_calcs.htm [34]

Assumptions and approximations:

1. The pitch diameter is used to calculate the shear cross-section area.
2. We assume that all screws in the same class are identical with the same pitch diameter. Screws with 6g tolerance with the lower tolerance limit for the pitch diameter will be used in the calculations.

Physical laws:

Shear force: $F = Ts \cdot A$

Cross-sectional area circle: $A = (\pi \cdot d^2)/4$

Properties:

Pitch diameter is found in a table from *EngineersEDGE* [35].

Calculations:

ISO metric thread designation	Pitch diameter [mm]	Area [mm^2]	Shear force one shear screw[N]*		Number of screws	Total shear strength [N]	
			Lower value	Upper value		Lower value	Upper value
M2x0.4	1.654	2.148	239.8	262.3	4	956.2	1049
					6	1439	1574
					8	1918	2098
M3x0.5	2.580	5.227	346.0	378.5	4	1384	1514
					6	2076	2271
					8	2768	3028
M4x0.7	3.433	9.256	612.7	670.1	4	2451	2680
					6	3676	4021
					8	4902	5361

*Calculating using $T_s=66.2$ and $T_s=72.4$ respectively lower value and upper value

To consider the worst case, the lower value for total shear strength is used to calculate factor of safety(FoS) for unintended separation. This is separation due to the pressure gradient at apogee. While the upper value for total shear strength is used to calculate the FoS for the intended separation. The total force here is the sum of the pressure gradient force and the pressure force from the separation system.

CO2-canister size (g)	Force separation system + pressure gradient [N]	ISO metric thread designation	Number of screws	FoS intended separation
25	5096	M2x0.4	4	4.86
			6	3.24

			8	2.43
			4	3.37
		M3x0.5	6	2.24
			8	1.68
		M4x0.7	4	1.90
			6	1.27
			8	0.95
33	6391		4	6.09
		M2x0.4	6	4.06
			8	3.05
		M3x0.5	4	4.22
			6	2.81
			8	2.11
		M4x0.7	4	2.38
			6	1.59
			8	1.19
45	8276		4	7.89
		M2x0.4	6	5.26
			8	3.94
		M3x0.5	4	5.47
			6	3.64
			8	2.73
		M4x0.7	4	3.09
			6	2.06
			8	1.54
Force from pressure gradient [N]	ISO metric thread designation	Number of screws	FoS unintended separation	

845.2	M2x0.4	4	1.13
		6	1.70
		8	2.27
	M3x0.5	4	1.64
		6	2.46
		8	3.27
	M4x0.7	4	2.90
		6	4.35
		8	5.80

Reasoning, discussion and verification:

Justifying assumptions

1. The approximation of using the pitch diameter is reasonable because the shear cross-section will include both the minor and major diameter of the screw.
2. The difference in pitch diameter is due to tolerances when making the screws. This difference is under 0.1mm. Making this difference neglectable.

The results seem valid at first glance. Still they will be validated via physical testing.

Final results:

The relevant combination of CO2-canister, shear screw type and amount are the ones who have a FoS above 2 for both unintended and intended separation.

CO2-canister (size g)	ISO metric thread designation	Number of screws	FoS unintended separation	FoS intended separation
25	M2x0.4	8	2.27	2.43
25	M3x0.5	6	2.46	2.24
33	M3x0.5	8	3.27	2.11
33	M4x0.7	4	2.90	2.38
45	M3x0.5	8	3.27	2.73
45	M4x0.7	4	4.35	3.09
45	M4x0.7	6	5.80	2.06

Drag difference aft and forward

Problem statement:

The difference in drag between aft and forward is to be determined. The following data is given from CFD-analysis:

Forces - Direction Vector (1 0 0)			
	Forces [N]		
Zone	Pressure	Viscous	Total
aft-tube	210.55231	-0.098898741	210.45341
boat-tail	10.827841	0.17049856	10.998339
fins	1139.7679	-0.26127521	1139.5066
main-tube	280.83505	12.087424	292.92247
nosecone	308.60218	3.9448742	312.54706
-----	-----	-----	-----
Net	1950.5853	15.842622	1966.4279

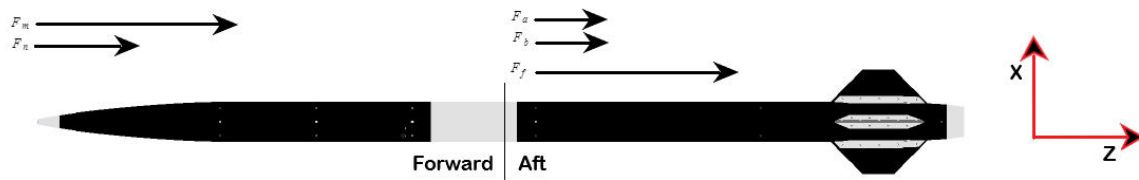
Forces - Direction Vector (0 1 0)			
	Forces [N]		
Zone	Pressure	Viscous	Total
aft-tube	180.70647	-0.31364821	180.39282
boat-tail	104.78241	-0.062369477	104.72004
fins	150.92459	1.9215007	152.84609
main-tube	1127.9069	7.6642929	1135.5712
nosecone	-32.932502	2.293294	-30.639208
-----	-----	-----	-----
Net	1531.3878	11.50307	1542.8909

Forces - Direction Vector (0 0 1)			
	Forces [N]		
Zone	Pressure	Viscous	Total
aft-tube	15.338822	7.217685	22.556507
boat-tail	21.061756	2.3013056	23.363061
fins	131.76282	38.8899	170.65272
main-tube	0.40075907	126.67528	127.07604
nosecone	33.387338	30.154491	63.541829
-----	-----	-----	-----
Net	201.95149	205.23866	407.19015

The coordinates relative to the rocket is shown in the figure below.

Figure:

F_a = Drag force aft - tube
 F_n = Drag force nose cone
 F_b = Drag force boat - tail
 F_f = Drag force fins
 F_m = Drag force main - tube



Assumptions and approximations:

Assuming only the forces in z-direction contribute to shear on the shear screws.

Physical laws:

Drag force equation:

$$F_D = \frac{1}{2} C_d \rho A v^2$$

Difference in drag between aft and forward:

$$\Delta F_D = F_{D,aft} - F_{D,forward}$$

Properties:

$$F_{D,aft} = F_a + F_b + F_f = 22.55N + 23.36N + 170.65N = 216.56N$$

$$F_{D,forward} = F_n + F_m = 63.54N + 127.07N = 190.61N$$

Calculations:

Difference in drag:

$$\Delta F_D = F_{D,aft} - F_{D,forward} = 216.56N - 190.61N = 25.95N$$

This is shear force in z-direction due to drag forces.

Reasoning, discussion and verification:

The assumption that only the drag forces in z-direction contribute to the shear force on the shear screws is not entirely correct. The forces in x- and y-direction will contribute as well as they induce a bending moment on the rocket that will also cause shear. Still this assumption is somewhat reasonable because the other screws(made of steel) will absorb most of the shear. Another factor is displacement. If the couplers have a loose fit, the bending moment will give an increased shear force. But because of tight tolerances between the lower and upper coupler there will be minimal displacement of the couplers and therefore a lower shear force due to this.

Final results:

Shear force on the screws is found to be 25.95N

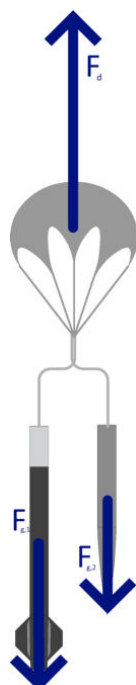
Chute calculations (Choosing chutes)

Problem statement:

Want to choose Drogue and Main chutes that follow DTEG 3.1

Therefore, the Drogue chute should descend with a velocity between 23 m/s and 46 m/s the whole descent. And when the Main chute is out the rocket should descend with a velocity below 9 m/s.

Figure:



Assumptions and approximations:

- Have assumed the chutes fold out instantaneously.
- Have assumed no drag from the rocket body, only the parachutes.
- Have assumed drag from the rocket was neglected
- Have assumed stable atmosphere and that air is an ideal gas
- Have assumed there exists a regression model that relates the projected area of each parachute style, based on its diameter in inches.
- Have assumed constant gravitational acceleration

Physical laws:

Drag force equation:

$$F_d = \frac{1}{2} C_d \rho A v^2,$$

where F_d is the drag force, C_d is the drag coefficient, ρ is the density of the fluid, A is the projected area and v is the velocity.

Rearranging the drag force gives the terminal velocity equation:

$$v_t = \sqrt{\frac{2mg}{\rho A C_d}}$$

where v_t is the terminal velocity, m is the weight and g is the gravitational acceleration

Clausius Clapeyron approximated:

$$e_s(T) = 611.2 \exp\left(\frac{L_v}{R_v}\left(\frac{1}{273.15} - \frac{1}{T}\right)\right),$$

Where L_v is the latent heat for vaporization, R_v is the gas constant for water vapor and T is temperature in Kelvin.

Density at altitude (with water pressure): [36]

$$\rho(z) = C \frac{p(z) - 0.378e(z)}{T(z)}$$

where C is a constant $C = \frac{1}{R_{air}}$, p is the pressure at an altitude z , e is the vapor pressure at z based on relative humidity w and temperature $T(z)$. This formula becomes the ideal gas law when $e = 0$.

Properties:

From [37], the air density at 10000m above sea level is 0.4135 kg/m^3 . The air density at apogee was estimated to be $\rho_{apogee} = 0.4035 \text{ kg/m}^3$ at apogee. Looking at weather data for October 2020 in Ponte de Sor [38], the lowest air density at the 450 m AGL was estimated to be $\rho_{450m} = 1.007 \text{ kg/m}^3$.

Parachute constants [39]:

Parachute	Drag coefficient	Projected Area
Drogue chute	1.5	0.44 m^2
Main chute	2.2	4.53 m^2

Mass of the rocket: $m = 23.79 \text{ kg}$

Using data from Fruity Chutes [39], created two regression models which relate the diameter of the given model to its projected area. The Drogue model is chosen to be the *Classical elliptical*, and the Main chute model is chosen to be the *Iris Ultra Compact*.

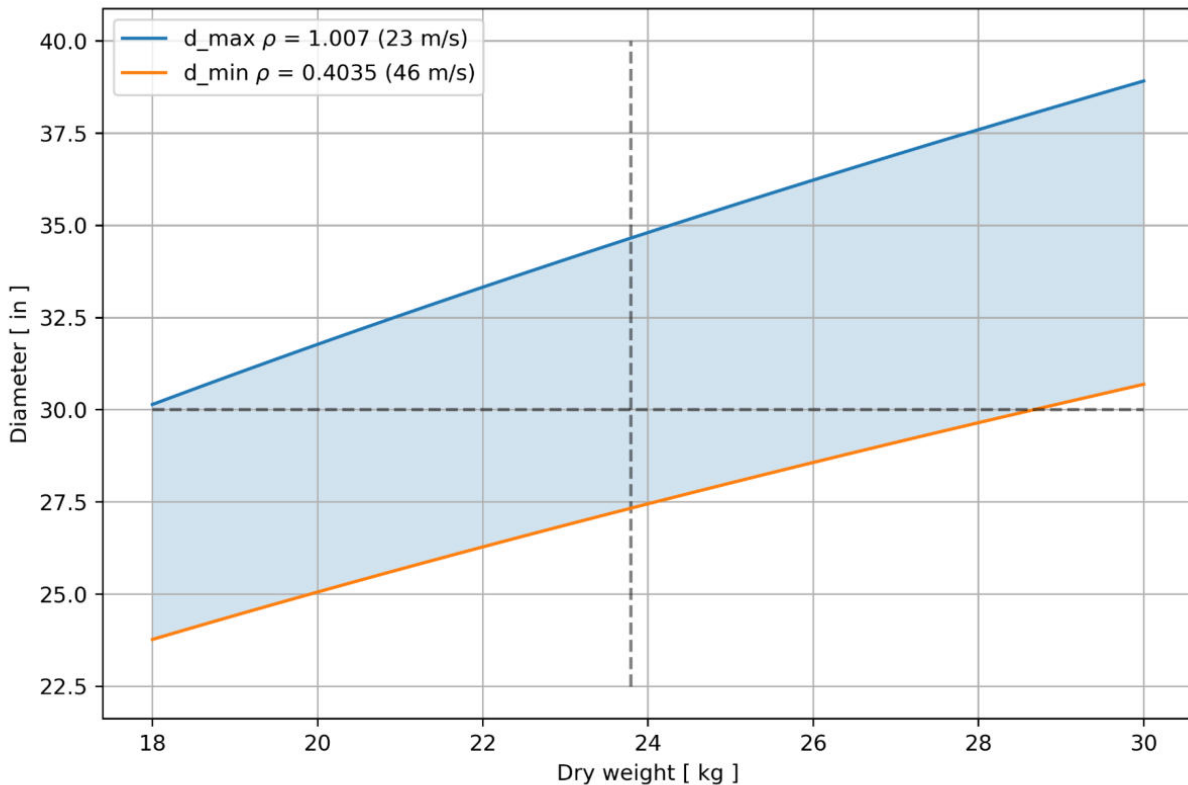
Calculations:

Rearranged the terminal velocity function to give a function for area as follows:

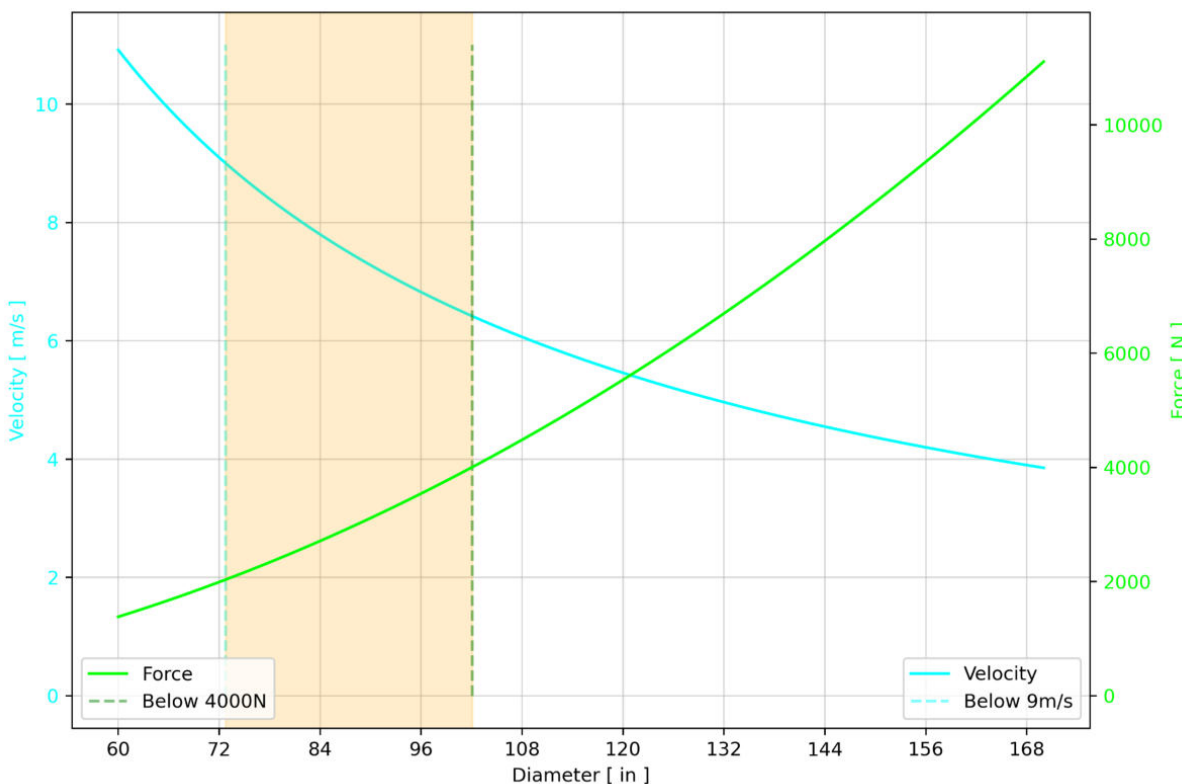
$$A = \frac{2mg}{\rho C_d v_t^2}$$

The two worst cases are, that either the Drogue chute goes to fast at apogee where $\rho = 0.4035$. Or that the Drogue chute goes too slow at the point where the Main chute will be released where $\rho_{450m} = 1.007kg/m^3$.

Thus boundaries can be plotted using the regression model to get the diameter of the chute at different dry weights of the rocket. The rocket has to have a velocity lower than 46m/s at apogee and a velocity larger than 23m/s at the point where the Main chute will be released. This gives the following plot below:



From the plot above it is easily seen that the 30 inch is within the two boundaries. Requirement S2.1.2, states that the force from the main chute should be below 4000 N, and from *DTEG 3.1.2 Main deployment event* the velocity should be below 9 m/s. The requirement was set, to limit the deployment force. Thus, using the terminal velocity equation for the Main chute alone gives one bound. Using the terminal velocity of the 30 inch Drogue chute in the Drag force equation, and then being below 4000 N gives the other bound. This can be visualized in the plot below which relates the velocity as well as the force to the diameter of the Main chute:



The slower the descent the smaller the impact, thus it is best to minimize the descent velocity. It can then be seen from the plot above that the 96 inch minimizes the descent velocity, and keeps the release force below 4000 N

Reasoning, discussion and verification:

Due to the spill hole in each of the parachutes, a regression model was chosen. This model has been fitted for all the available sizes for each model. Therefore, the projected area should be correct, and in the end it has to be rounded up or down, so the small errors have no effect on the calculations. The numbers seem reasonable as they come from the drag force equation, but they do neglect wind, so the forces might increase by a little bit. There are also some errors due to estimation of the air densities.

Final results:

Based on the plots above the Drogue chute has been chosen to be 30 inch, and the main chute has been chosen to be 96 inches.

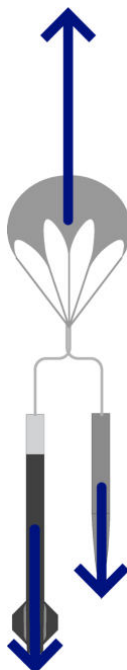
Parachute trajectory simulations

Problem statement:

Want to simulate the velocity and release force of the parachute system over time and get a parachute trajectory.

Figure:

Same as for chute calculations:



Assumptions and approximations:

Assumed a ISA [40], which briefly assumes that:

- Air is an ideal gas, and follows all ideal properties
- The atmosphere is stable, and therefore no winds
- The temperature with altitude follows a linear curve, with a Lapse rate of 6.49 K/km in the troposphere, which should be changed if the sea level temperature is increased.

Have assumed the chutes fold out instantaneously.

Have assumed constant Latent heat for vaporization.

Have assumed no drag from the rocket body, only the parachutes.

Physical laws:

Drag force equation:

$$F_d = \frac{1}{2} C_d \rho A v^2,$$

where F_d is the drag force, C_d is the drag coefficient, ρ is the density of the fluid, A is the projected area and v is the velocity.

Gravitational acceleration:

$$g(z) = \frac{GM}{r^2},$$

where M is the mass of the Earth, G is the gravitational constant, and r is the distance from the center of the Earth. z is included in the r .

Distance from Earth:

$$r(z) = r_{Earth} + h_{ASL} + z,$$

where r_{Earth} is the average radius of the Earth, h_{ASL} is the height above sea level and z is the altitude.

Temperature at altitude:

$$T(z) = T_0 - \Gamma_{ISA} z,$$

where T_0 is the temperature at ground level, Γ_{ISA} is the ISA lapse rate and z is the altitude.

Clausius clapeyron approximated:

$$e_s(T) = 611.2 \exp\left(\frac{L_v}{R_v} \left(\frac{1}{273.15} - \frac{1}{T}\right)\right),$$

Where L_v is the latent heat for vaporization, R_v is the gas constant for water vapor and T is temperature in Kelvin.

Pressure at altitude (assumed linear temperature profile):

$$p(z) = p_0 \left(\frac{T(z)}{T_0}\right)^{\frac{g(z)}{R_{air} \Gamma_{ISA}}},$$

where p_0 and T_0 is respectively the pressure and temperature at ground level, T is the temperature at an altitude z , g is the gravitational acceleration at an altitude z , R_{air} is the gas constant for air, Γ_{ISA} is the ISA lapse rate.

Density at altitude (with water pressure): [36]

$$\rho(z) = C \frac{p(z) - 0.378e(z)}{T(z)}$$

where C is a constant $C = \frac{1}{R_{air}}$, p is the pressure at an altitude z , e is the vapor pressure at z based on relative humidity w and temperature $T(z)$. This formula becomes the ideal gas law when $e = 0$.

Lastly the acceleration is set to:

$$\frac{dv}{dt} = g(z) - \frac{F_{d, drogue}}{m} - \frac{F_{d, main}}{m},$$

where $\frac{dv}{dt} = a$ is the acceleration of the system, g is the gravitational acceleration at z , m is the mass and F_d is the drag force.

Properties:

Parachute constants [39]:

Parachute	Drag coefficient	Projected Area
Drogue chute	1.5	0.44 m ²
Main chute	2.2	4.53 m ²

Atmospheric constants:

Constant	Value
R_{air}	287.05 J/K*kg
Γ_{ISA}	6.49 K/km
R_v	461.52 J/K*kg
L_v	2.50 MJ/kg

G	$6.67 \times 10^{-11} \text{ Nm}^2/\text{kg}^2$
C	$3.48 \times 10^{-3} \text{ K} \cdot \text{kg}/\text{J}$
M_{earth}	$5.97 \times 10^{24} \text{ kg}$
r_{earth}	6371 km
h_{ASL}	119 m [1]

Masses:

Object	Weight
m_{AFT}	9.81 kg
m_{FWD}	12.28 kg
m_{total}	22.09 kg

Atmospheric values for worst case (October 11 2020):

Parameter	Value
T_0	26 C°
p_0	102 kPa
w	19%

Start height (apogee): 8771.3 m [Section II.C Trajectory calculations]

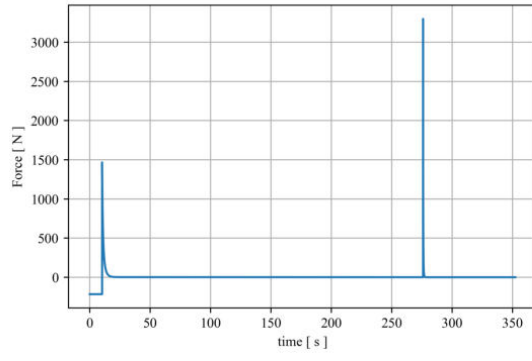
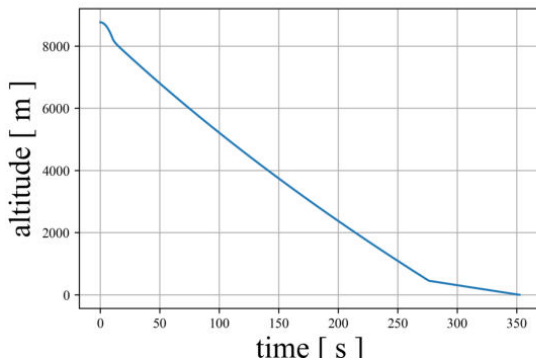
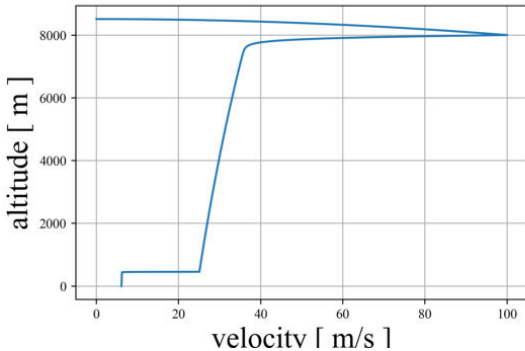
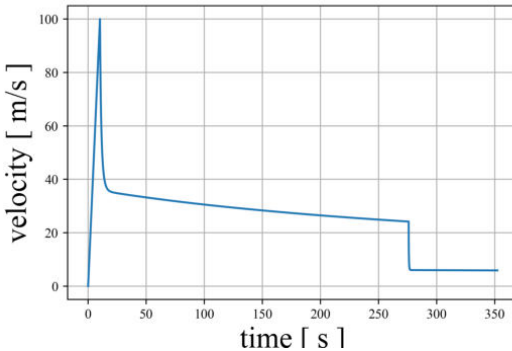
Calculations:

Have used python to implement a numerical equation solver with adaptive step size, which checks local error based on the (2,3) ordered pair of the Bogacki-Shampine model [41][42]. This method checks if a certain tolerance is met locally before accepting a new time step. This method takes in $(t_0, t_{end}, y_0, f, h_0, tol)$ and returns T, Y . Here t_0 is the start time, t_{end} is estimated descent time, y_0 is an array of initial values set to $[0, h_{apogee}]$, f is a function that returns the derivatives of each parameter in the array $y = [v, z]$. h_0 is estimated step size, but due to the adaptive step size this changes to meet the set tolerance tol . Throughout the calculations $tol = 10^{-6}$. All equations used are based on ISA standards.

The Drogue chute deployment was implemented by setting the $F_d = 0$ before a certain condition is met. For the Drogue chute the condition is set to $t > t_s$ where t_s is the time the drogue chute is deployed. For the Main chute this condition is that $z \leq 450m$.

Using the Bogacki-Shampine method, the atmospheric values above and with a drogue deployment time of

$t_s = \frac{100}{9.81}$ gives the following graphs:



And the worst case values:

Parachute	Release force	Final descent rate
Drogue chute	1466.39 N	24.16 m/s
Main chute	3298.10 N	5.87 m/s
Main chute (FWD only)	-	4.38 m/s*

*separate simulation with $m = m_{FWD}$

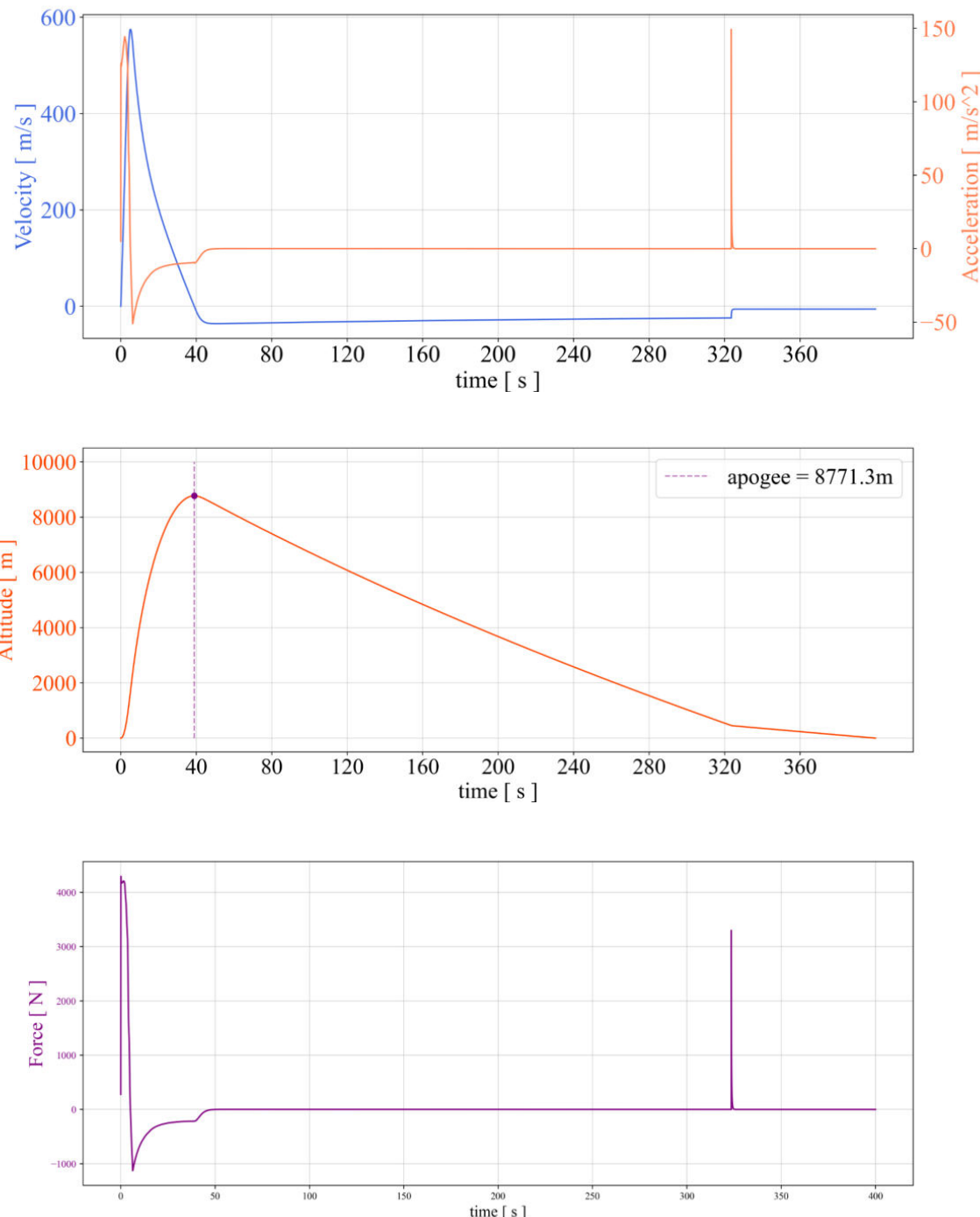
Reasoning, discussion and verification:

The results above are reasonable, since the curves are smooth, and also at each point one can dobbel check with the acceleration equation given above. Winds are being neglected, which might add some noise in the real trajectory, and the force might increase a little, but the general shape will remain. The result was also compared to the result using `scipy.integrate.solve_ivp`, and the values were the same up to the 5th decimal place.

Final results:

Since OpenRocket only accepts ISA standard temperatures (13°C , 101325 Pa) or an Isothermal atmosphere, a second simulation was used to give a compliance between the OpenRocket data for the propulsion trajectory with the recovery trajectory. This resulted in the graphs below.

Combined with OpenRocket data:



Here $t_s = 0$ and resulted in almost the same Main chute release force, but slower descent. Thus the worst case

values are as given in the table above:

Parachute	Release force	Final descent rate
Drogue chute	1498.30 N	24.16 m/s
Main chute	3553.23 N	5.87 m/s
Main chute (FWD only)	-	4.38 m/s*

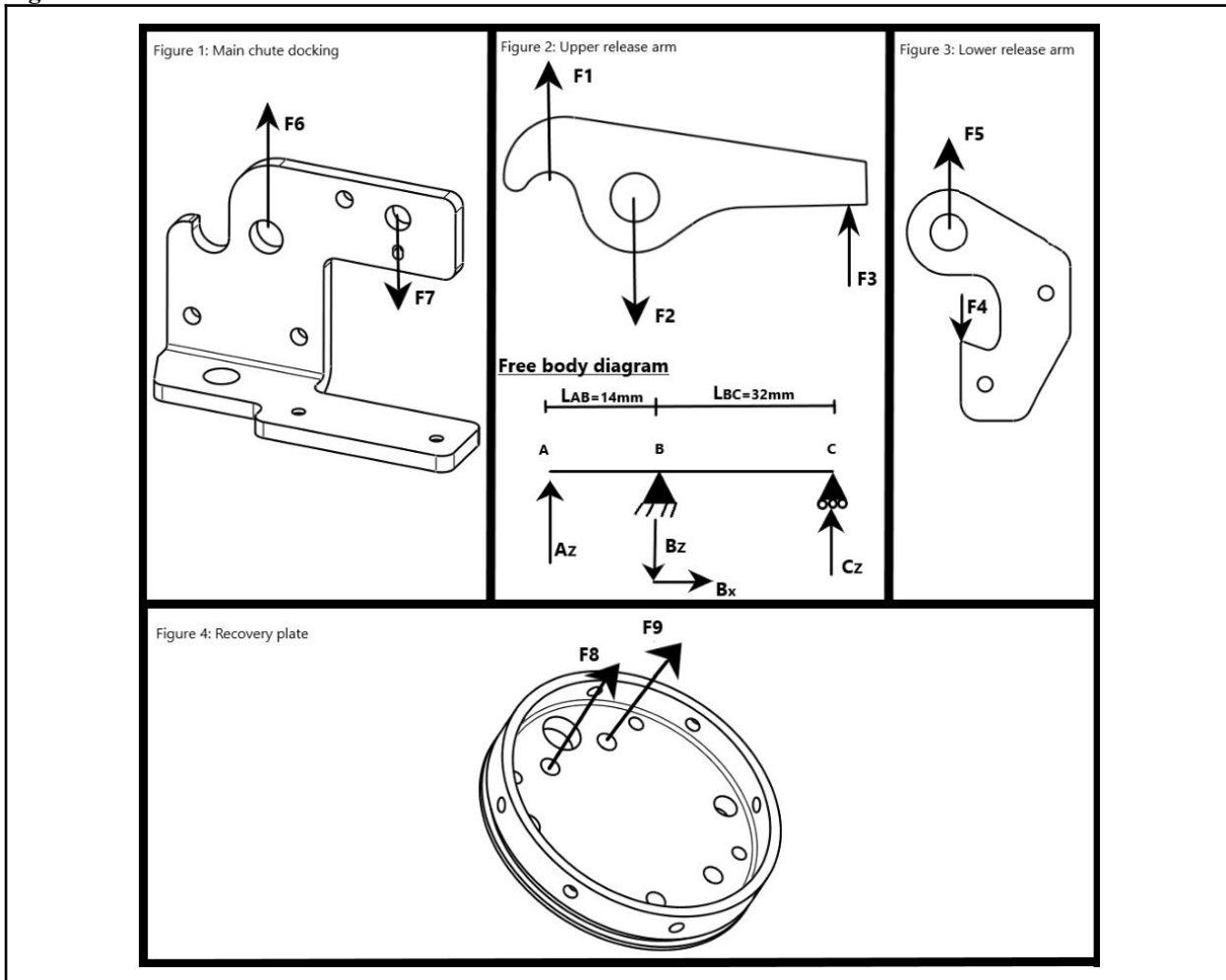
*separate simulation with $m = m_{FWD}$

Forces on MCRS and recovery plate

Problem statement:

The forces that act on the components in MCRS and the recovery plate are to be found.

Figure:



Assumptions and approximations:

Assuming that the system is in mechanical equilibrium.

Assuming the release forces from the drogue parachute and main parachute are evenly distributed between the aft and FWD based on their weight.

Physical laws:

Equilibrium equations:

$$\Sigma F_x = 0$$

$$\Sigma F_y = 0$$

$$\Sigma F_z = 0$$

$$\Sigma M = 0$$

$$F_1 = \frac{m_{FWD}}{m_{total}} \cdot F_{dc}, \text{ Force from drogue chute on FWD}$$

$$F_{mc,FWD} = \frac{m_{FWD}}{m_{total}} \cdot F_{mc}, \text{ Force from main chute on FWD}$$

Properties:

Given in *trajectory calculations*,

Parachute	Release force	Final descent rate
Drogue chute(F_{dc})	1290.57N	24.88 m/s
Main chute(F_{mc})	3551.77N	6.13m/s*

Object	Weight
m_{AFT}	10.18kg
m_{FWD}	13.61kg
m_{total}	23.79kg

Note that the properties used in this calculations are from an earlier *trajectory calculation*. Thats why these numbers are inconsistent with the numbers given in *trajectory calculations* above. We have chosen not to update the numbers here or conduct a new analysis since the calculation with the old numbers are more conservative, we calculate with a higher load.

Calculations:

$$F_1 = \frac{13.61 \text{ kg}}{23.79 \text{ kg}} \cdot 1290 \text{ N} \approx 738.3 \text{ N} \approx 738 \text{ N}$$

$$F_{mc,FWD} = \frac{13.61 \text{ kg}}{23.79 \text{ kg}} \cdot 3551.77 \text{ N} \approx 2032 \text{ N}$$

Forces on upper release arm:

Using $\Sigma M_c = 0$:

$$F_2 = B_z = \frac{F_1 \cdot (L_{AB} + L_{BC})}{L_{BC}} = \frac{738.3 \text{ N} \cdot (14 \text{ mm} + 32 \text{ mm})}{32 \text{ mm}} \simeq 1061.3 \text{ N}$$

Using $\Sigma F_z = 0$:

$$F_3 = C_z = B_z - F_1 = 1061.3 \text{ N} - 738.3 \text{ N} = 323.0 \text{ N}$$

Controlling the calculation using $\Sigma M_B = 0$

$$F_1 \cdot L_{AB} - C_z \cdot L_{BC} = 738.3 \text{ N} \cdot 14 \text{ mm} - 323.0 \text{ N} \cdot 32 \text{ mm} = 0.2 \text{ N} \text{ (rounding error)}$$

Forces on lower release arm:

Using $\Sigma F_z = 0$:

$$F_4 = F_5 = C_z \simeq 323 \text{ N}$$

Forces on the main chute docking:

$$F_6 = \frac{B_z}{2} = \frac{1061.3 \text{ N}}{2} \simeq 531 \text{ N}$$

$$F_7 = \frac{C_z}{2} = \frac{323.0 \text{ N}}{2} \simeq 162 \text{ N}$$

Forces on recovery plate:

$$F_{rec} = F_{mc,FWD} \simeq 2032 \text{ N}$$

$$F_8 = F_9 = \frac{F_{mc,FWD}}{2} = \frac{2032 \text{ N}}{2} = 1016 \text{ N}$$

Reasoning, discussion and verification:

The distribution seems reasonable

Final results:

$$F_1 = 738 \text{ N}$$

$$F_2 = 1061 \text{ N}$$

$$F_3 = 323 \text{ N}$$

$$F_4 = F_5 = 323 \text{ N}$$

$$F_6 = 531 \text{ N}$$

$$F_7 = 162 \text{ N}$$

$$F_8 = F_9 = 1016 \text{ N}$$

FEA on MCRS components and recovery plate

Problem statement:

The stress and displacement experienced by the following components are to be found:

- Upper release arm
- Lower release arm
- Main chute docking
- Recovery plate

Figure:

See *Forces on MCRS and recovery plate*

Assumptions and approximations:

Used solidworks FEA tool

Physical laws:

Used solidworks FEA tool

Properties:

Given in *Forces on MCRS and recovery plate*,

$$F_1 = 738 \text{ N}$$

$$F_2 = 1061 \text{ N}$$

$$F_3 = 323 \text{ N}$$

$$F_4 = F_5 = 323 \text{ N}$$

$$F_6 = 531 \text{ N}$$

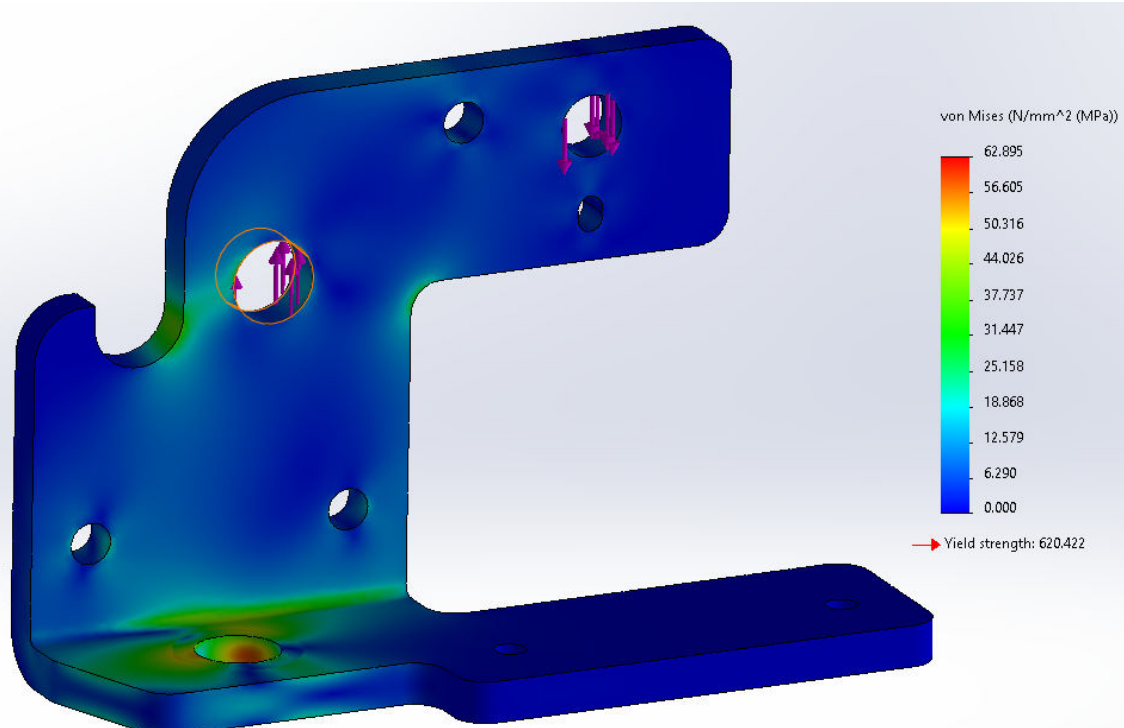
$$F_7 = 162 \text{ N}$$

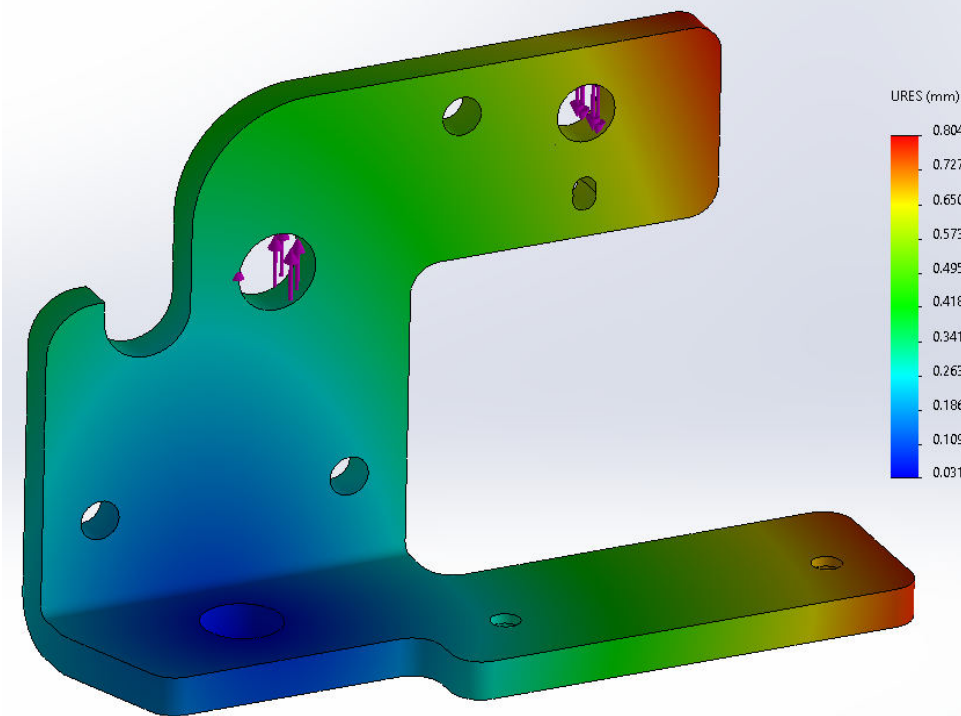
$$F_8 = F_9 = 1016 \text{ N}$$

Calculations:

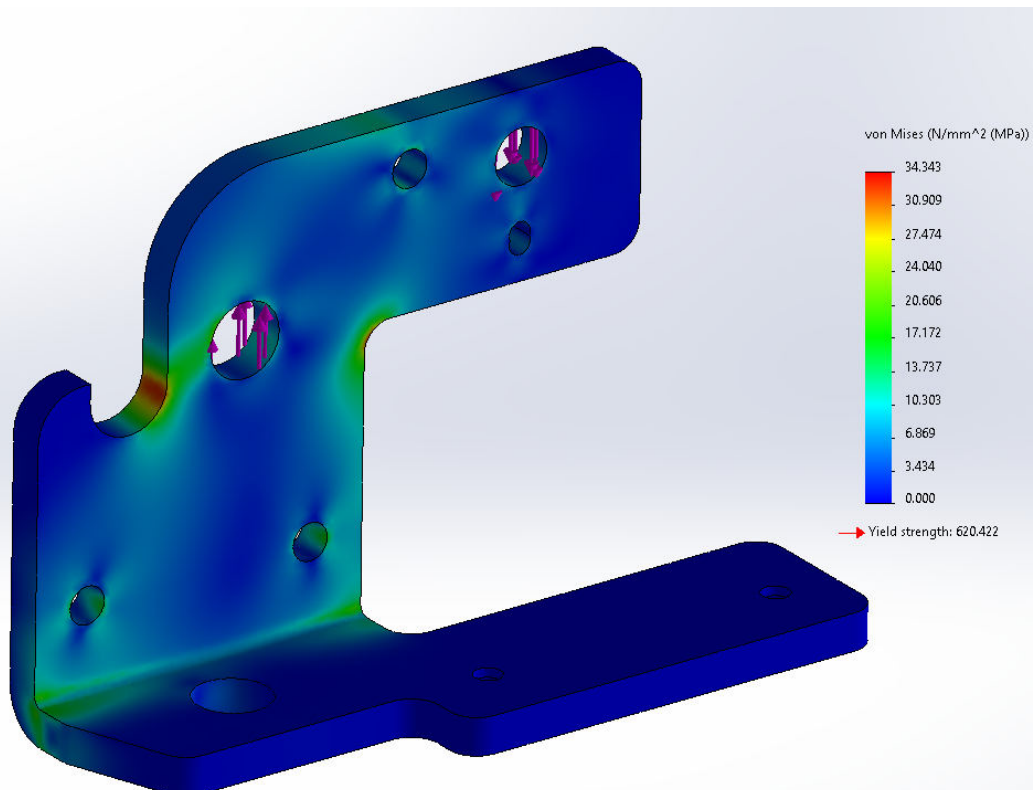
Stress and displacement **main chute docking:**

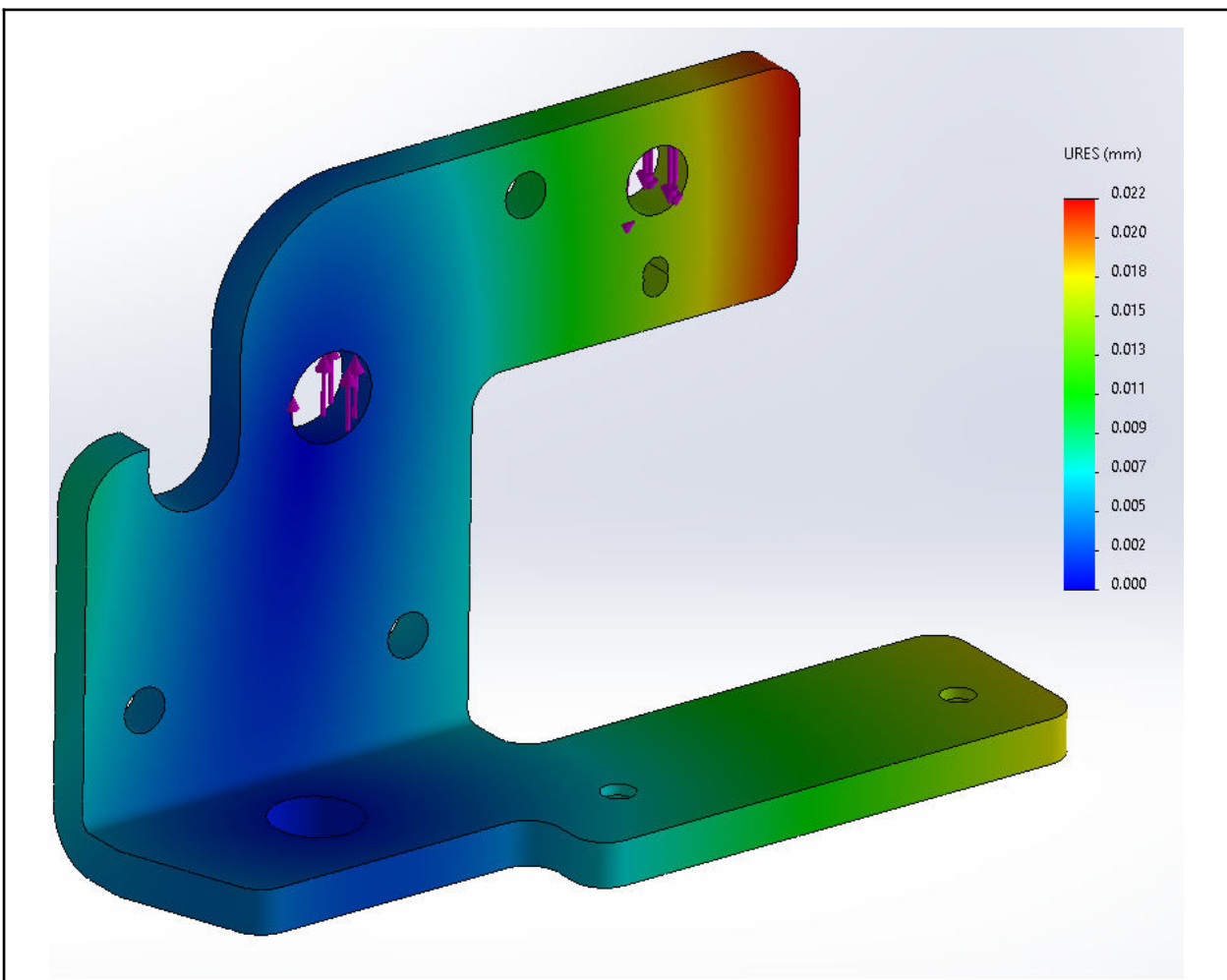
Without an elastic fixture at the bottom.



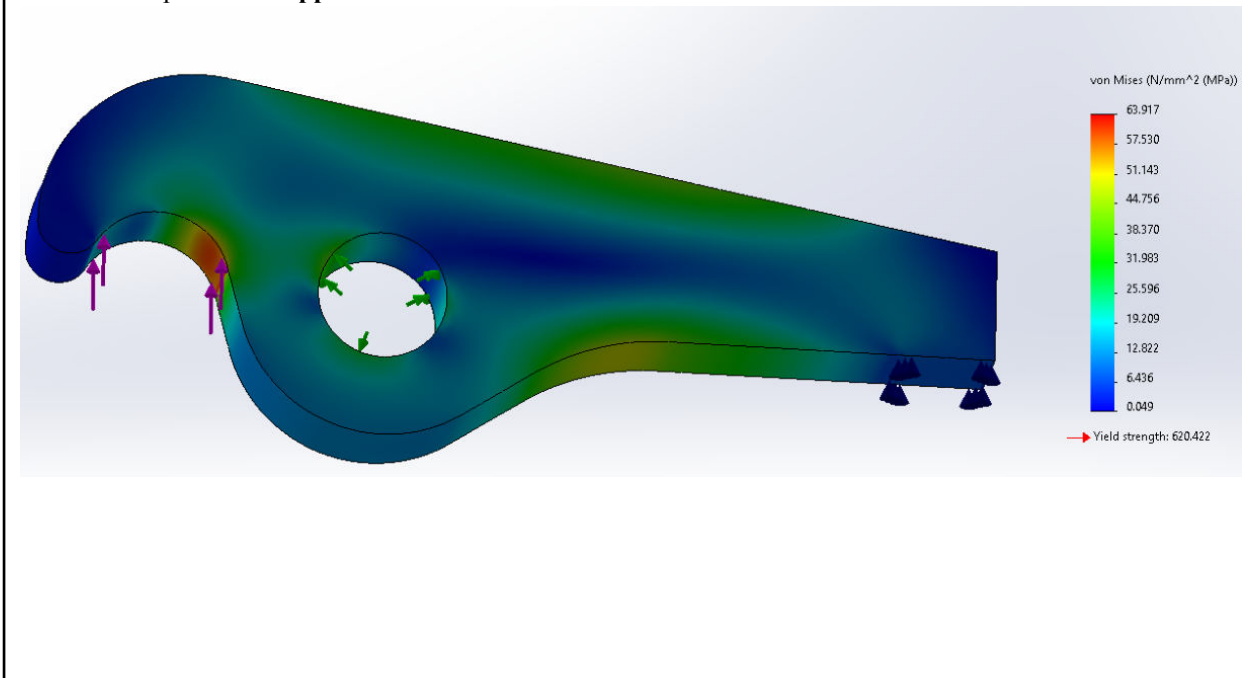


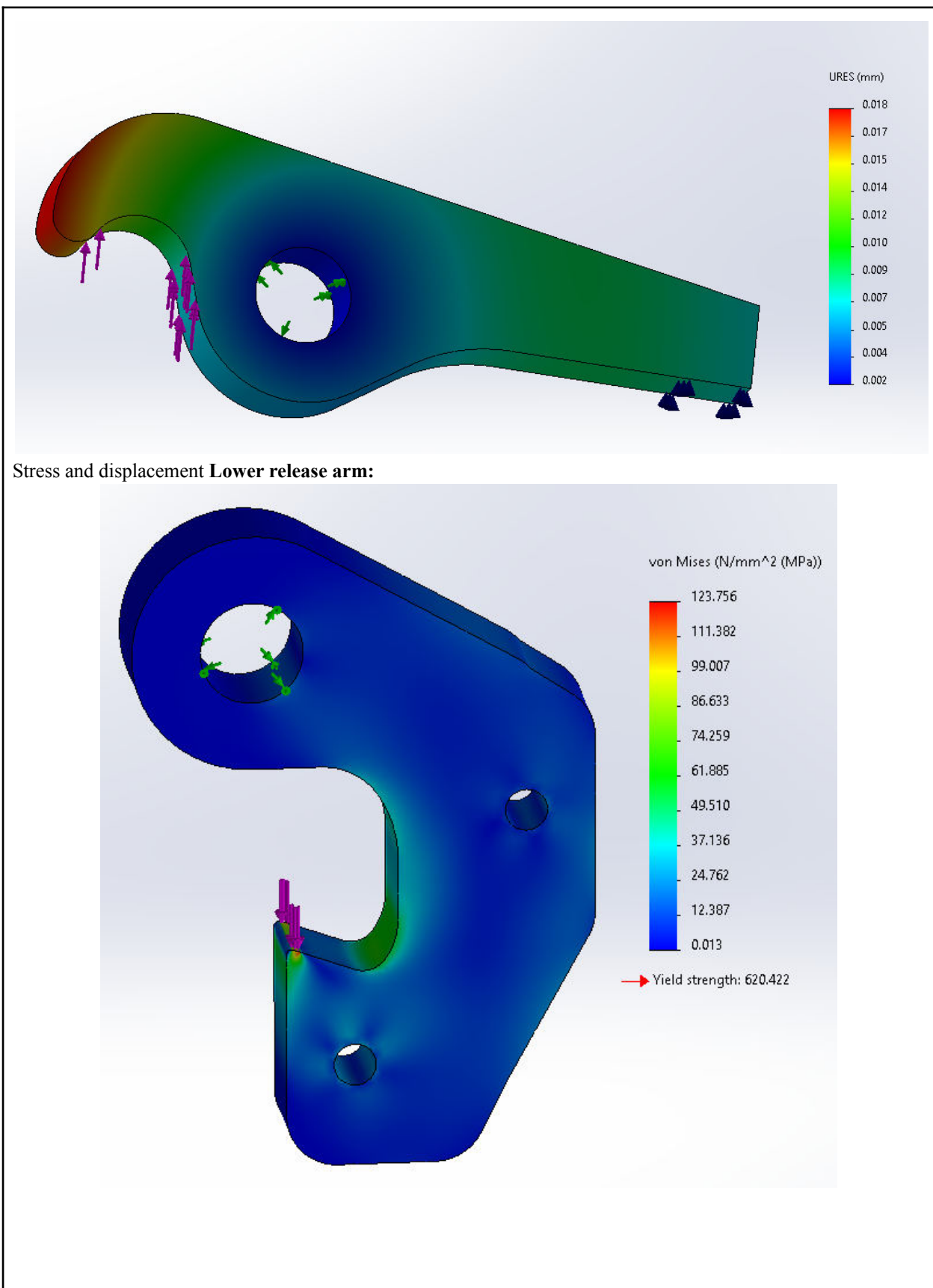
With elastic fixture at bottom

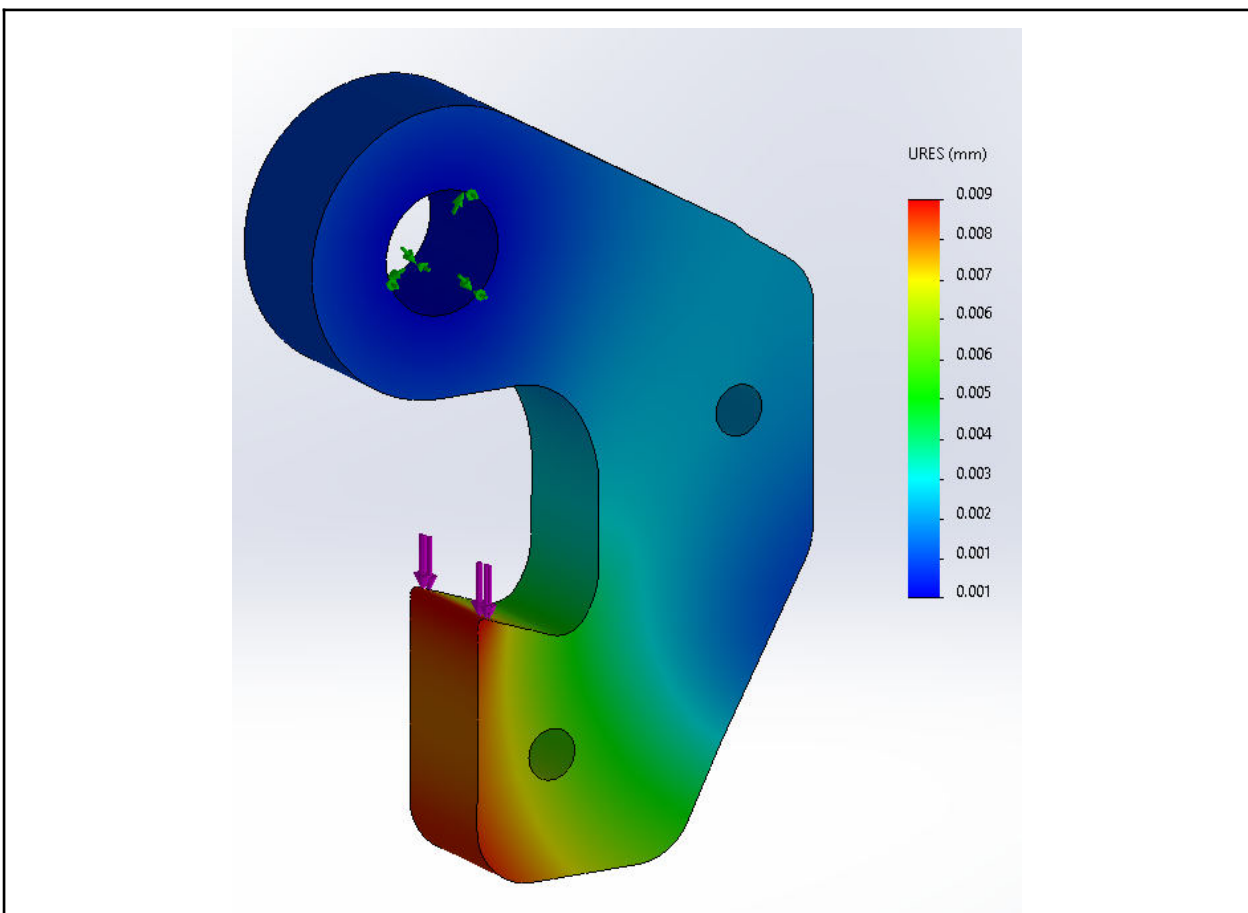




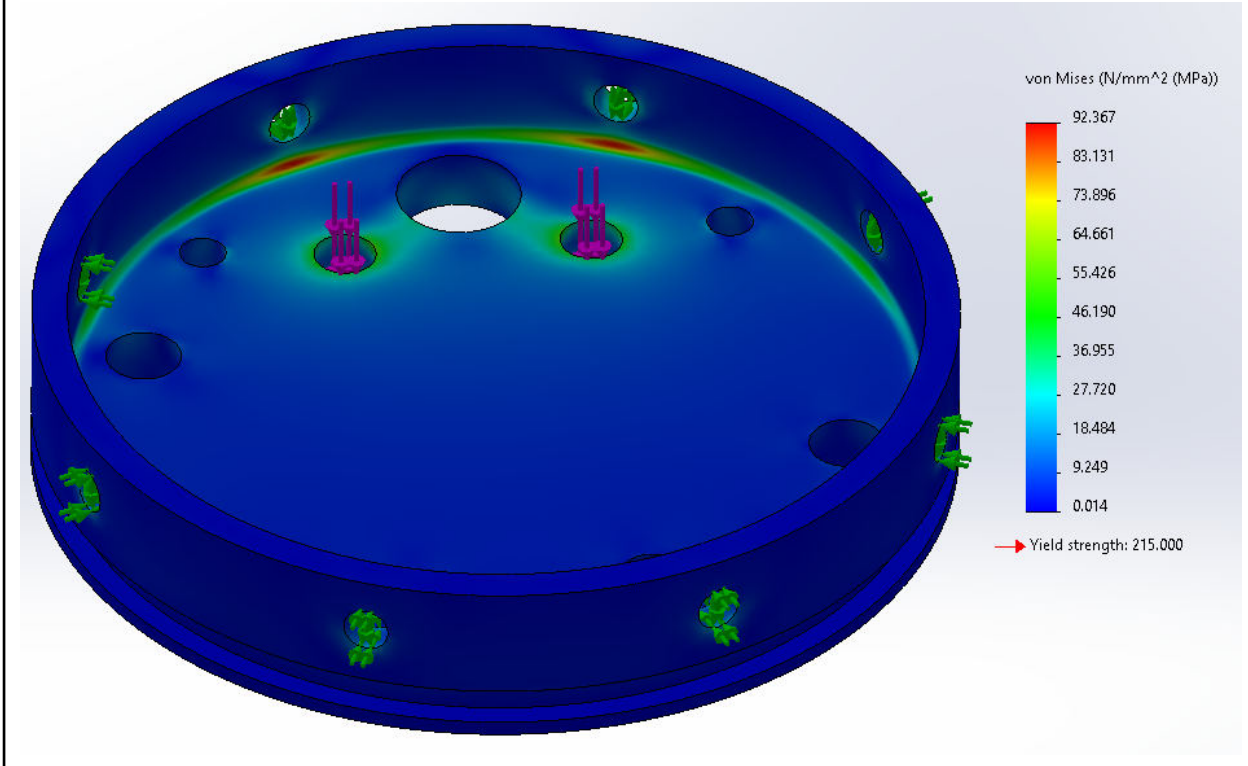
Stress and displacement **Upper release arm:**

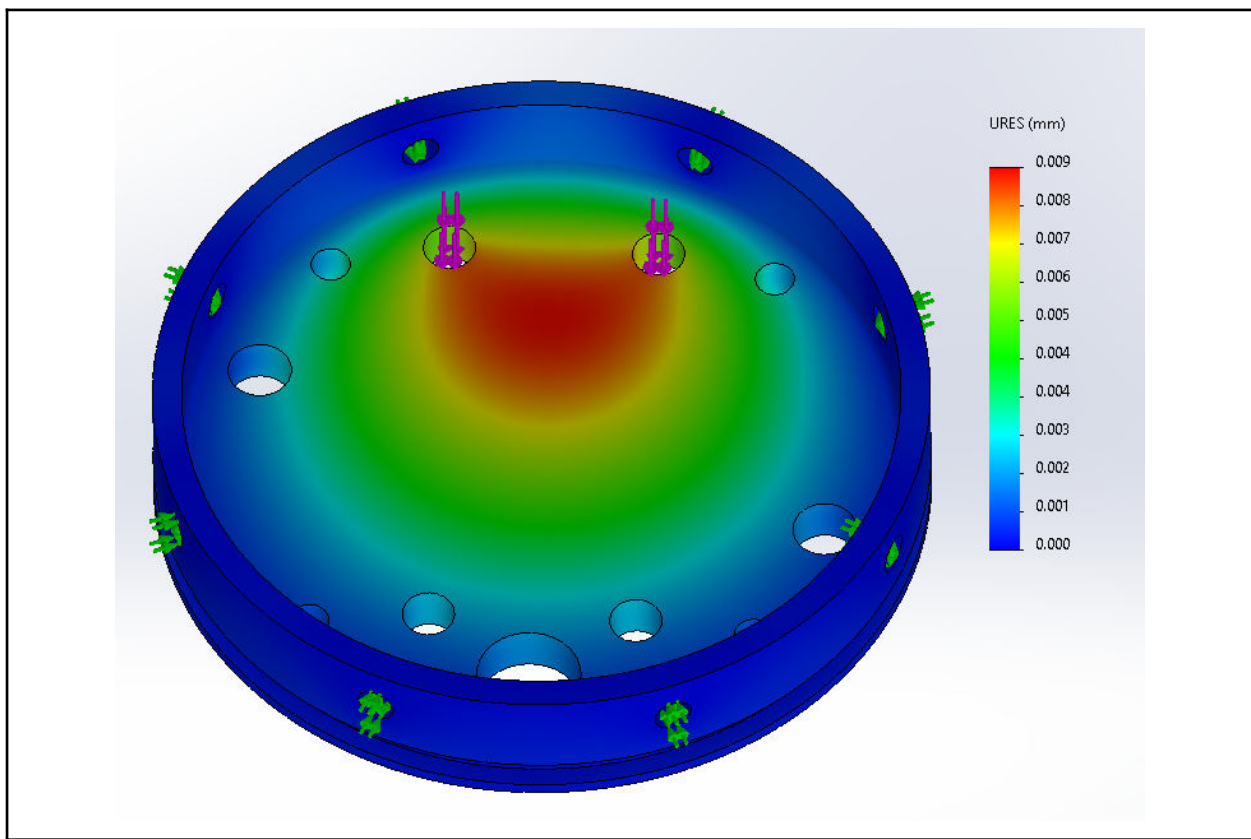






Stress and displacement Recovery plate:





Reasoning, discussion and verification:

The mesh is of high resolution, so the FEA captures stress concentrations.

Final results:

Part	Experienced stress[MPa]	Yield strength	FoS	Deformation[mm]
Main chute docking	62.8	650	10.3	0.804
Upper release arm	123	650	5.28	0.018
Lower release arm	124	650	5.25	0.009
Recovery plate	92.4	270	2.92	0.009

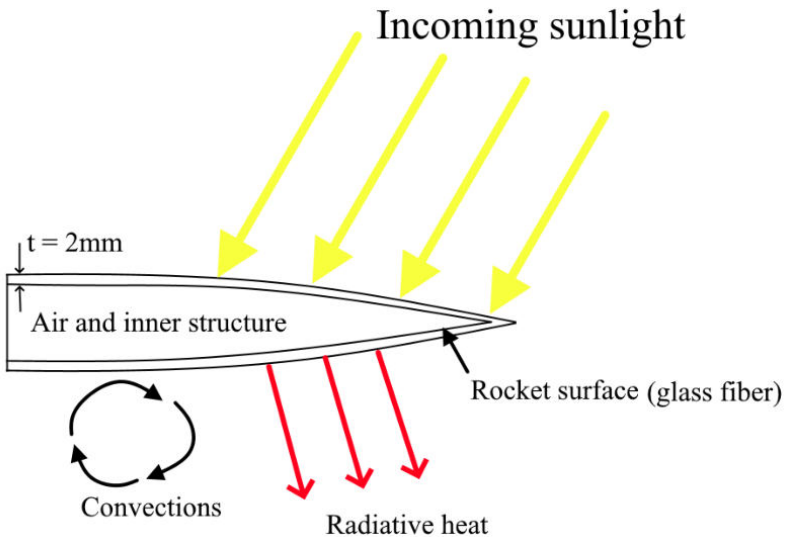
Other

Choosing color of forward airframe

Problem statement:

Want to see whether or not the forward airframe can be coated in black lacquer, or if it has to be painted white. Want to see how long it takes for the rocket, in direct sunlight, to reach its equilibrium temperature, and at what temperature it would reach equilibrium. A hard limit of 60 degrees celsius was set.

Figure:



Assumptions and approximations:

Assumed that:

- convections due to wind
- air is constantly removed by convection, so the air's temperature remains constant.
- incoming sunlight is normal to the surface so that all light is absorbed with the highest intensity.
- emissivity and solar absorptivity is constant.
- the air inside the rocket is heated uniformly.
- constant heat capacity
- 1D heat transfer through airframe

Physical laws:

Black body heating in an environment:

$$a * j_{net} = \epsilon\sigma(T^4 - T_{env}^4),$$

where a is the absorptivity, j_{net} is the net heat flow, ϵ is the emissivity in the infrared regime (long wavelengths), σ is the Stefan-Boltzmann constant and T and T_{env} is the temperature of the airframe and the temperature of the environment respectively.

Heat convection:

$$j_{conv} = hA(T - T_{avg}),$$

where h is the heat transfer coefficient, A is the surface area and T and

T_{env} is as stated above.

Heating of a material:

$$dQ = jdt$$

where dQ is heat, j is the heat transfer and dt is the time interval, which grows infinitesimally small.

Heat capacity (isobaric):

$$c = \left(\frac{dq}{dT}\right)_p,$$

where c is the heat capacity and $\left(\frac{dq}{dT}\right)_p$ is the change in heat for a change in temperature at a constant pressure.

Heat equation 1D:

$$j = -\kappa A \frac{dT}{dz},$$

where j is the heat transfer, κ is the thermal conductivity, A is the surface area and $\frac{dT}{dz}$ is the change in temperature with depth z into the material.

Properties:

The values below have meticulously been chosen to yield the worst case scenarios.

Environmental parameters/properties:

Parameter	Value
T_0	36 C°
T_{env}	36 C°
j_{sun}	640 W/m ² *
c_{air}	1.0035 J/g.K [44]

*47% of solar constant = 1367W/m² [43]

Paint properties [45]:

Name	Absorptivity	Emissivity
Black	0.95	0.75
White	0.25	0.89

Glass Fibre properties [46]:

Property	Value
Density ρ	2460 kg/m ³
Thermal conductivity κ	1.35 W/m.K
Specific heat c	735 J/kg.K

Constants:

Constant	Value
σ	$5.67 \times 10^{-8} \text{ W/m}^2 \text{ K}^4$
h	10 W/m^2 [47][48]

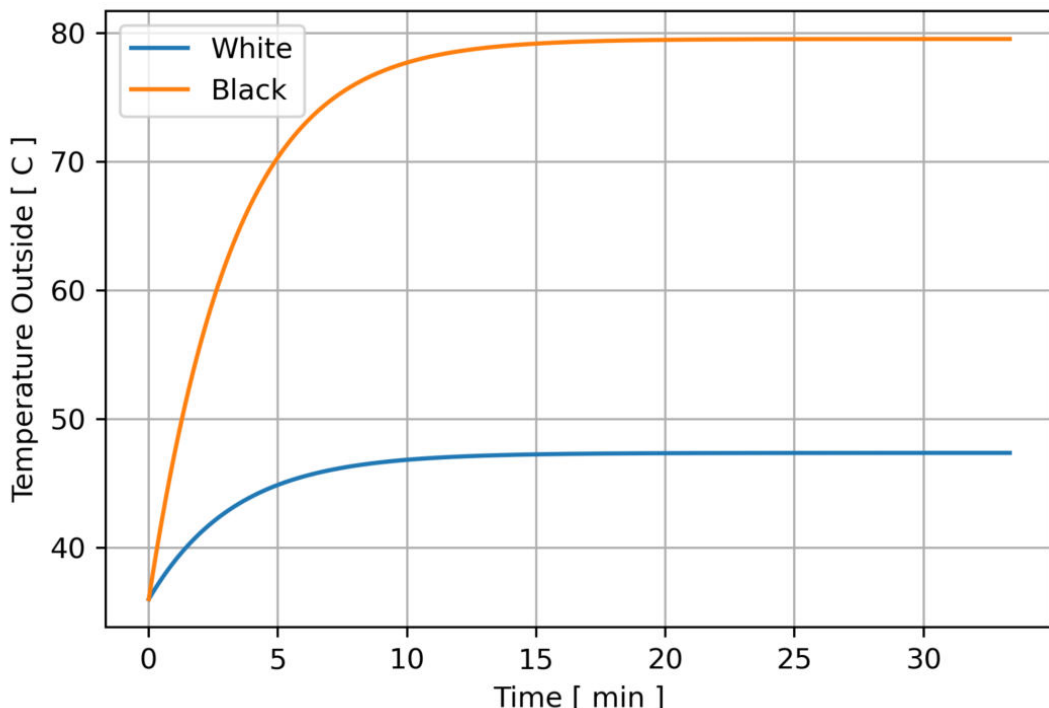
Rocket dimensions:

Dimension	Value
A	0.777 m^2
z	0.002 m

Calculations:**Rearring the equations above yields:**

$$\frac{dT}{dt} = \frac{1}{c} (aj_{\text{sun}} - hAT + hAT_{\text{env}} - \epsilon\sigma T^4 + \epsilon\sigma T_{\text{env}}^4).$$

This is a differential equation, which is solved using python with the `scipy.integrate.solve_ivp` method. Using (`rtol = 1e-13, atol = 1e-16`) over a long period of time with the properties above the following plot were obtained:



To see how long it takes to heat the air inside from the outside, the heat equation can be written as:

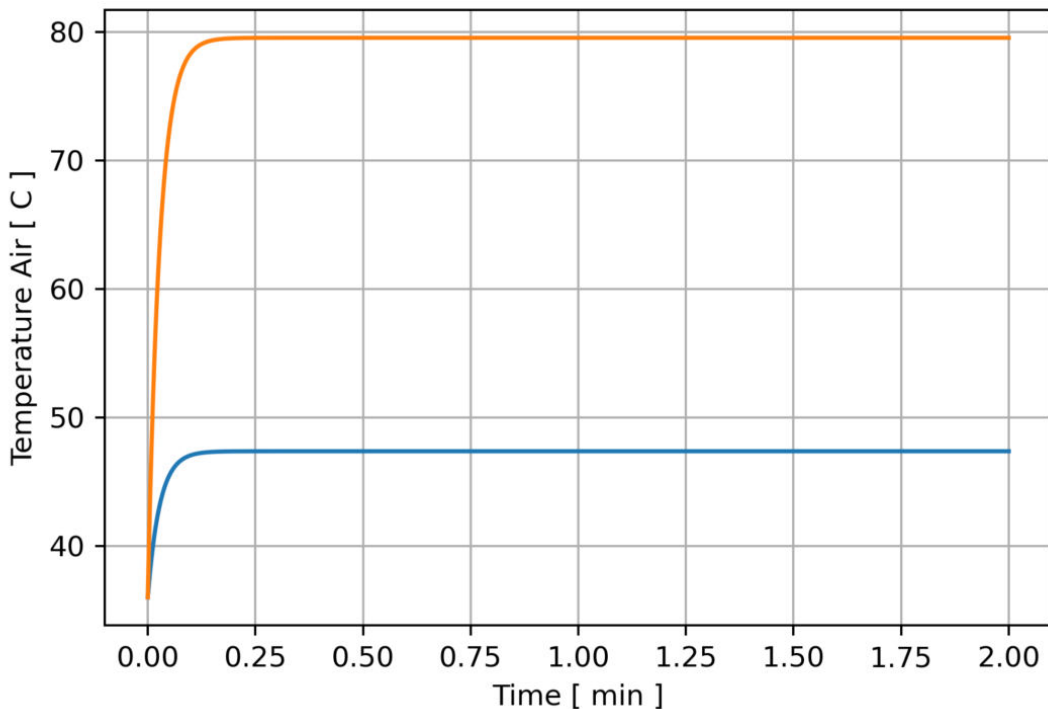
$$\frac{dT_{\text{air}}}{dt} = \frac{T_{\text{out}} - T_{\text{air}}}{zC_{\text{air}}} \kappa A,$$

where T_{air} is the temperature inside the rocket and T_{out} is the temperature of the surface area of the fuselage.

This differential equation can be solved, and yields:

$$T_{air} = T_{out} + c * \exp\left(-\frac{\kappa A}{cz} t\right),$$

Here T_{out} is assumed constant. From the initial value $T_{air}(0) = T_{env}$ which implies $c = T_{air}(0) - T_{out}$. Plotting the solution gives the following plot:



The calculations above yields the following equilibrium temperatures:

White: 47.4 °C

Black: 79.6 °C

Reasoning, discussion and verification:

Seeing as the absorbtivity is lower for the white lacquer than its emissivity, it makes sense that the white lacquer yields a lower equilibrium temperature than black lacquer. Which has absorbtivity almost close to its emissivity. It seems to take around 15 minutes for both colors to reach its equilibrium temperature at the outside. From the second plot it seems to be a tiny delay of 0.10 s between the temperature of the paint and the air inside. These numbers seem intuitive, as it is not too hot as to boil water in 1 atm.

Final results:

Since the black lacquer reaches an equilibrium temperature of 79.6 °C, which is larger than the limit of 60 °C. The black lacquer can not be used, and the forward airframe has to be coated in white lacquer, which reaches an equilibrium temperature of 47.4 °C in around 15 minutes.

Mandrel integrity

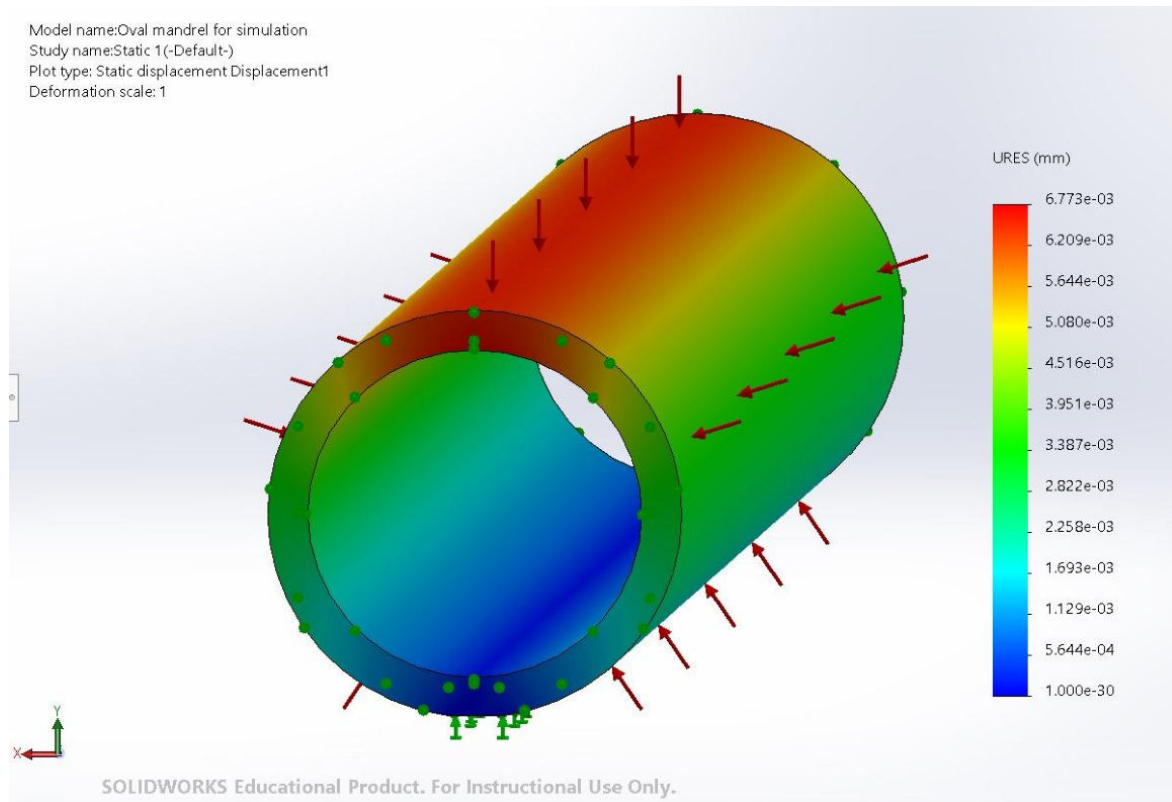
Problem statement:

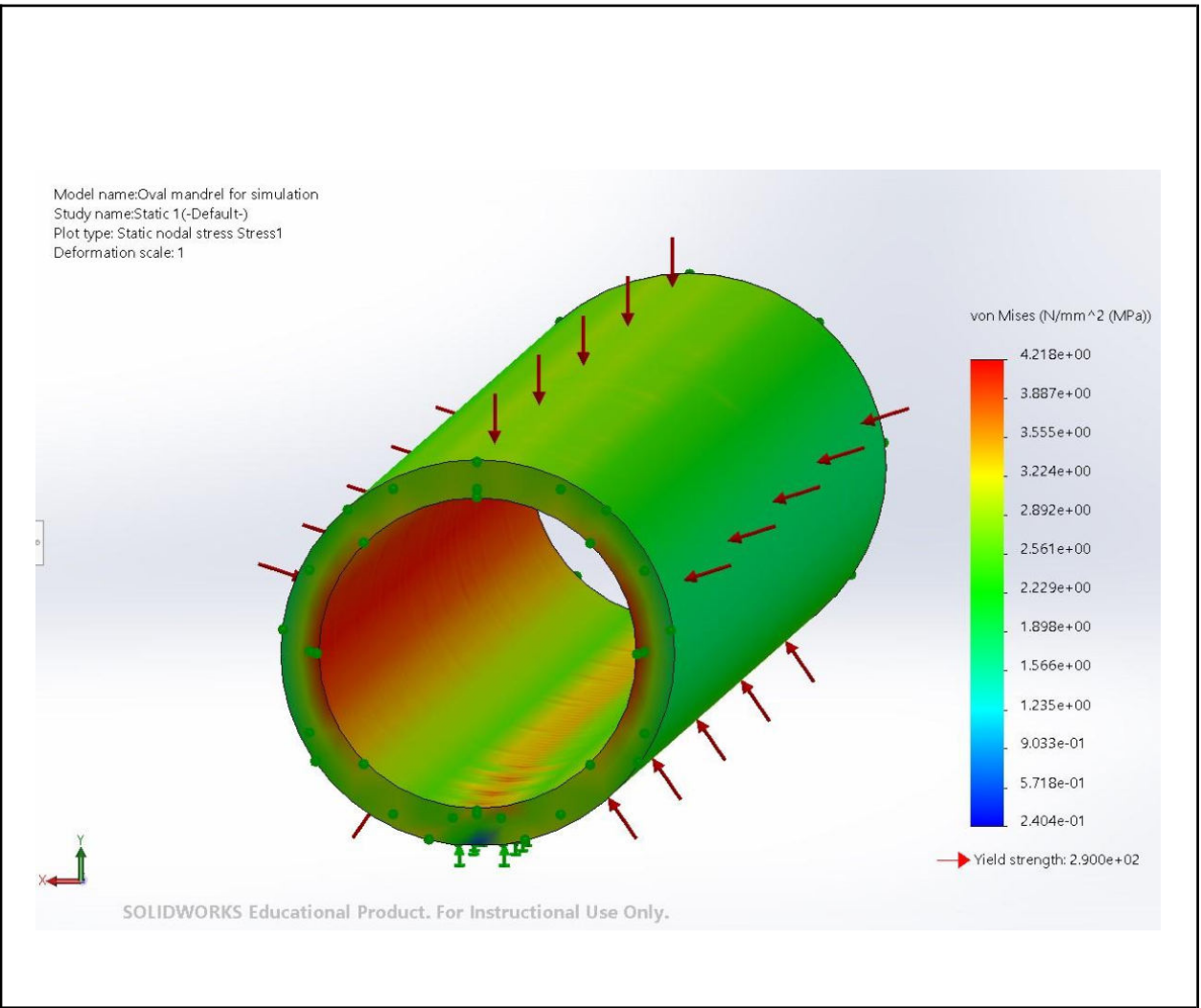
A secondary plan for the airframe is to produce it using an autoclave. The requirement for the mandrel was to be able to withstand 7 bar of external pressure. A FEA analysis was done in order to verify the mandrel's integrity. The goal of the analysis is to determine if the chosen thickness for the tube is adequate.

Assumptions and approximations:

A FEA was done to check stress and displacement. To simulate a non optimal case, a slight ovality of 2mm was added to the mandrel. The thickness of the tube is 12mm. The tube is fixed on a small surface at its bottom, as this was considered a simple way to constrain the mandrel.

Calculations:





Reasoning, discussion and verification:

The max displacement in the mandrel is less than a hundredth of a millimeter. The maximum stress is around 4 MPa, which is far below the yield strength of any aluminium alloy.

Final results:

A thickness of 12mm is adequate. A requirement will be set for the manufacturer not to use a tube with a smaller diameter than 12mm.

J. Production methods

PRODUCTION METHODS

Outer structure

Production Airframe

Mandrel

The material of choice for the mandrel is aluminium, due to its machinability, and potential for tight tolerances. The mandrel nose cone is machined out of a single bolt of aluminium, and follows the von karman shape offset 2 millimetres inwards. The fibers bunch up towards the tip of the nose, but they do so evenly and the resulting shape is close enough to the von karman shape to be aerodynamic. The forward and aft airframes are wound around the same mandrel, but are cut off the mandrel at different points. In order for the airframe parts to be cut off without damaging the mandrel, there are four o-ring grooves placed along the mandrel to allow the cutting tool through. These are filled with square o-rings which fills out the missing space. The mandrel can be seen in Figure 1.

If filament winding were not available as a production method, the mandrel can also be used with prepreg or wet layup. With these production techniques, the mandrel needs to be able to withstand 7 bars of external pressure. Refer to Appendix V.I - Mandrel Integrity for an FEM analysis of the stresses and displacements in the mandrel under these conditions.

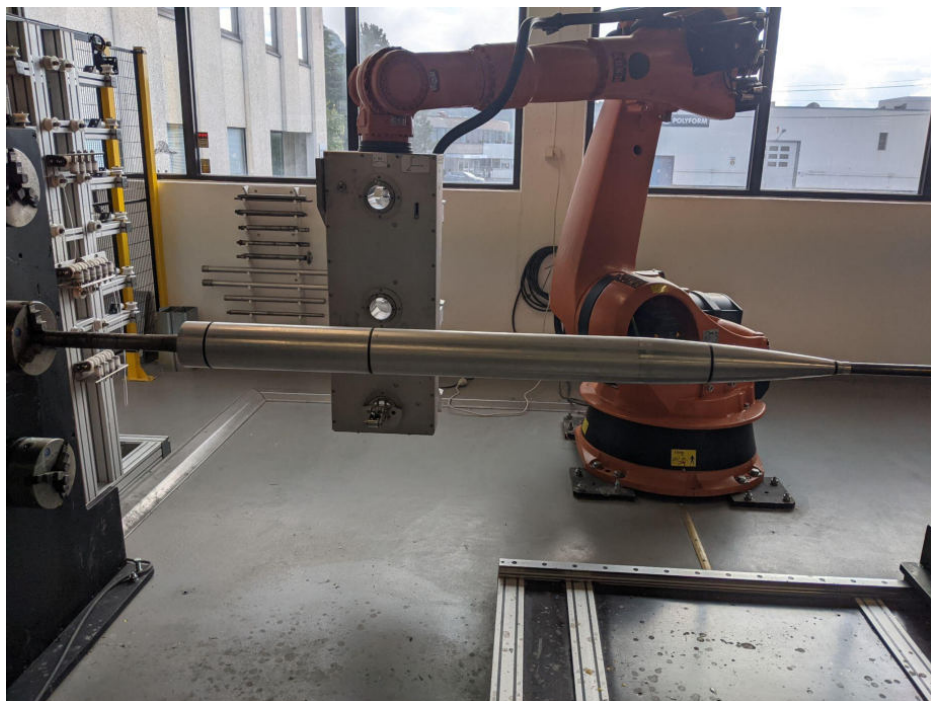


Figure 1. The mandrel in the winding robot at WindTec in Ålesund.

Filament winding

The airframe will be produced using filament winding.

Due to the requirement for RF-transparency [S4.3.1 Appendix V.H] the forward airframe is made out of glass fibre. The aft airframe is made out of carbon fibre due to its high strength to weight ratio as well as high stiffness. The glass fiber of choice is 758 Zentron, and the epoxy system is UF3369 TCR resin. The carbon fiber of choice is the Toray T700S, with the same epoxy system. These were chosen due to their availability at the winding company. More detailed information can be found in the datasheet linked to in Appendix V.K.

Before winding, the mandrel is polished and the o-rings inserted. A release agent is then applied to the mandrel, and pre-impregnated fiber is wound around the mandrel. After winding a strip of Peel-Ply is wound on top of the fiber. The part is then cured. After curing the airframe parts are cut to the right length and sanded. Holes are then drilled. The forward airframe is coated in a temperature resistant lacquer due to the high temperature mentioned in Section II.D.2.Computational Fluid Dynamics, that exceeds the glass transition temperature to the glass fiber. The aft airframe is coated in a clear lacquer. Lastly the logos and design are applied in the form of stickers. Figure 2 shows some of these steps.



Figure 2. Upper left: Winding in progress. Upper right: Sanding forward airframe. Lower left: Hole drilling. Lower right: Finished airframe prior to coating.

Surface finish and tolerance

The airframe will be glued and bolted to the upper and lower couplers. In order for the chosen glue [52] to adhere well, the diametrical clearance needs to be small. The winding process has a tolerance of (+0.2,-0). From figure 3 it is seen how a 124+-0.05 tolerance on the mandrel and a 124+-0.1 tolerance on the coupler will satisfy these criteria, given that an interference fit of 0.2mm diametrical overlap is accepted. The maximum possible diametrical clearance is 0.3mm, which is considered adequate. These tolerances were chosen because they were the tightest tolerances achievable at a reasonable price.

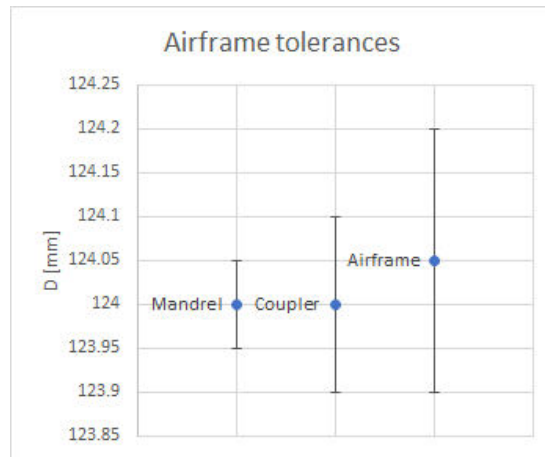


Figure 3. The cumulative tolerances for the airframe. Coupler and mandrel tolerances are also shown.

A good surface finish for the airframe is needed for good aerodynamic properties. The winding process leaves small pores in the intersections between fibers. Due to this a thorough sanding of the airframe prior to lacquer was agreed upon with the manufacturer. Whether this has a measurable effect on performance is unclear, but the sanded surface will leave a more professional look. The thickness of the stickers were also brought up as a concern, but the aerodynamic effect was judged to be negligible.

Layup selection

With winding we have the opportunity of choosing fiber layup directions between 88 and 5 degrees. One pass adds ~0.25mm of thickness. For every pass in one direction, there needs to be a pass in the opposite direction in the inverse layup direction. For an airframe thickness of 2mm, this allows us to choose 4 pairs of layup directions.

Our understanding of the most important general rules of thumb regarding fiber layups derived from “Structural Materials Handbook” [13] are the following:

- Around holes in the airframe there should be at least 50% +45.
- The fibers of adjacent layers should deviate as little as possible from the layer underneath.
- Break as few fibers as possible when making holes in the layup.
- The number of fiber directions should generally be at least 3.

The ESA handbook of composites is mainly concerned with unidirectional fiber layups, which is exactly what you get when winding.

In addition to these rules of thumb, certain manufacturing considerations need to be made. The winding machine has a limit for its lowest winding angle, being between 5 and 10 degrees. Because the layers have to be able to cover the entire surface as efficiently as possible with the available fiber width, the first layer was set to 10 degrees.

Based on these rules of thumb, and the manufacturing considerations, the chosen fiber layup is [-10/+10/+45/-45/-85/+85/+45/-45].

Ideally, we would like to run a FEM-analysis and a frequency analysis in ANSYS, where the anisotropy of the airframe is taken into account. This would allow us to better understand if the strength and stiffness of the airframe is adequate. This has proved too time consuming for this year's project, but will be pursued in the future.

Avionics

Production PCBs

The printed circuit boards (PCBs) were manufactured by our sponsor Ncab. A majority of the electrical components are surface mount devices (SMD). Therefore, a soldering oven was used, as this is both time efficient and often easier than doing it by hand with a soldering iron. Luckily, all major SMDs could handle the heat of the solder oven (around 240 C) and only through hole components, such as connectors were soldered on by hand. The soldering was verified under a microscope and fixed if needed before any verification tests occurred.

K. Component overview

Component overview

Mechanical components							
Reference	System	Sub-assembly	Name	Qty.	Mass [kg]	Material	Further information
IN.UP	Inner structure	Nose tip	Upper Nosetip	1	0.13	Aluminium 7075 T9	Appendix V.F - Dwg 1.1
IN.MP	Inner structure	Nose tip	Middle Nosetip	1	0.010	Aluminium 7075 T9	Appendix V.F - Dwg 1.2
IN.LP	Inner structure	Nose tip	Lower Nosetip	1	0.054	Aluminium 7075 T6	Appendix V.F - Dwg 1.3
IU.UTR	Inner structure	Upper threaded rod	Upper threaded rod	1	0.11	El.plated steel	
IU.UDB	Inner structure	Upper threaded rod	Upper disk bulkhead	1	0.018	Fiberglass	
IU.BH	Inner structure	Upper threaded rod	Battery holder	1	0.26	Plastic	
Altimax battery mount	Inner structure	Upper threaded rod	Lower disk bulkhead	1	0.030	Fiberglass	
IA.ABP	Inner structure	Avionics mount	Altimax battery plate	1	0.012	Fiberglass	
IA.BBP	Inner structure	Avionics mount	Black box plate	1	0.014	Fiberglass	
IA.BB	Inner structure	Avionics mount	Black box	1	0.065	Steel + epoxy	
IA.BBB	Inner structure	Avionics mount	Black box bracket	1	---	PLA	
IA.ABH	Inner structure	Avionics mount	Altimax battery housing	1	0.023	PLA	
IA.MP	Inner structure	Avionics mount	Middle plate	1	0.012	Fiberglass	

Mechanical components							
Reference	System	Sub-assembly	Name	Qty.	Mass [kg]	Material	Further information
IA.SPP	Inner structure	Avionics mount	Sensorboard + PSU plate	1	0.046	Fiberglass	
IA.RP	Inner structure	Avionics mount	Radionor plate	1	0.048	Fiberglass	
IA.GBH	Inner structure	Avionics mount	COTS GPS battery housing	1	0.0090	PLA	
IA.AGP	Inner structure	Avionics mount	Altimax + COTS GPS plate	1	0.029	Fiberglass	
IA.VEH	Inner structure	Avionics mount	Video encoder housing	1	0.045	PLA	
IA.VEP	Inner structure	Avionics mount	Video encoder plate	1	0.029	Fiberglass	
IA.LP	Inner structure	Avionics mount	Lower plate	1	0.0076	Fiberglass	
IP.B	Inner structure	Payload	Bulkhead	2	0.11	Aluminium 6082-T6	Appendix V.F - Dwg 2.2
IP.BR	Inner structure	Payload	Bulkhead ring	2	0.027	Aluminium 6082-T6	Appendix V.F - Dwg 2.1
IL.LTR	Inner structure	Lower threaded rods	Lower threaded rod	4	0.50	El. plated steel	Appendix V.I - Lower threaded rods analysis
IL.CM	Inner structure	Lower threaded rods	Camera mount	2	0.011	Aluminium	
IL.CP	Inner structure	Lower threaded rods	Camera plate	2	0.019	Aluminium	Appendix V.F - Dwg 3.2
IC.UC	Inner structure	Couplers	Upper coupler	1	1.0	Aluminium 6082-T6	Appendix V.F - Dwg 6.1 Appendix V.I - Upper and lower coupler analysis
IC.LC	Inner structure	Couplers	Lower coupler	1	0.80	Aluminium 6082-T6	Scotch-Weld DPX Adhesive DP490 [52] Appendix V.F - Dwg 6.2 Appendix V.I - Upper and lower coupler analysis

Mechanical components							
Reference	System	Sub-assembly	Name	Qty.	Mass [kg]	Material	Further information
IC.MM	Inner structure	Couplers	Motor mount	1	0.22	Aluminium 6082-T6	Appendix V.F - Dwg 6.3 Appendix V.I - Motor mount analysis
IAE.MCR	Inner structure	Aft end	Motor centering ring	1	0.046	Aluminium 6082-T6	Appendix V.F - Dwg 7
IAE.B	Inner Structure	Aft end	Boat tail	1	0.14	Aluminium 6082-T6	Appendix V.F - Dwg 9.3
IAE.BCR	Inner structure	Aft end	Boat tail centering ring	1	0.061	Aluminium 6082-T6	Appendix V.F - Dwg 9.2
IAE.BW	Inner structure	Aft end	Boat tail centering ring wedge	1	0.049	Aluminium 6082-T6	Appendix V.F - Dwg 9.1
IAE.M	Inner structure	Aft end	Cesaroni pro 98 6GXL	1	16.8	---	Refer to Cesaroni website.
OP.M	Outer structure	Production	Mandrel	1	---	Aluminium	Appendix V.F - Mandrel Assembly Appendix V.J. Production methods
	Outer structure	Upper half	Forward airframe	1	1.6	Fibreglass	Appendix V.I Choosing color of forward airframe Appendix V.J Production methods Appendix V.G Computational Fluid Dynamics 758 ZenTron datasheet [49]. UF3369 TCR Resin System. [50].
OU.AA	Outer structure	Upper half	Aft airframe	1	1.6	Carbon fibre	Appendix V.J Production methods Appendix V.G Computational Fluid Dynamics Toray T700S datasheet [51].
OL.FB	Outer structure	Lower half	Fin bracket	4	0.059	Aluminium	D. Outer structure - Fin Brackets Scotch-Weld DPX Adhesive DP490 [52] Appendix V.E - Dwg 8
OL.F	Outer structure	Lower half	Trapezoidal fin	4	0.15	Carbon fibre	Appendix V.I - Flutter boundary condition Appendix V.G. Computational Fluid Dynamics

RH.HP	Recovery	Hawk system	Hawk plate	2	0.064	Aluminum	Appendix V.F - Dwg 3.1
Mechanical components							
Reference	System	Sub-assembly	Name	Qty.	Mass [kg]	Material	Further information
RH.HSM	Recovery	Hawk system	Hawk servo motor	2	0.026	---	
RH.CS	Recovery	Hawk system	Compression spring	2	---	---	
RH.P	Recovery	Hawk system	Piston	2	---	---	
RH.F	Recovery	Hawk system	Fitting	2	0.024	Brass	
RH.GH	Recovery	Hawk system	Gas hose	2	0.81	---	
RH.ES	Recovery	Hawk system	Extension spring	2	---	---	
RH.RA	Recovery	Hawk system	Release arm	2	---	---	
RH.CO2	Recovery	Hawk system	CO ₂ -canister	2	0.41	---	
RH.HSP	Recovery	Hawk system	Hawk safety pin	2	0.0010	---	
RR.RP	Recovery	Recovery plate	Recovery plate	1	0.40	Aluminium 6082-T6	Appendix V.F - Dwg 4 Appendix V.I - Forces on MCRS and recovery plate Appendix VI- FEA on MCRS components and recovery plate
RR.CG	Recovery	Recovery plate	Cable gland	1	0.020	---	
RR.CM	Recovery	Recovery plate	Camera mount	1	0.02	Aluminium	
RM.MCRD	Recovery	MCRS	Main Chute release docking	2	0.22	Steel S650MC	Appendix V.F - Dwg 5 Appendix V.I - Forces on MCRS and recovery plate Appendix VI- FEA on MCRS components and recovery plate
RM.URA	Recovery	MCRS	Upper release arm	1	0.032	Steel S650MC	Appendix V.I - Forces on MCRS and recovery plate Appendix VI- FEA on MCRS components and recovery plate

	RM.LRA	Recovery	MCRS	Lower release arm	1	0.025	Steel S650MC	Appendix V.I - Forces on MCRS and recovery plate Appendix V.I- FEA on MCRS components and recovery plate
Mechanical components								
Reference	System	Sub-assembly	Name	Qty.	Mass [kg]	Material	Further information	
RM.SM	Recovery	MCRS	Servo mount	2	0.026			
RM.SMO	Recovery	MCRS	Servo motor	2	0.026			
RM.SPC	Recovery	MCRS	Spacers	3	0.0026			
RM.SE	Recovery	MCRS	Surface extender	1		PLA		
268	RM.SSA	Recovery	MCRS	Short spring attachment	2	Steel		
				Long spring attachment				
				Extension spring				
RC.MC	Recovery	Chutes	Main chute	1	0.46	Kevlar	Appendix V.I - Chute calculations Appendix V.I- FEA on MCRS components and recovery plate	
RC.DC	Recovery	Chutes	Drogue chute	1	0.088	Rip-stop, nylon shroud lines	Appendix V.I - Chute calculations Appendix V.I- FEA on MCRS components and recovery plate	
RC.UB	Recovery	Chutes	U bolt	1	0.071	Stainless steel		
RC.EB	Recovery	Chutes	Eye bolt	1	0.075	Stainless steel		
RC.DB	Recovery	Chutes	Deployment bag	1	0.071	Nylon		
RC.SWL	Recovery	Chutes	Swivel links	2	0.10	Stainless steel		
RC.QL	Recovery	Chutes	Quick links	2	0.14	Stainless steel		
RC.SCY	Recovery	Chutes	Shock cord Y	1	0.12	Kevlar		

RC.SCS	Recovery	Chutes	Shock cord straight	1	0.12	Kevler	
ORBIT	Orbit	Payload	Payload	1	4.0	---	
Mechanical components							
Reference	System	Sub-assembly	Name	Qty.	Mass [kg]	Material	Further information
RC.SOR	Recovery	Recovery plate	Static o-ring	1	-	EPDM	Appendix VI - O-ring calculations
RC.DOR	Recovery	Recovery plate	Dynamic o-ring	1	-	EPDM	Appendix VI - O-ring calculations

269

Fasteners								
Reference	Type	Interface				Dimensions	Qty	Material
F.1	Socket head	Radionor antenna (A.RC) Radionor plate (IA.RP)				M2.5x15	9	Steel
F.2	Socket head	Sensorboard + PSU (A.SB) Sensorboard + PSU plate (IA.SPP)				M4x14	4	Steel
F.3	Socket head	Video encoder housing (IA.VEH) Video encoder plate (IA.VEP)				M3x14	2	Steel
F.4	Socket head	COTS GPS (A.S5) Altimax + COTS GPS plate (IA.AGP)				M3x20	2	Steel
F.5	Socket head	Altimax (A.AM) Altimax + COTS GPS plate (IA.AGP)				M3x14	2	Steel
F.6	Socket head	COTS GPS battery housing (IA.GBH) Radionor plate (IA.RP)				M2.5x14	2	Steel
F.7	Socket head	Altimax battery housing (IA.ABH) Altimax battery plate (IA.ABP)				M3x18	2	Steel
F.8	Socket head	Black box housing (IA.BBH) Black box plate (IA.BBP)				M3x10	2	Steel

F.9	Countersunk	Lower coupler (IC.LC) Aft airframe (OL.AA)	M4x12	8	Steel
F.10	Insert	Lower coupler (IC.LC) Aft airframe (OL.AA)	M4x7,5	8	Steel
Fasteners					
Reference	Type	Interface	Dimensions	Qty	Material
F.11	Shear screw	Upper coupler (IC.UC) Lower coupler (IC.LC)	M3x8	8	Nylon
F.12	Countersunk	Nose tip middle part (IN.MP) Nose tip lower part (IN.LP)	M4x15	4	Steel
F.13	Socket head	Camera (A.C1) Camera mount (IL.CM)	M3x10	4	Steel
F.14	Socket head	Camera (A.C2) Camera mount (IL.CM)	M3x10	4	Steel
F.15	Countersunk	Bulkhead ring (IP.BR) Forward airframe (OU.FA)	M4x14	8	Steel
F.16	Insert	Bulkhead ring (IP.BR) Forward airframe (OU.FA)	M4x7,5	8	Steel
F.17	Countersunk	Bulkhead ring (IP.BR) Forward airframe (OU.FA)	M4x12	8	Steel
F.18	Insert	Bulkhead ring (IP.BR) Forward airframe (OU.FA)	M4x7,5	8	Steel
F.19	Countersunk	Bulkhead (IP.B) Payload	M4x14	8	Steel
F.20	Countersunk	Bulkhead (IP.B) Payload	M4x14	8	Steel
F.21	Insert	Upper coupler (IC.UC) Forward airframe (OU.FA)	M4x7,5	8	Steel
F.22	Countersunk	Forward airframe (OU.FA) Upper coupler (IC.UC) Recovery plate (RR.RP)	M4x24	8	Steel
F.23	Socket head	Main chute release docking (RM.MRD) Recovery plate (RR.RP)	M8x20	2	Steel

	F.24	Flat	Servo mount (RM.SM) Main chute release docking (RM.MRD)	M3x25	4	Steel
	F.25	Shoulder screw	Main chute release docking (RM.MRD) Lower release arm (RM.LRA)	M5x14	1	Alloy steel
Fasteners						
Reference	Type	Interface		Dimensions	Qty	Material
		Lower release arm(RM.LRA)				1074-1095
F.26	Ring shim	Main chute release docking (RM.MRD)		6mm ID	4	Spring Steel
		Shoulder screw	Main chute release docking (RM.MRD)			
F.27			Upper release arm (RM.URA)	M6x14	1	Alloy steel
			Main chute release docking (RM.MRD)			1074-1095
F.28	Ring shim	Upper release arm (RM.URA)		8mm ID	4	Spring steel
			Main chute release docking (RM.MRD)			
F.29	Socket head	Spacers (RM.SPC)		M4x20	3	Steel
F.30	Nylon-Insert locknut	Main chute release docking (RM.MRD)				
		Socket head (F.39)		M4x5,3	3	Steel
271	F.31	Flat	Hawk body (RH.HB) Hawk plate (RH.HP)	UNC 1/4"	8	Black-Oxide alloy steel
	F.32	Socket head	Camera (A.C3)			
			Camera mount (RR.CM)	M3x10	4	Steel
	F.33	Socket head	Recovery camera mount (RR.CM)			
			Recovery plate (RR.RP)	M3x10	4	Steel
	F.34	Countersunk	Motor centering ring (IAE.MCR)			
			Aft airframe (OL.AA)	M4x12	4	Steel
	F.35		Motor centering ring (IAE.MCR)			
	F.36	Insert	Aft airframe (OL.AA)	M4x7,5	4	Steel
			Aft airframe (OL.AA)			
	F.37	Countersunk	Boat tail centering ring (IAE.BCR)			
			Boat tail centering ring wedge (IAE.BW)	M4x7	4	Steel
	F.38	Insert	Aft airframe (OL.AA)			
			Boat tail centering ring (IAE.BCR)			
			Boat tail centering ring wedge (IAE.BW)	M4x7,5	4	Steel
	F.39	Flat head	Trapezoidal fin (OL.F)	M3x5	32	Black-Oxide

		Fin bracket (OL.FB)			Alloy Steel
F.40	Flat head	Fin bracket (OL.FB) Aft airframe (OL.AA)	M4x12	40	Steel
Fasteners					
Reference	Type	Interface	Dimensions	Qty	Material
F.41	Socket head	Lower release arm (RM.LRA)	M3x30	1	Black-Oxide Alloy Steel
F.42	Flat	Hawk body (RH.HB) Hawk plate (RH.HP)	UNC ¼"	4	Black-Oxide alloy steel

Referen ce	Avionics sensors						
	Sensor Type	Sensor Name	Quantity	Sensor Measurement	Sensor Placement	Sensor output [Unit]	Sensor Range [Lower / Upper]
A.S1	Barometer	MS561101BA03 -50	3	Pressure	Sensor board	mbar, °C	Pressure: 10 / 1200mbar, Temp: -40/+85°C
A.S2	IMU	ICM-20649	3	6DoF, accelerometer + gyro	Sensor board	Acc: g, Gyro: °/s	Acc: 30, Gyro: 4000
A.S3	Analog temperature sensor	LM19CIZ	1	Temperature	Main board	°C	-55 / 130
A.S4	Analog pressure sensor	BPS130-HA300 P-1SGCT-ND	1	Pressure	Main board	psi	0 / 300 PSI
A.S5	GPS	Adafruit ultimate gps	1	Position	Sensor board	GPRMC	1.8m position accuracy

Avionics Components						
Reference	Component Type	Component	Voltage [V]	Power Consumption [W]	Run Time	Flight Stage Active periode [Phase]
A.RCG	Radio Communications	CRE2-189	19-55	40.6-250W	1h, 30min	IDLE -> RECOVERY PHASE
A.SB	Sensor board + PSU	PCB	7.2 V	0.3W (max)	1h, 30min	FULL FLIGHT
A.MB	Mainboard	PCB	5V	0.25W (max)	1h, 30min	FULL FLIGHT
A.MBP	MB power PCB	PCB			1h, 30min	FULL FLIGHT
A.RP	Recovery PDB	PCB			1h, 30min	FULL FLIGHT
A.AM	COTS Flight computer	Altimax G3	7.2 V (Separate battery)		1h, 30min	FULL FLIGHT
	COTS GPS tracker + altitude	Eggtimer TRS GPS altimeter	7.2 V (Separate battery)		1h, 30min	FULL FLIGHT
A.RC	Radio Communications	CRE2-144-LW	15	8-25W	1h, 30min	IDLE->RECOVERY PHASE
A.VE	Video encoder	AVC-2K, H.264 Video Encoder	5	1.8W	1h, 30min	IDLE->RECOVERY PHASE
A.C1	Camera 1 (Horizon view)	Hawkeye 4K Firefly Split mini	15	4.125W	15 min	ARMED->RECOVERY PHASE
A.C2	Camera 2 (Fisheye view, livestream)	Hawkeye 4K Firefly Split mini	15	4.125W	15 min	ARMED->RECOVERY PHASE
A.C3	Camera 3 (Recovery)	Runcam split 3 nano whoop	15	~3W	15 min	ARMED->RECOVERY PHASE
A.C4	Camera 4(Recovery)	Runcam split 4	15	~3W	15 min	ARMED->RECOVERY PHASE

A.GG	Generator (Ground)					FULL FLIGHT
A.PC	Ground Station Computer	Laptop			3h	FULL FLIGHT
A.MCU	Microcontroller	STM32F103C8T 6	3.3V	0.165W (max)	1h 30min	FULL FLIGHT
A.BP	Main battery	4x 18650 cells	7.2V (2 in series)		1h 30min	FULL FLIGHT
Avionics Components						
Reference	Component Type	Component	Voltage [V]	Power Consumption [W]	Run Time	Flight Stage Active periode [Phase]
A.V1	Low-dropout regulator	TL1963A-33 DCYR	5V	~50% efficiency	1h 30 min	FULL FLIGHT
A.V2	Buck converter	TPS82140SILR	7.2V		1h 30min	FULL FLIGHT
A.V3	Boost converter	Pololu U3V70F15	7.2V		1h 30min	FULL FLIGHT
		Armored SD card	--V	--W	2 min	ARMED->RECOVERY PHASE
A.BB	Blackbox					
A.SW	Magnetic Arming Switch	Featherweight magnetic switch	--V	--W	From assembly (?? min)	FROM ASSEMBLY AND ONWARDS

Payload - Mechanical Components							
Reference	Sub-assembly	Name	Function		Material	Quantit y	Mass [kg]
P.CH	Lower section	Camera holder	Holds the camera in right position to film		Plastic, PLA	1	5
P.FF	Lower section	Ferrofluid	Used in experiment		Water with iron	1	N/A
P.FFC	Lower section	Ferrofluid container	Container for the ferrofluid		Acrylic plastic	1	34

P.MAG	Lower section	Magnet	Induce magnetic behaviour of the ferrofluid	Neodymium	1	22
P.CF	Lower, upper, middle	Cylindrical frame	Main body of the payload	Steel A2	1	1500
P.PLL	Lower section	Lower lid	Screwed on the bottom to make the frame watertight	Steel A2	1	504
P.UL	Upper section	Upper lid	Screwed on the top of the frame to insert the inner structure.	Steel A2	1	563

Payload - Mechanical Components

Reference	Sub-assembly	Name	Function	Material	Quantity	Mass [kg]
P.BP	Lower section	Bottom horizontal plate	This is used to fasten the threaded rods on the bottom, and anchor the structure to the bottom to prevent vibrations	Steel A2	1	177
P.BHP	Lower section	Battery holder plate	Supports the weights of the battery holders	Steel A2	2	35
P.BB	Lower section	Black Box	Resilient container for the SD-card	Steel A2	1	116
P.ROD	Lower, middle, upper section	Threaded rods	Framework for the inner structure		6	25
P.BHS	Upper section	Battery holder	Holds 2 batteries	Plastic, PLA	1	56
P.CVW	Upper section	Center vertical mounting wall	Wall for mounting the OBC and EPS	Plastic, PLA	1	60
P.OVW		Outer vertical mounting wall	Wall for mounting PI and SH	Plastic, PLA	1	40
P.SCW	Lower, middle, upper section	Screws	Fasten components	Stainless steel	N/A	N/A

Payload - Sensors						
Name	Sensor Type	Sensor Name	Sensor Measurement	Sensor Placement	Sensor output [Unit]	Sensor Range [Upper/Lower]
276	1. Gyroscope 2. Accelerometer 3. Magnetometer 4. Thermometer 5. Barometer 6. Humidity sensor	SenseHat	1. Rotation, 2. Acceleration 3. Magnetic flux 4. Temperature 5. Pressure 6. Humidity	Middle section	1. °/s 2. g 3. gauss 4. °C 5. hPa 6. % humidity	1. Max 20000 dps 2. Max 16g 3. ±16 gauss 4. 0-65°C 5. 260-1260hPa 6. 20-80%
P.SH						
P.IMU	IMU	LSM9DS1	1. Gyroscope 2. Acceleration 3. Magnetic flux	OBC	1. °/s 2. g 3. gauss	1. max 2000dps 2. g 3. gauss

Payload - Electrical Components						
Name	Component Type	Component	Voltage [V]	Power Consumption [mA]	Run Time	Flight Stage Active periode [Phase]
P.SDC	SD-card	SanDisk MicroSDXC High Endurance	--	--	30 min	Active, flying, landed
P.PI	Payload computer	Raspberry Pi 4B	5	640	30 min	Active, flying, landed
P.MIC	Microphone	Adafruit MAX4466	5	0.6	30 min	Active, flying, landed
P.ADC	Analog to digital converter	ADS1115	5	0.15	30 min	Active, flying, landed
P.CMR	Camera	Raspberry Pi camera module V2	Draws from PI	Draws from PI	30 min	Active, flying, landed
P.LED	LED	N/A	3.3	30	30 min	Active, flying, landed
P.OBC	On-board computer	N/A ¹	3.3	80	30 min	Active, flying, landed
P.EPS	Electrical power supply	N/A ²	N/A	N/A	30 min	Active, flying, landed
P.BLI	Battery	18650 LI-ION	--	--	30 min	Active, flying, landed

¹ This component is designed by Orbit NTNU.

² Ibid.

L. Detailed Telemetry Architecture

DETAILED TELEMETRY ARCHITECTURE

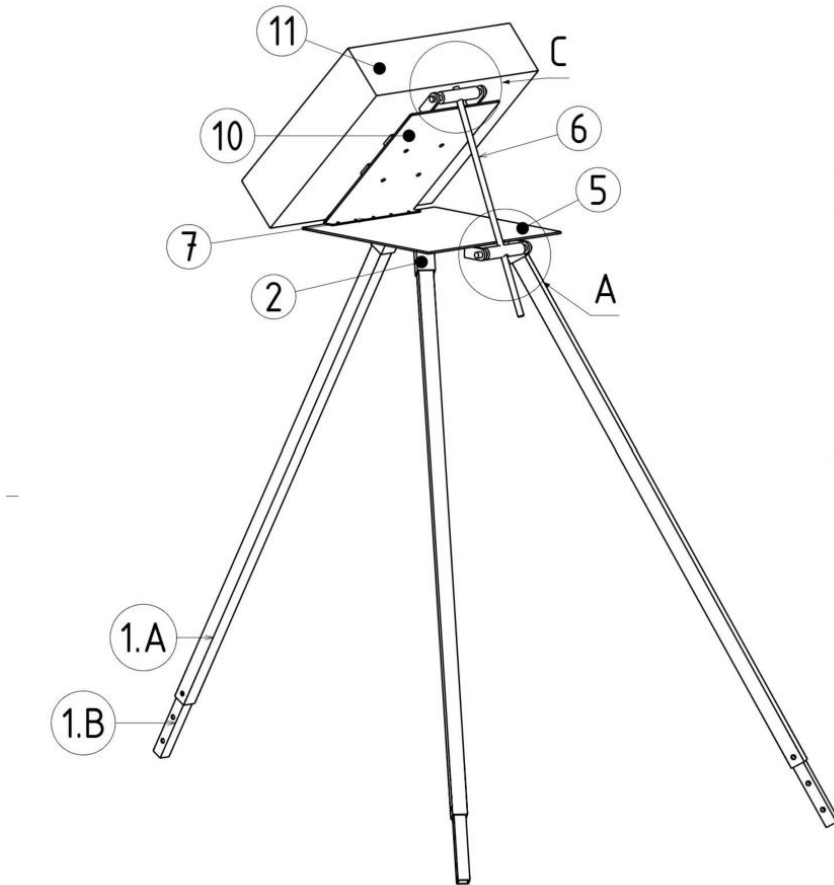
Ground station hardware

Radio specs overview

	Rocket radio	Ground radio
Component name	CRE2-144-LW	CRE2-189
Connectors	Power, Ethernet & UART	Power & Ethernet
Voltage range	10-32 V DC	19-55 V DC
Power draw	8-25 W	27-250 W
Frequency range	4900 MHz to 5900 MHz	4900 MHz to 5900 MHz
Channel width	14 MHz	14 Mhz
Tx power	2 W	4 W
Antenna gain	Dependent on antenna configuration	24 dBi
Transmission rate	15 Mbps	15 Mbps

Tripod

Since the CRE2-189 has a 90° field of view, it will be mounted on a 45 degree angle, so that it will be able to see both the horizon and straight above it. The mount is an adjustable tripod made of steel made in the design shown below.



Computer

The computer will be responsible for handling, storing and displaying the data received by the radio. The exact model is not important, but it will need to have an ethernet plug and an HDMI plug.

Monitor

The monitor will be connected to the computer through HDMI, and will simply act as an additional screen. It will be used for displaying the live video streamed from the rocket.

Power supply unit (CRE2-230VAC-24VDC):

The PSU on the ground is from the same supplier as the radios and is made to fit the ground station radio's power socket and supply a voltage in the radios voltage range. It receives power from the generator and can be plugged in directly.

Generator

1-Phase 230VAC CEE 7/3 “Schuko” sockets, powered from a low-power generator (maximum 2kW available for all of mission control) (provided by EuRoC)

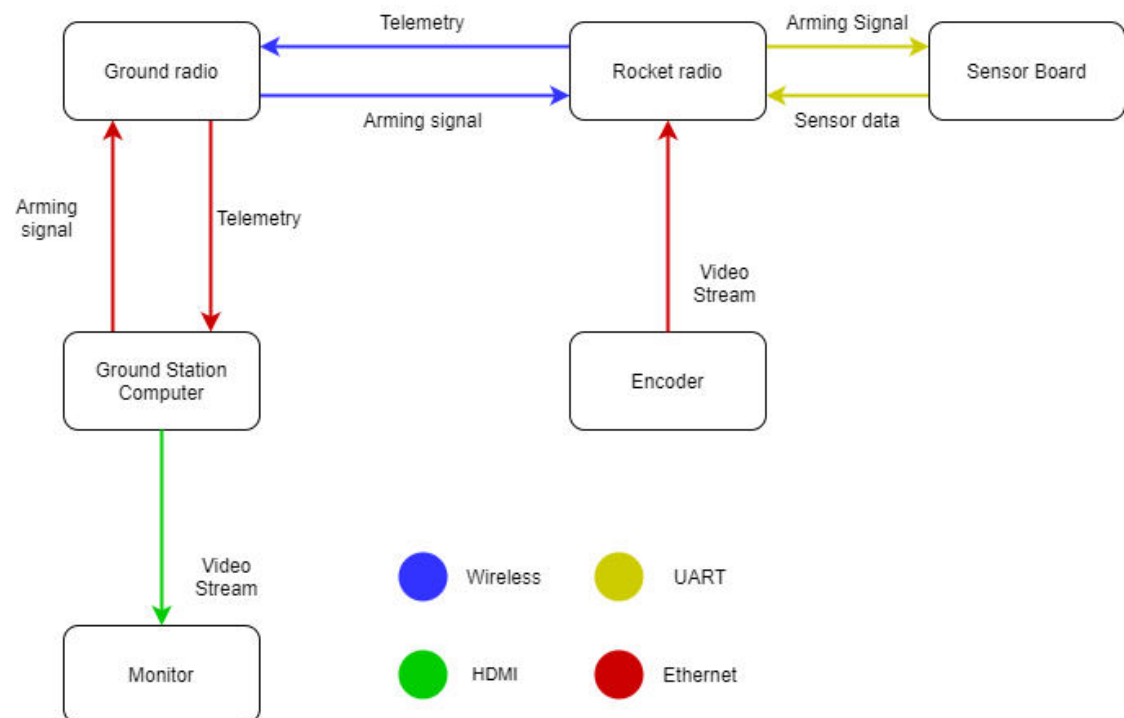
Software

The CRE2 radio system has built-in support for IP routing and the two radios used (A.RC + A.RCG) will be configured to the same network prior to assembly. Once configured, transmitting sensor data from the rocket is as simple as writing to the radio’s UART connectors.

The ground computer is connected to the ground radio through Ethernet, and will be able to communicate with the rocket’s sensor board by opening a network socket bound to the rocket radio’s IP address on port 20000. The video encoder will also need to be preconfigured to send to the IP address of the ground station PC. The livestream can be viewed in VLC media player by entering the encoder’s IP address as a streaming source. The sensor data will be transmitted by the radio using UDP (User Datagram Protocol), and the video stream will be transmitted using RTSP (Real Time Streaming Protocol)

The computer will be running a python server for handling the incoming data and passing it on the graphical user interface. The graphical user interface is a simple HTML file viewed in the browser and is capable of receiving data from the python server and displaying it live as numbers and graphs.

Telemetry information flow overview



Graphical user interface mockup

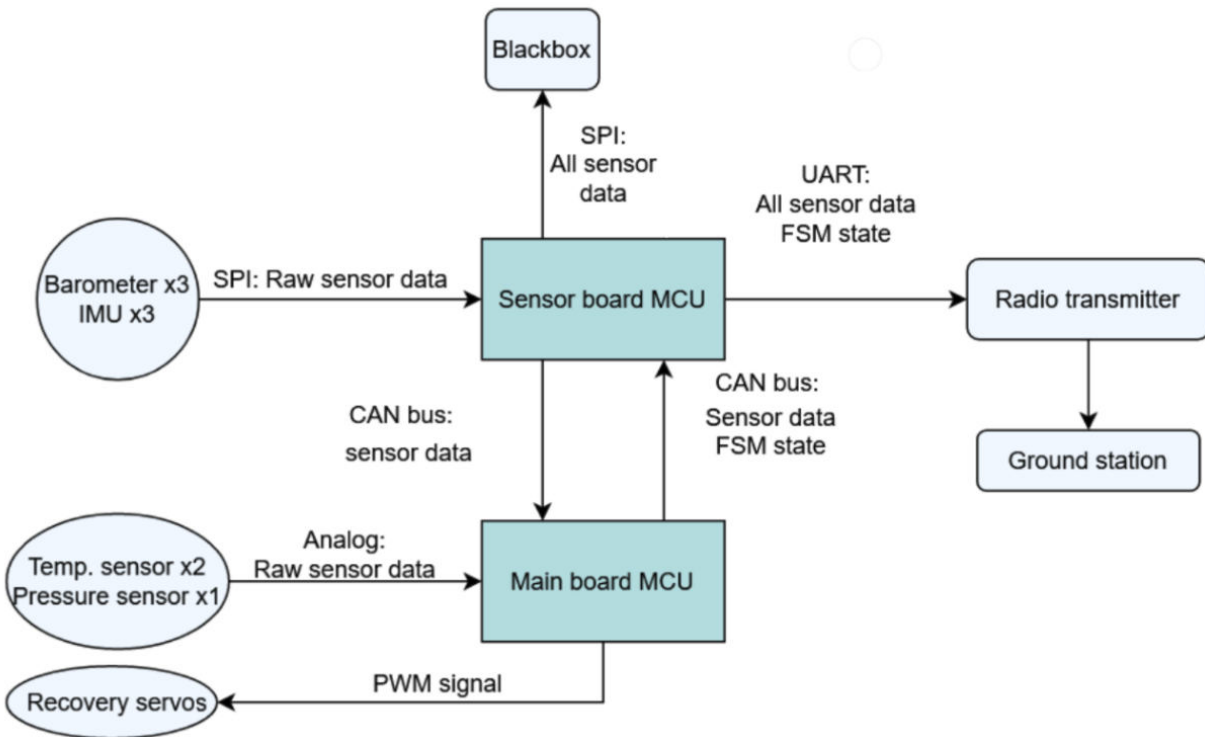


M. Detailed Software Architecture

DETAILED SOFTWARE ARCHITECTURE

Overview

The flight computer is divided into two parts; the main board and sensor board. On both of these, the microcontroller being used is an STM32F103C8T6 (A.MCU). This has a 32-bit ARM Cortex-M3 CPU architecture, and runs at 72 MHz. To fulfill main functions of the avionics system, there is a finite state machine(FSM) and Kalman filter running on the main board, while the sensor board reads, sends and stores the sensor data.



Sensor data

The sensor board communicates with the sensors over SPI. This ensures that no address collisions between the identical sensors can occur, in addition to simplifying the software development by having all of the sensors using the same interface. To reduce noise and measurement error, the system has three IMUs (A.S2) and barometers (A.S1). By then taking the average of all sensor readings, the measurement variance is reduced. This initial filtering also ignores any data that is unreasonable, like being too far from the others or no reading at all. Then a time stamp is added to identify the measurements when they are being sent to the main board and back.

A separate SPI bus is then used to interface with an SD-card inside of a blackbox, where all the sensor data is saved. The same data is also sent to the ground station via the radio.

In addition to the sensor board, there are also three analog sensors connected to the main board. These being two thermometers (A.S3) and one barometer (A.S4), which are used to monitor the status of the recovery system. This data is sent to the sensor board through the CAN bus.

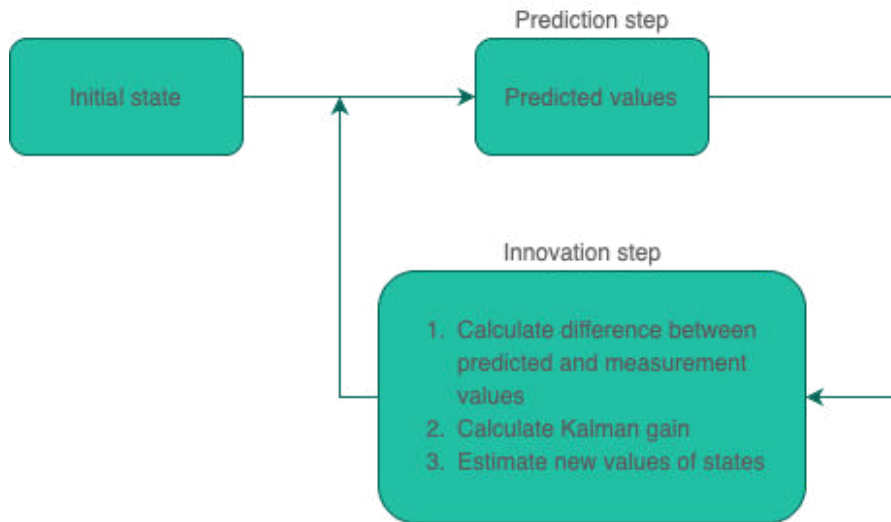
After collecting data on the sensor board, it is passed on to the main board through the CAN bus, where it is used as input to a Kalman filter. The FSM then uses this filtered data to predict which phase of the flight the rocket is in, before sending all the sensor data and FSM state back to the sensor board. All this ensures that the system has data stored in multiple places, increasing redundancy and reliability.

Kalman filter

To filter out noise from the sensor data we use a discrete Kalman filter, an algorithm used to estimate the true values of chosen states. This is a common method for data filtering in dynamic systems like a rocket. The main Kalman filter will estimate altitude and velocity by combining barometer and accelerometer data. This gives a better estimate of the rocket's altitude than if we were to rely on raw barometer data. This noise suppression is especially relevant when the rocket is in the trans and super sonic state. However, the filtered data will mainly be used for apogee detection and main chute deployment. Furthermore there is a separate filter that also estimates altitude and velocity in three dimensions by combining GPS position and accelerometer data. As GPSs (A.S5) are vulnerable to signal loss this filter will primarily be used for flight tracking.

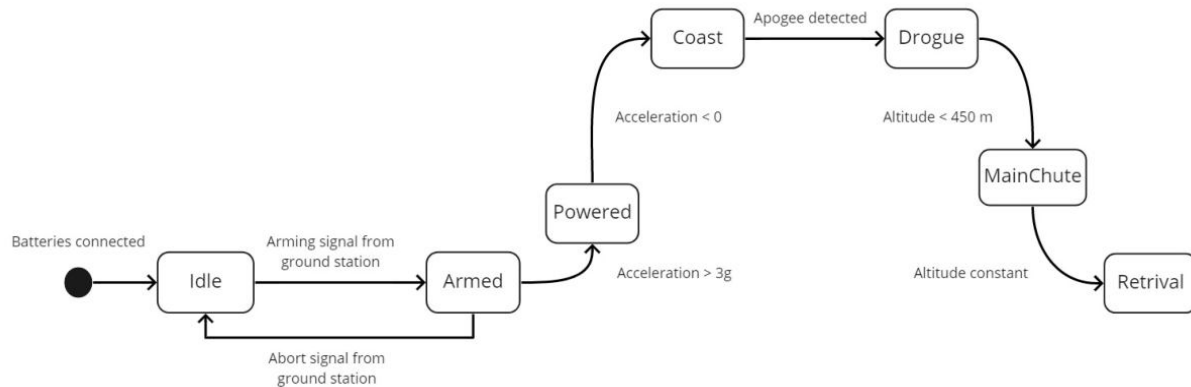
The IMU (A.S2) will measure acceleration in the body frame of the rocket, which means that the acceleration readings will be affected by orientation. We have experimented with an algorithm to calculate the orientation of the rocket. This is done by transforming the acceleration vector to the inertial frame using a rotation matrix which is calculated using gyroscope data and quaternions. This will make sure our acceleration data is always relative to the inertial frame.

The Kalman filter algorithm consists mainly of two steps; prediction and innovation. In the prediction step we make an educated guess of the value and the error in our states, based on the previous iteration of the algorithm and a model. Using the error prediction and the error in the measurements, the *Kalman gain* is calculated. Finally in the innovation step, we make an estimate of our state and error using the *Kalman gain* to decide if we trust our prediction or our measurements more.



Finite State Machine

The FSM is a tool that lets the software keep track of the flight phase of the rocket and allows it to execute the desired functionality associated with the state. This part will go further in detail with each state and transition used in the FSM.



States

The following table gives an overview of the states used in the FSM and their functionality.

FSM State	Rocket state and functionality
Idle	When the rocket is first powered on, this is the state it enters. Microcontrollers and radio the transmitter will power on. Corresponds to phase 0 in Mission concept overview.
Armed	Still waiting on the launchpad. Cameras will power up, live stream begins and

	logging of data starts. Corresponds to phase 1 in Mission concept overview.
Powered	While the rocket engine is burning. Corresponds to phase 4 and 5 in Mission concept overview.
Coast	After burn is done, but before apogee. Apogee detection starts. Corresponds to phase 6 in Mission concept overview.
Drogue	After apogee, when this state is entered the rocket will separate and drogue chute will deploy. Corresponds to phase 9 in Mission concept overview.
MainChute	When below 450m, main parachute releases when this state is entered. Corresponds to phase 10 in Mission concept overview.
Retrieval	When the rocket has landed. After a while data logging will stop and cameras will shut off. Corresponds to phase 12 in Mission concept overview.

Transitions

The following table gives an overview of the transitions used in the FSM and some of the reasoning behind it.

Transition	Trigger	Justification
Turned off → Idle	Batteries are connected /arming switches screwed in.	A screw switch is used to finish the circuit the batteries are connected to. These switches should minimize the chance of the system losing power due to vibrations in the rocket.
Idle → Armed	Arming signal from Ground station.	The arming signal from ground turns on the cameras, starts logging sensor data to SD-card and sends enable signal pulse to the payload. This step state is activated not long before launch and is used to save battery and storage space on the sd-card.
Armed → Powered	High G's detected. Acceleration > 3 g	There is an upper bound to what accelerations that could come from sensor uncertainty or small movements of the rocket. 3 g should be above this bound with a clear margin.

Powered → Coast	Negative acceleration detected. Acceleration < 0	As the rocket starts to slow down after burnout, negative acceleration should be detectable.
Coast → Drogue	Apogee detected. Maximum altitude reached.	Crucial transition where the apogee detection algorithm has the main responsibility to detect when the highest altitude is reached. Both the Kalman filter and a moving average of the last measurements is ensuring that the apogee is as accurate as possible.
Drogue → Main Chute	Altitude < 1500 ft.	450m AGL is set as the upper limit to what altitude main chute can be deployed. To reduce the rocket's decent rate as quickly as possible, the main chute is therefore deployed right after reaching 450m.
MainChute → Retrieval	Altitude constant.	If the altitude stays constant over some time interval, the rocket should have landed and it can enter retrieval state.

Detection Algorithm

The FSM uses a detection algorithm to ensure that the transition to the next state is correct and not a case of sensor uncertainty. The algorithm consists of a moving average of the last ten measurements. For each new measurement the average is updated. There is an average for both altitude and acceleration, as these are the measurements that the transitions between states are dependent on. The apogee detection, the most critical transition, consists of another step where the difference between the previous maximum average altitude and the current average altitude is calculated. If this difference is larger than a set margin, the apogee is detected and the drogue can be deployed.

N. Detailed Electrical Architecture

DETAILED ELECTRICAL ARCHITECTURE

This appendix details information about the electronic hardware in the rocket. Detailing important design decisions and specifications regarding the major components.

Printed Circuit Board

The PCBs used for the SRAD flight computer system are self developed. There are in total 4 circuit boards, the two holding microcontrollers are 4 layer PCBs where the two middle layers are used as a ground plane and power plane. The last two circuit boards are more simple 2 layer pbc's and are only used for routing and distributing power in a neat way. The microcontroller used is an STM32f103C8T6 (A.MCU), this MCU was chosen because it has adequate performance and capabilities, and there exists a lot of online resources for helping development.

On all PCBs there are multiple plugs to connect to other components. All connectors used for distributing power from the main battery pack are XT60 plugs. These plugs were chosen because they provide a strong connection which can allow for high current to pass through. The other plugs on the boards are nano-fit molex plugs, these plugs allow for a very customized and safe solution. The plugs have a snap-fit connection which should make all plugs stay connected even during high vibration and large acceleration. To further ensure that the plugs stay connected during flight we have oriented all the plugs so that they can't be disconnected by pulling in the direction of acceleration when the rocket launches.

Sensor Board components		
Part name	Part ID	Part type
STM32f103C8T6	A.MCU	Microcontroller
MS561101BA03-50	A.S1	Sensor, Barometer
ICM-20649	A.S2	Sensor, IMU
Adafruit ultimate gps	A.S5	Sensor, GPS breakout board
TL1963A-33DCYR	A.V1	Low-dropout regulator (LDO)
TPS82140SILR	A.V2	Buck converter
MB power PCB	A.MBP	Pcb for housing A.V3 and plugs for external power
Pololu U3V70F15	A.V3	Boost converter

Main Board components		
Part name	Part ID	Part type
STM32f103C8T6	A.MCU	Microcontroller
LM19CIZ	A.S3	Analog temperature sensor, connected externally via a plug.
HSCMANN300PGAA3	A.S4	Analog pressure sensor, connected externally via a plug
TL1963A-33DCYR	A.V1	Low-dropout regulator (LDO)



Figure 1: renderers of main board and sensor board.

Camera

Below you can see an overview of the different cameras and their settings/properties that they will be running for the launch. Below that you can see a visualization of their placement and what they will see.

Cam nr.	Camera model	Component name	Resolution	Framerate	Field of view	Streamed
1.	Firefly split 4k	A.C1	4096x2160	30 fps	160	no
2.	Firefly split 4k	A.C2	1920x1080	60 fps	185	yes
3.	RunCam Split 3 Nano whoop	A.C3	1920x1080	60 fps	165	no
4.	RunCam Split 4	A.C4	2704x2028	60 fps	140	no

Table 1 - Overview of camera specifications.

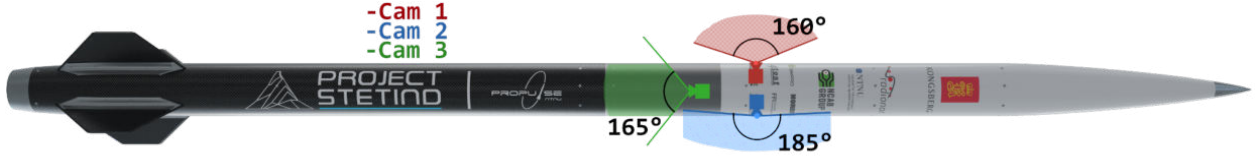


Figure 2 - Visualization of camera placement.

Camera purposes

Camera 1 will record a 4k video of the horizon, its purpose is to capture a cool looking video as the rocket flies. The file will only be stored locally on a micro SD-card.

Camera 2 will record a HD video of the horizon, but with a special 185 degree lens it will also be able to capture parts of the rocket, of which the fins are of special interest. Its purpose is to provide data of flight performance. To ensure that we capture and save this data it is stored locally on a micro SD-card, but also transmitted to the ground using our 5 Ghz transceiver.

The transmission of data happens via a video encoder onboard the rocket. The encoder takes in an HDMI signal from the camera and converts it into Real Time Streaming Protocol (RTSP) which carries a 1080p 30fps video stream at a bitrate TBD. This signal is then sent to the radio transceiver via ethernet and transmitted to the ground station where it is saved again. Further details on how the transmission from the transceiver works and how it's handled on the ground can be found in Appendix V.L.

Camera 3 is placed inside the recovery bay pointing out of the coupler, its purpose is to record main parachute deployment. This will be stored locally on the rocket on a micro SD-card.

Camera 4 is placed in nearly the same location as camera 3, but instead of pointing out of the coupler, it is pointed towards the MCRS. Its goal is to capture the MCRS releasing the main parachute which should provide interesting data post flight. This will be stored locally on the rocket on a micro SD-card.

Recovery monitoring sensors

The functionality of this system is explained in section G.Avionics of the report. Ths paragraph provides further details.

The temperature sensor (A.S3) is an LM19CIZ. This sensor uses a voltage of 3.3 V and outputs an analog voltage which the microcontroller (A.MCU) can read. A transfer function defined in the sensor's datasheet is then used to translate the measured voltage to centigrade. The sensor is rated to measure a temperature between -55 C° to 130 C°, which is more than sufficient for our use.

For attaching the temperature sensor to the CO₂ canister, a small 3D printed mount for the sensor is used to house it, which is then taped to the canister using tape. To ensure good thermal conductivity between the sensor and CO₂ canister there will be a thin thermal pad placed between the two.

The barometer sensor (A.S4) is an HSCMANN100PGAA3. This sensor uses a voltage of 5v and outputs an analog voltage between 0.5 and 4.5. To read this on the microcontroller a voltage divider is placed in

between to lower the max output voltage to 3.3 V as this is the highest the MCU can use. The sensor is rated to measure a pressure of 0 to 300 psi, and survive a pressure of up to 600 psi which is more than sufficient for our use.

Blackbox

On the rocket we will have a blackbox whose purpose is to safely store data even in the event where the rocket crashes. The blackbox is at its core just an SD-card encapsulated inside an aluminium box filled with resin.

Power supply

There are in total five power supplies/voltage converters in the rocket. Three of them are located on the sensor board, where the battery voltage of 7.2 V is converted to 15 V and 5 V. The 5 V is also converted to 3.3 V for the mcu and other components located on the PCB. Both the 5 V and 15 V are distributed to the mainboard, while the 5 V is additionally connected directly to the video encoder. The mainboard further distributes the 5 V to the Hawk and MCRS servo motors, and distributes the 15 V to the four cameras located in the rocket. On the mainboard there is also a voltage regulator which converts the 5 V to 3.3V for the MCU and other components on the PCB. Lastly there is a 15 V voltage converter connected to the Radio transceiver which receives power from the main battery. Below in figure 4 you can see this power distribution illustrated.

Originally we had designed a single SRAD 15 V power supply using a TSP61288 capable of providing 3 A of current. This was supposed to be located on the main power supply, but due to the shortage of electrical components we were unable to buy the necessary ICs. For that reason we decided to instead use two Pololu U3V70F15 15 V Step-Up Converters. This PSU is only capable of providing ~2 A of current, so we are implementing two of them as a replacement of the original design. One is located on the Sensor board in the main power supply and functioning as a direct replacement of the original PSU we designed, the other is directly connected to the radio transceiver, both of them are connected to the main battery in parallel.

TPS82140 converter from Texas Instruments will supply the encoder and the hawk servo motors with 5 V. The buck converter has a relatively high current limit of 2 A and an integrated inductor. The integrated inductor results in a much smaller footprint in addition to greater simplicity. Additionally, the converter offers a high efficiency of around 90 % in typical conditions.

TL1963A will convert the 5 V into 3.3 V for the MCU, SD cards and sensors. The 3.3 V components represent a small part of the total power consumption. Therefore little emphasis was placed on the efficiency of this part and simplicity and footprint were much more important factors. TL1963A offers both a small footprint and an incredibly simple circuit design. In addition, the converters can achieve an efficacy of ~50 % in typical conditions when the converter takes the 5 V from the buck converter as input.

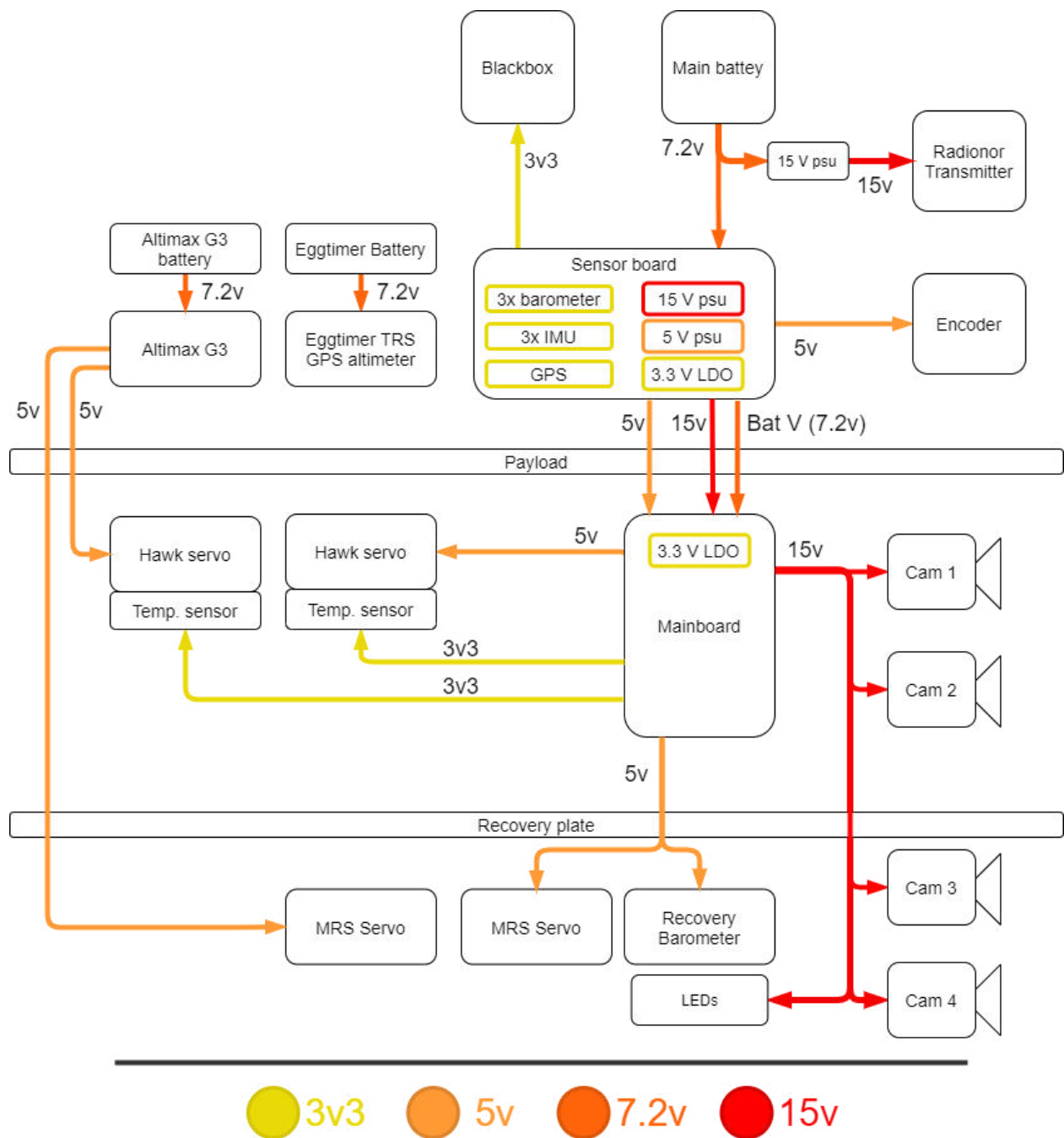


Figure 4. Diagram of power distribution through all components in the rocket.

O. Mechanical Interface Control Document for Payload

Mechanical Design Trade-Off

Payload



Issue statement

For this trade-off, the payload team seeks to find the optimal design for the mechanical design of the outer frame of the payload. The frame has to be cylindrical, in order to fit within the host rocket. It also has to be waterproof. This allows us to conduct experiments with liquids, because this gives the Propulse team a certainty that our liquid will not interfere with their system.

The payload team reckons that the inner structure for the liquid container does not have to be completely waterproof in case of an incident. This is because we believe that the physical structures will be strong enough that if the container is destroyed, the rest of the project is also compromised, and therefore there is no need to protect our systems. In other words, if the liquid container is broken, the rest of the system is most likely also broken.

All of our solutions will be made of steel. This is because it will be easy to work with if we decide to weld some pieces together.

Trade-off Objective

As previously mentioned, the frame has to be cylindrical and waterproof. Further, it has to fulfill some other criterias. These are listed below with the most important criterias first. In addition, we face some “yes or no”-criterias, which has to be fulfilled for the design to be applicable.

However, we will not list waterproof as a criteria, because we will not be considering options that are not waterproof. The same goes for robustness in design, which is a benefit, but we reckon that most of our designs will be more than sufficiable when it comes to robustness.

Physical dimensions is also a “yes-or-no”-criteria that we have not elaborated on in this trade-off. This is because all our alternatives need to have an outer diameter of 110mm, and an inner diameter of 90mm, in order to fit an On-Board Computer (OBC). Therefore, we will not consider alternatives that do not fulfill these structural criterias.

Selection criteria 1 - Ease of use

- The frame has to be built in such a way that it is easy to put the complete system together, and also be able to take it apart. This is relevant for the cause of trouble-shooting for the electrical components, and similar situations.

- Perhaps most importantly, the aspect that relies most on ease of use is how the cable from the payload to the bus is going to be implemented.
- An aspect that goes under ease of use is that we believe that having a separation between the bus and the payload might be beneficial because it allows us to work on one of them without disturbing the other.
- It should also be easy for the Propulse team to integrate the satellite with the rocket, in case the payload team is not present.

Selection criteria 2 - Simplicity in design

- A simpler, more elegant design allows for easier manufacturing, and possibly also lower costs and production time.
- If the design is simple, it may also allow us to produce the frame by ourselves to a larger degree. This is preferable, both because it gives us a greater potential of learning, and also it lowers the cost and possibly also production time.

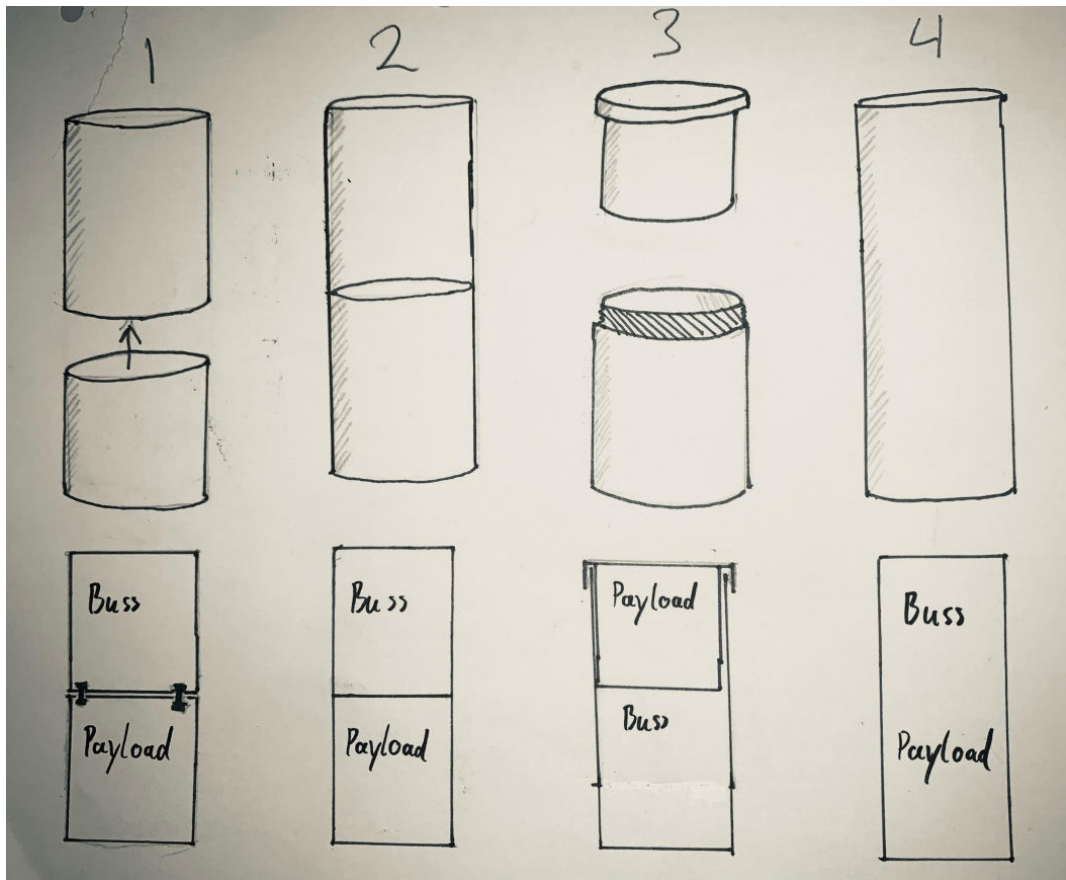
Selection criteria 3 - Production time - YES/NO

- This is a “yes or no”-criteria, because the frame has to be finished before the payload is handed over to Propulse. However, we consider a low production time as a benefit

Selection criteria 4 - Production cost - YES/NO

- This is a “yes or no”-criteria, because the cost of manufacturing has to be in line with an economical frame. However, there is no hard cap in our budget, but we will consider a low cost as a benefit.

Identify alternatives



Solution 1

Two cylinders with a sealed end that are mounted together.

Solution 2

A cylinder, where we will insert a separating wall between the bus and the payload.

Solution 3

A cylinder with a separate cylindrical box that is mounted in one end.

Solution 4

An empty cylinder.

Name	1	2	3	4
------	---	---	---	---

Ease of use	-Cable management +Separation	-Cable management +Separation	-Cable management +Separation	+simple to assemble and disassemble +no problem with cabling
Simplicity in design	+Easy to produce	-Hard to implement wall	-Hard to implement a separate container	+Easy to produce
Time	-	-	-	Low
Money	-	-	-	Affordable

We researched the manufacturing price and ease of production for the solution that we recognized as most optimal, solution 4. It became clear that it was both easy to produce and affordable, along with a time frame that fits with our program. Therefore, we did not research the price and manufacturing possibilities for the other solutions. The reason for this is that solution 4 is the simplest solution, and therefore we also assume that is the cheapest and easiest to produce.

Qualitative Considerations

Solution 1

Positive aspects

- This solution is simple to produce. Either to have it produced by a separate manufacturer as two cylinders with a closed end, or to use two cylinders and implement walls on one side of both of them.
- Having a separation between the payload and bus might be more practical.

Negative aspects

- The biggest drawback with this solution is that there has to go a cable between the separate compartments. The reason why this is a problem is that the camera will be on one side of the wall separating the compartments, while the rest of the bus is on the other side. In order to enable the bus to be taken out of the frame, the camera has to be threaded through a hole in the wall every time it is taken apart, or the cable has to be long enough so that the bus can be taken out of the frame, without having to disturb the camera. Both of these solutions raise problems, because threading the

camera through a hole may prove difficult. For the second solution to the problem, a long cable will have to be stored somewhere in the bus. This may prove to be problematic, as it will be moveable during flight and testing, and it is generally experienced that moveable parts are more susceptible to breaking.

Solution 2

Positive aspects

- Having one unit will be easier to produce, we may be able to find a steel tube that fits our dimensions, and only have to implement a separating wall by ourselves.
- As seen with solution 1, it may be beneficial to have separate compartments for the bus and payload.

Negative aspects

- Implementing a separating wall in the tube might prove to be difficult. We will have to either weld it in place, or use screws in some way to fasten it to the walls of the cylinder. Welding especially may be a challenge, because the welding tool will not be able to go inside a narrow cylinder.
- The separating wall will also raise the problem of cabling, as seen in the negative aspect of solution 1.

Solution 3

Positive aspects

- This solution makes it easy to separate between the bus and payload.

Negative aspects

- The cabling problem seen in other solutions also appears here.
- The way to implement the separate container for the payload seems hard to design and produce.

Solution 4

Positive aspects

- When having an open solution with no separating wall, the cabling management between the payload and the bus becomes easier. This also allows for the bus and payload to be assembled and taken apart easier
- Similarly to Solution 2, having only one unit will be easier to produce. Along with ease of production comes lower price and production time, which is also a benefit.

Negative aspects

- Without separation between the payload and the bus, we will have to interact with both the bus and payload when we want to interact with only one of them. We believe this might be impractical, and a minor drawback.

Alternative comparison

Name	1	2	3	4
Ease of use	Medium	Medium	Medium	Good
Simplicity in design	Good	Bad	Bad	Good
Time	-	-	-	Low
Money	-	-	-	Affordable

Discussion of results

We consider solution 4 to be sufficient. It fulfills our requirements, both in being easy to use, and having simplicity in design. It also comes at a reasonable cost.

P. Detailed Software Architecture Payload

Software Architecture Payload



Summary

In this document we give an overview of the overall structure of the software architecture for the payload.

Satellite definition

In this document, the rocket's payload is referred to as the satellite and the payload's experiment referred to as the satellite's payload. The reason for this is that the Sub-Orbital team in Orbit NTNU views the experiment as a sub-payload, and this is to avoid confusion between the rocket's payload and the satellite's payload.

Operating system

The OBC uses ErlendOS as an operating system. Link to the systems wiki can be found here:
<https://git.erlendjs.no/erlends-os/kernel/kernel/-/wikis/home>.

The Raspberry Pi uses Raspbian as the operating system.

Raspberry Pi

Sensors

A Raspberry Pi sensor board, SenseHat, is connected directly to the Raspberry Pi. The senseHat has the following sensor types:

- Gyroscope (°/s)
- Accelerometer (g)
- Magnetometer (gauss)
- Temperature (°C)
- Barometric pressure (hPa)

- Humidity (% humidity)

Decibel measurers (microphones) are used to gather data on the sound levels inside the rocket. Three are used, with different gain, to detect the varying levels of sound.

The sound level will be represented through three differential voltage signals, one from each measurer.

Raspberry Pi main program

Description

The main program on the Raspberry Pi. This program handles telemetry and communication between the OBC and the Raspberry Pi.

Usage

`payload_main.py`

Features

- Taking measurements from the sensors
- Filming
- Housekeeping
- Communication with the main computer

Housekeeping

This module handles getting and logging the status of the sensors on the Raspberry Pi. To do so, it includes a `getStatus` function, which collects the status of the `camera`, `senseHat` and `decibelMeasurer`. The `watchdogWriteToFile(data)` function saves the argument `data` together with a timestamp to a file. This function is used by most functions throughout the program to log everything that happens to the file.

Measurements from the sensors

The sensors the main program reads from are the sound sensors, called `decibelMeasurer`, and the telemetry sensor, called `senseHat`. By calling their respective turn on functions, both `decibelMeasurer` and `senseHat` are turned on and start saving their data to a file. The functions run concurrently using a thread for each function, unless the sensors are stopped and rebooted by an OBC command. This would happen when the OBC detects that they have failed to save their data to a file. See Appendix V.N Electrical interface control document for more details about what databusses the sensors are using.

Filming

The main program also calls a start recording function from the `camera` module. This function starts the Raspberry Pi camera and takes 1 second long videos concurrently using a thread. This will run forever unless the OBC detects that the camera is not running or the videos are not being saved, in which case the whole program will be rebooted. The reason that the whole program is rebooted for the camera, and does not do so for other sensors, is because the camera is the most important sensor, and the only sensor that records the experiment.

Communication

Raspberry Pi <-> OBC

The format for the messages sent between the OBC and the Raspberry Pi is always an array of 4 elements. The Raspberry Pi will receive commands from the OBC, and in return it will send an answer, for example an array containing status about the sensors [S111].

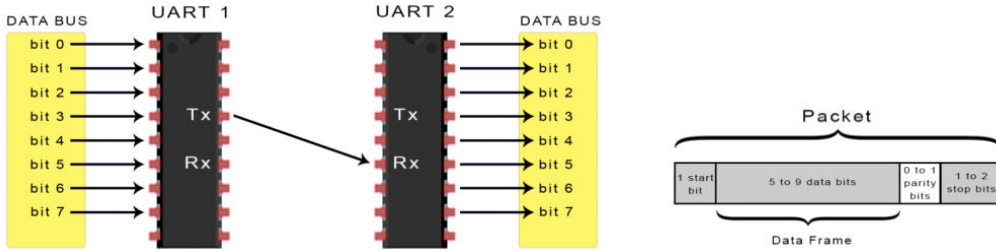
The message between the OBC and Raspberry Pi typically contains two fields

- Command/data information [0]
- Data [1-3]

Data[0]	Meaning
G	Get status from sensors and camera on the Raspberry Pi
K	Rebooting Raspberry Pi (“KILL”)
H	Shutdown Raspberry Pi (“HALT”)
S	Sending Status to OBC
Data[i+1]	Meaning
0	Sensor is not working
1	Sensor is working

Implementation

The communication is implemented using UART, where data is transferred between Tx and Rx pins on the Raspberry Pi and the OBC. The Raspberry Pi is using the python serial library “pyserial” to read/write on the Tx and Rx pins.



The Raspberry Pi Serial port is configured to match the OBC's serial port configuration. Therefore the Raspberry Pi serial port is configured to:

- port = `ttyS0` (standard port for serial communication on the RPi)
- bytesize= `EIGHTBITS`
- parity = `PARITY_NONE`
- stopbits = `STOPBITS_ONE`
- baudrate = `38400`
- timeout = `1`

NB: Since we are converting directly the data from the serial bus to a string, we get three non-data chars such as “ ‘[]’ ” which are omitted from the data packet.

On-Board Computer

OBC main program

Description

The main program running on the OBC. This program runs on a finite state machine (FSM), and handles communication with the rocket from Propulse, and communication with and systemcheck of our Raspberry Pi.

Usage

`CanSat_main`

To make the usage as simple as possible, `CanSat_main` takes no input arguments.

Features

- Finite state machine
- Watchdog module
- Housekeeping
- Communication with Raspberry Pi

Finite state machine

Definition: When referring to the word *states*, the states of the FSM are the ones referred to.

The FSM is a finite state machine implemented through the use of enum type 'State' returns. In each state, a function corresponding to the state will be run, and the return will be a new state, i.e. at boot the state is 'Init', which will run the 'FSM_init' function, which then could return the 'GettingStatus' state. None of the state functions will require input arguments.

The FSM has these 4 states:

- Init
- GettingStatus
- Ground
- Launch

Init

This state is our initial state, and will only run at boot on the OBC. The init state gives RPi time to boot before communication starts between the RPi and the OBC.

GettingStatus

In this state we will get status from the Raspberry Pi. This state is only exited once the status reading is successful. If status reading fails, the Raspberry Pi will be rebooted.

The return state from 'GettingStatus' is 'Ground' if the satellite has not yet sent a confirmation to the rocket that our Raspberry Pi is running, indicating that they are not going to launch.

This launch variable will be global, and will be set to true in the 'Ground' state. Once the launch variable is set to true, it will stay true during the rest of the launch.

The return state from 'GettingStatus' is 'Launch' if the launch variable is set to true.

Ground

In this state, the data in the status array from the Raspberry Pi is interpreted. The values from the status array will tell the OBC if the system is ready for launch or not.

If the array is [111], the launch variable will be set to true, and the return state will be 'Launch'.

If the array is not [111], the OBC decides which components to reboot or if it needs to reboot the whole Raspberry Pi. The return state when launch is not set to true, will be 'GettingStatus'.

Launch

In this state, the data in the status array from the Raspberry Pi is interpreted, and the OBC decides which components to reboot or if the Raspberry Pi needs rebooting based on the status array. The return state from 'Launch' is 'GettingStatus'.

Watchdog

The main purpose of the OBC is to act as a watchdog towards the Raspberry Pi, and therefore this module contains functions that send commands to the Raspberry Pi determined by the interpretation of the status array that the Raspberry Pi sends. (See the communication table for better clarification of what the different symbols mean.) For example if we get an array with the following data: [S101], this means that the camera is not working and it will trigger the function `watchdogOBC_sendRaspberryPiReboot()` which will make the Raspberry Pi reboot.

Housekeeping

All activity on the OBC, which includes commands, error messages, status checks, data and more, will be saved to a text-file. The activity can then be analyzed after retrieval.

Communication

The format for the messages sent between the OBC and Raspberry Pi is always an array of 4 elements. The Raspberry Pi will receive commands from the OBC, and in return the Raspberry Pi will send an answer, for example an array containing status about the sensors [S111].

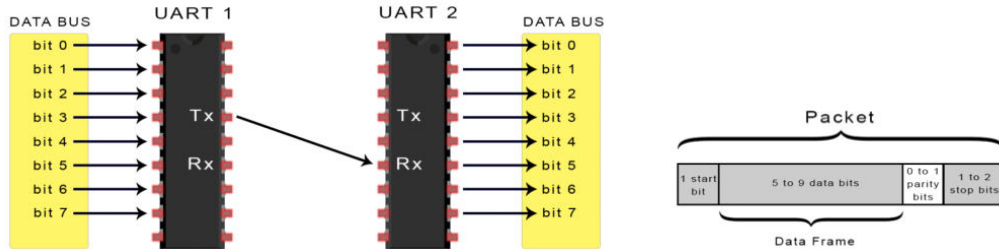
The message between the OBC and Raspberry Pi typically contains two fields

- Command/ data information [0]
- Data [1-3]

Data[0]	Meaning
G	Get status from sensors and camera on the Raspberry Pi
R	Reboot sound sensors
K	Rebooting Raspberry Pi (“KILL”)
H	Shutdown Raspberry Pi (“HALT”)
S	Sending Status to OBC
Data[1+i]	Meaning
0	Sensor is not working
1	Sensor is working

Implementation

The communication is implemented using UART, where data is transferred between Tx and Rx pins on the Raspberry Pi and the OBC. The OBC is using functions from ErlendOS to enable serial communications, by opening a serial port by using open(), and using read() and write() to interact with the Tx and Rx pins on the OBC.



The OBC has the current configuration on the serial port

- port = tty1
- bytesize= EIGHTBITS
- parity = PARITY_NONE
- stopbits = STOPBITS_ONE
- baudrate = 38400

External bus connections and interfaces

Uart is the communication protocol used between the OBC and Raspberry Pi computer.

I2C is used between the Raspberry Pi and the SenseHat.

The EPS is used to give power directly to the LED's.

EPS

If no status is received from RPi after 5 reads on the RX pin on the OBC, the OBC will send a “halt” warning to RPi, telling it to stop all processes and then send a ping to EPS to stop the power supply to the RPi.

Data storage redundancy

Telemetry and video footage on the RPi is stored on an industrial grade SD-card. IMU data on the OBC is saved on flash drives on the OBC. The card is stored in a steel container for physical protection. Sensor data is stored in a string format in a text file.

For the video footage, a crash is more significant. Since video is captured continuously, there might be a problem in case the electrical system goes down in the middle of a video. To avoid this problem, and limit the damage potential, video is captured in one second intervals. This is implemented to make fewer video files corrupted in case of a crash. To illustrate the point, the absolute opposite would have been to capture one long video, but then if the electrical system goes down, the whole video file is at risk of being corrupted.

However, testing revealed that more video files than the one currently being filmed were corrupted. For more details on this, please see the Black box test report¹.

¹ [Black box test report](#)

Q. Electrical Interface Control Document

Electrical Interface Control Document Payload



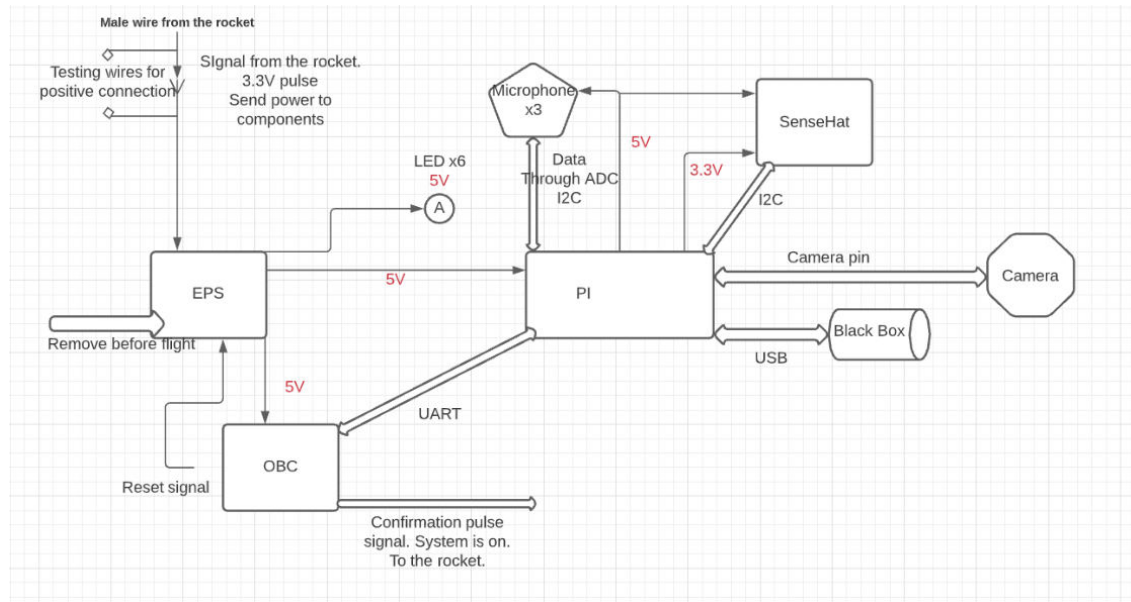
Summary

The purpose of this document is to give the reader a complete understanding of the electrical interface. This document covers the interface of the electrical system.

Satellite definition

In this document, the rocket's payload is referred to as the satellite and the payload's experiment referred to as the satellite's payload. The reason for this is that the Sub-Orbital team views the experiment as a sub-payload, and this is to avoid confusion between the rocket's payload and the satellite's payload.

Interface overview



Power

- 5 V directly from EPS to OBC.
- 5 V directly from EPS to Raspberry Pi.
- Raspberry Pi will distribute power to the camera, blackbox and sensors.
- 5 V directly from EPS to the LEDs.
- 5V and 3.3V from Raspberry Pi to the Sense Hat.

The OBC can power on and off the Pi by sending high voltage to a mosfet connected to the powerline between the Raspberry Pi and the EPS.

OBC

Information will be transferred by UART from OBC (Master) to Raspberry Pi (Slave).

There is also a wire from the OBC to the rocket that will ping back a pulse when all systems are running properly. It is a confirmation signal for the rocket that the system is functioning. The ping is a digital pulse of 3.3V.

EPS

Remove-before-flight pin is connected to the EPS. It will turn the EPS to Idle mode from off mode when removed. After that it will wait for a signal from the rocket to go active and supply all the components with power. The signal is referred to as the launch signal and will come a few minutes before the rocket will launch. This signal is the same signal as the rocket's arming signal.

This will make the EPS switch to on mode, and send power to the rest of the system. The pulse from the rocket will be made a permanent signal with a simple logic unit on the EPS, which then will make it turn on. The signal is one simple square pulse. It can also turn the EPS back to idle mode, if the signal is sent again. That will be used if the launch is delayed, for power saving.

The signal from the rocket will be received by a cable that sticks out of the top lid of the satellite. This will be a male to female cable that will be able to easily connect during the integration phase. It will not be very sturdy, however, there is no need for it. The cable only has to be intact before the launch, in order to receive a signal, and after that stage it has no other use. Therefore, if the acceleration causes it to loosen, it does not matter, because the cable is expendable at this point.

Two lithium ion 18650 batteries will supply the power to the EPS. They are connected in series and are connected with two power wires and one ground. The EPS will read the power difference from the two power cables and use the reading to supply power further to the system.

Two batteries is enough to power our system far longer than what is needed.

Raspberry Pi

The Raspberry Pi is the payload computer for the satellite.

- Sense Hat is connected to the Raspberry Pi via I2C and receives power from EPS.

- Data storage is located in Black Box, and is connected through an USB.
- Raspberry Pi Camera module is connected by specially designed cable, made by Pi.
- The Volume sensors use PINS 33, 35 and 37 one for each for data transfer to the Pi.
- The LED will be used to light up the inside of the satellite, so the camera will be able to film. They are connected directly to the EPS.

SenseHat

The senseHat is a sensor board designed by Raspberry Pi, and this is located on top of the Raspberry Pi. The senseHat has the following sensor types:

- Gyroscope (°/s)
- Accelerometer (g)
- Magnetometer (gauss)
- Temperature (°C)
- Barometric pressure (hPa)
- Humidity (% humidity)

Microphones

Microphones are used to measure the sound level of the noise in the rocket. Three microphones are used with different gain to be able to record different noise levels. The signal from the microphones are sent through an ADC in order for them to be interpreted by the Raspberry Pi.

Lighting

LED diodes are connected to the EPS to light up the experiment. This is in order to be able to film, since there is no natural light in the satellite.

Interface with the Rocket

The OBC will send pings to the rocket's avionics when all systems are running. If the rocket does not get a signal from the OBC after it has sent the launch signal to the EPS, it will try sending the launch signal again. If the launch is delayed, the same signal can be sent to make the satellite go back to idle mode. There are three wires; one ground wire from the EPS, the launch signal wire from the rocket to the EPS and the ping wire from the OBC to the rocket. These cables are pulled through the lid of the satellite, and run across the body of the satellite, to the rockets avionics board.

Wiring

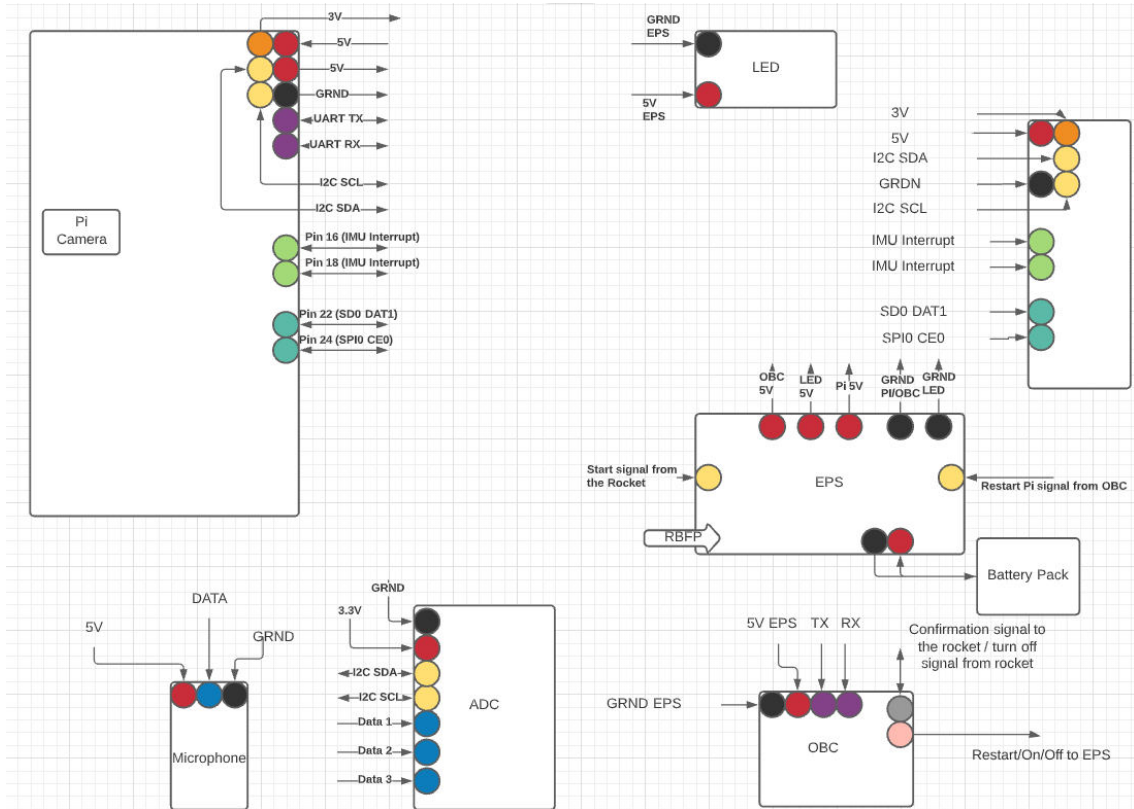


Figure 1: Wiring between the PI, Sense Hat, OBC, Microphones, EPS.

3v3 Power	1	2	5v Power
GPIO 2 (I2C1 SDA)	3	4	5v Power
GPIO 3 (I2C1 SCL)	5	6	Ground
GPIO 4 (GPCLK0)	7	8	GPIO 14 (UART TX)
Ground	9	10	GPIO 15 (UART RX)
GPIO 17	11	12	GPIO 18 (PCM CLK)
GPIO 27	13	14	Ground
GPIO 22	15	16	GPIO 23 (IMU Interrupt)
3v3 Power	17	18	GPIO 24 (IMU Interrupt)
GPIO 10 (SPI0 MOSI)	19	20	Ground
GPIO 9 (SPI0 MISO)	21	22	GPIO 25 (Atmel Prog Reset)
GPIO 11 (SPI0 SCLK)	23	24	GPIO 8 (Atmel Chip Select)
Ground	25	26	GPIO 7

Figure 2: Pinout for sense hat

The sense hat and raspberry pi are connected on the same pinouts.

Pin (PI)	Component	Description
2	EPS	5V From EPS
4	DB measurers, SenseHat	5V (VCC)
1	ADC, SenseHat	3V3
6	EPS	Ground to EPS
3 (GPIO2)	Sense Hat, ADC	I2C (SDA1)
5 (GPIO3)	Sense Hat, ADC	i2C (SCL1)
9	ADC	Ground
34	DB measurers	Ground
8 (GPIO14)	OBC	UART TX Send
10 (GPIO15)	OBC	UART RX Receive
22 (GPIO25)	Sense Hat	Atmel Prog
24 (GPIO8)	Sense Hat	Atmel Prog
16 (GPIO23)	Sense Hat	IMU
18 (GPIO24)	Sense Hat	IMU

Pin (OBC)	Component	Description
5V pin	EPS	5V Power from EPS
Ground pin	EPS	Ground to EPS
UART TX	PI	Send to Pi
UART RX	PI	Receive from Pi
GPIO 0	Rocket	Confirmation signal
GPIO 3	EPS	Turn ON/OFF Pi

Pin (EPS)	Component	Description
5V on/off	Pi	5V to Pi

5V	OBC	5V to OBC
Ground	OBC, Pi	Ground for OBC and Pi
5V	LED	5V to LED
Ground	LED	Ground to LED
RBF	RBF	Remove Before Flight to turn on EPS
ON/OFF Signal 5V	OBC	Signal from OBC turn Pi ON/OFF
Turn ON/Off power to system (SET pin)	Rocket	Start signal from rocket
Ground	Rocket	Ground to rocket avionics

R. Requirements Payload

Requirements Payload



Purpose

The purpose of this document is to explain the requirements for the Sub-Orbital 2021 project, which gives context to the design choices that are made for the payload.

Summary

The document consists of the following:

- Requirements from Spaceport America Cup / European rocketry challenge
- Requirements in relation to the rocket
- Structural and physical requirements
- System requirements

Satellite definition

In this document, the rocket's payload is referred to as the satellite and the payload's experiment referred to as the satellite's payload. The reason for this is that the Sub-Orbital team views the experiment as a sub-payload, and this is to avoid confusion between the rocket's payload and the satellite's payload.

Requirements from Spaceport America Cup /European Rocketry Challenge

R-1: Integration with the rocket

Description:	The satellite has to be able to easily separate from the rocket during the rocket's integration phase to be weighed. No irreversible connections must be made between the rocket and the satellite.
Rationale:	The satellite will be taken out of the rocket during the integration phase of the rocket to be weighed. Because of this it has to be able to be separated from the rocket easily, and also be simple to put into the rocket again after weighing. Easy integration is also beneficial in case the S.O. team is not attending the contest, and the Propulse team has to be responsible for the integration.

Requirements in relation to the rocket

R-2: Weight

Description:	The satellite shall weigh at least 4 kg, where a maximum of 1kg is consisting of dead weight. The satellite can weigh more than 4kg, but should be avoided since it makes the whole rocket heavier.
Rationale:	Having a satellite with a weight of 4kg is desirable for the Propulse team. It forces them to challenge themselves when it comes to design, in order to have a rocket that can transport a payload.

R-3: Stability

Description:	The satellite shall have a stable center of mass.
Rationale:	This is beneficial for the rocket, seeing that a stable center of mass does not add any more uncertainties to the rocket during flight,

R-4: Battery capacity - idle

Description:	The batteries of the satellite have to be able to stay in idle phase from 15 to 20 hours.
Rationale:	The rocket will be assembled the night before the contest at the earliest, and seeing that the launch time is not specified, we estimate that the longest time it will have to stay in idle mode is 20 hours. This is defined as a requirement in relation to the rocket, since the rocket's timeframe decides how long the satellite stays in idle phase.

R-5: Battery capacity - active

Description:	The batteries of the satellite have to be able to stay in the active and flying phase for at least 15 minutes.
Rationale:	The satellite will receive a launch signal approximately 10 minutes before launch. This makes the satellite go into the active phase, where all the systems are on. Following this, the flight which will take approximately 5 minutes, during this time all the systems are on. This is defined as a requirement in relation to the rocket, since the rocket's timeframe decides how long the satellite stays in active phase.

R-6: Size

Description:	The outer body shall have a length of 300mm, and a diameter of maximum 110mm.
Rationale:	The outer diameter can be a maximum of 110 mm, this is to ensure sufficient spacing in the coupler of the rocket.

Structural and physical requirements

R-7: Waterproof

Description:	The outer body of the satellite must be waterproof.
Rationale:	The payload of the satellite will conduct an experiment using fluids, and in order to guarantee the safety of the rocket's equipment, the mechanical interface must be water resistant.

R-8: G-force

Description:	The hardware must be resistant to g-force, up to 15g.
Rationale:	Maximum estimated amount of g-force is 15g, during the first seconds of the flight.

R-9: Vibrations

Description:	The satellite has to be able to function during high levels of vibration.
Rationale:	The electrical interface has to be able to stay still within the mechanical frame. The camera also has to be able to film the experiment with satisfying quality, although this is not a mission critical requirement.

R-10: Data retrieval

Description:	The data captured must be retrievable after launch, in case of a crash landing of the rocket, or other significant rocket failure.
Rationale:	This is in order to see how the satellite functioned during the flight, and also to get the experiment footage. Without the data, the S.O. team can not get a chance to validate the system if the satellite crashes.

System requirements

R-11: Launch signal

Description:	The satellite has to be able to respond to a launch signal given by the rocket. This will be a digital signal sent as a pulse. The same signal has to make the satellite go back to idle mode.
Rationale:	This signal will be received by a cable, and both the electrical and software interface has to be able to respond accordingly to this. Upon receiving the signal, the electrical interface shall be able to turn the system on, and the software interface initiates the functions used in the Active phase. The signal will be a digital pulse.

R-12: On-Board computer

Description:	The satellite has to use a main computer designed by the SelfieSat team.
Rationale:	SelfieSat's main computer is one of the most critical components of the SelfieSat, and it is valuable for the S.O. team to have experience using it if they decide to join the SelfieSat team after the mission.

R-13: Raspberry Pi

Description:	The satellite has to make use of a Raspberry Pi
Rationale:	Similarly to the main computer and R-13, the Raspberry Pi is an important component of the SelfieSat, and the S.O. team may benefit later from having experience with the Raspberry Pi.

R-14: Storage capacity

Description:	The satellite has to have an SD-card of a minimum of storage space to store sensor data and video in high resolution for at least 20 minutes. In case of a crash, as little of the video footage should be deleted or corrupted.
Rationale:	The SD-card must be large enough to capture video from the active and flying phase, for a total of approximately 20 min. This is similar to the battery capacity requirements, but unlike those, this requirement is listed as a system requirement. The reason for this is that the battery capacity has a more direct correlation with the rocket's timeframe, and

	also our choice of storing data is more adaptable than the choices behind battery capacity.
--	---

R-15: Boot time

Description:	The system has to boot and be set for launch within 5 minutes.
Rationale:	The satellite has to be able boot and calibrate IMU within five minutes. This is to ensure that the rocket's battery capacity and launch window is not compromised by the boot time of the satellite.

R-16: Software functionality

Description:	The software programs work as intended, and can handle random errors. This includes abnormal sensor data and sensor failure. The software must be able to write data to file correctly, in case of unexpected events
Rationale:	Case test the software programs and verify that the programs respond accordingly.

S. Payload Sub-assembly checklist

Payload sub-assembly



Purpose

This document is meant to give the person preparing the payload for launch a comprehensive list of all the things that must be done before the payload is ready for launch.

Required tools

- M4 screw driver
- Protective glasses
- Protective gloves
- Ferrofluid bottle
- Shear pliers

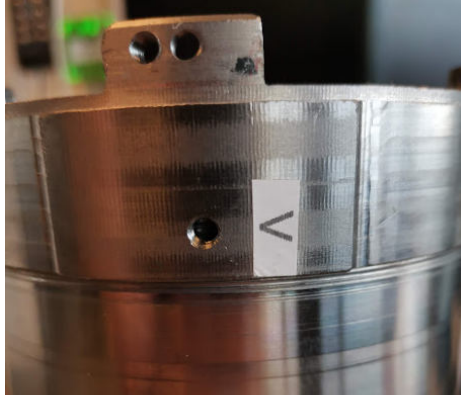
Before assembly

What to do	Required tools	Comment / picture	Mark when done
Charge batteries.	--	Charge for a maximum of 12 hours.	
Place batteries in the battery holder.	--	Batteries are labeled with "UP" on the side that is up.	
Strip batteries into place.	--	Strips are threaded in the battery holder, tighten them.	
Press the button on the side of the battery holder to verify that batteries are inserted correctly.	--	The batteries are inserted correctly if the LED lights up. 	

--	--	--	--

During assembly

What to do	Required tools	Comment / picture	Mark when done
Insert ferrofluid into the ferrofluid-container. The container is located in the bottom of the inner structure.	-Ferrofluid bottle -Protective glasses -Protective gloves	A circle is marked inside of the ferrofluid container to indicate how much fluid that shall be applied. After this point, avoid shaking and turning the payload upside down.	
Attach the lid on the ferrofluid container.	--		
Remove the remove before flight-pin.	--	Marked red, is located in the upper section of the inner structure.	
Screw the inner structure into the cylinder.	--	Screw clockwise. It is supposed to be able to rotate many times. Stop rotating when the labels with arrows are touching. 	
Insert grubber screws in the four holes in the side of the upper lid.	M4 screw driver	The screw holes are located on the side of the lid. Screw the screws in tightly enough so that the cylinder lid is not able to rotate.	

			
Connect ground cable from the satellite to the rocket.	--	This sticks out of the lid of the satellite, and is labeled with “GROUND”.	
Connect launch signal cable from the satellite to the rocket.	--	This sticks out of the lid of the satellite, and is labeled with “LAUNCH SIGNAL”.	
Connect ping cable from the satellite to the rocket.	--	This sticks out of the lid of the satellite, and is labeled with “PING”.	
Attach bulkheads to the lids.	--	The left holes are the ones that are used. 	
The complete system is booted when the ping to the rocket is received.	--	If ping is not received after an extended period, send a new signal to the payload to make it go back to idle, and then a new signal to turn it back to active.	

In case of delayed launch

What to do	Required tools	Comment / picture	Mark when done
Send de-arm signal to make satellite go back to idle mode.	--		
Cut strips and place new batteries in the battery holder.	Shear pliers	Batteries are labeled with "UP" on the side that is up.	
Strip batteries into place.	--	Easiest done by inserting one end at one side, and from the backside of the holder bend it back into the other hole.	
Press the button on the side of the battery holder to verify that batteries are inserted correctly.	--	The batteries are inserted correctly if the LED lights up.	

Acknowledgment

The team would like to thank our mentors for feedback and guidance throughout the project.

External mentors: Mariusz Eivind Grøtte at the Department of Engineering Cybernetics, NTNU, Arve Tokheim at 4Test Instruments, Cecilia Haskins at the Department of MechanicalEngineering, NTNU, Vegar Melvær at Byåsen VGS, Peder August Aune at Kongsberg Defence & Aerospace, Simen Ekornåsvåg at Kongsberg Defence & Aerospace and Jarle Øye at Nammo.

Mentors who are Propulse NTNU Alumni: Jonas Aannestad, Inge Eide, Eirin Fanebust, Eivind Rydningen, Henrik Øvrebø, Frederik Hiort, Jon Petter Stokmo, Abraham Sørdsalen, Tobias Winter and Rannveig Marie Færgestad.

References

- [1] SkyVector, “LPSO - Ponte De Sor Airport,” 2021. URL <https://skyvector.com/airport/LPS0/Ponte-De-Sor-Airport>.
- [2] Rogers, C. D., C. E., “Rogers Aeroscience RASAero II Aerodynamic Analysis and Flight Simulation Program,” 2019. URL <http://www.rasaero.com/dloads/RASAero%20II%20Users%20Manual.pdf>.
- [3] Tokheim, A., personal communication, April 2021.
- [4] Alm, C., personal communication, November 2021.
- [5] Øya, I. J., personal communication, November 2021.
- [6] Jameson, A., and Schmidt, W., “Some Recent Developments in Numerical Methods,” *COMPUTER METHODS IN APPLIED MECHANICS AND ENGINEERING*, Vol. 51, 1984, pp. 467–468. URL http://aero-comlab.stanford.edu/Papers/jameson_CMAME_v51_1985.pdf.
- [7] Anderson, J. D., *Fundamentals of Aerodynamics*, 6th ed., McGraw-Hill Education, New York, 2017.
- [8] Hall, N., “The drag equation,” Cited May 2nd 2021. URL <https://www.grc.nasa.gov/www/k-12/airplane/drageq.html#:~:text=The%20drag%20equation%20states%20that,times%20the%20reference%20area%20A.&text=For%20given%20air%20conditions%2C%20shape,for%20Cd%20to%20determine%20drag>.
- [9] A. Crowell Sr., G., “The descriptive geometry of nose cones,” Cited May 2nd 2021. URL https://web.archive.org/web/20110411143013/http://www.if.sc.usp.br/~projetosulfos/artigos/NoseCone_EQN2.PDF.
- [10] Kurowski, P. M., *Engineering Analysis with SolidWorks Simulation 2017*, SDC Publications, 2017.
- [11] Aune, P. A., personal communication, January 2021.
- [12] Ekornåsvåg, S., personal communication, January 2021.
- [13] Agency, E. S., “Structural Materials Handbook,” 1994. URL https://www.apc.univ-paris7.fr/APC_CS/Labo/Espace_Qualite/tch/normes/ESA/PSS%2003%20203%20Vol.1%20Structural.pdf.
- [14] James, C. J. R., S. C., “NACA RM A53D02 - Research Memorandum, Experimental Investigation of the Zero-Lift Drag of a Fin-Stabilized Body of Fineness Ratio 10 at Mach Numbers Between 0.6 and 10.” 1953. URL https://www.google.com/url?sa=t&rct=j&q=&esrc=s&source=web&cd=&ved=2ahUKEwiN6vTPwqvAhUslosKHQXLDRMQFjAAegQIAxAD&url=http%3A%2F%2Fwww.rasaero.com%2Fdloads%2FNACA%2520RM%2520A53D02.pdf&usg=A0vVaw3Hyfzr6wT6Y0Y6DG_knhV8.
- [15] Stephen Whitmore, C. B., “Effects of Wing Sweep,” Cited April 23rd 2021. URL http://mae-nas.eng.usu.edu/MAE_5420_Web/section7/section.7.3.pdf.
- [16] Summers, C. Y. e. a., T. P., “Overview of aluminum alloy mechanical properties during and after fires,” 2015. <https://doi.org/10.1186/s40038-015-0007-5>.
- [17] Components, A., “Shock Cords for Dual-Deployment Rockets,” April 9th 2018. URL <https://www.youtube.com/watch?v=isMdw3JXQIE>.
- [18] Chris’RocketSupplies, “Cesaroni O3400 Imax Rocket Motor,” Cited May 1st 2021. URL <https://www.csrocketry.com/rocket-motors/cesaroni/motors/pro-98/6gx1-reloads/cesaroni-o3400-imax-rocket-motor.html>.
- [19] Instrumart, “Keller LEO2 Digital Pressure Gauge,” Cited March 22th 2021. URL <https://www.instrumart.com/products/30984/keller-leo2-digital-pressure-gauge>.
- [20] MatWeb, “Overview of materials for Nylon 66/6, 30Reinforced,” April 24th 2018. URL <http://www.matweb.com/search/DataSheet.aspx?MatGUID=ea22ae239763477e8c21dcbf717695f6&ckck=1>.

- [21] Douglas B., W. C., and H., R., “Tracker,” Cited March 22th 2021. URL <https://physlets.org/tracker/>.
- [22] RASAero, “RASAero Altitude Prediction Accuracy,” Cited April 23rd 2021. URL <https://www.rocketryforum.com/attachments/rasaero-altitude-prediction-accuracy-pdf.387822/>.
- [23] RASAero, “RASAero II Comparisons with ARCAS Cp and Cd Data,” Cited April 24rd 2021. URL <https://www.rocketryforum.com/attachments/rasaero-ii-comparisons-with-arcas-cp-and-cd-data-pdf.277901/>.
- [24] “Exponential Approximation of Air Density with Altitude,” Cited April 23rd 2021. URL https://en.wikipedia.org/wiki/Density_of_air.
- [25] Ansys, “7.3.2 Using Flow Boundary Conditions,” Cited April 24th 2021. URL <https://www.afs.enea.it/project/neptunius/docs/fluent/html/ug/node238.htm>.
- [26] Incropera, D. D. P. B. T. L. L. A. S., F. P., *Incropera's, Principles of Heat and Mass Transfer*, 1st ed., John Wiley Sons Inc, 2017.
- [27] ApogeeComponents, “Peak of flight Newsletter,” July 19th 2011. URL <https://apogeerockets.com/education/downloads/Newsletter291.pdf>.
- [28] FlippingPhysics, “You can’t run from Momentum,” Cited March 4th 2021. URL https://www.flippingphysics.com/uploads/2/1/1/0/21103672/06-01_lecture_notes_compilation_-_momentum_and_impulse.pdf.
- [29] Nanoavionics, “Environmental Test Requirements for Falcon 9 Auxiliary Nanosatellites,” December 6 2019.
- [30] GmbH, D., “Joule-Thomson Coefficient (isenthalpic dT/dP) of Carbon dioxide,” Cited April 10rd 2021. URL http://www.ddbst.com/en/EED/PCP/JTC_C1050.php.
- [31] Wikipedia, “Van der Waals constants (data page),” , Cited April 10rd 2021. URL [https://en.wikipedia.org/wiki/Van_der_Waals_constants_\(data_page\)](https://en.wikipedia.org/wiki/Van_der_Waals_constants_(data_page)).
- [32] Rubber, A., “O-ring Basics,” Cited April 23rd 2021. URL <https://www.applerubber.com/src/pdf/section3-o-ring-basics.pdf>.
- [33] EngineersEDGE, “Shear Pin/Screw Calculations,” Cited May 5th 2021. URL [http://www.feretich.com/Rocketry/Resources/shearPins.html#:~:text=Shear%20strength%20is%20measured%20by,per%20square%20inch%20\(psi\).](http://www.feretich.com/Rocketry/Resources/shearPins.html#:~:text=Shear%20strength%20is%20measured%20by,per%20square%20inch%20(psi).)
- [34] EngineersEDGE, “Bolt or Pin In Single Shear Equation and Calculator,” Cited May 5th 2021. URL https://www.engineersedge.com/material_science/bolt_single_shear_calcs.htm.
- [35] EngineersEDGE, “External Metric Thread Table Chart and Fastener Sizes M1.6 - M18,” Cited May 5th 2021. URL <https://www.engineersedge.com/hardware/metric-external-thread-sizes1.htm>.
- [36] Williams, N. R., “The Calculation of Air Density in Various Units,” 1949, p. 319–320. URL https://journals.ametsoc.org/view/journals/bams/30/9/1520-0477-30_9_319.xml?tab_body=pdf.
- [37] ToolBox, E., “U.S. Standard Atmosphere,” Cited October 11th 2020. URL https://www.engineeringtoolbox.com/standard-atmosphere-d_604.html.
- [38] Time, and Date, “Weather in Ponte de Sor, October 15th 2020,” Cited August 16th 2021. URL <https://www.worldweatheronline.com/ponte-de-sor-weather-averages/portalegre/pt.aspx>.
- [39] FruityChutes, “Fruitychute website,” , Cited March 3rd 2021. URL <https://fruitychutes.com/>.
- [40] Wikipedia, “International Standard Atmosphere,” , Cited April 29th 2021. URL https://en.wikipedia.org/wiki/International_Standard_Atmosphere.
- [41] Wikipedia, “Bogacki–Shampine method,” , Cited April 12th 2021. URL https://en.wikipedia.org/wiki/Bogacki%20&%20Shampine_method.

- [42] Wikipedia, “Adaptive step size,” , Cited April 12th 2021. URL https://en.wikipedia.org/wiki/Adaptive_step_size.
- [43] Hartmann, A. K. T. M. R. L. A. S. B. Y. C. F. D. E. D. D. E. A. K. B. S. P. T. M. W., D.L., and Zhai, P., *Observations: Atmosphere and Surface*, 1st ed., Cambridge University Press, 2013. URL https://www.ipcc.ch/site/assets/uploads/2017/09/WG1AR5_Chapter02_FINAL.pdf.
- [44] ToolBox, E., “Air - Specific Heat at Constant Pressure and Varying Temperature,” Cited April 15th 2021. URL https://www.engineeringtoolbox.com/air-specific-heat-capacity-d_705.html.
- [45] Johnson, D., “Table of absorptivity and emissivity of common materials and coatings,” , Cited April 15th 2021. URL <http://www.solarmirror.com/fom/fom-serve/cache/43.html>.
- [46] AZOMaterials, “Properties: S-Glass Fibre,” Cited April 15th 2021. URL https://www_azom_com/properties.aspx?ArticleID=769.
- [47] ToolBox, E., “Convective Heat Transfer,” Cited April 15th 2021. URL [https://www.engineeringtoolbox.com/convective-heat-transfer-d_430.html#:~:text=Typical%20convective%20heat%20transfer%20coefficients,%2F\(mK\)\)](https://www.engineeringtoolbox.com/convective-heat-transfer-d_430.html#:~:text=Typical%20convective%20heat%20transfer%20coefficients,%2F(mK))).
- [48] Shitzer, A., “Convective heat transfer coefficients vs. wind speed,” , Cited April 15th 2021. URL https://www.researchgate.net/figure/Convective-heat-transfer-coefficients-vs-wind-speed_fig3_7373482.
- [49] Agy, “758 ZenTron® Roving,” Cited April 28th 2021. URL http://www.agy.com/wp-content/uploads/2014/03/758_ZenTron_Roving-Industrial_and_Automotive.pdf.
- [50] Tcrcomposites, “UF3369 TCR Resin System,” Cited April 28th 2021. URL <http://www.tcrcomposites.com/lib/TDS-RD-0001-R002-UF3369.pdf>.
- [51] TorayCarbonFibersAmericaINC, “T700S DATA SHEET,” Cited April 28th 2021. URL <https://www.rockwestcomposites.com/media/wysiwyg/T700SDatasheet.pdf>.
- [52] 3M, “EPX Adhesive DP490,” Cited April 28th 2021. URL <https://multimedia.3m.com/mws/media/82790O/dp490-scotch-weld-tm-adhesive.pdf>.